INESTABILIDADES SUBMARINAS: CARACTERIZACIÓN SEDIMENTARIA Y FACTORES DE CONTROL

David Casas Layola

Tesis Doctoral

2005

Universitat de Barcelona

Institut de Ciències del Mar CSIC

Departament d'Estratigrafia, Paleontologia i Geociències Marines
Universitat de Barcelona
Programa: **"Registre Sedimentari i Evolució Paleoambiental"**
Bienni 1998-2000

INESTABILIDADES SUBMARINAS: CARACTERIZACIÓN SEDIMENTARIA Y FACTORES DE CONTROL

Memoria Presentada por
DAVID CASAS LAYOLA
para optar al título de
Doctor en Ciencias Geológicas

Directoras de la Tesis:

Dra. Gemma Ercilla
Departament de Geologia Marina i
Oceanografia Física
Institut de Ciències del Mar
CMIMA-CSIC
Barcelona

Dra. Belén Alonso
Departament de Geologia Marina i
Oceanografia Física
Institut de Ciències del Mar
CMIMA-CSIC
Barcelona

ÍNDICE GENERAL

AGRADECIMIENTOS

Es seguro que no conseguiré expresar en esta página la gratitud que debo a un incontable número de personas que directamente o indirectamente han influido en el trabajo que finalmente se materializa en esta Tesis Doctoral.

En primer lugar debo dar las gracias a mis directoras de Tesis, las Doctoras Gemma Ercilla y Belén Alonso. Está claro que sin ellas y su apuesta clara y rotunda nada de esto existiría.

A Ferran, el compañero de trabajo ideal, con el que espero poder colaborar tantos años como este mundo nos permita.

A Marcel·lí, Marga y el resto de compañeros del grupo de geología marina, siempre es un placer estar rodeado de buena gente. A Bene por su ayuda en el trabajo de laboratorio.

A Pablo, Javi, Toni y el resto del personal de la UTM, por su soporte técnico demasiadas veces por encima de sus obligaciones.

También querría agradecer la cooperación Homa Lee y los miembros del equipo de geología marina del "Western Region Coastal and Marine Geology, U.S Geological survey (USGS)" que me acogieron durante mi estancia en California y con los que fue un placer trabajar.

Finalmente, esta Tesis doctoral y los trabajos que la forman se han realizado gracias al soporte de diferentes proyectos de investigación financiados por instituciones nacionales y europeas. Se deben mencionar los proyectos *Hyace* (MAS3-CT97-0102), *Anaximander* (EVK3-2001-00123), financiados por la comunidad Europea y *Marconi* (REN2000-0336-C03), *Marsibal* (REN2001-3868-C03), "*Arquitectura, estratigrafía, y sedimentología de los márgenes y cuencas al Norte de la Península Antártica: procesos sedimentarios de origen glacial y marino, y reconstrucción paleoambiental durante el Cuaternario*" (ANT97-0584) y "*Geología reciente de la Plataforma en Bahía Sur (Isla Livingston): Estudio sismoestratigráfico y morfosedimentario*" (ANT1999-1462-E) financiados por el Ministerio de Ciencia y Tecnología. Debo también mencionar el soporte económico de la Generalitat de Catalunya por la beca predoctoral (1999FI 00002CSIC PG) que me fue concedida.

PRÓLOGO

El estudio de los movimientos de masa submarinos en márgenes continentales y cuencas marinas tiene importancia desde el punto de vista científico y aplicado así como una gran relevancia estratégica y social, al permitir predecir, determinar y evaluar áreas con potenciales riesgos geológicos y los posibles efectos derivados de estos, como por ejemplo los maremotos. El estudio de las inestabilidades del fondo marino tiene también una gran importancia para el diseño y construcción de infraestructuras submarinas como tendidos de cables y tuberías, para el posicionamiento y anclaje de torres y plataformas así como para la selección de áreas probables donde efectuar vertidos de residuos industriales y nucleares. El interés en el conocimiento de los procesos de inestabilidad sedimentaria y sus características deposicionales queda plasmado en los grandes proyectos científicos nacionales e internacionales que están directamente relacionados con el estudio de los movimientos de masa submarinos. Entre estos proyectos destacan: ADFEX (Arctic Delta Failure Experiment, 1989-1992), GLORIA (Geological Long-Range Inclined Asdic, 1984-1991), STEAM (Sediment Transport on European Atlantic Margins, 1993-1996), ENAM II (European North Atlantic Margin, 1996-1999), STRATAFORM (1995-2001), COSTA (Continental Slope Stability, 2000-2004) o IGCP-511 (Submarine Mass Movements and Their Consequences, 2005-2009).

Esta Tesis Doctoral representa una contribución al conocimiento de las inestabilidades submarinas al abordar aspectos fundamentales en su estudio con distintas técnicas, diferentes grados de resolución y contextos geológicos. En los trabajos presentados en este volumen, se hace especial hincapié en el análisis de las propiedades físicas de los sedimentos marinos como uno de los aspectos centrales en el estudio de las inestabilidades submarinas. En este sentido, el trabajo realizado utilizando herramientas como el “Multi Sensor Core Logger” de forma rutinaria se puede considerar novedoso en nuestro país. Aunque esta herramienta se está convirtiendo en un estándar en el análisis de testigos de sedimentos marinos, su implantación en los centros de investigación españoles es hasta el momento minoritario.

Esta memoria presentada como tesis doctoral, se ha concebido como una integración de tres trabajos publicados y dos en proceso de publicación en revistas científicas incluidas en el “science citation index”. Este formato de tesis doctoral, aceptado desde hace tiempo en la Universitat de Barcelona, tiene por su propia concepción unas características diferenciadoras de las tesis “clásicas”; en este sentido

en la presente memoria y atendiendo tanto a los precedentes existentes como a la norma escrita, se ha optado por incorporar una corta introducción (capítulo 1) donde se detallan los aspectos más relevantes para la justificación y comprensión del trabajo en su conjunto. A continuación se presentan cinco artículos (capítulos 2 a 6) que reflejan aspectos fundamentales en el estudio de inestabilidades submarinas en márgenes continentales y cuencas, y en diferentes marcos geológicos. Por último, en el capítulo 7 se discute y resume las principales conclusiones de la tesis doctoral.

La integración de diferentes artículos publicados según las normas editoriales impuestas por diferentes editores en un único trabajo, fuerza a tomar decisiones respecto al formato final de la memoria. En este sentido se ha optado por homogeneizar la estructura del texto para facilitar su lectura y proporcionar coherencia al volumen. Pero se han respetado algunos aspectos concretos de cada formato original como es el caso del idioma, la estructura de los títulos o de la bibliografía entendiendo que, ésta al estar separada por artículos no supone ningún obstáculo para la correcta comprensión y seguimiento del trabajo.

OBJETIVOS

El objetivo fundamental de esta Tesis Doctoral es profundizar en el conocimiento de las inestabilidades sedimentarias en márgenes continentales y su evolución, abordando para este fín cuatro aspectos fundamentales de estos procesos sedimentarios y la valoración de sus consecuencias:

a) caracterización del margen continental y registro histórico de las inestabilidades observables en un talud continental,

b) definición de facies sedimentarias, geometría, dinámica de rotura y evolución de los deslizamientos submarinos observados,

c) estudio de las propiedades físicas, mecánicas y elásticas del sedimento y

d) determinación de las fuerzas y procesos mecánicos que pueden controlar la detonación de deslizamientos y su evolución.

La estrategia de estudio para abordar los cuatro aspectos fundamentales ha implicado una aproximación multidisciplinar (facies acústicas, morfología, sedimentología, propiedades físicas y geotécnicas…) y multiescala (desde kilométrica a micrométrica).

Cada uno de los artículos que forman la Tesis Doctoral (capítulos 2, 3, 4, 5 y 6) trata uno o más de estos aspectos enumerados. Aunque como entidades individuales centradas en áreas y contextos geológicos diferentes, pueden extenderse más allá de cada uno de los puntos citados anteriormente.

El primer aspecto fundamental enunciado (**a**) se ha trabajado básicamente en el margen continental del Ebro (capítulo 2) y Golfo de Cádiz (capítulo 3). El trabajo realizado en el margen continental del Ebro se centra en la distribución espacial y variabilidad de las inestabilidades observadas. El estudio en el Golfo de Cádiz se focaliza en las diferentes características existentes asociadas a la presencia de gas e hidratos de gas en sedimentos, como uno de los parámetros importantes en la valoración del riesgo geológico.

El segundo punto (**b**) se ha trabajado en el margen continental del Ebro (capítulo 2) haciendo especial hincapié en el análisis de la geometría de los cuerpos deslizados y sus facies sísmicas para poder establecer los mecanismos de rotura, evolución y sus posibles factores de control.

El tercer aspecto (**c**) se ha trabajado en sedimentos distales de la Llanura Abisal de Madeira (capítulo 4), sedimentos depositados por procesos asociados a volcanes de fango en las montañas submarinas Anaximander (capítulo 5) y en sedimentos del margen glaciomarino de la Península Antártica (capítulo 6). Estos estudios se han centrado en la caracterización de las propiedades físicas de estos sedimentos así como su asociación a procesos sedimentarios y la cuantificación de las variables sedimentológicas que controlan dichas propiedades. En el capítulo 6 también se han estudiado las propiedades mecánicas de dichos sedimentos.

Finalmente, los procesos que pueden controlar la detonación de las inestabilidades observadas (**d**) se han discutido principalmente en tres áreas de estudio, el margen continental del Ebro, Golfo de Cádiz y Península Antártica.

CAPÍTULO 1

INTRODUCCIÓN

CAPÍTULO 1: INTRODUCCIÓN

INTRODUCCIÓN

1. Sedimentos Marinos e Inestabilidades

Las inestabilidades submarinas tienen un impacto significante en la construcción de márgenes continentales y en la transferencia de sedimentos a zonas profundas de los océanos, y al mismo tiempo pueden tener un gran impacto económico si afectan a estructuras submarinas o costeras construidas por el hombre. El estudio de las inestabilidades submarinas permite reconstruir y modelizar la evolución temporal y espacial de los márgenes continentales y las cuencas oceánicas. Los modelos obtenidos son, además, aplicables al estudio sedimentario de una gran variedad de contextos geológicos, por lo que resultan de gran valor para la interpretación de registros sedimentarios antiguos, la evaluación de la interacción de numerosos procesos geológicos (aporte sedimentario, eustatismo, tectónica, sismicidad) en la evolución sedimentaria de márgenes y cuencas, así como para la predicción de los riesgos geológicos potenciales.

Las inestabilidades del fondo marino son la fuente de los eventos catastróficos como deslizamientos, coladas de derrubios y corrientes de turbidez. Por tanto, tienen una influencia relevante en la evolución de la morfología y estratigrafía de los fondos marinos ya que controlan dónde, cuándo y qué cantidad de sedimento es transferido desde aguas someras a profundas, con la gravedad como principal mecanismo de transporte. Además, como las inestabilidades son parte inherente al carácter físico de los márgenes continentales, estos continúan hoy en día produciendo eventos incluso en áreas donde el nivel del mar es alto y la sismicidad y aporte de sedimento es bajo. Estos procesos además representan en especial un elevado riesgo en las zonas costeras donde la actividad humana es muy intensa. Son por lo tanto, un importante factor a tener en cuenta tanto en la exploración como en la utilización de los márgenes continentales, cuencas oceánicas y sus recursos.

Todas las provincias fisiográficas del margen continental presentan fenómenos de inestabilidad sedimentaria desde la línea de costa hasta las cuencas oceánicas. Pero el número de inestabilidades presentes es significativamente más alto en el talud continental. Una de las razones más obvias es que es el área con más pendiente y por tanto donde la fuerza de la gravedad tiene un papel más importante. Otra razón, menos evidente, es que el talud continental tiende a ser la provincia donde la acumulación de

sedimento es más alta por el balance positivo entre progradación y agradación de los márgenes en general (Pratson, 2001).

1.1. El medio marino versus el continental

Las inestabilidades sedimentarias se dan en ambientes terrestres y subacuaticos aunque estas vienen condicionadas por las características propias de cada medio. Los mayores deslizamientos descritos en la Tierra se dan en los márgenes continentales y cuencas oceánicas. Deslizamientos y coladas de derrubios individuales pueden involucrar varios miles de kilómetros cúbicos de material. Por ejemplo, el mayor de los deslizamientos descritos en la Isla Hawai tiene hasta 2 km de espesor y un volumen de 5000 km^3 (Moore et al., 1989; Masson et al., 1996). Otros deslizamientos destacables podrían ser el "Aghulas Slide" en Sur África, el "Storegga Slide" en Noruega (Bugge, 1983; Evans et al., 1996; Canals et al., 2004), o las coladas de derrubios de Canarias y del Sahara en el Atlántico occidental, tienen un recorrido de entre 600 y 800 km y la mayoría se dan en áreas con pendientes de menos de 0,5º (Weaver et al., 1992; Masson et al., 1997). Respecto a las corrientes de turbidez, el volumen de sedimento que pueden transportar es un orden de magnitud menor que el del mayor deslizamiento o colada de derrubios conocido. Por ejemplo, se han descrito algunas turbiditas individuales de 100-200 km^3 en varias llanuras abisales atlánticas (Weaver et al., 1992). Aunque la distancia de transporte son normalmente espectaculares y frecuentemente exceden los 1000 km (Locat et al., 2002).

Este hecho diferenciador respecto al medio terrestre es consecuencia directa del relieve y la forma de las cuencas oceánicas y de la gran cantidad de sedimento no consolidado (en condiciones geotécnicas sólo marginalmente a favor de la estabilidad), o parcialmente consolidado presente en los taludes de los márgenes continentales (Masson et al., 1996). A este factor hay que añadir que la densidad de los sedimentos movilizados es del mismo orden de magnitud, aunque ligeramente mayor que la del medio acuático (Parsons et al., 2005) hecho que da la capacidad a los sedimentos para viajar mayores distancias. Otra característica relevante y diferenciadora respecto el medio terrestre es que en general, en el medio marino hay menos variación espacial, es decir que las propiedades físicas de los sedimentos pueden ser muy similares en áreas relativamente extensas (Silva et al., 2004).

Un sedimento marino es una mezcla de diversos componentes entre los que se incluyen electrolitos, partículas sólidas de formas y características muy variables, a menudo con gases y normalmente saturado en agua; esto confiere a los sedimentos un carácter físico y geotécnico particular. Las principales características del sedimento marino que lo diferencian del terrestre pueden resumirse en:

- Saturación en un 100% en la mayor parte de los depósitos,
- Agua salada como fluido intersticial (salinidad 0-3,5%),
- Ausencia de crosta desecada en la superficie,
- Material poco consistente en la parte superior de la columna estratigráfica,
- Tendencia a la subconsolidación y presencia de gas en sedimentos depositados rápidamente (gas disuelto, libre o sólido bajo un enterramiento profundo) y
- Partículas biogénicas con formas y texturas características, frágiles y en ocasiones químicamente activas.

1.2. Definiciones, tipos y clasificación de las inestabilidades submarinas

El término movimientos de masa submarinos ("submarine mass-movement") utilizado ampliamente en esta memoria, es un término general que incluye diferentes tipos de inestabilidad, desde deslizamientos hasta corrientes de turbidez, tal y como la ISSMGE (International Society for Soil Mechanics and Geotechnical Engineering) establece. Muchos estudios han utilizado este término (Casas et al., 2004) aunque existen otros términos sinónimos utilizados por otros autores, como por ejemplo "mass wasting", inestabilidades o deslizamientos submarinos ("submarine landslides") (Hampton et al.,1996), "offshore mass-movements" (Mulder y Cochonat, 1996) y "gravity-driven sediment flows" (Masson et al., 1996), que también se han utilizado en esta memoria. Aunque el término movimientos de masa submarinos ha sido utilizado anteriormente por autores como Nardin et al. (1979), su clasificación de los procesos es diferente de la propuesta por la ISSMGE. El objetivo de todas estas clasificaciones es organizar los diferentes eventos dando información sobre los mecanismos detonadores, el movimiento estrictamente y el depósito resultante.

Los diferentes tipos de inestabilidades submarinas se pueden definir siguiendo la clasificación para movimientos de masa subaéreos propuesta por la ISSMGE (Locat y Lee, 2000) (Tabla 1), ya que en los ambientes acuáticos (marinos y continentales) se dan básicamente los mismos tipos que en los ambientes terrestres, con algunas excepciones, que son exclusivas del medio marino como las corrientes de turbidez. Todos los tipos indicados se excluyen mutuamente aunque por supuesto cualquiera de ellos puede generar otro tipo de inestabilidad (por ejemplo, un deslizamiento puede transformarse en un flujo). Se pueden presentar diferentes subdivisiones (Prior, 1984; Norem et al., 1990; Mulder y Cochonat, 1996) pero los términos presentados en esta clasificación (Tabla 1) cubren la gran mayoría de fenómenos observados.

Procesos como los flujos turbidíticos o corrientes de turbidez, exclusivos del medio marino, están ausentes de la literatura científica anterior a 1950. No fue hasta que una corriente de turbidez rompió varios cables de comunicaciones transatlánticos cuando se pensó en un nuevo tipo de corriente con flotabilidad negativa producida por el mismo sedimento (Heezen y Ewing, 1952).

Tipos de movimientos de masa submarinos	"Topples" (Vuelcos/ Desplomes)		
	"Slides" (Deslizamientos)	"Slumps" (D. Rotacionales)	
		"Slides" (D. Traslacionales)	
	"Spreads" (Desparramientos)		Corrientes de turbidez
	"Falls" (Desprendimientos)	"Avalanches" (Avalanchas)	
	"Flows" (Flujos)	"Debris flow" (Colada de derrubios)	
		"Mud flows" (Flujos de fango)	

Tabla 1. Clasificación de los movimientos de masa submarinos adaptada de la clasificación subaérea propuesta por el comité técnico ISSMGE (Locat y Lee, 2000).

La concentración también es un criterio efectivo para definir y clasificar los diferentes tipos de inestabilidades. Según este criterio, se distinguen cuatro tipos básicos y cada uno tiene un rango de concentraciones, número de Reynolds (Re), duración y tamaño de grano típico (Tablas 2 y 3).

Flujo	Duración	Velocidad	Concentración (kg/m^3)	Tamaño de grano máximo	Reología	Re
Desliza-miento	minutos	> 1 m/s (3,6 km/h)	>1000	Bloques (> 100 m^3)	No-Newtoniano?	<1
Colada derrubios	minutos a horas	0.1-10 m/s (0,36-36 km/h)	>1000	Bloques (<100 m^3)	No-Newtoniano	<100
Flujos fangosos	horas	5-30 cm/s (0,18-1 km/h)	>10	Limo y arena?	No-Newtoniano?	$1\text{-}10^4$
Corrient. turbidez	minutos a días	30 cm/s (1km/h)	<10	Arena gruesa	Newtoniano	$>10^4$

Tabla 2. Principales características de los movimientos de masa submarinos (Parson et al., 2005)

De entre los diferentes tipos de movimientos de masa submarinos existentes, los deslizamientos, coladas de derrubios y las corrientes de turbidez son quizás los más abundantes y los que transportan volúmenes importantes de sedimento hacia las zonas más profundas de los océanos (Masson et al., 1996).

Los *deslizamientos* se definen como el movimiento de un cuerpo sobre una superficie basal de rotura, del que resulta grandes bloques de material coherente, con una deformación interna que puede variar de nula a significante (Fig.1). Son movimientos de masa de gran escala, donde las interacciones partícula-partícula tienen un papel mucho más importante que la presión de poro del fluido intersticial y no se pueden tratar simplemente con modelos continuos de mecánica de fluidos (Parsons et al., 2005).

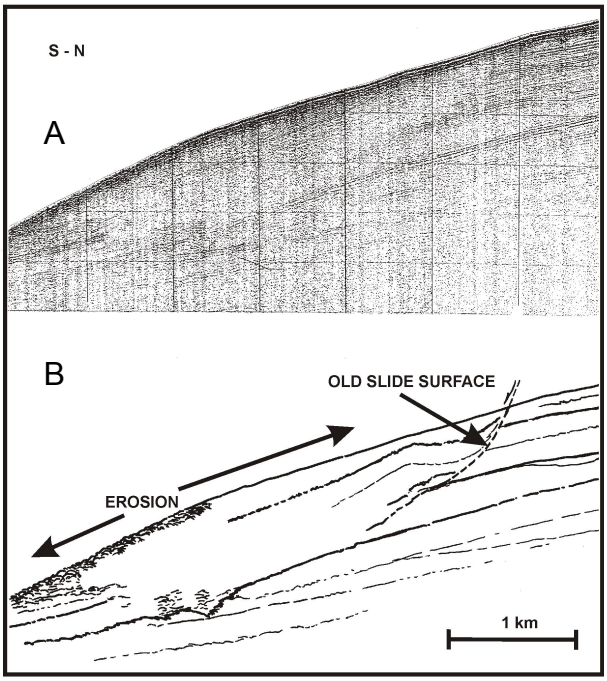

Fig. 1. Ejemplo de deslizamiento en un perfil sísmico Geopulse (A) y su interpretación (B).

Las *coladas de derrubios* (Figs. 2 y 3) son masas de material poco seleccionado donde las interacciones partícula-partícula son importantes y su reología es función de la presión de poro del fluido intersticial y de la fricción interna (Parsons et al., 2005). Se definen como el movimiento de sólidos granulares, a veces mezclados con pequeñas cantidades de agua, en zonas de pendientes bajas. La mayoría de los estudios en detalle de coladas de derrubios se han hecho en eventos sub-aéreos, pero no hay razones para pensar que los submarinos difieren substancialmente. El flujo es predominantemente laminar, aunque es necesaria una mezcla interna para que se produzca la estructura caótica observada en la mayoría de eventos (Tabla 3). En teoría, los clastos en los derrubios están soportados principalmente por la combinación de su flotabilidad y por la fuerza de cohesión de la matriz, aunque en algunos casos los clastos mayores no pueden ser soportados totalmente por la matriz y su transporte implica un componente de deslizamiento y otro de rotación con la matriz actuando de lubricante mientras proporciona cierta flotabilidad. En movimientos submarinos parece que este mecanismo es crucial para explicar la dinámica de los mayores bloques arrastrados por diferentes eventos (Urgeles et al., 1997).

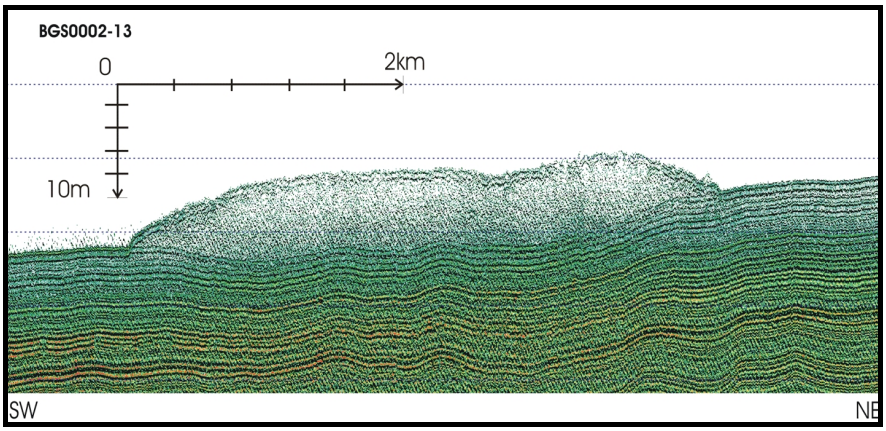

Fig. 2. Sección de un perfil sísmico de alta resolución mostrando una colada de derrubios (Wilson et al., 2003).

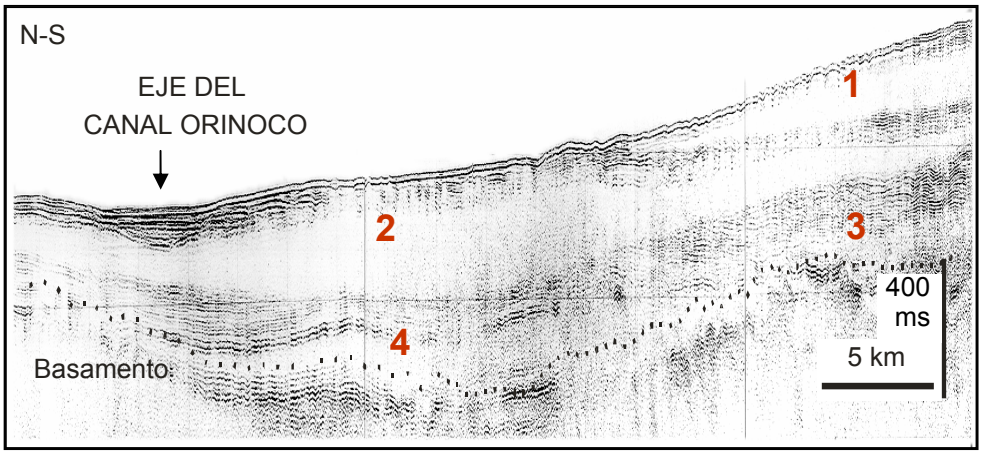

Fig. 3. Ejemplo de perfil sísmico de alta resolución mostrando diferentes depósitos de coladas de derrubios (1 a 4).

Los deslizamientos y coladas de derrubios están claramente emparentados y se diferencian principalmente por el grado de fluidez, deformación y mezcla de clastos (por ejemplo, fragmentos de niveles rotos). Un deslizamiento puede transformarse en una colada de derrubios si durante el movimiento el cuerpo original se desintegra y diluye progresivamente (Norem, 1990; Piper et al., 1999; Locat et al., 2002). Muchos de los deslizamientos descritos en la literatura aparecen como eventos complejos que involucran ambos procesos (Locat et al., 2002; Parsons et al., 2005).

Reología	**Tipo de flujo**	**Depósito**	**Mecanismo de soporte**
Fluido Newtoniano	*Corriente de turbidez* (turbulento)	Turbidita	Turbulencia
Variable (parcialmente Newtoniano y no-Newtoniano)	*Flujo denso* (parcialmente turbulento y laminar)	Densita	Presión dispersiva, turbulencia, escape fluido intersticial, esfuerzo de la matriz
Fluido dilatante no-Newtoniano (Plástico) Bingham	*Colada de derrubios* (laminar)	Debrita	Presión dispersiva Esfuerzo de la matriz
(Plástico) Bingham	*Deslizamiento-Deslizamiento rotacional*	Deslizamiento-Deslizamiento rotacional	Esfuerzo de la matriz

Tabla 3. Principales características de los diferentes tipos de flujos y los depósitos resultantes (modificado de Gani, 2004). Los flujos densos, por estar a caballo entre los flujos turbidíticos y las coladas de derrubios, a menudo han recibido diferentes nombres asociados a uno u otro tipo como son: "High-density turbidity currents" (Lowe, 1982), "Sandy debris flows" (Shanmugam, 1996), "Slurry flows" (Lowe y Guy, 2000) y "Concentrated density flows" (Mulder y Alexander, 2001).

Las *corrientes de turbidez* (Fig. 4) son flujos diluidos (< 10 g/l) y totalmente turbulentos (Re > 10^4) de sedimento pobremente seleccionado. Las corrientes turbidíticas pueden tener una capa basal, a menudo llamada capa de tracción, con alta concentración pero dominada por el flujo turbulento. Las corrientes de turbidez son movilizadas por el gradiente de presión horizontal producido por el incremento de la presión hidrostática dentro de la corriente debido a la incorporación de partículas (Pratson et al., 2000; Parsons et al., 2005). Por las complejas interacciones que se dan dentro de estas corrientes, las turbiditas resultantes pueden ser extremadamente variables en espesor, tamaño de grano y composición.

Las corrientes de turbidez pueden ser generadas directamente por la alta concentración de sedimentos en suspensión que llegan al borde de la plataforma continental gracias a agentes como corrientes de marea, ríos o tormentas (Mulder y Syvitski, 1995; Mulder et al., 1998) y otras parecen tener su origen en inestabilidades que se dan en el talud continental. En este caso, las corrientes de turbidez evolucionan desde las coladas de derrubios por un mecanismo parecido al que los deslizamientos podían evolucionar a una colada de derrubios (Hampton, 1972; Normak y Piper, 1991; Piper et

al., 1999; Floquet y Hennvy, 2003). Esta evolución requiere la dilución del flujo por incorporación de agua y una transformación del flujo de laminar a turbulento (Masson et al., 1996).

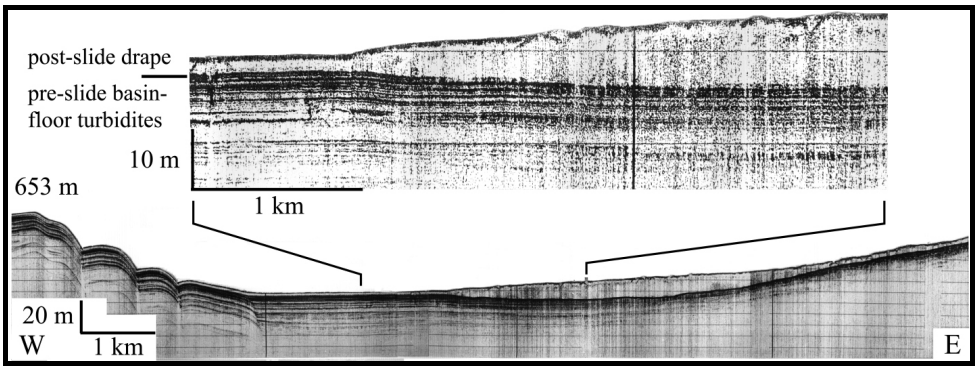

Fig. 4. Ejemplo de depósitos turbidíticos distales observados en un perfil sísmico (3,5-kHz) (Trincardi et al., 2003). Las turbiditas forman niveles de alta continuidad lateral que están limitados basalmente por superficies de alta reflectividad acústica.

Para explicar el comportamiento de los cuerpos movilizados se debe tener en cuenta la proporción relativa de las fases sólida y líquida que contienen. Según esta relación el comportamiento de la mezcla se podrá describir con los principios de mecánica (suelo-roca) o de mecánica de fluidos. Esto quiere decir, por ejemplo, que un flujo fangoso donde la velocidad del movimiento es suficientemente rápida como para evitar la disipación del exceso de la presión de poro, se debería explicar con los principios de mecánica de fluidos (Iverson, 1997). El comportamiento de los cuerpos movilizados se complica cuando hablamos de corrientes de turbidez ya que es producto de la compleja interacción entre flotabilidad, transporte o deposición de partículas y turbulencia. Uno de los conceptos básicos en la relación de estos parámetros es el de la autosuspensión o ignición, que se refiere a la capacidad de una corriente de turbidez para incrementar su carga y por tanto su densidad en el tiempo. El incremento de las fuerzas de “conducción” (por ejemplo la flotabilidad negativa) impulsa el flujo dando más capacidad de transporte y acelerándolo (Bagnold, 1962).

Para valorar la extensión potencial (Fig. 5) de un movimiento en masa se deben tener en cuenta todos los componentes involucrados, como la iniciación, la posible transformación del cuerpo deslizado durante el movimiento, la transición de un

deslizamiento a colada de derrubios (Norem et al., 1990) o la subsiguiente formación de corrientes de turbidez (Normark y Piper, 1991) y el movimiento hasta la deposición final.

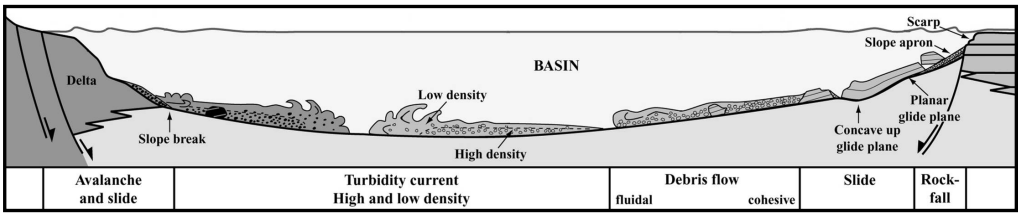

Fig. 5. Diagrama esquemático en el que se muestra la ocurrencia y extensión de los principales movimientos de masa submarinos (modificado de Floquet y Hennvy, 2003).

1.3. Caracterización de los movimientos de masa

La modelización de los movimientos de masa y sus consecuencias (entendidos como los sistemas complejos que son), es compleja ya que la base de cualquier modelo es la determinación de las relaciones existentes entre los diferentes estados de las variables que lo constituyen. Para cada modelo, estas relaciones son utilizadas para determinar los estados desconocidos de variables en base a estados conocidos de otras. El problema en los sistemas naturales es que la predicción de los estados desconocidos de las variables no tienen una solución única, y son por tanto, sistemas no deterministas donde la incertidumbre tiene un papel protagonista. Cuando se construye un modelo con un objetivo dado, se busca que este sea lo máximo de útil para ese objetivo. Esto quiere decir que el modelo ha de tener tres características fundamentales: credibilidad, complejidad e incertidumbre. Idealmente se busca un modelo con la máxima credibilidad y la mínima complejidad e incertidumbre posibles. Lamentablemente estos tres criterios entran en contradicción y la relación entre ellos aún no se conoce suficientemente bien.

A pesar de la complejidad en la modelización, se pueden hacer aproximaciones en el conocimiento de las inestabilidades submarinas y sus consecuencias utilizando un gran espectro de técnicas y métodos como son la batimetría multihaz, sonar de barrido lateral, perfiladores sísmicos, muestreo sedimentario y geotécnico y técnicas de datación. Para el muestreo geotécnico, es importante obtener muestras de sedimento de calidad por lo que es recomendable la utilización de sistemas muestreadores como los sacatestigos de gravedad o pistón de gran longitud y diámetro. Utilizando herramientas como el “Multi Sensor Core Logger” (MSCL) y diversas técnicas geotécnicas se pueden

determinar las propiedades físicas y geotécnicas de los sedimentos en zonas aparentemente estables y no alteradas (sin deslizamientos), para compararlas con zonas equivalentes con inestabilidades submarinas (Silva et al., 2004).

A partir de ensayos de consolidación, que proporcionan datos sobre la historia del estrés (balance de esfuerzos a los que ha estado sometido el sedimento) se pueden obtener evidencias de deslizamientos tanto recientes como antiguos. La datación de inestabilidades recientes podría permitir realizar aproximaciones sobre los posibles mecanismos desencadenantes de los eventos observados (por ejemplo si se pueden relacionar con seísmos datados históricamente) y podría ser una herramienta valiosa para la estimación del período de recurrencia de eventos como las corrientes turbidíticas. La disponibilidad de métodos fiables y relativamente económicos para obtener datos exactos de la extensión de las áreas inestables, muestras de sedimento no alteradas para obtener parámetros geotécnicos, o medidas “in-situ” es un factor básico para poder modelizar la estabilidad de los taludes submarinos.

1.4. Caracterización del riesgo geológico

Los movimientos de masa submarinos pueden tener consecuencias importantes, desde cambios en hábitats marinos o en la morfología y naturaleza del suelo marino hasta afectar o destruir infraestructuras humanas como cables de comunicación o plataformas petroleras (Norem et al., 1990). También pueden ser precursores de tsunamis (Tappin, 2001; Lee et al., 2003; Trifunac et al., 2003) que pueden generar consecuencias desastrosas en zonas costeras. Así pues, el análisis de las consecuencias de los deslizamientos submarinos tiene mucho que ver con el análisis de riesgos y su gestión, e involucra aspectos como el marco geológico (factores internos o inherentes al sedimento), factores externos (naturales o antrópicos), la evaluación del riesgo, los elementos que pueden verse afectados y finalmente su gestión o las medidas necesarias para mitigar los efectos sobre estos elementos (Tabla 4).

Leroueil et al. (1996) propone que para valorar el riesgo asociado a los deslizamientos submarinos se deben tener en cuenta todos los componentes del fenómeno, incluyendo la caracterización geotécnica de los movimientos de masa. Esto incluye tres elementos básicos: los materiales, el tipo de movimiento y los estadios de este movimiento.

Marco geológico →	Fuerzas ambientales →	Evaluación de riesgo →	Elementos en riesgo →	Valoración del riesgo
Sedimento: Estratigrafía, geomorfología, propiedades geotécnicas. **Fluidos**: Presión intersticial, gas libre, hidratos de gas.	Terremotos, diapirismo, tasas de erosión y sedimentación, corrientes, amplitud de marea.	**Primario:** Frecuencia Extensión **Secundario:** Tsunami Polución etc.…	Plataformas petrolíferas, líneas de comunicación, gasoductos, estructuras costeras, ecosistemas, etc.…	Gestión Mitigación

Tabla 4. Esquema para la valoración del riesgo asociado a las inestabilidades submarinas y sus consecuencias (Locat et al., 2001).

Los tipos de materiales que podemos encontrar en ambientes submarinos son esencialmente los mismos que en los terrestres, con la excepción de suelos residuales e insaturados (ver apartado 1.1). Los estadios de los movimientos son básicamente cuatro: el estadio pre-rotura (cuando el sedimento está en estado de equilibrio e intacto), el estadio de rotura, el estadio post-rotura (el comportamiento de la masa movilizada hasta que ésta se detiene) y el estadio de reactivación (relacionado con la presencia de planos de deslizamiento o cuerpos deslizados preexistentes). Es en el estadio post-rotura donde las diferencias con los movimientos en los continentes son más evidentes (Moore et al., 1989; Masson et al., 1996). La división de los movimientos en cuatro estadios diferentes refleja el aspecto dinámico de los movimientos de masa submarinos y por tanto el hecho de que las leyes y parámetros que controlan cada uno de estos estadios pueden ser diferentes. Según esto la caracterización del riesgo geológico asociado a los deslizamientos submarinos también debe abordar tres aspectos: a) leyes y parámetros de control del movimiento, b) factores de predisposición, detonantes y revelantes de las inestabilidades (Tabla 5) y c) consecuencias del movimiento. Es importante diferenciar los factores de predisposición de los detonantes. Por ejemplo, la presencia de hidratos de gas constituye un factor de predisposición pero es la disociación de los hidratos por el decrecimiento de la presión o incremento de temperatura que puede ser un factor detonante (Sultan et al., 2004). Se pueden añadir a los hidratos de gas otros elementos específicos del medio submarino como las olas de tormenta, subconsolidación, formación de diapiros o cambios del nivel del mar (Leroueil et al., 2003).

Factores de Predisposición	• Zona de actividad sísmica • Niveles “débiles” • Hidratos de gas/ gas libre • Presencia de actividad volcánica • Materia orgánica en descomposición • Erosión • Altas tasas de sedimentación • Estratigrafía desfavorable (p.e. material denso sobre material menos denso)
Factores detonantes o agravantes	• Terremotos • Actividad volcánica • Disociación de hidratos de gas • Sedimentos cargados de gas libre • Oleaje de tormenta • Sobreinclinación (función de erosión y sedimentación) • Subconsolidación: presión intersticial (función de permeabilidad y tasa de sedimentación) • Formación de diapiros • Cambios en el nivel mareal
Factores Revelantes	• Evidencia de inestabilidades previas • Evidencia de licuefacción por actividad sísmica • Presencia de reptación o grietas • “Pockmarks” • Diapirismo

Tabla 5. Principales factores que influyen o revelan inestabilidades submarinas (Leroueil et al., 2003).

2. Metodología

El análisis de las inestabilidades submarinas se puede acometer mediante metodologías diversas. La más extendidas son las técnicas acústicas, como sondas multihaz, perfiladores de sísmica y sonografías de barrido lateral, y las técnicas de muestreo (sacatestigos de sedimento y sondeos). Los primeros tienen el valor de ofrecer una visión regional, integral y de detalle, y los segundos permiten obtener una visión física del sedimento deslizado, informando sobre sus características sedimentológicas, geoquímicas y físicas. Estas técnicas se han aplicado con éxito en la caracterización de la geometría, estructura interna, tipo de sedimento, cronología, etc. de diferentes movimientos de masa submarinos.

No obstante, para la comprensión de las inestabilidades submarinas es necesaria la utilización de metodologías que comprenden desde observaciones experimentales en laboratorio (propiedades físicas y geotécnicas), mediciones de sus propiedades físicas "in situ" con sistemas como "puppi" (www.geotek.co.uk) y "penfeld" (www.ifremer.fr), y utilización de modelos (cuantitativos) físicos para describir su iniciación, comportamiento, deposición, conocer su mecánica y características (volumen, velocidad, densidad…), así como el depósito resultante. Quizás las técnicas menos frecuentes en otros trabajos de geología marina son los que proporcionan datos como las propiedades físicas y geotécnicas, incluyendo en este grupo variables como las propiedades índice (densidad de grano, porosidad, contenido en agua….), propiedades físicas (densidad total, velocidad de ondas P, susceptibilidad magnética) y características geotécnicas (estado de consolidación y resistencia a la cizalla). Todas estas variables se comentan se abordan en los capítulos siguientes, pero de entre este grupo de datos, las propiedades físicas por su relevancia, versatilidad y creciente implantación en los protocolos de los laboratorios de geología marina merecen una atención especial.

Una aproximación tridimensional a las inestabilidades submarinas es posible mediante programas informáticos de representación e interpretación geofísica (Kingdom Suite) y la creación de modelos digitales del terreno (Lee, 2000; León, 2005). Este tipo de aproximación permite profundizar en el conocimiento de la estructura interna de las masas deslizadas y del área circundante y por tanto mejorar los modelos probabilísticos de estabilidad.

2.1. Propiedades físicas

Las propiedades físicas de sedimentos se utilizan cada día con más intensidad por un gran número de científicos con objetivos diferentes ya que pueden ser indicadores de composición, formación o de las condiciones ambientales de los depósitos. Algunas propiedades físicas se pueden medir fácil y rápidamente a alta resolución ("core logging") y servir como una aproximación a la caracterización de la compleja mezcla de minerales y fluidos que forman los sedimentos. En sedimentos marinos semiconsolidados las propiedades físicas son una buena aproximación al conocimiento de su composición, controlada por el área fuente, los procesos erosivos y deposicionales, cambios climáticos y oceanográficos así como procesos postdeposicionales como consolidación y diagénesis temprana. En sedimentos consolidados y rocas ígneas, los procesos diagenéticos, incluyendo la cementación, cambios litológicos y estructuras como fallas, tienden a dominar la mayoría de propiedades físicas, por lo que son útiles, por ejemplo, para detectar una posible circulación hidrotermal. Una de las principales aplicaciones del registro a alta resolución (intervalos centimétricos) de propiedades como la susceptibilidad magnética, el color, densidad y radiación natural- Gamma es la correlación entre testigos de sedimento que es esencial para los estudios crono-estratigráficos.

2.2. Multi Sensor Core Logger (MSCL)

El MSCL es un sistema automatizado que permite registrar en continuo y a alta resolución las propiedades físicas en testigos de sedimentos marinos. El sistema puede incorporar diferentes sensores instalados secuencialmente a través de los que pasan los testigos a intervalos predeterminados (Fig. 6). Los sensores básicos que incorpora el sistema son los que permiten medir los siguientes parámetros:

- Densidad total por atenuación de rayos Gamma (Fig. 7),
- Susceptibilidad Magnética (Fig. 9) y
- Velocidad de ondas P (Fig. 10).

El MSCL se está convirtiendo en un estándar en el análisis de testigos marinos al ser un test rutinario en muchos centros de investigación así como en el protocolo de actuación del "Ocean Drilling Program".

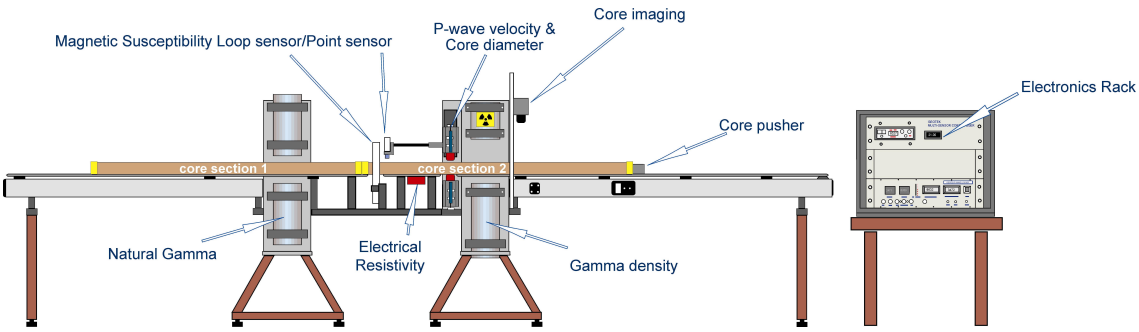

Fig. 6. “Multi sensor core logger” con todos los sensores que puede incorporar.

2.2.1. Densidad

La densidad del sedimento (densidad total) es estimada a partir de la atenuación de rayos Gamma que pasan a través del sedimento (Tittman y Wahl, 1965; Evans, 1965) (Fig. 7). El sistema se basa en los efectos producidos por la interacción de radiación electromagnética con la materia (en este caso sedimento). Para la energía utilizada (0,1-1 MeV) el efecto Compton y el fotoeléctrico son las dos interacciones dominantes y en los que se basa el cálculo de la densidad.

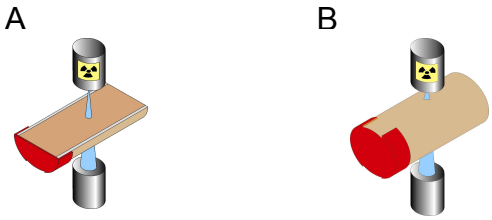

Fig. 7. Par emisor - receptor de rayos Gamma que forman el sensor de densidad, para testigos abiertos (A) y testigos enteros (B).

El efecto fotoeléctrico consiste en la absorción de un fotón por un átomo con la emisión subsiguiente de un electrón. El átomo residual queda ionizado en una capa profunda y, en consecuencia, el efecto fotoeléctrico va acompañado de una cascada de rayos X característicos del material considerado (Fig. 8). La probabilidad de que se produzca el efecto fotoeléctrico disminuye rápidamente con la energía del fotón incidente. El efecto fotoeléctrico es importante para energías bajas del fotón y absorbentes de elevado número atómico.

Los rayos X o Gamma de energías comprendidas entre unos pocos keV y unos MeV pueden sufrir una dispersión en sus colisiones con electrones atómicos de las capas externas y experimentar una desviación en su dirección de propagación, así como una disminución de su energía y por tanto una disminución de su frecuencia. El electrón atómico es expulsado del átomo que queda ionizado. Es lo que llamamos efecto Compton (Fig. 8). Habitualmente, la mayor parte de la energía se la lleva el rayo X o Gamma dispersado, que puede dar lugar a otras dispersiones Compton hasta terminar absorbido fotoeléctricamente.

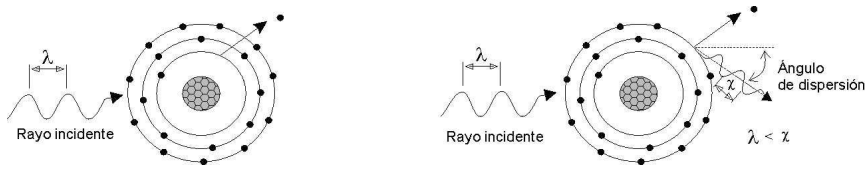

Fig. 8. Efecto fotoeléctrico (A) y efecto Compton (B).

La mayoría de los elementos que forman sedimentos y rocas tienen un coeficiente de atenuación de Compton similar y la densidad electrónica medida puede ser fácilmente relacionada con la densidad del sedimento. Normalmente se utiliza Cesio (^{137}Cs) como fuente radioactiva emisora de los rayos Gamma, con una energía de 662 keV, energía para la que en principio el efecto Compton es el dominante (Tipler, 1992), pero en el caso en que el medio tenga un número atómico alto se produce el efecto fotoeléctrico.

La transmisión de rayos Gamma (atenuación) a través del sedimento se puede relacionar con la densidad electrónica con la expresión:

$$\mathbf{I = I_0 e^{-\mu\rho d}} \quad \mathbf{(1)}$$

donde I_0 representa la intensidad de los rayos Gamma en el aire, I es la intensidad después de pasar por el sedimento de espesor d (cm), μ es el coeficiente de absorción en masa (cm^2/gr), que es una constante de cada material y ρ es la densidad electrónica de la formación. Así, de esta expresión…

$$\rho = (1/-\mu d)*\ln I/I_0 \quad (2)$$

La densidad electrónica de un material es una función lineal del logaritmo de la intensidad de los rayos Gamma detectados; en una primera aproximación la densidad electrónica es proporcional a la densidad de la formación. El número de rayos Gamma detectados es pequeño cuando la densidad es alta. La densidad total o "*bulk density*" (ρ_b) de un sedimento queda entonces relacionada con la densidad electrónica según la expresión:

$$\rho=\rho_b (Z/A)N \quad (3)$$

donde Z es el número atómico, A la masa atómica y N el número de Avogadro. Para la mayoría de los elementos constituyentes de sedimentos y rocas, esta relación es inferior a 0.5 (Tipler, 1992), excepto para el hidrógeno que es próxima a 1. Según las relaciones descritas, la densidad total también se puede expresar como:

$$\rho_b = \ln (I/I_0) / \mu d \quad (4)$$

2.2.2. Susceptibilidad magnética

La susceptibilidad magnética es el grado en el que un material puede ser magnetizado por un campo externo. Este parámetro puede ayudar a identificar minerales presentes en el sedimento, calcular su concentración o volumen total, clasificar diferentes tipos de sedimento o identificar procesos en la formación y transporte del sedimento.

Si la magnetización se expresa por unidad de volumen, la **susceptibilidad volumétrica (κ),** que representa la relación entre el campo magnético aplicado y la magnetización resultante se expresa como:

$$\kappa=M/H \quad (5)$$

donde M es la magnetización inducida sobre el material de susceptibilidad κ por un campo H. La susceptibilidad volumétrica es adimensional y la magnitud depende del sistema de medida utilizado, por ejemplo en el sistema internacional: κ (SI) = $4\pi k$ (cgs) = $4\pi G\ Oe^{-1}$, donde G y Oe son abreviaciones de Gauss y Orstedt respectivamente. La magnitud típica cuando se trabaja en el sistema internacional es de 10^{-5}, aunque las medias de κ dependen de la frecuencia con la que se mide, que puede ser 0,46 o 4,6 kHz. Esto se puede utilizar para detectar la presencia en las muestras de minerales magnéticos ultrafinos (<0,3 micras). Las muestras donde hay minerales ultrafinos darán lecturas bajas cuando se mide a alta frecuencia y las muestras sin estos minerales darán unas κ idénticas para las dos frecuencias.

Las medidas de susceptibilidad volumétrica son relativas, y las diferencias observadas pueden estar relacionadas con el contenido de agua o la densidad del sedimento, por tanto, normalmente se obtiene la **Susceptibilidad específica en masa**, resultado de dividir la susceptibilidad volumétrica por la densidad de la muestra:

$$\chi=\kappa/\rho \quad \textbf{(6)}$$

donde ρ es la densidad de la muestra con una susceptibilidad magnética volumétrica κ. La susceptibilidad específica en masa tiene como unidades $\mu m^3\ kg^{-1}$.

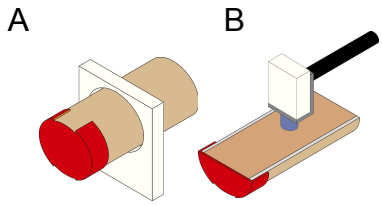

Fig. 9. Sensores para medir la susceptibilidad magnética que incorpora el MSCL. El primer esquema (A) corresponde a un sensor (tipo "loop") diseñado para trabajar con testigos enteros y el segundo (B) para trabajar con secciones de testigos abiertos.

El magnetismo es una propiedad inherente a fuerzas creadas por los electrones de los átomos de los materiales. Todo electrón gira alrededor de un eje propio y del núcleo atómico. El sentido y alineación en que se mueven los diferentes electrones determina la energía magnética total de las moléculas que forman los materiales. Hay diferentes grupos de materiales con comportamientos o propiedades magnéticas diferentes (Tabla 6). El primer grupo, el **ferromagnético**, es el de materiales altamente

magnéticos, como el hierro puro. Estas sustancias tienen una susceptibilidad magnética muy alta, pero normalmente no se encuentran en forma pura en el ambiente. El comportamiento magnético más importante que se detecta en materiales naturales es el **ferrimagnetismo**. Esta categoría incluye la magnetita y otros minerales que contienen hierro con una susceptibilidad magnética alta. Una baja susceptibilidad magnética se obtiene por minerales **antiferromagnéticos** como la hematites. Valores parecidos se dan en minerales **paramagnéticos** de los que hay muchos ejemplos y es común que contengan hierro (biotita o pirita). Finalmente, los materiales **diamagnéticos** dan valores muy bajos e incluso negativos de susceptibilidad magnética. Estos incluyen minerales que no contienen hierro como el cuarzo o el carbonato cálcico, o sustancias como el agua o la materia orgánica (Thompson y Oldfield, 1986).

Comportamiento magnético	**Susceptibilidad magnética**
Ferromagnético	Susceptibilidad magnética alta y positiva (hierro puro, níquel, cromo)
Ferrimagnético	Susceptibilidad magnética alta y positiva (óxidos de hierro y sulfidos como magnetita, maghemita, pirrotina...)
Antiferromagnético	Susceptibilidad moderada y positiva (óxido de hierro como hematites o gohetita)
Paramagnético	Susceptibilidad débil y positiva (minerales con hierro y sales, como biotita, olivina, sulfatos...)
Diamagnético	Susceptibilidad débil y negativa (agua, materia orgánica, plásticos, cuarzo, feldespato, carbonato cálcico...)

Tabla 6. Susceptibilidad magnética asociada a cada tipo de comportamiento magnético.

La susceptibilidad magnética de un medio determinado será la suma de todas las susceptibilidades (ferrimagnética, antiferrimagnética y paramagnética) menos la susceptibilidad diamagnética. Normalmente la componente diamagnética es muy baja comparada con las otras y se puede despreciar su efecto excepto en el caso que dominen el cuarzo, la materia orgánica o que la muestra esté saturada en agua. Las muestras no contaminadas por metales ferrosos no contienen normalmente materiales ferromagnéticos, y en su ausencia la susceptibilidad es controlada sobre todo por minerales ferrimagnéticos y algo menos por minerales de otras categorías. La magnetita (que contiene aproximadamente un 69% de Fe^{3+}, un 31% de Fe^{2+} y cantidades variables de óxidos de titanio, cobre y magnesio) es por ejemplo 1000 veces más magnética que el mineral antiferromagnético con una señal más fuerte.

2.2.3. Velocidad de ondas P (Pw)

Las ondas P (de compresión o longitudinales) son aquellas que producen en las partículas un movimiento en una dirección paralela a la de propagación de la onda. Su velocidad de propagación es, con diferencia, la más alta comparando con otros tipos de ondas, además de ser la única onda capaz de propagarse por medios líquidos.

La Pw mide la velocidad de las ondas compresionales ultrasónicas en el sedimento mediante pulsaciones que atraviesan diametralmente los testigos. Un par de transductores (transmisor y receptor) se colocan diametralmente en contacto con las paredes de los testigos (Fig. 10).

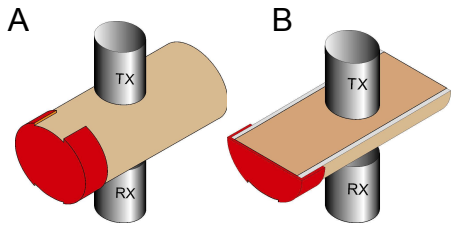

Fig. 10. Disposición del par emisor (TX)-receptor (RX) del Pw para testigos enteros (A) y abiertos (B).

La estructura mecánica del emisor y el receptor es idéntica, y constan de una carcasa de aluminio donde se monta un disco piezoeléctrico de cerámica. El contacto con el testigo se produce a través de una cubierta que maximiza la energía transmitida. El transmisor es excitado con un pulso (150 V durante 0.5 μs) y produce una onda compresional corta de 500 kHz que se propaga por el testigo y es detectada por el receptor. El funcionamiento del sistema depende en gran parte de la precisión en la medida del tiempo que tarda en cruzar el pulso por el testigo.

Las diferencias de diámetro que existen en la camisa del testigo introducen en el cálculo de la velocidad un factor de error importante, ya que varía el tiempo del recorrido del pulso por el testigo. Por eso se necesita conocer estas variaciones o cómo varía la distancia entre los dos transductores ultrasónicos. Para conseguirlo se montan y conectan en el bloque de los transductores ultrasónicos un par de transductores de desplazamiento. Estos transductores se conectan en serie y la diferencia entre sus salidas es proporcional a la distancia entre los transductores ultrasónicos. Con estos datos es fácil la corrección del tiempo de viaje del pulso emitido.

La velocidad del pulso, V, en el sedimento viene dada por V = D/T donde D es el diámetro interior del testigo y T el tiempo de recorrido en el sedimento. De manera que:

$$D = D_1 - 2d \quad (7) \qquad y \qquad T = T_f - T_e - T_p - 2t \quad (8)$$

donde D_1 es el diámetro exterior del testigo, d es el grosor de la pared de la camisa del testigo, T_f es el tiempo total registrado por Pw, T_e es el retardo, T_p es el tiempo de corrección (diferencia entre onset del pulso y el cero detectado por Pw) y t es el tiempo que tarda el pulso en atravesar la camisa.

La velocidad de las ondas P, o el tiempo que tarda el pulso emitido en atravesar el sedimento, depende de diferentes factores:

- De la litología del sedimento, su densidad y de los parámetros de elasticidad de sus componentes,
- De la naturaleza de los fluidos presentes,
- De la textura, el tamaño y forma de los granos o componentes, repartición y conexión de los poros,
- De la estructura, homogeneidad o heterogeneidad, presencia de laminaciones, fracturas, pendiente de las capas o fracturas y
- De la presión y temperatura.

2.3. Propiedades físicas y tiempo de almacenaje de los testigos de sedimento

El registro continuo y de alta resolución de las propiedades físicas de sedimentos marinos, como ya se ha citado, representa un conocimiento básico y crítico con un gran abanico de aplicaciones. En este sentido es necesario tener un control exhaustivo sobre la calidad de los datos obtenidos, ya que estos pueden variar no sólo por las condiciones de trabajo, sino también por la calidad del sedimento analizado. El control de este factor requiere estudios a largo plazo para poder caracterizar el comportamiento del sedimento con el paso del tiempo, una vez recuperado del fondo del mar. Uno de los pocos estudios existentes es el realizado por Dave Gun del British Geological Survey (comunicación personal), en el que se relaciona el tiempo transcurrido desde la obtención de los testigos de sedimento hasta el análisis de éstos con el MSCL, para así poder calibrar las desviaciones que pueden sufrir los resultados en los registros de las propiedades físicas.

El conocimiento de estos efectos es muy importante si se asume el objetivo de recopilar colecciones de referencia de testigos de sedimento en diferentes áreas y ambientes sedimentarios, y bases de datos lo suficientemente amplias y fiables de las propiedades físicas de dichos sedimentos. Las Tablas 7 y 8 muestran de manera resumida cuales son los efectos del paso del tiempo en los sedimentos almacenados (en unas condiciones determinadas) y sus repercusiones en las propiedades físicas.

	Tiempo (horas)	Amplitud Pw	Velocidad Pw	Densidad	Espesor
Tiempo abierto a 23 ºC	0	Las secciones recién abiertas presentan un perfil continuo de más de 80mV con alguna reducción de la señal por la alta atenuación natural de los tramos limosos.	El perfil de velocidad es relativamente continuo, con picos en los tramos limosos.	Cuando se registra cada 2 s en lugar de 5 s, la señal presenta más ruido. A medida que el sedimento se seca se hace menos denso pero cuando pierde agua también se pueden producir grietas que provocarán un mayor número de picos de baja densidad en el registro.	La progresiva y gradual reducción de espesor se puede observar a medida que este se seca, y puede llegar a ser de hasta el 85% del espesor original.
	24	Pocos cambios, pero los tramos limosos presentan una reducción de la señal por efecto del rápido drenaje de los sedimentos de grano grueso.	Al secarse el sedimento, hay una perdida de señal en los tramos de grano grueso. El sedimento más fino presenta cambios muy pequeños generalmente en forma de incremento gradual de la velocidad después de 24h.		
	24-48	Bajada significante de la amplitud a las 40 horas. La atenuación de la señal aumenta con el tamaño de grano en la base de las turbiditas.	Cuando aparecen las primeras grietas en el sedimento más fino hay un incremento significativo de la velocidad (20m/s) y una reducción de la amplitud de la señal.		
	40-72	La amplitud continúa decreciendo con el progresivo drenaje o desecación del sedimento.	Aparece ruido en el perfil de velocidad. Atenuación de la señal en los tramos de limo de la base de las turbiditas.		
	72-186	Amplitud 0 (<20mV) cuando el sedimento esta seco.	Señal muy débil. El sistema no puede reconstruir la forma de la onda. La velocidad registrada no es válida.		

Tabla 7. Cambios observados en el registro de las propiedades físicas según el tiempo de almacenamiento de los testigos a 23 ºC.

Tiempo de almacenaje	Cambios observados
0	Testigo nuevo, recuperado y abierto inmediatamente.
24h	Arenas y limos empiezan a drenarse. La oxidación actúa sobre sedimentos anóxicos cuando se exponen al aire observando un cambio de color hacia tonos verdosos.
0.5 años	Las arcillas pierden el brillo de la humedad en superficie. Las arenas y limos están completamente drenados. El cambio de color por oxidación ha penetrado unos 5 mm.
2 años	Arcillas se mantienen húmedas al tacto, las arenas y limos están secos. Primeros signos de crecimiento de moldes en superficie.
10 años	Primeros signos de drenaje en arcillas por la aparición de grietas transversales. Grietas son comunes.
24 años	Aparecen grietas longitudinales. Arcillas están secas al tacto. Disminución del espesor del sedimento. Arcillas endurecidas. Presencia general de grietas y cero contenido en agua.

Tabla 8. Cambios observados en el sedimento según el tiempo de almacenamiento de las secciones de testigos.

3. Cinco Marcos Geológicos

Los trabajos que forman esta Tesis Doctoral se han realizado en cinco áreas geográficas diferenciadas (Fig. 11), con cinco marcos geológicos diferentes y procesos sedimentarios específicos: el talud continental del Ebro (Mediterráneo Occidental), el talud continental del Golfo de Cádiz (Atlántico Central), la Llanura Abisal de Madeira (Atlántico Central), las montañas submarinas Anaximander (Mediterráneo Oriental) y finalmente el talud continental de la Península Antártica y zona profunda de la Cuenca de Bransfield (Estrecho de Bransfield).

Fig. 11. Localización geográfica de las áreas de estudio: 1. talud continental del Ebro, 2. talud continental del Golfo de Cádiz, 3. Llanura Abisal de Madeira, 4. Montañas submarinas Anaximander y 5. Península Antártica y Estrecho de Bransfield.

El talud continental del Ebro, en el Mediterráneo noroccidental, se caracteriza por ser un margen pasivo joven que ha progradado desde el Mioceno (Dañobeitia et al., 1990). Situado en una cuenca restringida entre dos bloques continentales (la Península Ibérica y la Plataforma Balear), es un margen con una de las áreas fuente más importante en el Mediterráneo (Río Ebro) y cuya evolución sedimentaria ha estado controlada

principalmente por los cambios de nivel del mar, favoreciendo el desarrollo de deltas en la plataforma, valles submarinos, sistemas turbidíticos e inestabilidades sedimentarias en el margen continental distal (Maldonado y Nelson, 1990).

El Golfo de Cádiz es un margen en forma de arco que se caracteriza por su compleja estructura geológica producida por la intersección de estructuras como el sistema de fallas Azores- Gibraltar, el sistema NE-SW de deformación alpina del sur de Europa y el límite occidental del arco de Gibraltar (Biju-Duval et al., 1977; Nelson et al., 1993; Maestro et al., 2003; Medialdea et al., 2004). La estructura sedimentaria reciente del talud continental resulta de una compleja interacción entre la estructura tectónica, cambios de nivel del mar, procesos oceanográficos asociados a la corriente Mediterránea profunda y múltiples áreas fuente continentales (Somoza et al., 2003; León, 2005). Todo ello ha favorecido la presencia de gas bajo diversas formas como gas libre o hidratos de gas (Fig.12) condicionando la estabilidad sedimentaria de forma variable.

Fig. 12. Hidratos de gas recuperados en el volcán de fango Ámsterdam, en la zona de Anaximander durante el mes de octubre de 2004, en el marco del proyecto europeo Anaximander (Casas et al., 2004).

La Llanura Abisal de Madeira (Atlántico norte) está limitada por altos al norte, sur y oeste y por un cambio de pendiente al este, desde un gradiente suave en el ascenso (1:300 a 1:1000 aproximadamente) a la llanura virtualmente plana (1:3000) (Searle, 1987). Esta llanura representa el área final de deposición de sedimentos que provienen del continente africano, Islas Canarias y montes submarinos que son depositados mediante corrientes de turbidez de distintas características (Weaver et al., 1992; Masson, 1994). El resultado es un registro sedimentario caracterizado por depósitos de diferente

naturaleza, génesis y áreas fuente, que configura un escenario propicio para el análisis de las propiedades físicas de sedimentos gravitativos.

Las montañas Anaximander, al SW del margen de Turquía, en el Mediterráneo oriental, configuran una área de volcanismo de fango activo y son un complejo de tres montes submarinos que se elevan más de 1000 m por encima del área que los rodean (Woodside et al., 1998; Zitter, 2004). Los volcanes de fango son resultado de la extrusión de fluidos ricos en fango (Casas et al., 2004) y han sido observados tanto en medios marinos como aéreos, y en diferentes contextos geológicos, que pueden ser tectónicamente activos o márgenes pasivos (Fig. 13). El interés científico en los volcanes de fango es cada día mayor debido a los procesos que se asocian a este fenómeno, como son la expulsión de gases invernadero a la atmósfera, la producción de energía para ecosistemas basados en la quimiosíntesis, la acumulación de hidratos de gas (Fig. 12) o la génesis de petróleo (Cita et al., 1981; Zitter, 2004; León, 2005).

El talud continental de la Península Antártica y la Cuenca de Bransfield (en el Estrecho de Bransfield) forman parte de un margen glaciomarino privilegiado para el estudio de la interacción entre procesos tectónicos, glaciales y marinos, además de ser un modelo moderno de condiciones interglaciales relativamente cálidas en la Antártida. Su evolución sedimentaria estuvo controlada inicialmente por la tectónica (Barker y Austin, 1994; Gràcia et al., 1996) y finalmente por el avance y retroceso de masas de hielo produciendo una estructura sedimentaria compleja donde interactúan los procesos glaciares, glaciomarinos y marinos (Anderson, 1999).

Fig. 13. Ejemplo de un volcán de fango submarino (A) registrado con sonar de barrido lateral en el Mar de Alborán (Comas y Ivanov, 2003). El edificio volcánico tiene unas dimensiones de 80 m alto y 300 m ancho. La morfología de los volcanes de fango submarinos es similar a los descritos en medios aéreos, como se muestra en las fotografías; (B) cráter, (C) colada de fango y (D , E) conos volcánicos.

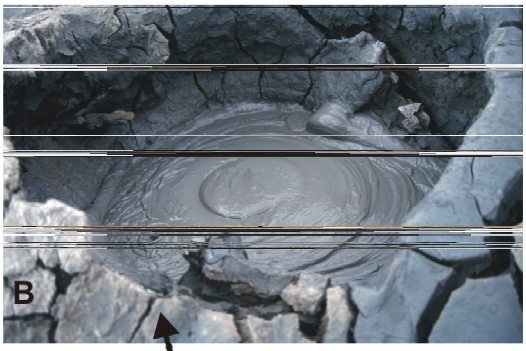

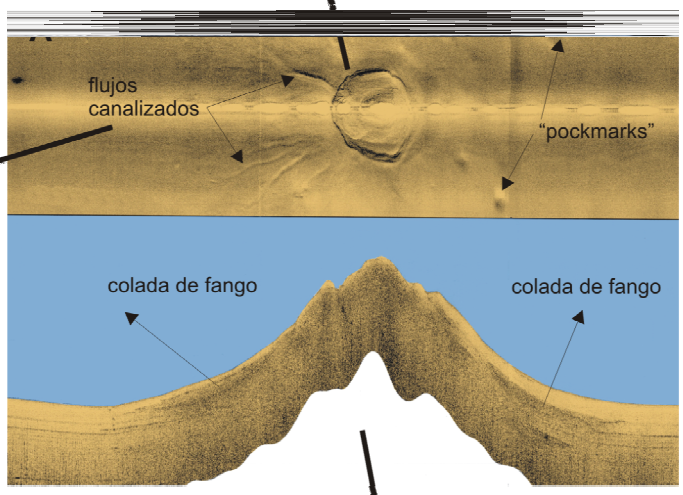

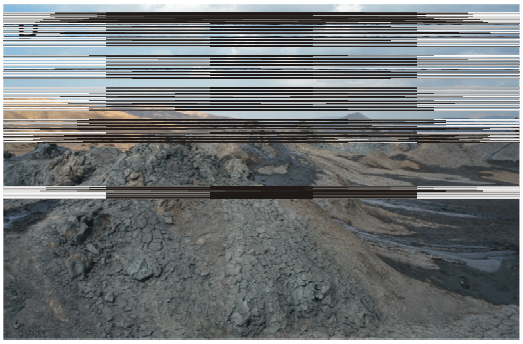

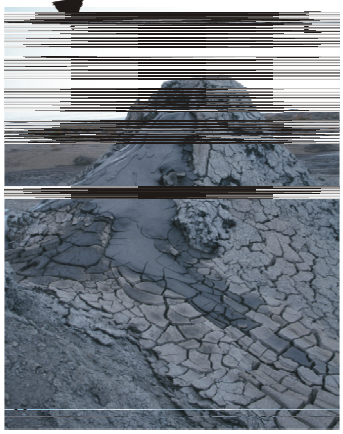

Fotografías realizadas de un campo de volcanes de fango ("Dashgil Mud Volcano") en Azerbayan.

Bibliografía

Anderson, B. J., 1999. Antarctic Marine Geology. Cambridge University Press. 287 p.

Bagnold, R. A., 1962. Auto-suspension of transported sediment; turbidity currents. Proceedings of the Royal Society of London. Series A, Mathematical and Physical Sciences, 1322: 315-319.

Barker, D.H.N., Austin, J.A., 1994. Crustal diapirism in Bransfield Strait, West Antarctica. Evidence for distributed extension in marginal basin formation. Geology, 22: 657-660.

Biju-Duval, B., Dercourt, J., Le Pichon, X., 1977. From the Tethys Ocean to Mediterranean Seas: a plate tectonic model of the evolution of the western Alpine system. International Symposium on the Structural History of the Mediterranean Basins. Technip, Paris, pp. 143-164.

Bugge, T., 1983. Submarine slides on the Norwegian continental margin, with special emphasis on the Storegga area. Publ. Continental Shelf Inst. 110:152.

Canals, M., Lastras, G., Urgeles, R., Casamor, J.L., Mienert, J., Cattaneo, A., De Batist, M., Haflidason, H., Imbo, Y., Laberg, J.S., Locat, J., Long, D., Longva, O., Masson, D.G., Sultan, N., Trincardi, F., Bryn, P., 2004. Slope failure dynamics and impacts from seafloor and shallow sub-seafloor geophysical data: case studies from the COSTA Project. Marine Geology, 213: 9- 72.

Casas, D., Ercilla, G., Baraza, J., Alonso, B., Maldonado, A., 2004. Reply to comments by Lastras et al., on “Recent mass-movement processes on the Ebro continental slope (NW Mediterranean)”. Marine and Petroleum Geology, 21: 135-139.

Casas, D., Ercilla, G., Lykousis, V., Georgiou, P., Roussakis. G., 2004. Physical properties and their relationship to texture and consolidation effects in sediments from mud volcanoes in the Anaximander Mountains (Eastern Mediterranean). CIESM 37th Congress. 7-11 June. Barcelona.

Cita, M.B., Ryan, W.B.F., Paggi, L., 1981. Prometeus mud breccia. An example of shale diapirism in the Western Mediterranean Ridge. Annales Gélogiques des Pays Hélléniques, 30: 543-569.

Comas, M. y Ivanov, M., 2003. Alboran Basin (Leg 3). Preliminary results of investigations during the TTR-12 cruise of RV Professor Logachev. June-August 2002. IOC Technical Series nº. 67: 51-71.

Dañobeitia, J.J., Alonso, B., Maldonado, A., 1990. Geological framework of the Ebro continental margin and surrounding areas. En C.H. Nelson, A. Maldonado (Eds.), The Ebro margin. Marine Geology, 95: 265-287.

Evans, 1965. GRAPE- A device for continuous determination of material density and porosity. SPWLA, 6th Ann. Symposium, 2: 25.

Evans, D., King, E.L., Kenyon, N.H., Brett, C., Wallis, D., 1996. Evidence for long-term instability in the Storegga Slide region off western Norway. Marine Geology, 130: 281-292.

Floquet, M., Hennuy, J., 2003. Evolutionary gravity flow deposits in the Middle Turonian - Early Coniacian southern Provence Basin (Se France): origins and depositional processes. En J. Locat, J. Mienert (Eds.), Submarine Mass Movements and Their Consequences. Advances in Natural and Technological Hazards Research, 19: 417-424. Netherlands, Kluwer Academic Publishers.

Gani, R. M., 2004. From Turbid to Lucid: A straightforward approach to sediment gravity flows and their deposits. The Sedimentary Record. SEPM. 2(3) September.

Gràcia, E., Canals, M., Farran, M., Prieto, M.J., Sorribas, J., Gebra team. 1996. Morphostructure and evolution of the Central and Eastern Bransfield Basin (NW Antarctic Peninsula). Marine Geophysics Research, 18: 429-448.

Hampton, A. M., 1972. The role of subaqueous debris flow in generating turbidity currents. Journal of Sedimentary Petrology, 42: 775-793.

Hampton, A. M., Lee, H., Locat, J., 1996. Submarine landslides. Reviews of Geophysics, 34(1): 33-59.

Heezen, B. C., Ewing, W. M., 1952. Turbidity currents and submarine slumps, and the 1929 Grand Banks earthquake. American Journal of Science, 250: 849-873.

Iverson, R.M., 1997. The physics of debris flows. Reviews of Geophysics, 35: 245-296.

Lee, H., 2000. A GIS-based regional analysis of the potential for shallow-seated submarine slope failure. Proc. 8 International Symposium on Landslides. June. Cardiff, Wales.

Lee. H.J., Kayen, R.E., Gardner, J.V., Locat, J., 2003. Characteristics of several tsunamigenic submarine landslides. En J. Locat, J. Mienert (Eds.), Submarine Mass Movements and Their Consequences. Advances in Natural and Technological Hazards Research, 19: 357-366. Netherlands, Kluwer Academic Publishers.

León, R., 2005. Modelo S.I.G. del campo de estabilidad de los hidratos de gas: aplicación a las estructuras geológicas ligadas a las emisiones submarinas de fluidos hidrocarburos en el Golfo de Cádiz. Tesis Doctoral. Universidad Complutense de Madrid. pp. 463.

Leroueil, S., Vaunat, J., Picarelli, L., Locat, J., Lee, H., Faure, R., 1996. Geotechnical characterization of slope movements. En Proceedings of the 7th International Symposium on Landslides, Trondheim. 1: 53-74.

Leroueil, S., Locat, J., Levesque, C., Lee, H.J., 2003. Towards an approach for the assessment of risk associated with submarine mass movements. En J. Locat, J. Mienert (Eds.), Submarine Mass Movements and Their Consequences. Advances in

Natural and Technological Hazards Research, 19: 59-68. Netherlands, Kluwer Academic Publishers.

Locat, J., Lee, H., 2000. Submarine landslides: Advances and challenges. Proceedings of the 8th International Symposium on Landslides, Cardiff.

Locat, J., 2001. Instabilities along ocean margins: a geomorphological and geotechnical perspective. Marine and Petroleum Geology, 18: 503-518.

Locat, J., Lee, H., 2002. Submarine landslides: advances and challenges. Canadian Geotechnical Journal, 39: 193-212.

Lowe, D.R., 1982. Sediment gravity flows, II. Depositional models with special reference to the deposits of high-density turbidity currents. Journal of Sedimentary Petrology, 52: 279-297.

Lowe, D.R., Guy, M., 2000. Slurry-flows deposits in the Britannia Formation (Lower Cretaceous), North Sea: a new perspective on the turbidity current and debris flow problem. Sedimentology, 47: 31-70.

Maestro, A., Somoza, L., Medialdea, T., Christopher J. T., Lowrie, A., Vazquez, J. T., Diaz-del-Rio, V., 2003. Large-scale slope failure involving Triassic and Middle Miocene salt and shale in the Gulf of Cadiz (Atlantic Iberian Margin). Terra Nova, 15(6): 380-391.

Maldonado, A., Nelson, H., 1990. The Ebro margin study, northwestern Mediterranean Sea - an introduction. Marine Geology, 95(3-4):157-163.

Masson, D.G., 1994. Late Quaternary turbidity current pathways to the Madeira Abyssal Plain and some constraints on turbidity current mechanisms. Basin Research, 6: 17-33.

Masson, D. G., Kenyon, N. H., Weaver, P.P.E., 1996. Slides, debris flows and turbidity currents. En C.P. Summerhayes, S.A. Thorpe (Eds.), Oceanography. An Illustrated Guide. pp. 136-151. Paris, Manson.

Masson, D.G., van Niel, B., Weaver, P.P.E., 1997. Flow processes and sediment deformation in the Canary Debris Flow on the NW African Continental Rise. Sedimentary Geology, 110: 163-179.

Medialdea, T., Vegas, R., Somoza, L., Vázquez, J. T., Maldonado, A., Díaz-del-Río, V., Maestro, A., Córdoba D., Fernández-Puga M. C., 2004. Structure and evolution of the "Olistostrome" complex of the Gibraltar Arc in the Gulf of Cádiz (eastern Central Atlantic): evidence from two long seismic cross-sections. Marine Geology, 209(1-4): 173-198.

Moore, J.G., Clague, D.A., Holcomb, R.T., Lipman, P.W., Normark, W.R. Torresan, M.T., 1989. Prodigious submarine landslides on the Hawaiian Ridge. Journal of Geophysical Research, 94: 17465-17484

Mulder, T., Syvitski, J. P. M., 1995. Turbidity currents generated at river mouths during exceptional discharges to the world oceans. Journal of Geology, 103: 285-299.

Mulder, T., Cochonat, P., 1996. Classification of offshore mass movements. Journal of Sedimentary Research, 66: 43-47.

Mulder, T., Syvitski, J. P. M., Skene, K., 1998. Modelling of erosion and deposition by sediment gravity flows generated at river mouths. Journal of Sedimentary Research, 67: 124-137.

Mulder, T., Alexander, J., 2001. The physical character of subaqueous sedimentary density flows and their deposits. Sedimentology, 48: 269-299.

Nardin, T.R., Hein, F.J., Gorsline, D.S. Edwards, B.D., 1979. A review of mass movement processes, sediment and acoustic characteristics, and contrasts in slope and base-of slope systems versus canyons-fan-basin floor systems. En L.J. Doyle, O.H. Pilkey (Eds.), Geology of Continental Slopes. Special Publication, 27: 61-73. Texas, Society of Economic Paleontologists and Mineralogists.

Nelson, CH., Baraza, J., Maldonado, A., 1993. Mediterranean undercurrent sandy contourites, Gulf of Cadiz, Spain. Sedimentary Geology, 82: 103-131.

Norem, H., Locat, J., Schieldrop, B., 1990. An approach to the physics and the modelling of submarine landslides. Marine Geotechnology, 9: 93-111.

Normark, W.R., Piper, D.J.W., 1991. Initiation processes and flow evolution of turbidity currents: implications for the depositional record. En Form Shoreline to Abyssal. Society of Economic Palaeontologists and Mineralogists, Special Publication 46: 20-230. R.H. Osborne.

Parsons, J. D., Friedrichs, C. T., Traykovski, P., Mohrig, D., Imran, J., Syvitski, J. P. M.G., Parker, Puig, P., García, M. H., 2005. En revisión. Capítulo 7: The Mechanics of Marine Sediment Gravity Flows In review. En Nittrouer et. al. (Eds.), STRATAFORM Master Volume Textbook, Continental-Margin Sedimentation: Transport to Sequence.

Piper, D.J., Cochonat, P., Morrison, M.L., 1999. The sequence of events around the epicentre of the 1929 Grand Banks earthquake: initiation of debris flow and turbidity currents inferred from sidescan sonar. Sedimentology, 46: 79-97.

Pratson, L.F., 2001. A perspective on what is known and not known about seafloor instability in the context of continental margin evolution. Marine and Petroleum Geology, 18: 499-501.

Pratson, L., Imran, J., Parker, G., Syvitski, J. P., Hutton, E., 2000. Debris flow versus turbidity currents: a modelling comparison of their dynamics and deposits. A. Bouma (Ed.), SEPM Special Publication, 68: 57-71.

Prior, D.B., 1984. Submarine landslides. En Proceedings of the 4th International Symposium on Landslides, Toronto, 2: 179-196.

Searle, R.C., 1987. Regional setting and geophysical characterization of the Geat Meteor East area in the Madeira Abyssal Plain. En P.P.E. Weaver, J. Thomson (Eds.), Geology and Geochemistry of Abyssal Plains, Special Publications, 31: 49-70. London, Geological Society.

Shanmugam, G., 1996. High-density turbidity currents: are they sandy debris flows? Journal of Sedimentary Research, 66: 2-10.

Silva, A.J., Baxter, C.D.P., LaRosa, P.T., Bryan, W.R., 2004. Investigation of mass wasting on the continental slope and rise. Marine Geology, 203: 355-366.

Somoza, L., Díaz-del-Río, V., León, R., Ivanov, M., Fernández-Puga, M.C., Gardner, J.M., Hernández-Molina, F. J., Pinheiro, L.M., Rodero, J., Lobato, A., Maestro, A., Vázquez , J.T., Medialdea, T., Fernández-Salas, L.M., 2003. Seabed morphology and hydrocarbon seepage in the Gulf of Cádiz mud volcano area: acoustic imagery, multibeam and ultra-high resolution seismic data. Sedimentary Processes and Seafloor Hydrocarbon Emission on Deep European Continental Margins. Marine Geology, 195(1-4): 153-176.

Sultan, N., Foucher, J.P., Cochonat, P., Tonnerre, T., Bourillet, J.F., Ondreas, H., Cauquil, E., Grauls, D., 2004. Dynamics of gas hydrate: case of the Congo continental slope. Marine Geology, 206: 1-18.

Tappin, D.R., Watts, P., Mcmurtry, G.M., Lafoy, Y., Matsumoto, T., 2001. The Sissano, Papua New Guinea tsunami of july 1998- offshore evidence on the source mechanism. Marine Geology, 175: 1-23.

Tipler, P. A., 1992. Física, 2: 597-1171. Barcelona, Reverté. ISBN 8429143661.

Tittman, J., Wahl, J.S., 1965. The physical foundations of formation density logging (Gamma-Gamma). Geophysics, 30: 284–294.

Thompson, R., Oldfield, F., 1986. Environmental Magnetism. London, Allen and Unwin.

Trifunac, M.D., Todorovska, M.I., 2003. Tsunami source parameters of submarine earthquakes and slides. En J. Locat, J. Mienert (Eds.), Submarine Mass Movements and Their Consequences. Advances in Natural and Technological Hazards Research, 19: 121-128. Netherlands, Kluwer Academic Publishers.

Trincardi, F., Cattaneo, A., Correggiari, A., Mongardi, S., Breda, A., Asioli, A., 2003. Submarine slides during relative sea level rise: two examples from the eastern Tyrrhenian margin. En J. Locat, J. Mienert (Eds.), Submarine Mass Movements and Their Consequences. Advances in Natural and Technological Hazards Research, 19: 469-478. Netherlands, Kluwer Academic Publishers.

Urgeles, R., Canals, M., Baraza, J., Alonso, B., Masson, D.G., 1997. The most recent megalandslides of the Canary Islands: the El Golfo debris avalanche and the Canary debris flow, west El Hierro Island. Journal of Geophysics Research, 102: 20305-20323.

Weaver, P.P.E., Rothwell, R.G., Ebbing, J., Gunn, D.E., Hunter, P.M., 1992. Correlation, frequency of emplacement and source directions of megaturbidites on the Madeira Abyssal Plain. Marine Geology, 109: 1-20.

Wilson, C.K., Long, D., Bulat. J., 2003. The Afen slide – a multistaged slope failure in the Faroe-Shetland channel. En J. Locat, J. Mienert (Eds.), Submarine Mass Movements and Their Consequences. Advances in Natural and Technological Hazards Research, 19: 317-324. Netherlands, Kluwer Academic Publishers.

Woodside, J.M., Ivanov, M.K., Limonov, A.F., 1998. Shallow gas and gas hydrates in the Anaximander Mountains region, eastern Mediterranean Sea. En JP. Henriet, J. Mienert (Eds.), Gas hydrates: relevance to world margin stability and climate change, Geological Society, 137: 177-193. London, Special Publications.

Zitter, T.A.C., 2004. Mud volcanism and fluid emissions in Eastern Mediterranean neotectonic zones. PhD thesis. 140 p. Amsterdam.

CAPÍTULO 2

Recent mass-movement processes on the Ebro continental slope (NW Mediterranean). D. Casas, G. Ercilla, J. Baraza, B. Alonso, A. Maldonado. *Marine and Petroleum Geology*, 20: 445-457. 2003.

ELSEVIER

Marine and Petroleum Geology 20 (2003) 445–457

Marine and Petroleum Geology

www.elsevier.com/locate/marpetgeo

Recent mass-movement processes on the Ebro continental slope (NW Mediterranean)

David Casas[a,*], Gemma Ercilla[a], Jesús Baraza[a,@], Belén Alonso[a], Andrés Maldonado[b]

[a]*Institut de Ciències del Mar—CMIMA (CSIC), Passeig Marítim de la Barceloneta 37-49, Barcelona 08003, Spain*
[b]*Instituto Andaluz de Ciencias de la Tierra (CSIC), Facultad de Ciencias, Granada 18002, Spain*

Received 26 September 2002; received in revised form 5 April 2003; accepted 17 May 2003

Abstract

Mass-movement is an important process controlling the sedimentary structure and growth patterns of the Ebro continental slope during recent time (at least Quaternary). About 37% of the slope surface is affected by mass-movement features, which are variable in distribution, size and morphology. The northern and central sectors are mainly affected by erosive canyons with gullies on their upper courses and massive and chaotic slump bodies on the middle and lower courses; the southern sector is mainly affected by large-scale slides (>10 km), and debris-flow deposits. In the three sectors, the slope is also locally affected by small-scale slides (<4 km long). The overall development of mass-movement features on the Ebro continental slope has been favoured by the local tectonism and the high sedimentation rates on the upper slope sediments, which correspond to regressive deltaic deposits. Under these conditions, the possible triggering mechanisms of the mass-movement features are the gravity loading, earthquakes, and the impinging of storm and internal waves onto the seafloor during the lowstand stages. The spatial distribution, the variability in the types of mass-movement and the post-failure evolution are influenced by several independent factors. These factors include the uneven volume of sediment supply, the frequency of failures, the sediment thickness involved in the failures, the slope gradients and the proximity to earthquake epicenters.

Keywords: Ebro; Continental slope; Submarine mass-movements

1. Introduction

Mass-movements play an important role in molding continental margins. During recent years there has been an important growth in the level of study of these features due to the increasing development of deep-water exploration activity. An understanding of the types, mechanisms and controlling factors of slope instability processes are relevant to assessment of this hazard.

The Ebro continental slope, in the Spanish NW Mediterranean Sea, is an area of significant sedimentological interest (Nelson & Maldonado, 1990). The slope is adjacent to the Ebro continental shelf (70 km wide, Díaz, Nelson, Barber, & Gràcia, 1990) the Ebro Turbidite System and the Valencia Trough, which were developed as result of the large sediment supply from numerous point sources influenced by sea-level changes and tectonic controls (Fig. 1). Previous studies of this region have largely concentrated on the stratigraphy, sedimentology, and geologic history of the Ebro continental margin (Nelson & Maldonado, 1990). In contrast, the study of mass-movement features on the continental slope has received comparatively less attention (Baraza, Lee, Kayen, & Hampton, 1990; Lastras et al., 2002; Willmott, Canals, Lastras, & Casas, 2001). In this paper, we present a detailed description of seismic characteristics of recent mass-movement features in order to discuss their geological significance and possible controlling factors. Based on indirect observations this work shows where mass-movements occur and how we see them in terms of slide plane, scale of failure, slide geometry, internal structure, run-out distances, and variability of failures. This work also assesses some questions related to the variability in the distribution, types and scales of mass-movement features.

* Corresponding author. Tel.: +34-932309500; fax: +34-932309555.
E-mail address: davidc@icm.csic.es (D. Casas).
@ Deceased.

0264-8172/03/$ - see front matter © 2003 Elsevier Ltd. All rights reserved.
doi:10.1016/S0264-8172(03)00078-3

CAPÍTULO 2: RECENT MASS-MOVEMENT PROCESSES ON THE EBRO CONTINENTAL SLOPE (NW MEDITERRANEAN)

RECENT MASS-MOVEMENT PROCESSES ON THE EBRO CONTINENTAL SLOPE (NW MEDITERRANEAN)

David Casas[a *], Gemma Ercilla[a], Jesús Baraza[a†], Belén Alonso[a], Andrés Maldonado[b].

[a] *Institut de Ciències del Mar - CMIMA (CSIC). Passeig Marítim de la Barceloneta, 37-49. 08003 Barcelona. Spain.*

[b] *Instituto Andaluz de Ciencias de la Tierra (CSIC). Facultad de Ciencias.18002 Granada. Spain.*

Abstract

Mass movement is an important process controlling the sedimentary structure and growth patterns of the Ebro continental slope during recent time (at least Quaternary). About 37% of the slope surface is affected by mass-movement features, which are variable in distribution, size and morphology. The northern and central sectors are mainly affected by erosive canyons with gullies on their upper courses and massive and chaotic slump bodies on the middle and lower courses; the southern sector is mainly affected by large-scale slides (> 10 km), and debris-flow deposits. In the three sectors, the slope is also locally affected by small-scale slides (< 4 km long). The overall development of mass-movement features on the Ebro continental slope has been favoured by the local tectonism and the high sedimentation rates on the upper slope sediments, which correspond to regressive deltaic deposits. Under these conditions, the possible triggering mechanisms of the mass-movement features are the gravity loading, earthquakes, and the impinging of storm and internal waves onto the seafloor during the lowstand stages. The spatial distribution, the variability in the types of mass-movement and the post-failure evolution are influenced by several independent factors. These factors include the uneven volume of sediment supply, the frequency of failures, the sediment thickness involved in the failures, the slope gradients and the proximity to earthquake epicenters.

Keywords: Ebro, Continental slope, Submarine mass-movements.

1. Introduction

Mass-movements play an important role in molding continental margins. During recent years there has been an important growth in the level of study of these features due to the increasing development of deep water exploration activity. An understanding of the types, mechanisms and controlling factors of slope instability processes are relevant to assessment of this hazard.

The Ebro continental slope, in the Spanish NW Mediterranean Sea, is an area of significant sedimentological interest (Nelson & Maldonado, 1990). The slope is adjacent to the Ebro continental shelf (70 km wide, Díaz, Nelson, Barber, & Giró, 1990) the Ebro Turbidite System and the Valencia Trough, which were developed as result of the large sediment supply from numerous point sources influenced by sea-level changes and tectonic controls (Fig.1). Previous studies of this region have largely concentrated on the stratigraphy, sedimentology, and geologic history of the Ebro continental margin (Nelson & Maldonado, 1990). In contrast, the study of mass-movement features on the continental slope has received comparatively less attention (Baraza, Lee, Kayen & Hampton, 1990; Willmott, Canals, Lastras & Casas, 2001; Lastras, Canals, Hughes-Clarke, Moreno, DeBatist, Masson & Cochonat, 2002). In this paper, we present a detailed description of seismic characteristics of recent mass-movement features in order to discuss their geological significance and possible controlling factors. Based on indirect observations this work shows where mass-movements occur and how we see them in terms of slide plane, scale of failure, slide geometry, internal structure, run-out distances, and variability of failures. This work also assesses some questions related to the variability in the distribution, types and scales of mass-movement features.

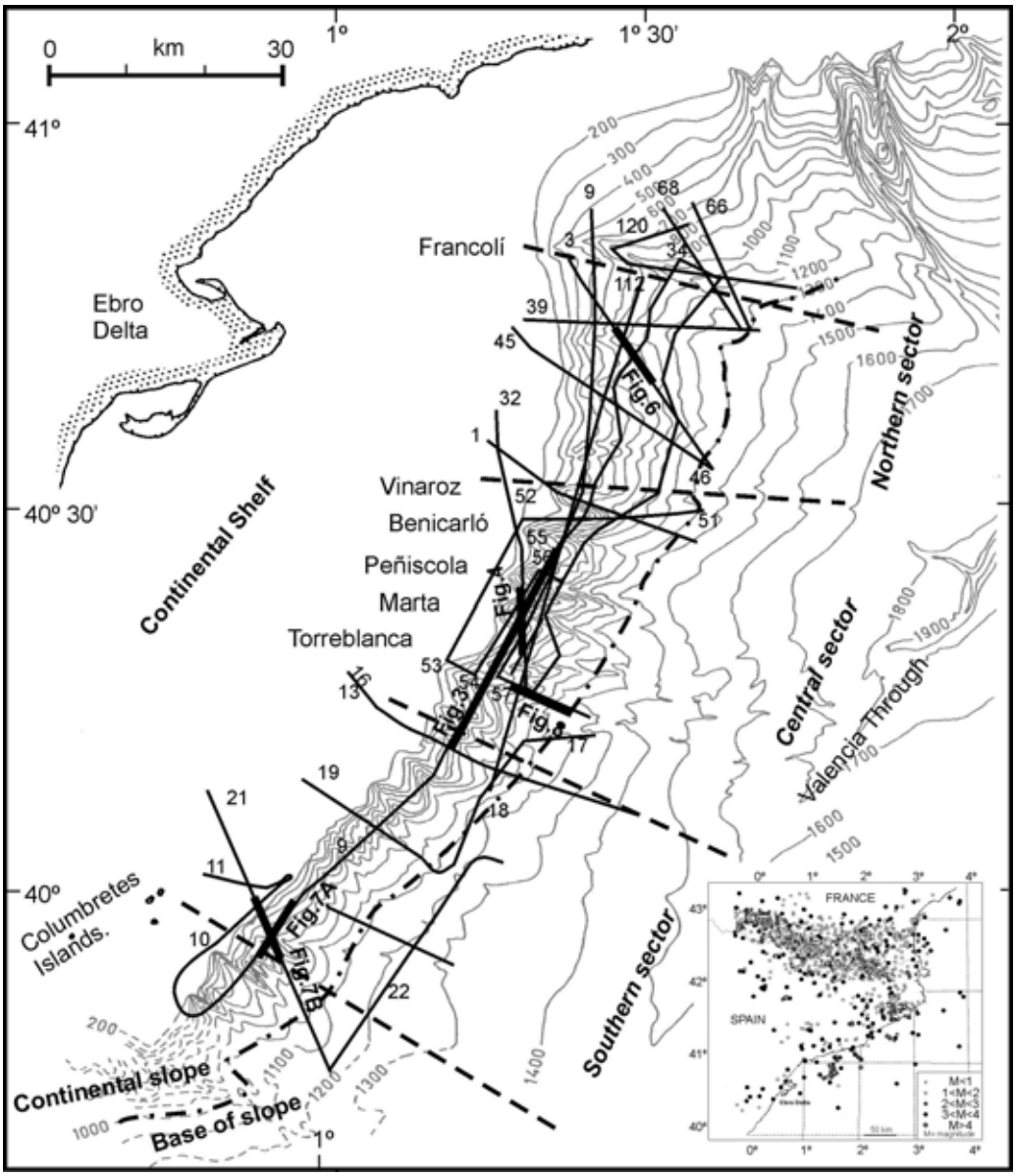

Fig. 1. - Maps of location of the study area and bathymetry of Ebro margin (grey lines) showing the three geographic sectors (northern, central and southern) defined on the slope. The seismic profiles (black continuous lines) used for this study are displayed. Numbers (3 to 8) show the locations of the profiles illustrated in figures. The map on lower right corner shows the location and magnitude of seismic epicentres on the area, recorded between 1986-2001 (after Institut Cartogràfic de Catalunya).

2. Setting

2.1. Structural features and sedimentary structure

The Ebro continental margin is a NE-SW trending passive, prograding margin initiated during the late Oligocene (Dañobeitia, Alonso, & Maldonado, 1990). The present structure results from several successive extensional episodes during the Oligocene-Miocene followed by continuous subsidence through the Late Pliocene and Quaternary. The tectonic adjustments along faults that bound the Tertiary grabens may have been active as late as to the Upper Pliocene and the Quaternary. Volcanic activity occurred during the Neogene and Quaternary and formed the Columbretes Islands. The depositional sequences above the Mesozoic basement may reach up to 4 km in thickness and infill the grabens bounded by faults striking parallel to the coast. The uppermost Pliocene to Quaternary deposits form progradational sequences up to 2 km thick near the shelf edge (Dañobeitia et al., 1990).

The Pliocene-Quaternary sedimentary structure of the Ebro continental margin is characterised by vertically stacked shelf-margin deltas on the outer continental shelf and upper slope, which are defined by prograding sedimentary wedges, thickest at the shelf break (Farran & Maldonado, 1990; Chiocci, Ercilla, & Torres, 1997). The continental slope is also characterised by the formation of submarine canyons due to mass-movement processes (Farran & Maldonado, 1990; Alonso, Díaz, Farran, Giró, Maldonado & Vázquez, 1984). The base-of-slope is characterised by turbidite channel-levee complexes (Alonso & Maldonado, 1990). The three sedimentary systems, shelf-margin deltas, submarine canyons and turbidite complexes, mainly developed during sea-level falls and lowstand stages (Alonso & Maldonado, 1990). Low energy, hemipelagic sedimentation prevailed over the entire margin during the high sea-level periods such as the present (Alonso & Maldonado, 1990; Baraza et al., 1990; Nelson & Maldonado, 1990). Today, the Ebro continental slope is inactive as a depositional system because most of the sediment supplied by the Ebro River is trapped by the dams upstream and in the delta (Palanques, Plana & Maldonado 1989). Only the finer sediment supply bypasses the delta front and results in a mud blanket that extends southward over the inner and middle continental shelf (Díaz et al., 1990).

Sedimentological and geotechnical analysis indicate that the most recent sediments of the Ebro continental slope can be grouped into two main types (Baraza et al., 1990): silty clays with low water content (34% dry weight), low plasticity, and high overconsolidation near the seafloor on the upper continental slope, and silts and clays with a high water content (90 %), high plasticity, and low to moderate degree of overconsolidation near the sediment surface, on the lower continental slope.

2.2. Oceanography

The dominant winds in the area are from northwest and northeast, and have speeds between 20 and 50 km/h. Wind speeds greater that 50 km/h occur for approximately 14 % of the year and can produce waves up to 4 m high. Wind-driven surface currents from the northwest extending to water depths of 150-200 m constitute permanent flows along the shelf and upper continental slope, modified by the interactions with the slope topography. Evaporation exceeds precipitation during each month of the year because of high insolation and the few storms, so that the sea is highly saline. During the summer a well-defined thermocline with temperature gradient of 0.17ºC/m develops by the end of July. During periods of water-mass stratification, internal waves may form on the interface between water masses of different density (Font, Salat & Julià 1990).

2.3. Seismicity

The seismicity of the Ebro continental margin has been studied from both historic (Glabis, 1940; Fontsere & Iglesias, 1971; Surinach & Roca, 1982) and instrumental data (Roca, 1975; Gaibar-Puertas, 1979; Mezcua & Martinez Solares, 1983). Epicenters on the northwestern Mediterranean margin (Fig.1), are associated with the main tectonic units, for example part of the Ebro continental margin is included within the southern boundary of the Catalan seismogenic coastal zone (Surinach & Roca, 1982). In fact, 7 epicenters among the 11 earthquakes with a magnitude over 4 registered between 1986 and 1996, are located offshore.

Three earthquakes were recorded during the last century (1907-1979) on the Ebro continental margin with peak intensities between 4 and 6 (MSK scale), and form a belt of epicenters roughly parallel to the coastline and 60 km offshore. On the coastal zone and offshore areas shallow earthquakes are predominant, showing foci shallower

than 10 km (Surinach & Roca, 1982). The relative scarcity of known offshore earthquakes may correspond to the instrumental difficulty of recording earthquakes of low intensity from onshore stations situated at long distances.

Seismicity in the Valencia Trough is fairly moderate, with two main earthquakes of magnitudes between 4 and 5 (Gallart, Guimera, & Olivera, 1989). Surinach & Roca (1982), from statistical parameters of the peak intensities distribution, calculated the return period of earthquakes in the studied region and surroundings. The return period on the Ebro margin for an intensity 4 earthquake is 7±1 years; for an intensity 5 of 13 ± 3 yrs; and for a 6 earthquake of 40 ± 20 yrs.

3. Methods

A total of 825 km of single-channel, high-resolution seismic-reflection profiles were collected between 1979 and 1986 using Sparker (1000J) and airgun (40 and 20 in^3) seismic sources (Fig.1). Navigation was by Loran C, Syledis and Decca. The configuration of discontinuities, the nature of bounding reflectors, the acoustic facies and their configuration have been used to define and interpret the types of mass-movements. The definition of the term “mass-movement” proposed by the Committee on landslides of the I.S.S.M.G.E (Locat & Lee, 2000) is applied in this study. This general term involves different types of instabilities, from slides to turbidity currents (Locat & Lee, 2000) and is defined as the movement of sediment driven by gravity rather than by interstitial fluid motion (Hampton, Lee, & Locat, 1986).

4. Morphology

The Ebro continental slope is less than 25 km wide with an average gradient of 4.5º and extends from the shelf break at 160±20 m down to 1100 ± 200 m water depth (Fig.1). It is characterised by the presence of numerous morphological irregularities mostly in the form of gullies, short and straight submarine canyons and banks (Field & Gardner, 1990). The Ebro continental slope has been divided into northern, central and southern sectors. These are characterised by a relative decrease in width and increasing slope gradient from north to south, and by a more important development of submarine canyons in the central sector (Fig.1). Table 1 shows the geometric parameters of the submarine canyons and gullies that characterise the sectors. The

canyons that reach the base-of-slope evolve into channel-levee complexes forming the Ebro Turbidite System (Alonso et al., 1984; Alonso, 1986; Alonso & Maldonado, 1990).

Sectors	Gradients	Width (km)	Maximum Depth (m)	Canyons
North	2.5º to 3º	20	1300	2
Central	2.5º to 4º	25	1200 to 1300	6
South	3.8º to 5.8º	10 to 15	1000 to 1200	2

Table 1. Comparative table showing the three geographic sectors (northern, central and southern) defined on the slope of the Ebro margin.

5. Seismic Evidences of Mass-Movement Features on the Ebro Continental Slope

Recent mass-movement features on the Ebro continental slope are recognised by the disappearance of sediment packages and by deformational structures. The removal of sediment packages results in: (1) erosional surfaces associated with submarine canyons, and (2) slide scars. Deformational structures have two different styles based on their location: (3) slides associated with submarine canyons and (4) slides and mass-flow deposits located on the open continental slope. Herein, the open continental slope is considered to be that segment of the continental slope where submarine canyons and gullies are absent.

5.1. Erosive surfaces associated to submarine canyons

Submarine canyons are the main morphologic features shaping the Ebro continental slope whose erosional origin is shown by the disappearance of sediment packages (Figs. 2, 3) as demonstrated by the following seismic and topographic characteristics:

a) Truncation of reflectors against canyon walls (Fig.3).
b) Several phases of scour and fill features on the canyon floor (Fig.3). The surface of some Ebro canyon floors is characterised by erosive surfaces that resemble paleovalleys and are infilled by onlapping stratified and chaotic facies, and locally appear to be vertically stacked.
c) Presence of gullies on the canyon heads and walls (Fig.4). The gullies appear as narrow valleys separated by sharp-edge interfluves, having average widths

between 160 and 400 m, and heights between 25 and 75 m. An erosional origin is suggested by the truncation of reflectors against the walls. The upper parts of the canyons, between 225 and 440 m water depth, show extensive side-wall gullying, whereas in the lower parts, gullies seems to be relatively less important (Alonso et al., 1984). The gullies form a herringbone pattern in relation to the canyon axes.

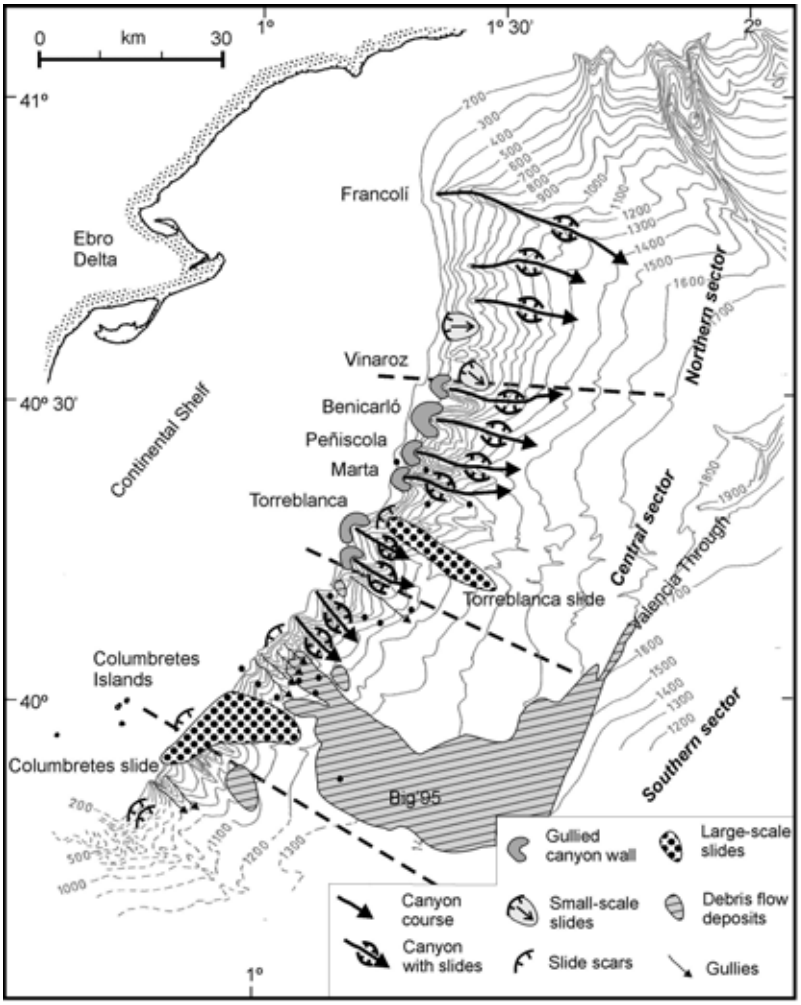

Fig. 2. - Map of location of the different mass-movement features identified on the Ebro slope. Black plots represent the position of sediment cores used for the geotechnical study. Discussion in the text.

5.2. Slides on submarine canyons

Slides on the Ebro continental slope are preferentially found along the courses of the canyons, on their walls and axes (Fig.3). The slides have dimensions varying between 20 and 80 ms (twt) in thickness, and from hundreds of meters to a few kilometres in length. They are mainly characterised by subbottom chaotic and transparent facies bounded by high amplitude surfaces that form bodies with local seafloor relief. Likewise, they are dominated by large, irregular overlapping hyperbolas with vortex elevations above the widely variable seafloor. Most of the slumped sediments lie adjacent to their respective scars, which are recognised by the abrupt relief displayed by the walls and the truncation of internal reflections. The presence of the slides originates an asymmetric image of the canyons in cross sections (Fig.3).

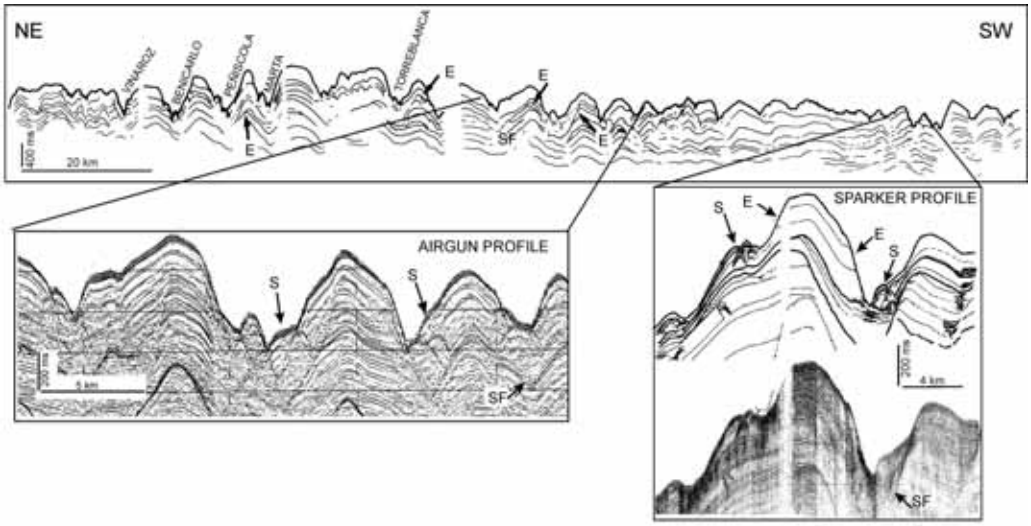

Fig. 3. - Representative seismic profile parallel to the slope and line drawing interpretation. Two selected segments of the profile are enlarged for details of the cross-sections of submarine canyons on the northern and central sectors. Legend: E, erosive surfaces suggested by the truncation of reflectors; S, slump deposits on the canyon walls and floor; SF, scour and fill features. Discussion in the text.

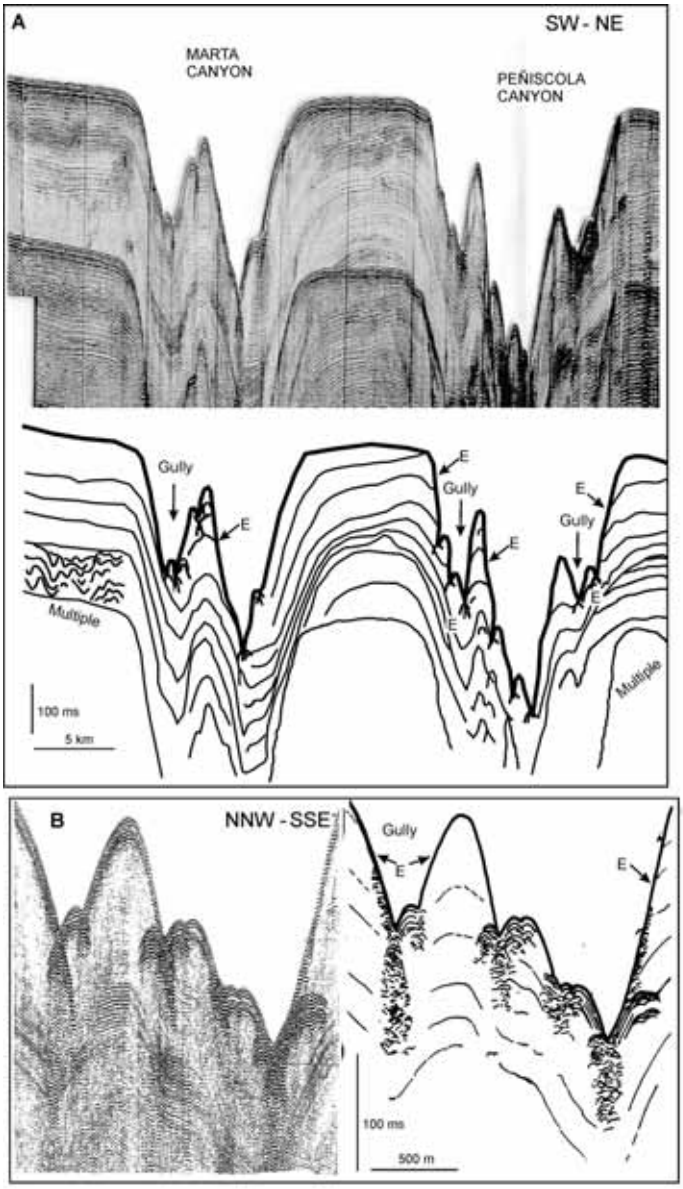

Fig. 4. - A) Seismic profile (sparker) and line drawing interpretation across the head of Marta and Peñiscola canyons (central sector) illustrating the presence of numerous gullies and the erosive character of the walls. B) Seismic profile (sparker) and line drawing interpretation showing the cross-section of gullies. Legend: E, erosive surfaces suggested by the truncation of reflectors.

5.3. Slides on the open continental slope

These occur on the entire Ebro continental slope (Fig. 2) and are mostly observed as morphologic relief on the seafloor, although they are also identified in the subbottom reflectors (Fig.5). The slides range in size from a few km to tens of km in length.

The smaller slides occuring mostly along the upper slope consist of sigmoidal and lenticular packages, up to 100 ms thick that extend downslope for < 4 km distances (Fig.5). They are internally characterised by a discontinuous stratified facies which is locally progradational. Some of these slides lie adjacent to steep scars (> 100 ms vertical offset) against which the upper reflections terminate sharply as result of truncation by failure. Locally, isolated slide scars are also identified, as shown by the sharp local increase in slope gradients and the truncation of subottom reflectors (Fig.6).

Two large-scale submarine slides also affect the Ebro continental slope: the Columbretes and the Torreblanca slides located on the southern sector and southernmost part of the central sector respectively (Fig.2). The Columbretes slide is rooted on the upper slope at 170 m water depth and ends near the base-of-slope, in approximately 1100 m water depth (Martinez del Olmo, 1984). The slide scar extends from 170 to 454 m water depth and is characterised by a steep (> 4º) slope surface that truncates the prograding deposits of the shelf break (Fig. 4B). The 20 km wide slide extends 10 km downslope and is about 150 ms (≈ 113 m) thick on average; the total volume is about 23 km^3. Actually, the thickness of the main body of the slide varies downslope (Fig.7B) and decreases in thickness toward the northeast along slope (from 150 to 80 ms) (Fig.7A). Seismically, the main body of the Columbretes slide can be identified as a chaotic deposit clearly differentiated from the well-stratified surrounding slope (Fig.7). The seabed is characterised by several side-by-side stacked hyperbolae, also observed within the slide. The failure plane is difficult to trace downslope, but along the slope it is discontinuous and appears to be mostly concordant with the regional stratification. Nevertheless, the slide appears as a structureless and acoustically chaotic body, whose clearly recognisable scar and failure plane identify it as a slump mass (irregular, chaotic) and not as a mass flow deposit (Fig.7).

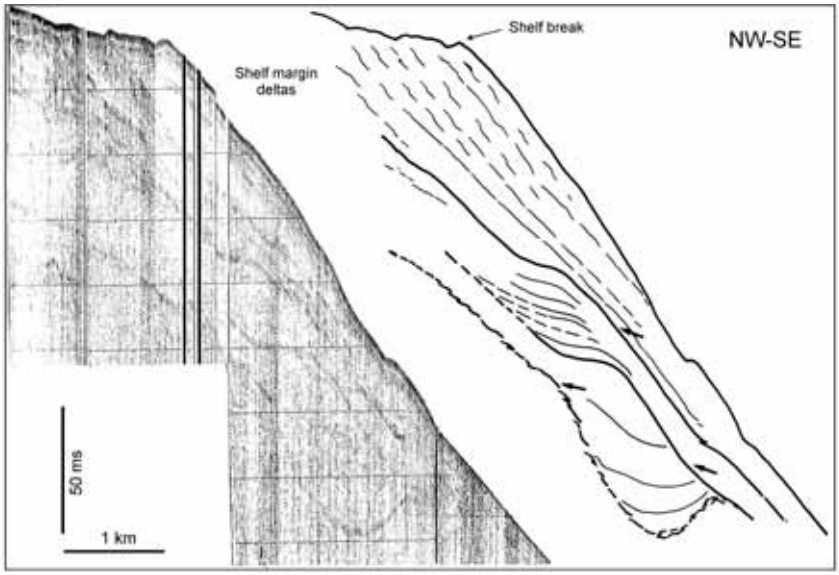

Fig. 5. - Seismic profile (sparker) and line drawing interpretation showing the small-scale slides identified on the upper slope. The arrows indicate truncation of sediments by failure.

The Torreblanca slide has been identified in the southernmost part of the central sector (Fig.2) and extends down to the base-of-slope (at least 1350 m water depth), beyond the study area. The more proximal part near the head of the Torreblanca Canyon is in about 360 m water depth, where the slope gradients display a sharp increase from about 15 to 29 %. This break marks the slide scar which has a vertical offset of approximately 300 m. Between the scarp and the main body of the slide at 655 m depth, there is a small V-shaped topographic feature (Fig.8) which corresponds to the tensional scar, characteristic of the headslope of many submarine landslides. The main body of the Torreblanca slide is seismically defined by discontinuous stratified reflections locally affected by chaotic and hyperbolic facies (Fig.8). This body has a length at least up to 40 km, and it displays a longitudinal lens-shape section. The slide has a rough upper surface and involves sediment up to 300 ms thick, affects a channel-levee complex (Fig.8). The failure plane of the Torreblanca slide is at depths of between 90 and 260 m below the top surface of the slide. The plane is quite continuous, concordant with the stratification, highlighted by parallel reflections but with high roughness.

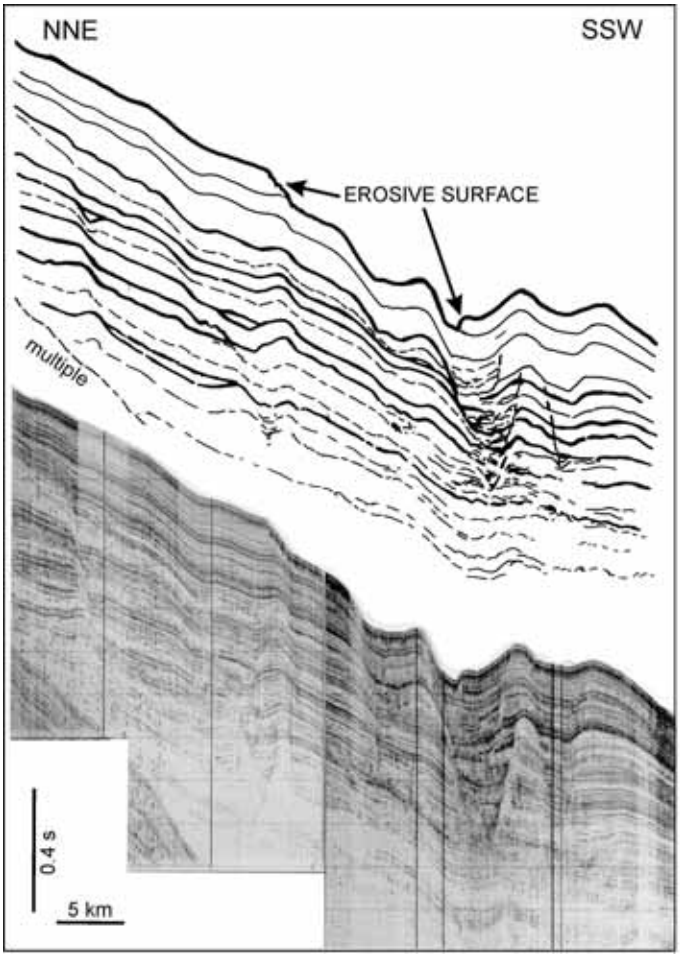

Fig. 6. - Seismic profile (sparker) and line drawing interpretation showing isolated slide scars identified on the upper part of the slope. These scars are associated to erosive surfaces that truncate the subottom reflectors.

5.4. Mass-flow deposits on the open continental slope

The presence of mass-movement features has been also recognised by the presence of depositional bodies formed by mass-flows (Fig.7). Recently, Canals et al. (2000) and Willmott et al. (2001) have recognized on the Ebro slope a major mass flow deposit (named BIG'95) from very high resolution seismic profiles (Lastras et al. 2002). Those authors show that the BIG'95 mass flow deposits are very recent in age and extend from the slope to the base-of-slope covering an area of 2000 km^2 (Lastras et al. 2002; Urgeles et al. 2003). Mass flow deposits are variable in scale, and only those of smaller scale have been recognised on our seismic profiles. These deposits are

characterised by chaotic facies with a lenticular shape up to 0.26 s thick and 8 km long that interrupt the lateral continuity of the surrounding stratified facies. They usually show a concave-upward base of high reflectivity, a very irregular upper surface, and terminate abruptly. Based on the external morphology, acoustic signature, types of boundaries, and also by comparison with the signatures of these deposits in high-resolution seismic profiles they can be interpreted as debris-flow deposits (Ercilla, Alonso & Baraza, 1994).

6. Discussion

6.1. Geological significance

The analysis of seismic profiles of the Ebro continental margin shows that mass-movements are a common recent process on the slope, in both submarine canyons and on the open slope. In fact, about 37 % of the Ebro slope is affected by these features (Fig.2). While a number of factors have been involved to explain the presence and development of canyons most imply sedimentary mass-movement processes (Twichell, 1986). In the case of the Ebro canyons, mass-movement processes also appear to be particularly important (Alonso et al., 1984; O'Connell & Normark, 1987; Alonso & Maldonado, 1990). The incision, enlargement and sculpting of these canyons have been attributed to submarine slides and mass flows which occurred mostly during Quaternary regressive episodes (Alonso & Maldonado, 1990). Submarine erosion by mass flows combined with headward and wall slumping are the main combination of events suggested to explain the truncation of reflections against the canyon walls. The occurrence of mass-movement processes in the canyons is also show by the presence of ancient cut and fill features, and the chaotic character of the infill (Fig.3). This character may reflect displaced sediments with an internally deformed structure, probably associated with the lateral collapse and mass flows running along the canyons. On the other hand, the presence of submarine canyons is also indicative of mass-movements because they represent areas of downslope evacuation of sediments. The sediments coming from the canyons were deposited at the base-of-slope forming channel-levee complexes during the Quaternary (Alonso & Maldonado, 1990).

The occurrence of mass-movement processes on the submarine canyons is also evidenced by individual slides on the walls and the canyon-head and wall gullying

(Figs. 3 and 4). The slides on the walls are favoured by the steep gradients (< 15º), in combination with wall erosion by mass flows running along the canyons. The gullies have developed basically as a result of small-scale submarine slides or other type of small-scale sediment mass-movements, as is suggested by the regularity and the proximity between them. The presence of several steps with a chaotic acoustic response on their transverse profiles suggests a growth of the gullies by coalescence, due to backward and lateral erosion by mass flows or gully headward and wall sliding (Fig.4B). The less common presence of gullies along the lower parts of the canyons may be related to a combination of the gentler sidewall gradients on the lower slope (Alonso et al., 1984) and distal location relative to the continental shelf (Fig.3).

The mass-movement features on the open continental slope are variable in size and morphology (Fig.*2)*. The smaller features occur in the form of small-scale slides and slide scars on the upper slope, and debris-flow deposits on the lower slope. The small-scale slides and slide scars affect regressive shelf-margin deltas (Farran & Maldonado, 1990) (Fig.5). High accumulation rates and the subsequent sedimentary loading favoured a state of underconsolidation with corresponding low values of shear strength on these thick prograding deltas (Baraza et al., 1990). The underconsolidation stage occurs because excess pore pressure occurs during periods of high sedimentation rates (Dimakis, Elverhøi, Høeg, Solheim, Harbitz, Laberg et al, 2000) Therefore, the small-scale slides and their scars could be interpreted as features resulting from delta front failures.

With respect to the debris-flow deposits, their preferential presence on the lower slope could be explained as a result of the downslope evolution of the mass-movement processes that occurred on the upper slope. The mapping of mass-movement features does not show a direct correlation between the presence of isolated slide scars and the location of debris-flow deposits (Fig. 2). Several studies have demonstrated, however, that slides often undergo rheologic changes during their passage downslope and may transform into mass-flow events, over relatively short distances (Parker, 1982; Cochonat & Piper, 1995; Mulder, Savoye, Piper & Syvtstki*,* 1998). More seismic information is necessary to assess this possible interpretation.

The mass-movement features of the Columbretes and Torreblanca slides represent events that involved large amounts of sediments (Fig.2). The lack of bedding in the Columbretes slide indicates that deposits have been displaced, distorted and mixed as the slide moved downslope (Fig.7). The variable depth of the failure plane

(shallower in the northeast) beneath the seafloor and the different stratigraphic levels that it affects, both suggest that failure is not rooted in a single incompetent layer (Fig.7B). Progressive failure propagation towards the northeast probably occurred. The Torreblanca slide displays different seismic and morphologic features of the Columbretes slide (Fig.8). Its internal structure indicates that sliding has slightly disturbed the sediment and that downslope transport only caused minor rumpling and folding. The slab slide seems to exist as a geometric entity, whereas progressive fragmentation seems to have occured during downslope movement of the Columbretes slide.

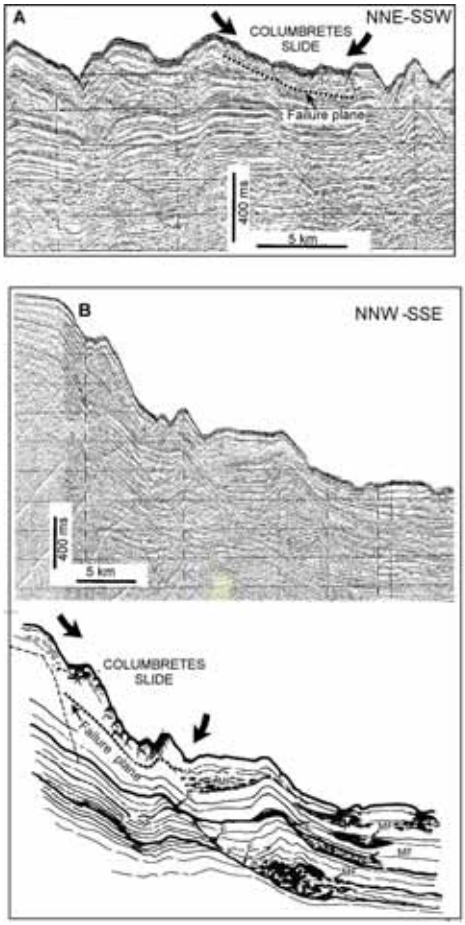

Fig. 7.- A) Seismic profile (airgun) parallel to the slope illustrating the Columbretes slide; the thick arrows indicate the lateral extension of the slide and the dotted line the failure plane. B) Seismic profile (airgun) along the Columbretes slide and line drawing interpretation showing the chaotic internal facies and the trace of the failure plane. The thick arrows indicate the lateral extension of the slide. This profile also shows the presence of mass-flow deposits (MF) on the lower slope. Legend: E, erosive surfaces.

6.2. *Triggering mechanisms*

Geotechnical studies done by Baraza et al. (1990) on surficial sediment cores (< 3 m long) indicate that the upper slope has a relatively high degree of stability under relatively rapid (undrained) static loading conditions, compared with the lower slope, which has a high degree of stability under long-term (drained) static loading conditions. Under cyclic loading (e.g., earthquakes) the upper slope should have a higher degree of stability than the lower slope. However, the results presented here indicate that sediment instability is common on the upper and lower slope. This contradiction may be due to the fact that the geotechnical analysis was done on surficial sediment cores (Fig.2), whereas the instability features affect thicker depositional packages with deeper levels of mechanical failure. The non-correlatable seismic and geotechnical modellings have been discussed in detail by Casas et al (2003) who suggest that the different failure events should be studied individually from a geotechnical point of view to better understand the failure dynamics and their impact on slope stability.

With respect to triggering mechanisms, Baraza et al. (1990) established that seismically induced instability seems unlikely on the Ebro slope and that other types of cyclic events, such as storms or internal waves do not appear to be a direct cause of instability at present. These processes, however, might have influenced instability during the past, when infrequent strong earthquakes occurred (Roca & Suriñach, 1982); in addition sea-level and sediment sources had different locations (Farran & Maldonado, 1990; Chiocci, et al., 1997), and oceanographic conditions affected the stability of the seafloor and subbottom. The following triggering mechanisms are evaluated as potential destabilising factors: gravity loading, storm and internal waves, earthquakes and tsunamis.

Gravity loading is probably the most common cause for mass-movement features in the submarine canyons, and small-scale slides, scar slides and debris-flow deposits on the open continental slope. It results from the interplay of the steep slope of the canyon walls (< 15º), regressive delta fronts (> 1º), the higher sediment supply to the slope and rapid deposition of fluvial sediment during regressive periods.

Likewise, storm waves and internal waves during low sea levels may act as trigger mechanisms of unstable features in submarine canyons and the small slides and scar slides of the upper slope. The oceanographic conditions during low sea level and glacial time are unknown. However it can be tentatively considered that during

sea-level falls, when high sedimentation rates favoured the development of underconsolidated sediment, storm waves and internal waves might have impinged onto the seafloor inducing slope failures.

Infrequent strong earthquakes with intensities of VI or greater and with a return period greater than 70 years can be tentatively considered as a major mechanism for the large-scale slides of Columbretes (Baraza et al., 1990) and Torreblanca. However their remarkable differences in size, volume of sediment, and location respect to the small-scale slides suggest a different trigger, or a particular combination of triggers. Earthquake stresses propagate upward from bedrock, whereas the stress produced by oceanographic conditions dissipates downward from the seafloor (Schwab & Lee, 1993). This implies that an earthquake has more capacity to reduce the strength of deep sediment; this reduction joined to lithostatic stress that increases with increasing depth would develop an unstable condition that affects relatively thick packages of sediments. The Columbretes slide was probably caused by earthquake shaking associated with volcanism in the Columbretes Islands (Field & Gardner, 1990) (Fig.2). This may have caused the main failure, in combination with the high sedimentation rates, steepness of the slope and the underconsolidation due to rapid sedimentation.

The chaotic seismic signature of this slide indicates several phases of deformation (Fig.7). This may have been caused by multiple tectonic events, related to volcanism at different times during the Neogene and Quaternary (Martínez del Olmo, 1984; Maldonado, 1985; Farran & Maldonado, 1990). Likewise, the main failure of the Torreblanca slide could be triggered by an important seismic shaking; it probably corresponds to a single important event, suggested by the limited deformation of the internal structure evidenced by the seismic reflectors (Fig.8). Similarly to the Columbretes slide, the Torreblanca slide could also be the end product of a combination of an earthquake plus other factors.

Tsunamis generated by seismic activity have affected the southern and eastern coast of Spain, caused mostly by strong earthquakes in Algeria (north Africa) (Sloviev, Solovieva, Go & Shchetnikov 2000). The tsunamis that affected the Westernmost Mediterranean Sea were weak (a few centimetres high), and we consider that they probably did not provide enough cyclic loading to induce slope failures, at least in the most recent sedimentary units of the Ebro continental slope.

6.3. Distribution and variability of mass-movement features

According to Pratson (2001) there are still unresolved questions about slope instability. For example it is unknown why one region of seafloor remains intact, and why another sector fails while the neighbouring region remains intact, and why a sector fails in the way that it does. The Ebro continental slope is a good case to assess some of these questions because of the variability in the distribution, types and scales of mass-movement features. The predominant features showing mass-movement processes on the Ebro slope are the submarine canyons. These canyons have collected sediment supply during low sea stands but have also favoured the development of mass-gravity processes due to the steepness of their side walls and the rapid accumulation of deposits in shelf margin deltas at the canyon heads (Fig. 2). The seismic stratigraphy of the Ebro shelf indicates that the direction of propagation of regressive shelf margin deltas was southward, with a maximum thickness in the central sector (Farrán & Maldonado, 1990). We can tentatively consider that the relative higher sediment supply received by the central sector slope plus the oversteepening of the slope favoured the relatively major occurrence of failures on this sector, where the canyons are bigger and numerous (Fig.2).

The small-scale-slides are predominant on the upper slope (Fig.2). The steep gradients and high sedimentation rates may have favoured slide development comparable to the failures observed in submarine canyons. The post failure behaviour, however, was different: the run-out distances on the small-scale slides were short whereas post-failure mobility was more important in the case of the canyons. Several qualitative assumptions about the post-failure behaviour may be inferred on the basis of the data available (Figs. 1, 2). Taking into account that the Ebro upper slope seems to be composed in the three sectors of fine-grained deposits (silty clays with high overconsolidation, Baraza et al., 1990), the post-failure behaviour may be explained at least by the interplay of two factors: frequency of failures and sediment thickness involved in the failures. Sectors with small-scale slides would be characterised by a lower frequency of failures and thicker slide packages, where canyons have a restricted development. In the sectors of the slope dominated by submarine canyons, the failure events would be frequent so that only thin packages of sediments were subject to sliding; this has been also observed on the Nice continental slope (northwestern Mediterranean) (Klaucke & Cochonat, 1999). The occurrence of

successive thin slides in relative steep slopes facilitates major post-failure mobility of the slides and the development of canyons.

The large-scale slides are concentrated mainly around the southernmost part of the central and southern sectors (Fig.2). Earthquakes were probably the main triggering mechanism, but the surrounding areas may be equally affected by the seismic activity although large slides are absent. The proximity of the volcanic Columbretes Islands to the southern sector might have been a primary factor in inducing failure, although relatively steeper gradients, large width and open conditions (less canyons or gullies) may also have favoured their development.

With respect to the debris-flow deposits, their presence implies long distance transport of slides. Most debris-flow deposits are concentrated in the lower slope (Fig.2). Long transport and their distorted structure result from the relative high gradients of the open slope segments and the absence of gullies or canyons that would interrupt the pathway of the flows. Their geotechnical properties may have also influenced the initiation of the displacement reducing the shear strength to facilitate sediment mobility.

7. Conclusions

Mass-movement is an important process controlling the growth patterns, morphology and sedimentary structure of the Ebro continental slope during recent times (at least Quaternary). The instability features comprise erosive surfaces associated with submarine valleys, gullies, slides on submarine canyons, small and large-scale slides, small-scale slide scars and debris-flow deposits on open slope segments (Table 2). The small and large-scale slides do not act as important agents of downslope dispersal of sediments because the slump packages retain their coherence. However, these processes modify the internal structure of the affected sediments. Submarine canyons, in contrast, are a major conduit for the downslope of material.

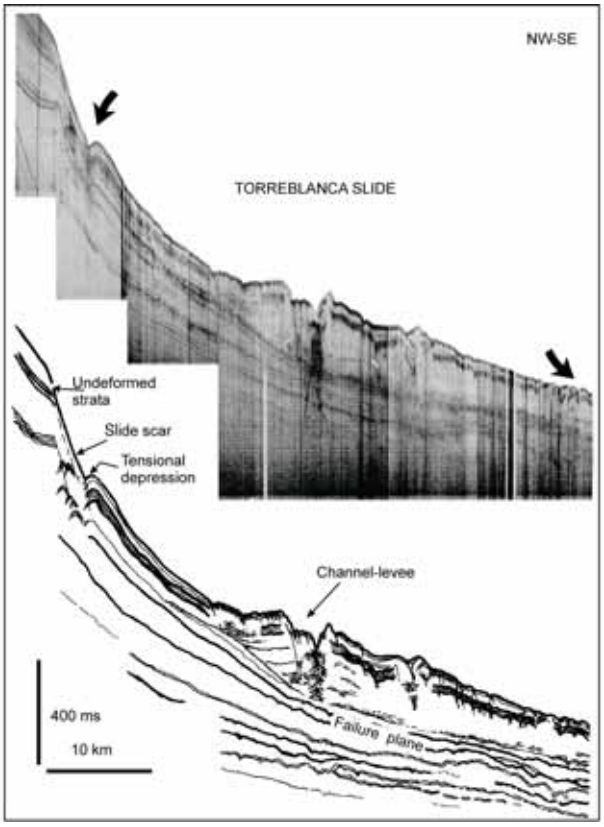

Fig. 8. - Seismic profile (sparker) along the Torreblanca slide displaying the different morphological and internal structure of reflectors and the failure plane. Discussion in the text.

The relatively high slope gradients and rapid deposition of sediments directly onto the upper slope during the low sea level stands were the main factors contributing to the state of underconsolidation and consequent degradation of the sediment shear strength. Under these conditions, gravity loading was probably sufficient to cause failure. This mechanism was, however, also favoured by the cyclic action of storm and internal waves during low sea levels. The debris-flow deposits located at the lower slope were emplaced as a result of sliding. Seismic loading is considered to be the main trigger mechanism responsible for the emplacement of the large-scale slides of Torreblanca and Columbretes, probably also favoured by other instability factors. The large variations in distribution, type and size of mass-movement features seem to be controlled by the local characteristics of the slope, which have governed not only their genesis but also the post-mobility of the gravity processes.

		Water depth	Type of movement	Height of scarp	Average Slope angle	Thickness
Open slope	Columbretes	170 m	Slide	280 m	> 4º	150 ms
	Torreblanca	360 m	Slide	300 m	4.9º	300 ms
	Big'95	700 m	Debris-flow	No data	4.5º	8-28 ms
	Small-scale slides	<500 m	Slide	> 75 m	4.5º	100 ms
	Small scale Mass-flow	>500 m	Mass-flow	No data	4.5º	260 ms
Canyons	Slides	Along courses	Slide	No data	No data	20 - 80 ms
	Erosive surfaces	Along courses	Erosion	No data	No data	-
	gullies	225-440 m	Erosion	19 - 56 m	No data	-

Table 2. Comparative table showing the different sediment mass movements features observed on the slope of the Ebro margin.

Acknowledgements

This work was founded by the European Commission ANAXIMANDER project (EVK3-2001-00123), and by the "Ministerio de Ciencia y Tecnología" MARCONI (REN2000-0336-C03) project, MARSIBAL (REN2001-3868-C03) project and ANT1999-1462-E. The support of these people and institutions is gratefully acknowledged. David Casas thanks the Generalitat de Catalunya for the PhD grant (1999FI 00002CSIC PG). We also thank David G. Roberts and anonymous journal reviewer for their helpful comments and editorial assistance.

References

Alonso, B. (1986). El sistema del Abanico profundo del Ebro. Ph.D. Thesis. Universidad de Barcelona, 384 p.

Alonso, B., & Mardonado, A. (1990). Late Quaternary sedimentation patterns of the Ebro turbidite systems (northwestern Mediterranean): Two styles of deep-sea deposition. In C.H. Nelson and A. Maldonado (Eds.), *The Ebro margin. Marine Geology,* 95, 353-377.

Alonso, B., Díaz, J.I., Farran, M., Giró., S., Maldonado, A., & Vázquez, A. (1984). Cañones submarinos del margen Catalán meridional: morfología y evolución. *I Congreso Español de Geología*, Segovia, (pp. 301-311).

Baraza, J., Lee, J., Kayen, R., & Hampton, M.A. (1990). Geotechnical characteristics and slope stability on the Ebro margin, western Mediterranean. In C.H. Nelson and A. Maldonado (Eds.), *The Ebro margin. Marine Geology,* 95, 379-393.

Canals, M., Casamor, J.L., Urgeles, R., Lastras, G., Calafat, A.M., Masson, D.G., Berné, S., & Alonso, B. (2000). The Ebro Continental Margin, Western Mediterranean Sea: Interplay between Canyon-Channel System and Mass Wasting Processes. GCSSEPM Foundation 20th Annual Research Conference Deep-Water Reservoirs of the World. 152-174. Houston, Texas.

Casas D., Ercilla G., Lee H., Alonso B., Maldonado A., & Baraza J. (2003). Submarine Mass Movement on The Ebro Slope. In J. Locat and J. Mienert (Eds.), *Submarine Mass Movements and Their Consequences*. *Advances in Natural and Technological Hazards Research. 19,* 393-400. Netherlands: Kluwer academic publishers.

Chiocci, F.L., Ercilla, G., & Torres, J. (1997). Stratal architecture of Western Mediterranean margins as the result of the stacking of Quaternary lowstand deposits below “glacio-eustatic fluctuation base-level”. *Sedimentary Geology*, 112, 198-217.

Cochonat, P., & Piper, D.J.W. (1995). Source area of sediments contributing to the “Grand Banks” 1929 turbidity current. In Pickering, K.T., Hiscott, R.N., Kenyon, N.H., Ricci-Lucchi, F., Smith, R.D.A. (Eds.), *Atlas of Deep Water Environments: Architectural Style in Turbidite Systems*. (pp. 12-13). London: Chapman &Hall.

Dañobeitia, J.J., Alonso, B., & Maldonado, A. (1990). Geological framework of the Ebro continental margin and surrounding areas. In C.H. Nelson and A. Maldonado (Eds.), *The Ebro margin. Marine Geology,* 95, 265-287.

Díaz, J.I., Nelson, C.H., Barber Jr., J.H., & Giró. S. (1990). Late Pleistocene and Holocene sedimentary facies on the Ebro continental shelf. In C.H. Nelson and A. Maldonado (Eds.)*, The Ebro margin. Marine Geology.* 95: 333-352.

Dimakis, P., Elverhøi, A., Høeg, K., Solheim, A., Harbitz, C., Laberg, J.S., Vorren, J.S. & Marr J. (2000). Submarine slope stability on high-latitude glaciated Svalbard-Barents Sea margin. *Marine Geology*, 162, 303-316.

Ercilla, G., Alonso B. & Baraza, J. (1994). Post-Calabrian sequence stratigraphy of the northwestern Alboran Sea. *Marine Geology*, 120, 249-265.

Farran, M., & Maldonado, A. (1990). The Ebro continental shelf: Quaternary seismic stratigraphy and growth patterns. In C.H. Nelson and A. Maldonado (Eds.), *The Ebro margin. Marine Geology,* 95, 289-312.

Field, E., & Gardener, V. (1990). Pliocene-Pleistocene growth of the Rio Ebro margin, northeast Spain: A prograding-slope model. The Geological Society of America Bulletin*, 102 (6), 721-733.*

Font, J., Salat, J., & Julià, A. (1990). Marine Circulation along the Ebro Continental Margin. In C.H. Nelson and A. Maldonado (Eds.)*, The Ebro margin. Marine Geology,* 95, 165-177.

Fontsere, E., & Iglesias, J. (1971). Recopilació de dades símiques de les terres catalanes entre 110 i 1906. (pp.546) Barcelona: Fundació Salvador Vives.

Gaibar-Puertas, C. (1979). Actividad sísmica de Cataluña durante los últimos 70 años: 1907-1976. *Acta Geológica Hispánica*. *"Homenatge a Lluis Solé i Sabaris"*, 14, 178-184.

Gallart, J., Guimera, J., & Olivera, C. (1989). Neogene Paleostresses and present seismotectonic results of the Valencia Trough and surrounding areas. *Terra Abstracts*, 1, 48.

Glabis, J. (1940). Catálogo sísmico de la zona comprendida entre los meridianos 5º E y 20ºN y paralelos 45º y 25ºN. Tomo II, (pp277) Madrid: Instituto Geográfico y Catastral.

Hampton, A.M., Lee, H., & Locat, J. (1996). Submarine landslides. *Reviews of Geophysics*, 34 (1), 33-59.

Lastras, G., Canals, M., Hughes-Clarke, J.E., Moreno, A., DeBatist, M., Masson, D.G., & Cochonat, P. (2002). Seafloor imagery from the BIG'95 debris flow, western Mediterranean. *Geology*, 30 (10), 871-874.

Locat, J., & Lee, H. J. (2000). Submarine landslides: Advanced and challenges. In *Proceedings of the 8th International Symposium on Landslides*, Cardiff.

Klaucke, I., & Cochonat. P. (1999). Analysis of past seafloor failures on the continental slope off Nice (SE France). *Geo-Marine Letters*, 19, 245-253.

Maldonado, A. (1985). Evolution of the Mediterranean basins and a detailed reconstruction of the Cenozoic paleoceanography. In R Margalef (Ed.), *Key Environments: western Mediterranean*, (pp. 17-59), Pergamon Press.

Martinez del Olmo, W. (1984). Un ejemplo actual y reciente de abanico turbidítico profundo: Columbretes Fan. *I Congreso Español de Geología, Segovia*, 5, 53-75.

Mezcua, J., & Martinez Solares, J.M. (1983). Sismicidad del área Ibero-Magrebí. Instituto Geográfico Nacional, Madrid, 301pp.

Mulder, T., Savoye, B., Piper, D.J.W., & Syvtstki, J.P.M. (1998). The Var submarine sedimentary system: understanding Holocene sediment delivery processes and their importance to the geological record. In Stoker, M.S., Evans, D., Cramps, A. (Eds.)*, Geological Processes on Continental Margins: Sedimentation, Mass-Wasting and Stability. Geological Society, Special Publications*. 129, 145-166.

Nelson, C.H., & Maldonado, A. (1990). Factors controlling late Cenozoic continental margin growth from the Ebro Delta to the western Mediterranean deep sea. In C.H. Nelson and A. Maldonado (Eds.)*, The Ebro margin. Marine Geology,* 95, 419-440.

O'Connell, R., & Normark, W.R. (1987). Modes of development of development of slope canyons and their relation to channel and levee features on the Ebro sediment apron, off-shore northeastern Spain. *Marine and Petroleum Geology*, 4, 308-319.

Palanques, A., Plana, F., & Maldonado, A. (1990). Recent influence of man on the Ebro margin sedimentation system (Northwestern Mediterranean Sea). In C.H. Nelson and A. Maldonado (Eds.)*, The Ebro margin. Marine Geology, 95, 419-440.*

Parker, G. (1982). Conditions for the ignition of catastrophically erosive turbidite currents. *Marine Geology*, 46, 307-182.

Pratson, L.F. (2001). A perspective on what is known and not known about seafloor instability in the context of continental margin evolution. *Marine and Petroleum Geology*, 18, 499-501.

Roca, A. (1975). Sismicidad de Cataluña 1907-1974 y relación señal-ruido en una estación para el estudio de la sismicidad local. *Phd Thesis*. Universidad de Barcelona, 120pp.

Sloviev, S.L., Solovieva, O.N., Go, Ch.N., & Shchetnikov, N.A. (2000). Tsunamis in the Mediterranean Sea 2000 B.C.-2000 A.D., Kluwer Academic Publishers, 237 pp.

Suriñach, E. & Roca, A. (1982). Catálogo de terremotos de Cataluña, Pirineos y zonas adyaentes. In: La sismicidad en la zona comprendida entre 40ºN-44ºN y 3ºW-5ºE NE de la Península Ibérica. *Publicaciones de la Cátedra de Península Ibérica nº 190. Universidad Complutense*, (pp. 9-53), Madrid.

Schwab, W.C., & Lee, H.J. (1993). Processes controlling the style of mass movement in glaciomarine sediment: Northeastern Gulf of Alaska. In W.C. Schwab, H.J. Leel, and D.C. Twichell (Eds)*, Submarine Landslides: Selected Studies in the U.S. Exclusive Economic Zone. U.S. Geological Survey Bulletin* 2002, 135-142.

Twichell, D.C. (1986). Geomorphic map of the U.S. Atlantic continental margin and upper rise between Hudson and Baltimore canyons. In David, W.F., Hathaway J.C. (Eds.)*. Conference on Continental margins Mass Wasting and Pleistocene Sea-level Changes. UGS* (pp.14- 20).

Urgeles, R., Lastras, G., Canals, M., Willmott, V., Moreno, A., Casas, D., Baraza, J., & Berné, S. (2003). The BIG'95 debris flow and adjacent unfailed sediments in the NW Mediterranean Sea: geotechnical-sedimentological properties, and dating. In J. Locat and J. Mienert (Eds.). *Submarine Mass Movements and Their Consequences. Advances in Natural and Technological Hazards Research 19,* 479-487. Netherlands: Kluwer academic publishers.

Willmott, V., Canals, M., Lastras, G., & Casas, D. (2001). Caracterización sedimentológica de un debris flow reciente en el margen continental del Ebro. Geotemas, *3(2), 117-120.*

CAPÍTULO 3

Acoustic evidences of gas in the continental slope sediments of the Gulf of Cadiz (E Atlantic). D. Casas, G. Ercilla, J. Baraza. *Geo-Marine Letters,* 23: 300-310. 2003.

Geo-Mar Lett (2003) 23: 300–310
DOI 10.1007/s00367-003-0160-z

ORIGINAL

D. Casas · G. Ercilla · J. Baraza

Acoustic evidences of gas in the continental slope sediments of the Gulf of Cadiz (E Atlantic)

Received: 28 January 2003 / Accepted: 7 October 2003 / Published online: 7 November 2003

Abstract Detailed reviews of high-resolution acoustic studies in the continental slope of the Gulf of Cadiz has revealed the following gas-related features: acoustic turbidity and blanking, bright spots, ancient and modern pockmarks, high-amplitude diffractions, acoustic plumes and turbidity in the water column, and BSRs. The origin of the gas is believed to be biogenic and thermogenic. The BSR-like acoustic anomalies occur intermittently in some areas of the upper slope and tend to occur in the volcanoes/diapirs. The pressure temperature conditions deduced for the location of those acoustic anomalies do not correspond to the conditions of stability of gas hydrates. It is suggested that these volcanoes/diapirs intrusions may locally induce anomalously higher pore pressure conditions on the immediately surrounding sediments, affecting the stability field of the gas hydrates.

Introduction

High and very high-resolution reflection seismic investigations have revealed the presence of gas-charged sediments around the world oceans at water depths, from coastal to deep water environments (Hovland 1983; 1984; Söderberg and Floden 1992; Taylor 1992; Solhëim and Elverhoi 1993; Chow et al. 2000; Judd and Curzi 2002). The gas-related acoustic features observed include mainly acoustic turbidity and blanking, bright spots, strong multiple reflections, pockmarks, acoustic plumes and turbidity in the water column, bottom simulating reflectors (BSRs), among others.

The BSRs are associated with the presence of gas hydrates. Gas hydrates are solid, ice-like substances formed by penta-hexagonal closed structures of water molecules that form cavities where gas molecules—essentially methane—are trapped. They are stable under conditions of high pressure and low temperature, and occur naturally where these appropriate conditions of temperature and pressure co-exist, such as the deeper sectors of the continental margins, and in deep ocean basins (Sloan 1990). In the marine environment, gas hydrates are present in the sediments of continental margins below some hundred meters down to 1,500 m water depth, and from the seafloor down to 500 m deep in the sediment column. The scientific study of the formation and stability of methane hydrates has increased largely in recent years (Henriet and Miienert 1998; Max 2000). The interest in gas hydrates is due to several factors, among which their use as a potential energy resource (Kvenvolden et al. 1993; McDonald 1990; Max and Lowrie 1993), their influence on seafloor slope stability (Kayen and Lee 1993; Popenoe et al. 1993; Kvenvolden 1998), and the implications as a control factor on the global climate change and the greenhouse effect (Kvenvolden and McMenamin 1980; McDonald 1990; Nisbet 1990; Kvenvolden 1993, 1998) can be cited.

Although the direct evidence for the presence of gas hydrates in marine sediments has only been obtained trough drilling and coring (Kvenvolden and Barnard 1983; Kvenvolden 1993), they can also be identified by means of acoustic methods using high-resolution seismic tools (Paull and Dillon 1981; Popenoe et al. 1993; Schmuck and Paull 1993; Kvenvolden 1998). The solid and rigid structure of the gas hydrates is characterised by a very high acoustic velocity (avg. 3.3 km/s) compared to the surrounding, hydrate-free sediments (avg. 1.7 km/s), and this results in a strong acoustic impedance contrasts. The presence of free gas in the sediment pores below the hydrate stable zone produces a strong decrease in the P wave velocity (Gregory 1977), which provides an even greater acoustic impedance contrast with hydrate-bearing sediments. This velocity contrast results in a high negative amplitude (Wood et al. 1994; Andreassen et al. 1995) and polarity (Neben et al. 1998),

D. Casas (✉) · G. Ercilla · J. Baraza
CSIC, Instituto de Ciencias del Mar.,
P Marítimo de la Barceloneta 37 49,
08003 Barcelona, Spain
E-mail: davidc@icm.csic.es

CAPÍTULO 3: ACOUSTIC EVIDENCES OF GAS IN THE CONTINENTAL SLOPE SEDIMENTS OF THE GULF OF CADIZ (E ATLANTIC)

ACOUSTIC EVIDENCES OF GAS IN THE CONTINENTAL SLOPE SEDIMENTS OF THE GULF OF CADIZ (E ATLANTIC)

D. Casas, G. Ercilla, and J. Baraza,

CSIC - Institut de Ciències del Mar. P. Marítim de la Barceloneta 37-49, 08003 Barcelona, Spain.

Abstract

Detailed reviews of high resolution acoustic studies in the continental slope of the Gulf of Cadiz has revealed the following gas-related features: acoustic turbidity and blanking, bright spots, ancient and modern pockmarks, high amplitude diffractions, acoustic plumes and turbidity in the water column, and BSRs. The origin of the gas is believed to be biogenic and thermogenic. The BSR-like acoustic anomalies occur intermittently in some areas of the upper slope and tend to occur in the volcanoes/diapirs. The Pressure/Temperature conditions deduced for the location of those acoustic anomalies do not correspond to the conditions of stability of gas hydrates. It is suggested that these volcanoes/diapirs intrusions may locally induce anomalously higher pore pressure conditions on the immediately surrounding sediments, affecting the stability field of the gas hydrates.

1. Introduction

High and very high resolution reflection seismic investigations have revealed the presence of gas-charged sediments around the world oceans at water depths, from coastal to deep water environments (Hovland, 1983; 1984, Söderberg and Flodén, 1992; Taylor, 1992; Solhëim and Elverhoi, 1993; Chow et al., 2000; Judd and Curzi, 2002). The gas related acoustic features observed include mainly acoustic turbidity and blanking, bright spots, strong multiple reflections, pockmarks, acoustic plumes and turbidity in the water column, Bottom Simulating Reflectors (BSRs), among others.

The BSRs are associated to the presence of gas hydrates. Gas hydrates are solid, ice-liked substances formed by penta-hexagonal closed structures of water molecules which form cavities where gas molecules -essentially methane- are trapped. They are stable under conditions of high pressure and low temperature, and occur naturally where these appropriate conditions of temperature and pressure co-exist, such as the deeper sectors of the continental margins, and in deep ocean basins (Sloan, 1990). In the marine environment gas hydrates are present in the sediments of continental margins below some hundred meters down to 1500 m water depth, and from the seafloor down to 500 m deep in the sediment column. The scientific study of the formation and stability of methane hydrates has increased largely in recent years (Henriet and Mienert, 1998; Max, 2000). The interest on gas hydrates is due to several facts, among which their use as a potential energy resource (Kvenvolden et al., 1993; McDonald 1990; Max and Lowrie, 1993), their influence on seafloor slope stability (Kayen and Lee, 1993; Popenoe et al., 1993; Kvenvolden, 1998), and the implications as a control factor on the global climate change and the greenhouse effect (Kvenvolden and McMenamin, 1980; McDonald, 1990; Nisbet, 1990; Kvenvolden, 1993; 1998) can be cited.

Although the direct evidence for the presence of gas hydrates in marine sediments has only been obtained trough drilling and coring (Kvenvolden and Barnard, 1983; Kvenvolden, 1993), they can also be identified by means of acoustic methods using high resolution seismic tools (Paull and Dillon, 1981; Popenoe et al., 1993; Schmuck and Paull, 1993; Kvenvolden, 1998). The solid and rigid structure of the gas hydrates is characterised by a very high acoustic velocity (avg. 3.3 km/sec) compared to the surrounding, hydrate-free sediments (avg. 1.7 km/sec), and this results in a strong acoustic impedance contrasts. The presence of free gas in the sediment pores below the hydrate stable zone produces a strong decrease in the P wave velocity (Gregory, 1977),

which provides an even greater acoustic impedance contrast with hydrate-bearing sediments. This velocity contrast results in a high negative amplitude (Wood et al., 1994; Andreassen et al, 1995) and polarity (Neben et al., 1998), very strong reflection paralleling the surface of the seafloor, known as “Bottom Simulating Reflector” (BSR) which marks the base of the stable hydrate layer (Kvenvolden and Barnard, 1983).

The aim of this work is to review in detail the previous acoustic evidence published by Baraza and Ercilla (1996), to analyse the possible evidence in the form of BSR-like acoustic anomalies seen on existing seismic records, and provide new insights on evidences supporting the existence of gas hydrates on continental margin sediments.

2. Methods

The present study is mainly based on the interpretation of seismic reflection profiles collected during several oceanographic cruises in the Gulf of Cadiz, onboard the B/O *Garcia del Cid* between 1986 and 1991 (Fig. 1). The main geophysical systems used on these surveys were bathymetric echosounder, high-resolution ORE 3.5 kHz subbottom profiler, Geopulse boomer, and a 20-40 cu. in airgun array. The vessel speed was 5.5-6.0 knots, and the shooting interval was 1 to 3 seconds. The receiver consisted on a 200 m long, single channel streamer containing two active sections, each one with 40 hydrophones. After being filtered with a 200 Hz low pass and 300 Hz high pass filter, the reflected signal was stored as an analogic record on an EPC 4800S graphic recorder. Depending on the sedimentary cover thickness the penetration achieved reached up to 700 ms with a vertical resolution of up to 6 m. Navigation was controlled by MAXIRAN, Loran C, and Transit satellite. The thickness of individual units has been calculated by converting travel time to thickness using an average acoustic velocity of 1600 m/s.

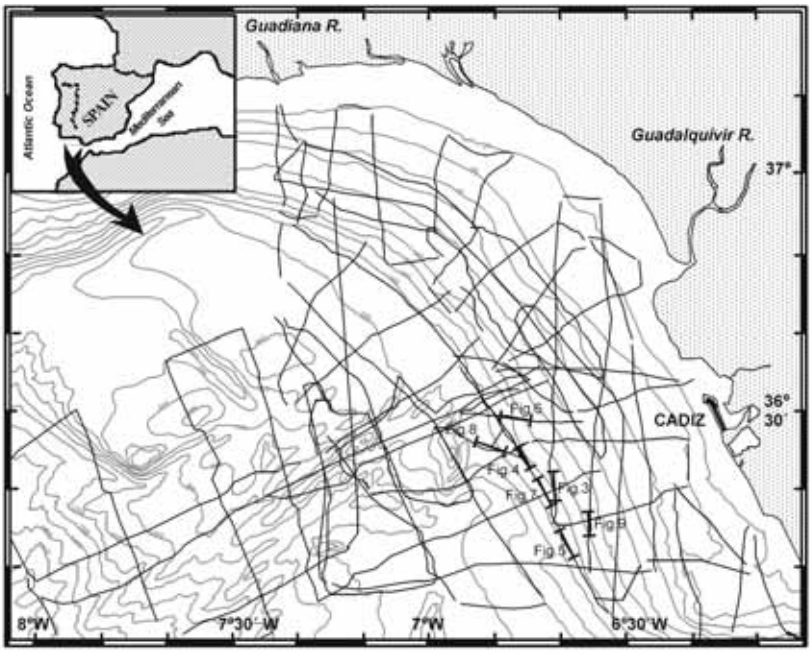

Fig. 1. Bathymetric map (in meters) of the Gulf of Cadiz showing the location of seismic profiles. Thick black short lines with numbers refer to seismic lines shown in Figs. 3 to 9.

3. Geological and Oceanographical Background

3.1. Geological background

The Gulf of Cadiz (Fig. 1) occupies a focal position between the westernmost segment of the Mediterranean and the Iberian-African boundary, and records a complex tectonic history including several phases of extension, convergence and strike-slip motion, and the tectonic emplacement of a large olistostrome following the westward thrust of the Gibraltar Arc (Maldonado et al., 1999). Such a tectonic complexity is reflected on the present seafloor morphology and structure of the Gulf, characterized by a prograding margin with a central slope area occupied by elongated highs of shale-diapiric/volcanic nature, separated by narrow, steep-walled valleys (Maldonado et al., 1992; Nelson et al., 1993; Baraza et al., 1999; Somoza et al., 2002).

Different aspects related to the Neogene and Quaternary seismic stratigraphy and architecture of the Gulf of Cadiz slope and deep areas have been already discussed elsewhere (Nelson et al., 1993; 1999; Riaza and Martínez del Olmo, 1996; Rodero et al, 1999). The Messinian deposits in the Gulf of Cadiz correspond to clays and interbedded

sand lenses with up to 450 m in thickness, that fill most of the existing irregularities and depressions and prograde into the basin deposits, draping the top of the allochtonous units (Maldonado et al., 1999). The sand units represent depositional fan lobes derived from the northern Gulf of Cadiz margin and mainly from the two major rivers in the area (Guadiana and Guadalquivir, Fig. 1) and contain substantial amounts of gas (Riaza and Martínez del Olmo, 1996; Maldonado et al., 1999). The top of these deposits is a basin-wide erosional unconformity above which the Lower Pliocene deposits are represented by a uniform unit between 50 and 300 m thick characterised by continuous stratified, parallel reflectors of high amplitude (Maldonado et al., 1999). These correspond to clays with interbedded sandy clays and some turbidite sand deposits (Riaza and Martínez del Olmo, 1996). The Upper Pliocene deposits are agradational above the Lower Pliocene unit or onlap onto the pre-existing slopes, reach from 150 to more than 500 m in thickness, and consist on interbedded clays and sands corresponding to hemipelagic deposits, turbidite sands and current-drift deposits. On seismic profiles these deposits appear as a sequence with transparent to discontinuous reflectors at the bottom, and higher amplitude, interfingered reflectors at the top, following an overall cyclic pattern (Maldonado and Nelson, 1999; Rodero et al., 1999; Hernández-Molina et al., 2003). On top of these deposits there is an unconformity over most of the basin which corresponds to the base of the Quaternary, above which there is a prograding and onlapping package consisting on several units of shelf margin deltas showing variations in facies and thickness that are controlled by the physiography of the margin, sediment sources and the intensity of bottom currents (Nelson et al., 1993; Rodero et al., 1999).

3.2. Oceanographic setting

The characteristic oceanographic setting and water mass structure of the Gulf of Cadiz is dominated by the plume of dense Mediterranean water that spreads westwards from Gibraltar Strait and descends the continental slope in the center of the Gulf. The presence of an eastward-moving upper layer of light and cold Atlantic water, and a westward-moving lower layer of dense and warmer Mediterranean water characterises a dynamic system of water masses whose vertical profiles in temperature and salinity depend on the geographical location, the physiography and the sea-level position (Zenk, 1970; Baringer and Price, 1999). The present sea-bottom topography has a very important effect upon the dynamics and path of the Mediterranean outflow water, and hence influences the sediment transport and grain size, bedform formation and gradation

(Nelson et al., 1993; Baringer and Price, 1999; Nelson et al., 1999). Temperature profile transects give temperatures for bottom waters ranging from 12.5 to 10.5 ºC between 400 and 1100 m water depth (Madelain, 1970). During the geologic past, however, the Atlantic and Mediterranean water-mass exchange may have been reduced due to smaller effective cross section through Gibraltar Strait, resulting from a lower sea-level position. Under these conditions the strength and volume of the Mediterranean outflow, as well as its interaction with the seafloor may have been different (Maldonado and Nelson, 1999). All these factors may have altered the characteristics of the water masses and their distribution and mixing along the Gulf of Cadiz, and would have resulted on very different temperature profiles compared to the present ones.

4. Geophysical Evidences of Gas in the Gulf of Cadiz

There are a number of geophysical evidences that support the presence of gas in the sediments of the Gulf of Cadiz slope (Fig. 2). The typical acoustic masking on seismic records caused by interstitial free gas, gas-escape craters (pockmarks), and free gas seeps trough the water column have been already described by Baraza and Ercilla (1996). They are reviewed in detail in this section.

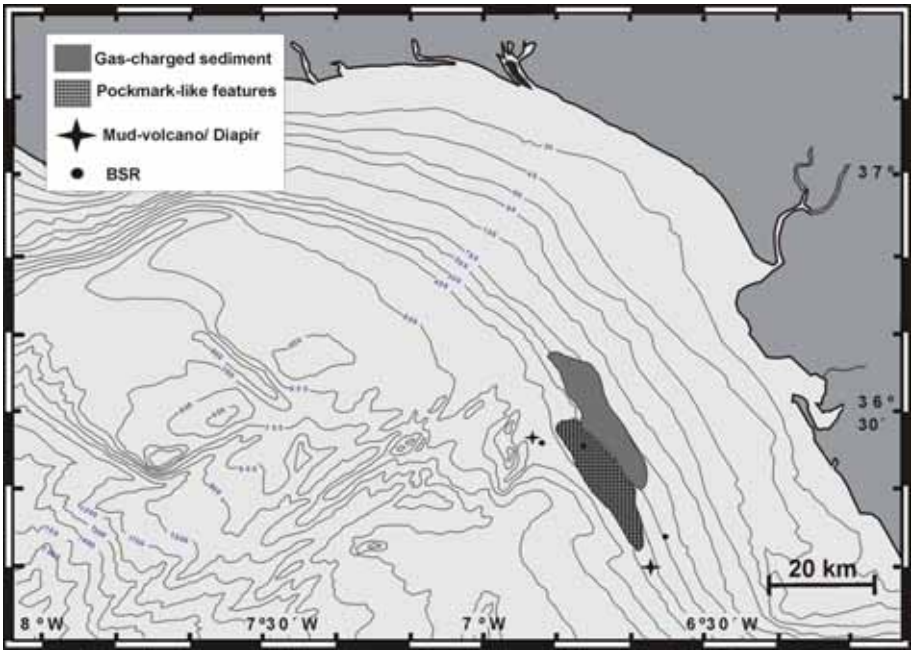

Fig. 2. Bathymetric map (in meters) of the Gulf of Cadiz showing the location of the areas with gas-charged sediments, pockmarks, BSRs and some of the mud volcanoes/diapirs identified in this study.

5. The Area with Gas Charged Sediments

The area with interstitial free gas is identified in the form of a “blanket” feature that appears as an acoustic turbidity on the seismic records (Fig. 3). It occurs on the uppermost slope between 130 and 300 m water depth forming a 35 km long by 5 to 7 km wide belt trending approximately parallel to the slope contours that covers an approximate area of 210 km^2 (Fig. 2). This feature indicates the presence of free gas within the sediments and forms by the absorption of nearly all the seismic energy (Field et al., 1980). The acoustic turbidity appears mostly free of seismic reflections in the central zone although locally some reflections can be identified in the external zones. Enhanced reflections are locally observed at the top of the acoustic turbidity and also in the lateral extremes, indicating local high concentration of gas. The upper limit of the acoustic turbidity is irregular and average 20 m of the seabed surface. The area with free gas is locally affected by gravitational processes in the form of slumps (Baraza et al., 1999). Likewise, slumps occur downslope to the westwards of the acoustically turbid zone. Locally, in the most proximal parts of the slumps they are underlined by gas and/or enhanced reflections in the form of bright spots.

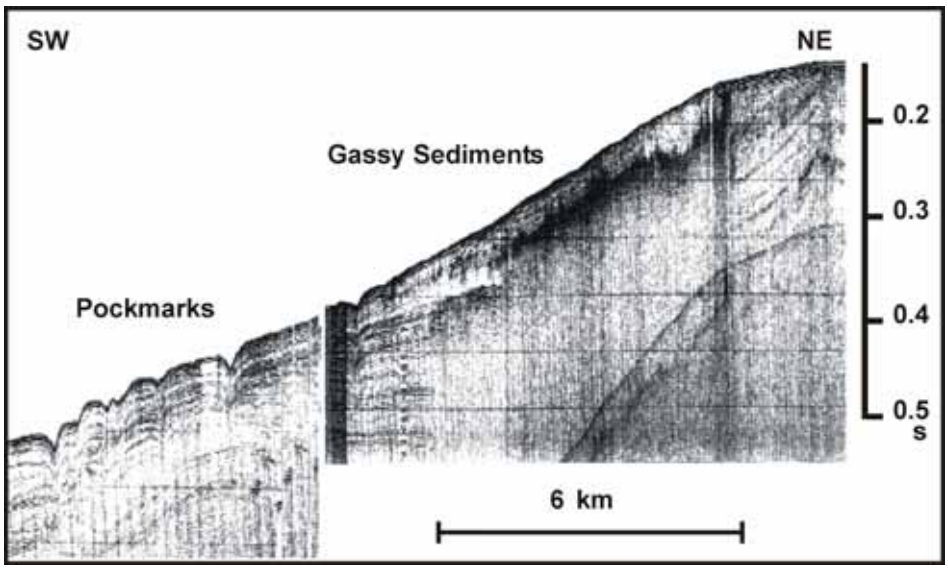

Fig. 3. GeoPulse seismic profile showing gas-charged sediment and pockmark-like features. Seismic line in Fig. 1.

6. Pockmark Area

With respect to the pockmarks they occur in a 30 km long by 2 to 7 km wide belt in the central-east upper slope (Fig. 2) between 300 and 400 m water depth, and display a wide range of sizes, with lengths between 125 and 850 m and depths between 1 and 19 m. The existence of seismic profiles that cut to those features approximately downslope (Fig. 3) and alongslope (Fig. 4) supports the interpretation that they are closed depressions (Baraza and Ercilla, 1996). The pockmarks are both modern (Figs. 3 and 4) and ancient (Fig. 5), and they are similar in shape cross-sections. Their size is variable and some ancient pockmarks grow in the vertical and have surficial expression whereas others are fossilised at different depths (Figs. 5 and 6). The pockmark area develops downslope from the gas-charged sediment area and surrounding diapirs (Figs. 2 and 6). Associated to the pockmarks there are acoustic disturbances with a narrow vertical column structure distributed along the vertical pockmark arrangements. These acoustic disturbances appear as diffractions mostly of high amplitude. These vertical acoustic anomalies may represent gas columns related to gas expulsion through the pockmarks (Figs. 5 and 6). Likewise, acoustically transparent columnar disturbances or wipe-outs are present in certain areas, immediately below and adjacent to the pockmarks (Fig. 5). They are interpreted as being caused by the presence of gas within the sediment. Enhanced reflections in the form of bright spots also occur in the vicinity of the ancient pockmarks in the sediment column, which indicate local high concentration of free gas.

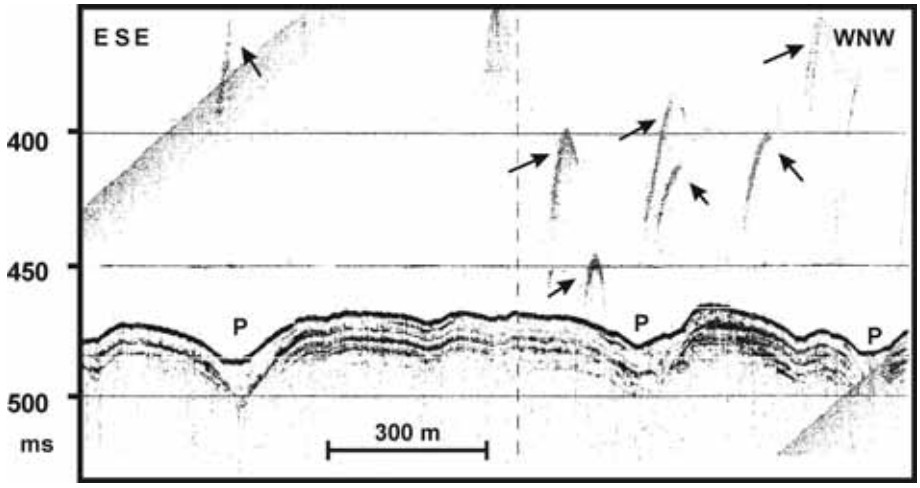

Fig. 4. Detail of a 3.5 kHz seismic profile showing modern pockmarks (P) and acoustic turbidity in the form of acoustic plumes (arrows) in the water column caused by ascending gas bubbles. Seismic line in Fig. 1.

7. Gas Seepage Area

Acoustically reflective plumes in the water column have been observed immediately above the pockmarks suggesting that these plumes represent the actual seepage from the near-surface upper slope sediment (Baraza and Ercilla, 1996). This gas seepage was observed in 3.5 kHz seismic profiles (Fig. 4). Moreover, the new analysis of bathymetric echosounders records also illustrates a possible indication for the actual seepage of gas from near-surface sediments on the upper slope and shelf-break sediments (Fig. 7). They appear as dark hyperbolas and columns ascending from the seafloor up to 50 m. Similar features can be caused by the presence of fish shoals, concentrations of suspended sediment among others (Hovland and Sommerville, 1985). But, in this case, the dark features extend vertically, seem to be bilaterally symmetrical, and are located above gas charged sediments and pockmarks. These observations suggest that the mentioned acoustic anomalies are gas plumes ascending along the water column (Judd et al., 1997).

Together with the above mentioned acoustic evidence of sediments containing free gas, or features that support the actual and past escape of gas from the sediments in the Gulf of Cadiz, there is new evidence, in the form of acoustic anomalies comparable to BSRs. They may constitute a proof for the presence of gas in the form of gas hydrates on the same area (Ercilla et al., 2002). These acoustic anomalies are described in the detail below.

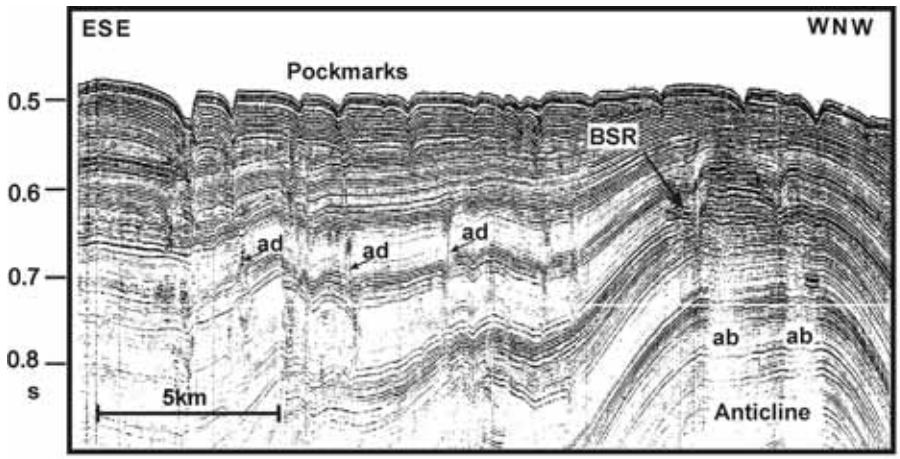

Fig. 5. Detail of an airgun seismic profile showing the pockmarks, and the presence of a BSR-like feature on top of an anticline feature. Note the presence of acoustic disturbances (ad) that occur along the vertical arrangement of pockmarks, and of acoustic blanking (ab) below the BSR-like feature. Seismic line in Fig. 1.

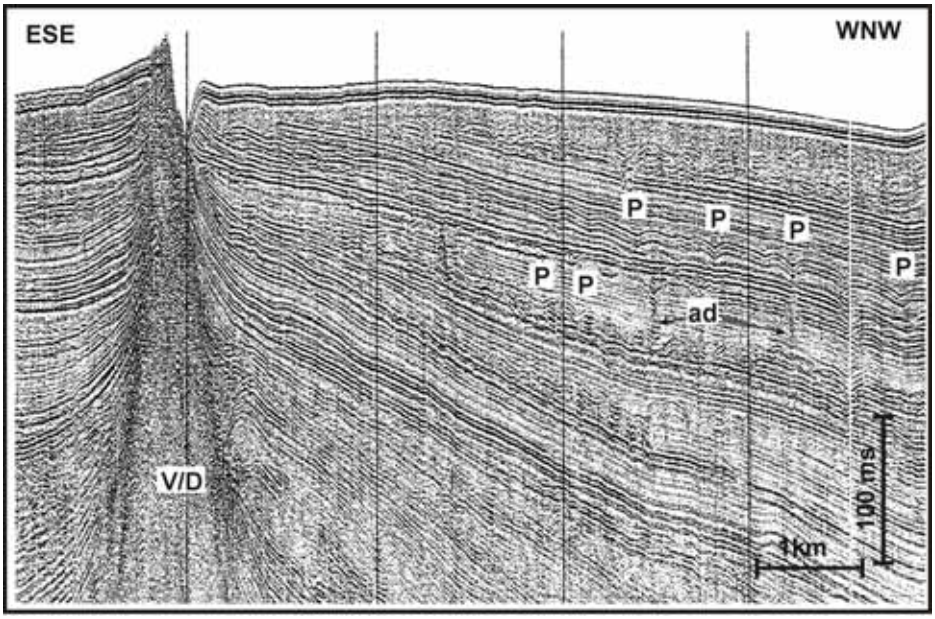

Fig. 6. Airgun seismic profile showing ancient pockmarks (P) fossilised at different depths and their close relationship with volcanic/diapir feature. Note the presence of acoustic disturbances (ad) in the form of high amplitude diffractions that occur along their vertical arrangement. Seismic line in Fig. 1.

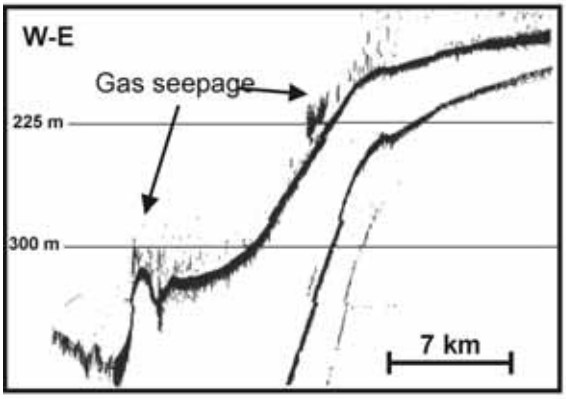

Fig. 7. Bathymetric echosounder profile showing acoustically reflective plumes in the water column. Seismic line in Fig. 1.

8. BSR-like Reflections

A detailed review of the existing seismic database from the Gulf of Cadiz reveals several local examples of acoustic anomalies similar to what are interpreted as indicative of the presence of gas hydrates in the sediment column. These appear mainly in the form of high-amplitude reflections and BSRs identified on high-resolution, single-channel airgun seismic records.

A strong, discontinuous, high-amplitude reflection of about 3 km long appears in a location of the central upper slope of the Gulf of Cadiz in the same area where both surficial and buried pockmarks develop (Fig. 5). This reflector appears parallel to the seafloor surface in an area where the stratification shows clear dipping. By its disposition with respect to both the surrounding reflectors and the seafloor surface, and, following the terminology of Shipley et al (1979), the reflector can be identified as a BSR. This BSR develops above an anticline structure on which other evidences for the presence and escapes of gas have also been identified (Baraza and Ercilla, 1999) (Fig. 5). Acoustic anomalies in the form of column-shaped acoustic wipe-outs develop immediately below the BSR, on what seems the evidence of free gas within the sediments below the hydrate zone. The area where the BSR is located lies at a water depth of 388 m, and a depth below the seafloor of about 150 ms. Assuming an average sonic velocity of 1,600 m/sec, and that both the hydrostatic and lithostatic pressure gradients are 0.1 atm m^{-1}, a pressure of about 50,8 atm can be expected at the depth of the acoustic anomalies. The Gulf of Cadiz area overlies a “normal” continental crust, and then an average geothermal gradient of 30 ºC/km can be assumed for this area. This will imply a temperature increase of about 3.6 ºC from the seafloor surface to the depth where the acoustic anomaly or BSR is located. Without applying any correction for the presence of seawater rather than pure water within the sediment pores, this leads to a temperature range estimate between 14.1 and 16.1 ºC for the position within the sediment column where the acoustic anomaly is located.

There is a second example of acoustic anomaly found in the upper slope of the Gulf of Cadiz. This has been identified on different locations along airgun seismic profiles obtained immediately below an outcropping volcano/diapir ridge on the Gulf of Cadiz slope (Fig. 8). The anomalous reflection shows a clear reverse polarity, compared to the seafloor reflection. The BSR is at 340 m water depth and about 80 ms deep in the sediment column and extends for about 3,5 km (Fig. 8). The volcanoe/diapir appears as a

penetrative structure cutting through more than 600 m of sedimentary units, probably along a fault that has been successively reactivated since the Pliocene. The sedimentary units are progressively thinner towards the diapir and show well-stratified, parallel seismic reflectors that abut against the diapir. Stratification is planar and horizontal and becomes more inclined, even sub-vertical, near the contact with the diapir, reflecting the simultaneity and continuity between sedimentation and diapir uplift (Fig. 8). Assuming the above mentioned values for average sonic velocity and hydrostatic and lithospheric pressure gradients, this acoustic anomaly would, theoretically develops at pressure of 40,4 atm under temperature conditions between 12,4 and 14,4 ºC .

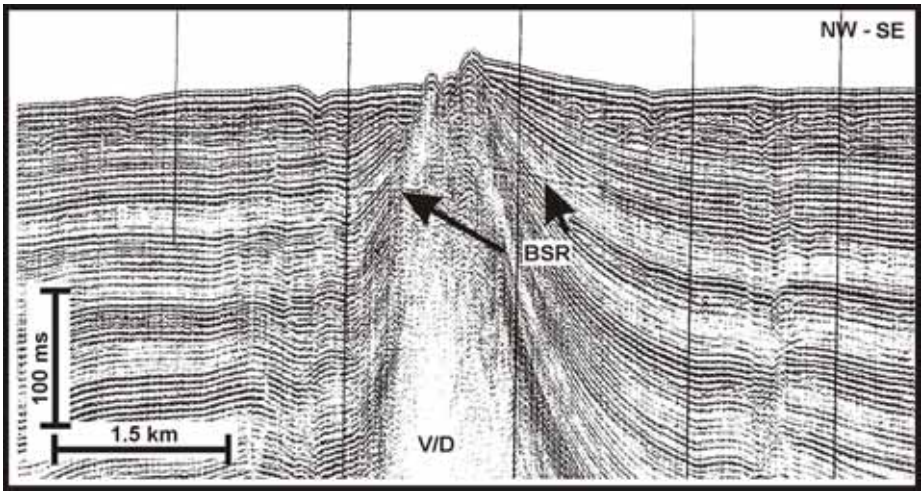

Fig. 8. Detail of an airgun seismic profile showing the location of the BSR-like feature around the top of a mud volcanoe/diapir (V/D). Seismic line in Fig. 1.

New examples of acoustic anomalies are found towards the SE along the upper slope of the Gulf of Cadiz, but these occur in locations where no diapirs or other gas-related features (pockmarks) appear. The more evident of these acoustic anomalies on the airgun seismic profiles appear in an area between the uppermost slope and the shelfbreak, between 140 and 220 m water depth (Fig. 9). The erosion caused by the strong Mediterranean Undercurrent affects the upper slope in this area. This is reflected in an irregular topography, the truncation of the reflectors of the surficial seismic units, the presence of seismic facies with acoustic signatures and features typical of high-energy environments, internal erosional surfaces, cut and fill features…etc. Under these reflections, an acoustic anomaly that cuts through the stratification extends for more than

12 km. The acoustic anomaly has a reverse polarity compared to the seafloor reflection, and appears paralleling the seafloor at a very continuous depth of 80 ms (Fig. 9). Assuming the above mentioned values for average sonic velocity and hydrostatic and lithospheric pressure gradients, these acoustic anomalies would, theoretically, develop at pressure conditions between 20,4 to 28 atm, and, given their location closer to Gibraltar Strait (and hence near the direct impact of the Mediterranean Undercurrent), under temperature conditions of pressure conditions between 12,4 and 14,4 ºC.

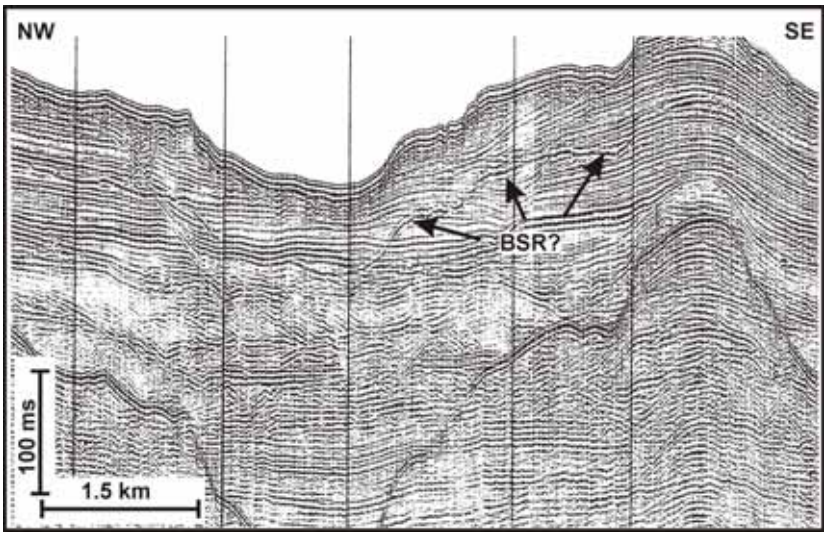

Fig. 9. Detail of an airgun seismic profile showing the location of the BSR-like feature, which mimics the morphology of the sea-floor. Seismic line in Fig. 1.

9. Discussion

The review of geophysical evidence that supports the presence of gas in the sediments of the Gulf of Cadiz slope by Baraza and Ercilla (1996), together the recent publications about direct evidence of gas on the Gulf of Cadiz (Kenyon et al., 2000; Mazaurenko et al., 2002; Somoza et al., 2002) have provided new information and evidence about the presence of gas and their origin.

Yun et al. (1988) infer the relative distribution of gas in the subsurface based on differences in seismic features displayed by the gas charged sediments: highly gas-charged areas, when the subsurface appears to be acoustically impenetrable; areas of

abundant gas, when acoustically turbid is present but coherent reflectors can be still discerned; and zones of sparse to no gas, where reflectors are coherent. In the sense of Yun et al. (1988) we may suggest that the concentration of gas within the area with charged sediment is higher in the central zones because the acoustic signal is totally obliterated; contrasting, the concentration is lower in the external zones because it is possible to see traces of acoustic reflections. The presence of free gas within the sediment could have played an important role in the formation of slumps. Free gas within sediment increases pore pressure and in consequence reduces its shear strength favouring sediment faulting and gas migration and expulsion (Kayen and Lee, 1993). In fact, enhanced reflections are still identified in proximal parts of slumps. Therefore, gas release can also occurs through the slump development, and not only through pockmarks.

The new analysis suggests the presence of pockmarks is not only related to sediment sorting whether they also seem to be related to diapirs. Baraza and Ercilla (1996) proposed that pockmarks occur where the near-surface sediments are sandier due to the action of the Mediterranean Undercurrent outflow (Nelson et al., 1999); the sandier sediments have high porosity allowing the interstitial gas escaping. We note that pockmarks presence could be related also to diapir structures. Recent studies have indicated that some of these diapirs correspond to mud volcanoes (Kenyon et al., 2000; Mazaurenko et al., 2002; Somoza et al., 2002). In fact, these studies have demonstrated the presence of gas hydrates, degassing structures, chemosynthetic fauna, and autigenic carbonates from samples recovered on the mud volcanoes. Our results also indicate the presence of gas and possible BSR features on the top of anticline structures. Then, we can tentatively consider that those pockmarks nearest to mud volcanoes/diapirs could be attributed to the expulsion of gas and/or fluids through migration paths related to the mud volcano/diapir structure. In fact, faults have been identified in the area where pockmarks develop (Baraza and Ercilla, 1996; Baraza et al., 1999). The fossilisation of the pockmarks at different depths would indicate gas and/or fluids expulsion was episodic, their activity ceased at different times and then migration paths also had a temporal character.

Baraza and Ercilla (1996) proposed a biogenic origin for the gas in the Gulf of Cadiz, resulting from the decay of organic matter contained within the rapidly developed regressive shelf-margin deltas. This origin can be attributed for the interstitial free gas identified in the uppermost slope area, where the shelf-margin deltas develop. But, recent geochemical data on gas-hydrate samples from mud volcanoes/diapirs indicate that gas has also a thermogenic origin (Mazurenko et al., 2002). Then, the origin of the gas

responsible of the pockmark formation can be both, biogenic for those pockmarks close to the gas-charged sediments, and thermogenic for those pockmarks adjacent to mud volcanoes/diapirs.

The analysis of bathymetric echosounder records indicates that the gas seepage area is present not only above the pockmark area, whether also above the gas-charged sediments. The presence of this acoustic anomaly in the water column above pockmarks is because the gas is venting through them. The presence of gas seepage above that area with free gas within the sediments could be linked to slump development (above mentioned) and permeability. Gas venting could occur through micro -faults and -fractures formed by elevated gas pressures and/or paths formed through interconnected pore spaces, which act as permeable conduits reaching the seafloor.

Some of the most interesting new data obtained from the detail review of acoustic records has been the identification of BSR-like reflections. In the following paragraphs we discuss in the detail the possible origin of this anomaly.

10. Origin of the BSR-like Reflections: Gas Hydrate Evidence?

The development of BSR-like reflections in the Gulf of Cadiz is constrained to very limited sectors of the upper slope that have some particular geological features. The most likely BSRs appear above anticline-like features and associated to mud volcanoes/diapirs (Figs. 5 and 8).

The P-T conditions in the area where the BSRs occur are apparently contradicted by their location on the hydrate P-T stability diagram, where their positions are not within the methane hydrate stability zone (Fig. 10). The Gulf of Cadiz acoustic anomalies plot on the areas of the P-T diagram where no stable gas hydrates are supposed to occur. Only one (maybe two) of the locations (those related to anticline or volcano/diapir structures) may really account for real BSRs caused by the presence of hydrates, providing that anomalous pressure or temperature conditions exist.

As shown on the seismic profiles, the lateral termination of the BSR appears to be very abrupt. But the seismic facies surrounding the BSR and the BSR-free sectors, which are related to overall changes in sediment type or composition, change sufficiently to explain this significant feature. Chemical composition of the gas could have displaced the hydrate stability field, but the high concentration of methane (81 %) measured in hydrates from a mud volcano in the Gulf of Cádiz by Mazurenko et al. (2002), does not explain

satisfactorily the BSR depths observed in this study (Lerche and Bagirov, 1998). Thus the pressure, the third critical component in the stability field of gas hydrate, and the deep structure of the area may be the responsible factors that we can tentatively consider.

Mud volcanoes/diapirs are commonly developed as a result of sediment deformation and fluid escape from underconsolidated sediments, under the weight of the overlying sediments or under tectonic stress. As a result of this, excess pore pressure develops which reduces the strength of the sediment and forces the sediment to deform and behave in a plastic way. Excess pore pressure can also dissipate along the sediment column in the vicinity of the diapirs, especially if geological discontinuities (such as faults or sharp lithologic contrasts) exist. Then, the pressure conditions in the vicinity of a mud/shale volcano/diapir may eventually differ (being locally higher), compared to the normal range controlled by the lithostatic/hydrostatic pressure conditions. However, there are examples that show that diapirs may have the opposite effect on the stability field of gas hydrates. The thermal conductivity of a salt diapir is greater than that of the surrounding muddy sediment, resulting in a local increase in heat flow away from the diapir and a compression of the isotherms above it (MacLeod, 1982). Contrasting, the low thermal conductivity of muds leads to a low temperature gradient which can contribute to the concentration of the hydrates at /or near the crests of the mud/shale diapirs (Barker, 1972; Lerche and Bagirov, 1998).

This process, in conjunction with the doming of the surrounding strata by the diapir, forms a trap for gas released by disintegrating gas hydrate above the diapir and gas migrating updip from strata surrounding the diapir. A fast decrease of pressure can, then, bring the hydrates to the zone of instability and, in such a case, explosive dissociation of the hydrates can occur, especially where their concentration is very high, resulting in the expulsion of gas onto the water column, where venting takes place and the formation of pockmarks occurs (Fig. 5). For instance, the tops of mud volcanoes/diapirs are very saturated in gas, then the gas in Gulf of Cadiz may get trapped by the doming of the gas hydrate-bearing sediment due to diapirism, as it has been observed in other areas (Dillon et al., 1980; Schmuck and Paull, 1993). Significant gas accumulations can then occur in the rotated strata around the diapirs, and above large diapirs in domed strata forming anticline-like structures. Gas occurrences in similar geologic settings have already been cited for the head of Cape Fear Slide area, US Atlantic margin (Schmuck and Paull, 1993).

The areas where the acoustic anomalies are not in relationship with diapir uplift or deformation do not appear to be the result of hydrate-bearing sediments (Fig. 9). The P-T conditions corresponding to the location of these anomalies are far from the stability conditions of hydrates, which makes very unlikely their interpretation as a result of impedance contrasts at the base of the gas hydrate. These anomalous reflections may be the result of some kind of reverberation of the received acoustic signals or their interaction with the geometry of the source-receiver-vessel system.

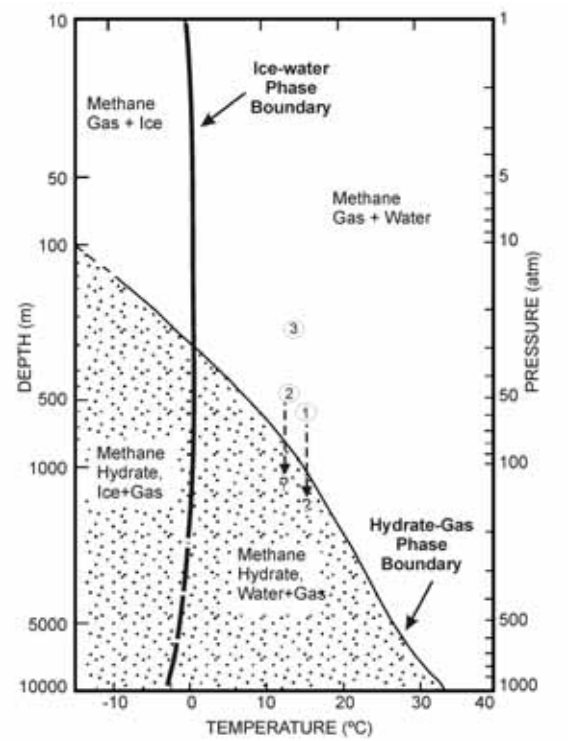

Fig. 10. Phase diagram showing the boundary between free methane gas (no pattern) and methane hydrate (pattern) for a pure water and methane system. Depth scale assumes lithostatic and hydrostatic pressure gradients of 10.1 kPa-1. (From Kvenvolden, 1998). The dots 1, 2 and 3 represent the local P-T conditions for the three examples BSR-like features discussed on the text. 1 corresponds to the BSR-like feature in Fig. 7, 2 in the Fig. 8 and 3 in Fig. 9.

11. Conclusions

1. The detailed review of the acoustic evidences previously identified in the Gulf of Cadiz has led to the acquisition of further evidence of the presence of gas. The gas-related features observed on the seismic records include acoustic turbidity and blanking, bright spots, ancient and modern pockmarks, high amplitude diffractions, acoustic plumes and turbidity in the water column, and BSRs.
2. This indirect evidence plus the recent sampling of sediment containing gas hydrate suggest the origin of the gas in the Gulf of Cadiz is not only biogenic as it has been suggested by Baraza and Ercilla (1996) whether thermogenic (Mazurenko et al., 2002).
3. The formation of pockmarks seems to be related to expulsion of biogenic gas and also to thermogenic gas coming from the volcanic/diapir fluids.
4. The emission of gas to the water column occurs through permeability conduits (micro -fractures and -faults and interconnected pore paths) in the area of gas charged sediment, and through slump and pockmark development.
5. The BSR-like acoustic anomalies occur intermittently in some areas of the upper slope, between 140 and 388 m water depth, and at 80 to 150 milliseconds (65 to 120 m) deep in the sediment column. This anomaly tends to occur in the vicinity of volcanoes/diapirs or immediately above anticline features formed as a result of diapir uplift.
6. The P-T conditions deduced for the location of the acoustic anomalies do not correspond to the conditions of stability of gas hydrates, although some of the observed examples plot close to the boundary between hydrates and free-gas. It is suggested that these diapiric intrusions may locally induce anomalously higher pore pressure conditions on the immediately surrounding sediments, affecting the stability field of the gas hydrates.

Acknowledgements

Geophysical data presented in this work were obtained within a co-operative project between the US Geological Survey, and the Spanish CSIC (Ref. CCA 8309/047). This report has been supported by the HYACE (MAS3-CT97-0102) and ANAXIMANDER (EVK3-CT-2002-00068) Projects.

References

Andreassen K, Hart PE, Grantz, A (1995) Seismic studies of a bottom simulating reflection related to gas hydrate beneath the continental margin of the Beafort Sea. J. Geophys. Res. 100: 12659-12673

Baraza J, Ercilla G (1996) Gas-Charged sediments and large pockmark-like features on the Gulf of Cadiz slope (SW Spain). Mar. Petrol. Geol. 13 (2): 253-261

Baraza J, Ercilla G, Nelson CH (1999) Potential geologic hazards on the eastern Gulf of Cadiz slope (SW Spain). Mar. Geol. 155: 191-215

Barker, PE (1972) Experiments on hydrocarbon gas hydrate in unconsolidated sand. In: Kaplan IR (ed) Natural Gases in Marine Sediments. New York, Plenum Press: 227-234.

Baringer MO, Price LF (1999) A review of the physical oceanography of the Mediterranean outflow. Mar Geol 155:63-82

Chow J, Lee J S, Sun R, Liu C S, Lundberg N (2000) Characteristics of the bottom simulating reflectors near mud diapirs: offshore southwestern Taiwan. Geo-Mar. Lett. 20: 3-9

Dillon WP, Grow JA, Paull CK (1980) Unconventional gas hydrate seals may trap gas off southeast US. Oil Gas J. 78: 124-130

Ercilla G, Casas D, Alonso B, Baraza J (2002) Acoustic evidences of gas-charged sediments, pockmarks, and BSRs on the Gulf of Cadiz slope sediments. IV Congress Gas in Marine Sediments. October, Baku, Azerbaijan

Field ME, Clarke SH, Kvenvolden, K (1980) Diapir-like ridges and possible hydrocarbon occurrence, northern California continental margin. Am. Assoc. Petrol. Geol. Bull. 64: 706

Gregory A (1977) Aspects of rock physics from laboratory and log data that are important to interpretation. In: Payton D (ed) Seismic Stratigraphy – Application of Petroleum Geologists Memoir 26: 15-46

Hernández-Molina FJ, Llave E, Somoza L, Hernández-Puga MC, Maestro A, León R, Medialdea T, Barnolas A, García M, Del Río V, Fernández-Salas LM, Vázquez T, Lobo Fº, Aveirinho JM, Rodero J, Gardner J (2003) Looking for clues to paleoceanographic imprints: A diagnosis of the Gulf of Cadiz contourite depositional systems. Geology 31(1): 19-22

Henriet JP, Mienert J (1998) Gas hydrate: the Gent debates. Outlook on research horizons and strategies. In: Henriet JP, Mienert, J (eds) Gas Hydrates. Relevance to world margin stability and climate change. Geol. Soc. Spec. Publ. 137: 1-9

Hovland M (1983) Elongated depressions associated with pockmarks in the western slope of the Norwegian Trench. Mar. Geol. 51: 35-46

Hovland M (1984) Gas-induced erosion features in the North Sea Earth Surf. Proc. Landforms 9: 209-228

Hovland M, Sommerville JH (1985) Characteristics of two natural seepages in the North Sea. Mar. Pet. Geol. 2: 319-326

Judd A, Davies D, Wilson J, Holmes R, Baron G, Bryden I (1997) Contributions to atmospheric methane by natural seepages on the U.K. continental shelf Mar. Geol. 137: 165-189

Judd A G, Curzi P V (2002) The rising influence of shallow gas: an introduction to the Bologna Conference on Gas in Marine Sediments. Cont. Shelf Res. 22: 2267-2271

Kayen RE, Lee HJ (1993) Slope stability in regions of sea-floor gas hydrate: Beafort sea continental slope. In: Submarine landslides: selected studies in the US exclusive economic zone. USGS Bul. 2002: 97-103

Kenyon NH, Ivanov M, Akhmetzhanov GC (2000) Multidisciplinary study of geological processes on the North East Atlantic and Western Mediterranean margins. Preliminary results of geological and geophysical investigations during the TTR-9 crusie of R./V Professor Logachev, June-July, 1999. IOC Tech. Series 56. UNESCO, Paris.

Kvenvolden K, Barnard L (1983) Hydrates of natural gas in continental margins. In: Watkings J, Drake C (eds) Studies in continental margins. AAPG Mem. 34: 631-640.

Kvenvolden K, McMenamin M (1980) Hydrates of natural gas: A review of their geologic occurrence. USGS Circular, 825.

Kvenvolden K, Ginsburg G, Solovyev V (1993) Worlwide distribution of subaquiatic gas hydrate. Geo-Mar. Lett. 13: 32-40.

Kvenvolden K (1998) A primer on the geological occurrence of gas hydrate. Henriet JP, Mienert, J (eds) Gas Hydrates. Relevance to world margin stability and climate change. Geol. Soc. Spec. Publ. 137: 9-30.

Lerche I, Bagirov E (1998) Guide to gas hydrate stability in various geological settings. Mar. Petrol. Geol. 15: 427-437.

MacLeod MK (1982) Gas hydrates in ocean bottom sediments. Am. Asoc. Petrol. Geol. Bull. 66: 2649-2662.

Madelain F (1970) Influence de la topographie du fond sur l'écoulement méditerranéen entre le Détroit de Gibraltar et le Cap Saint Vicent, Paris Cah. Océanogr. 22(1): 43-61

Maldonado A, Campillo AC, Mauffret A, Alonso B, Woodside J, Campos J (1992) Alborán Sea Late Cenozoic tectonic and stratigraphic evolution. Geo-Mar. Lett. 12: 179-186

Maldonado A, Nelson CH (1999) The Cadiz margin study off Spain: and introduction. Mar. Geol. 155: 3-8

Maldonado A, Somoza L, Pallarés L (1999) The Betic orogen and the Iberian-African boundary in the Gulf of Cadiz: geological evolution (central North Atlantic). Mar. Geol. 155: 9-43

Max MD (2000) Natural Gas Hydrate in Oceanic and Permafrost Environments. Max MD (ed) Kluwer Academic Publishers , 414 pp.

Max MD, Lowrie A (1993) Natural gas hydrates: Artic and Nordic Sea potential. In: Vorren TO, Bergsager E, Dahl-Stammes OA, Holter E, Johanse B, Lie E, Lund TB (eds) Artic Geology and Petroleum Potential. Proceedings of the Norwegian Petroleum Society Conference. Norwegian Petroleum Society (NPF) Special Publication 2 Elsevier, Amsterdam: 2753

Mazurenko LL, Soloviev VA, Belenkaya I, Ivanov MK, Pinheiro LM (2002) Mud volcanoes gas hydrates in the Gulf of Cadiz. Terra Nova 14(5): 321-329

McDonald G (1990) The future of methane as an energy resource. Annual Review of Energy 15: 53-83

Neben S, Hinz K, Beiersdorf H (1998) Reflection Characteristics, depth and geographically distribution of bottom simulating reflectors within the accretionary wedge of Sulawesi. In: Henriet JP, Mienert, J (eds) Gas Hydrates. Relevance to world margin stability and climate change. Geol. Soc. Spec. Publ. 137: 255-265.

Nelson, CH, Baraza J, Maldonado A (1993) Mediterranean undercurrent sandy contourites, Gulf of Cadiz, Spain. Sediment. Geol. 82: 103-131

Nelson CH, Baraza J, Maldonado A, Roderot C, Escutia C, Barber JH (1999) Late Quaternary seismic facies of the Gulf of Cadiz Spanish margin: depositional processes influenced by sea-level change and tectonic controls. Mar. Geol. 155: 99-130

Nisbet EG (1990) The end of ice age: Canadian Journal of Earth Sciences 27: 148-157

Paull CK, Dillon WP (1981) The appearance and distribution of the gas hydrate reflector off the southeastern United States. U.S. Geological Survey Open File Report 80-88. 24pp

Popenoe P, Schmuck E A, Dillon W P (1993) The cape Fear Landslide: Slope failure associated with diapirism and gas hydrate decomposition. In: Submarine Landslides: Selective Studies in the U.S. Exclusive Economic Zone. U.S. Geol. Survey Bull. 2002: 40-53

Riaza C, Martínez del Olmo W (1996) Depositional model of the Guadalquivir-Gulf of Cadiz Tertiary basin. In: Friend PF, Dabrio CJ (eds) Tertiary Basins of Spain. The Stratigraphic Record of Crustal Kinematics (World and Regional Geology, 6) Cambridge Univ Press, Cambridge: 330-338

Rodero J, Pallarés L, Maldonado A (1999) Late Quaternary seismic facies of the Gulf of Cadiz Spanish margin: depositional processes influenced by sea-level change and tectonic controls (Central North-Atlantic). Mar. Geol. 155: 131-156

Schmuck E A, Paull C K (1993) Evidence for gas accumulation associated with diapirism and gas hydrates at the head of the Cape Fear slide. Geo-Mar. Lett. 13: 145-152

Shipley T, Houston M, Buffler R et al. (1979) Seismic reflection evidence for the widespread occurrence of possible gas-hydrate horizons on continental slopes and rises. AAPG Bull. 63: 2204-2213

Sloan E D (1990) Clathrate Hydrates of Natural Gas. Marcel Dekker, New York.

Söderberg P, Flodén P (1992) Gas seepages, gas eruptions and degassing structures in the seafloor along the Stömma tectonic lineament in the crystalline Stockholm Archipelago, East Sweden. Cont. Shelf. Res. 112 (10): 1157-1171

Solhëim A, Elverhoi A (1993) Gas-related sea floor craters in the Barents Sea. Geo. Mar. Lett. 13: 235-243

Somoza L, Gardener JM, Díaz del Río V, Vázquez T, Pinheiro LM, Hernández-Molina FJ (2002) Bumerous methane gas-related sea floor structures identified in Gulf of Cádiz. EOS Transactions, Am. Geophys. U. 83 (47): 541-547

Taylor D I (1992) Nearshore shallow gas around the UK coast. Cont. Shelf. Res. 12 (10): 1135-1144

Wood W, Stoffa P, Shipley T (1994) Quantitative detection of methane through high-resolution seismic velocity analysis. J. Geophys. Res. 99: 9681-9695

Yunn JW, Orange DL, Filed ME (1999) Subsurface gas offshore of northern California and its link to submarine geomorphology. Mar. Geol. 154: 357-368

Zenk W (1970) On the temperature and salinity structure of the Mediterranean water in the N.E. Atlantic. Deep-Sea Res. 17: 627-632

CAPÍTULO 4

Physical properties and their relationship to texture and consolidation effects in Pliocene-Quaternary sediments from Madeira Abyssal Plain**.** D. Casas, G. Ercilla, J. Baraza, B. Coakley. *Marine Georesources & Geotechnology*. Enviado 2005. Aceptado 2006.

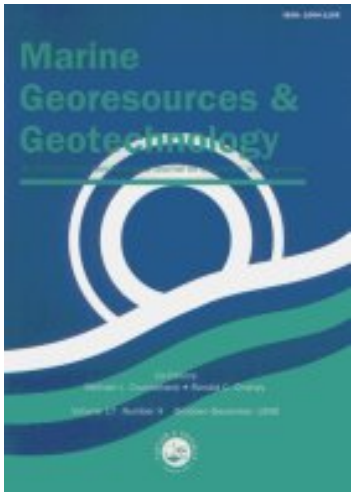

CAPÍTULO 4: PHYSICAL PROPERTIES AND THEIR RELATIONSHIP TO TEXTURE AND CONSOLIDATION EFFECTS IN PLIOCENE-QUATERNARY SEDIMENTS FROM MADEIRA ABYSSAL PLAIN

PHYSICAL PROPERTIES AND THEIR RELATIONSHIP TO TEXTURE AND CONSOLIDATION EFFECTS IN PLIOCENE-QUATERNARY SEDIMENTS FROM MADEIRA ABYSSAL PLAIN.

D. Casas[1*], G. Ercilla[1], J. Baraza[1], B. Coakley[2].

[1] Institut de Ciències del Mar-CSIC. P. Marítim de la Barceloneta, 37-49. 08003, Barcelona. SPAIN.
[2] Department of Geology & Geophysics**.** University of Alaska Fairbanks. P.O. Box 755780, Fairbanks AK 99775-5780.

***** Fax: +34 932309555/ davidc@icm.csic.es

Abstract

Multi Sensor Core Logger data and index properties were measured onboard the JOIDES resolution during ODP Leg 157 and compared with grain size distribution and carbonate contents measured in the on-shore laboratory. Cored sediments are similar in grain size, but very variable in carbonate content. Magnetic susceptibility clearly defines the volcanic turbidite layers, whereas GRAPE density and acoustic velocity help to define the coarser (silty) bases of some organic or calcareous turbidite layers. Index properties are mostly controlled by consolidation effects.

Keywords: physical properties, sediment texture, index property, shear strength.

1. Introduction

Physical properties of marine sediments are important variables to understand geological events of marine environments. Several studies have been conducted to examine the relationship between physical and textural parameters of marine sediments (Hamilton and Bachman, 1982; Orsi, Dunn, 1991; Weber et al., 1997; Kim et al., 2001). Sediment physical properties depend to a large extent on the lithology, the grain size and composition of the sediment (clay, quartz, biogenic carbonate, and silica) (Hamilton et al., 1982; Nobes et al, 1991). The wet-bulk density, for example, is related to porosity, grain density and is partially controlled by grain size (Johnson and Olhoeft, 1984). The acoustic velocity is controlled by porosity, carbonate and clay contents (Hamilton et al., 1982; Mienert, 1984; Nobes et al., 1986). Physical properties are also influenced by diagenetic effects, not only decrease of porosity with increasing compaction, but also cementation and carbonate dissolution (Nobes et al., 1992).

Continuous coring at sites *950a* to *952a* of ODP Leg 157 recovered more than 1000 m thick sediment sequence, from the deep floor of the Madeira Abyssal Plain (Fig. 1). Four lithologic units define the Eocene to Quaternary sedimentary stratigraphy of the Madeira Abyssal Plain (Schmincke et al. 1995). Unit I (Pleistocene to middle Miocene) consists of turbidite layers interbedded with pelagic nannafossil oozes. There are three primary types of turbidites (volcaniclastic, organic-rich and calcareous), originated from volcanic islands, northwestern African margin and seamounts respectivelly. Unit II (Middle Miocene) consists of massive calcarenite composed of coarse shallow-water carbonate clasts that originated from the seamount complex. Unit III consists of dominantly red pelagic clays interbedded with nanofossils and volcanic ash. Unit IV consists of two units of volcaniclastic siltstone and sandstone layers interlayered with a clay layer.

A continuous record of the physical properties of the sediments was acquired after core recovery, which have been published as preliminary results (Baraza et al., 1996; ODP Leg 157 Shipboard Scientific Party, 1995; Schmincke et al. 1995). More detailed observations of sediment physical properties are presented here, as well as the results of post-cruise sedimentological analyses. The aim of this paper is to determine the relationship of sedimentologic changes (composition and texture of turbiditic *vs.* volcaniclastic *vs.* pelagic sediments) with physical properties of the sediments recovered on the Madeira Abyssal Plain and compare these to similar effects caused by consolidation and diagenetic processes.

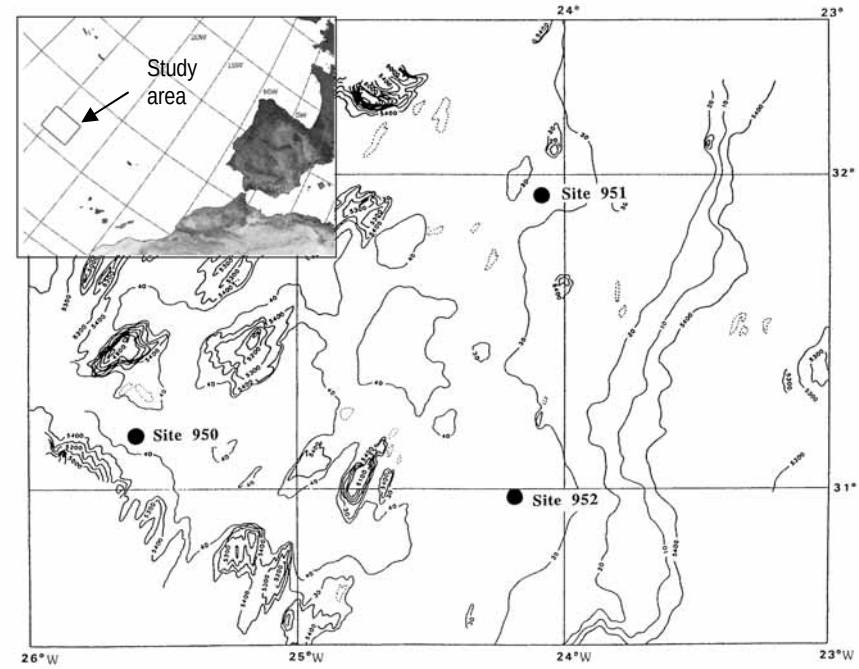

Fig. 1. Location map of ODP sites *950a*, *951a* and 952 in the Madeira Abyssal Plain.

2. Methodology

The methodology comprises measurements made on-board and post cruise laboratory analysis. The on-board measurements were made for physical and index properties of the types of sediments; the physical properties were continuously measured whereas the index properties were made on discrete samples. The post-cruise laboratory analysis was made on texture and composition of discrete samples. The samples were selected based on observations and preliminary sedimentological analysis made onboard (ODP Leg 157 Shipboard Scientific Party, 1995).

2.1. On-board measurements

2.1.1. Multi-sensor core logger

Continuous, non-destructive high-resolution measurements of physical properties were obtained by using a multi-sensor core logger (MSCL), at room temperature (22º).

The measured parameters include wet-bulk density (by Gamma Ray Attenuation, GRAPE), magnetic susceptibility (MS) and P-wave velocity (Shipboard Scientific Party, 1995; Weber, 1997). Typical sampling rate was one measurement every 1-2 cm for GRAPE, 5.10 cm for MS, and 2.5 cm for P-wave velocity measurement throughout the entire cores at sites *950a* to *952a*. The process of extended core barrel (XCB) coring creates an annular disturbance around the center of the core. Therefore, the cores recovered with this technique are partially disturbed and the data measured through the liner can be significantly affected (Pisciotto et al., 1990). Because this disturbance, P-wave velocity was measured only down to 160 mbsf (meters below sea floor) at *950a*, 118 mbsf at 951a, and 143 mbsf at *952a.* This study focuses on data obtained from the upper 200 mbsf on each site (Unit I), where the APC (advanced piston core) was used, minimizing core disturbance.

2.1.2. Discrete measurements

Discrete samples for physical properties were taken about once per section (about every 1.5 m) in holes *950a* to *952a*, with two main goals: (1) sampling was intended to include all lithologies present; and (2) samples selected were relatively undisturbed and intended to be representative of in-situ conditions. Discrete measurement of physical properties included index properties (porosity, wet density, dry density, grain density, and water content), as well as undrained shear strength and compressional-wave velocity (Shipboard Scientific Party, 1995). Index properties were determined by gravimetric techniques using the salt-corrected weights and volumes as outlined by Hamilton (1970) assuming an interstitial pore-water salinity of 35%.

In soft sediments, samples of 5 to 10 cm^3 of sediment were sampled with a syringe, and placed in precalibrated aluminium beakers. Mean sample weights were determined from multiple discrete weights by using a Scitech electronic balance to a precision of ±0.005 g with a confidence level of 99.5%. Sample volumes were determined using a helium-displacement Quatachrome Penta Pycnometer, with a precision of ±0.03 cm^3. The samples were placed in an oven for 24 hr at about 105ºC, and the dry weight and volume were again measured. More consolidated sediments were sampled by placing small chunks of the sediments in the calibrated cylinders and their weight and volume measured by repeating the preceding process. The calculation procedures to determine index properties, are detailed in "Explanatory Notes" chapter, Leg 151 (Shipboard Scientific Party, 1995).

The motorized vane shear (Wyckeham-Farrance, laboratory miniature vane shear device) and the handheld penetrometer (CL-700) were used to measure the sediment strength. The two instruments correlate well throughout over which both measurements were made. Measurements were performed at an average rate of one per core section during the first 100 mbsf, and every other section below this depth.

The undrained shear strength can be determined using a vane that is inserted into soft sediment and rotated until the sediment fails. Failure can be defined as the maximum principal stress difference, which is the same as the (unconfined) compressive strength of the specimen. At a prescribed strain, shear strength is related to compressive strength which is determined by reading the vertical strain, such us with the pocket penetrometer. The value must be divided by 2 to obtain the shear strength.

The undrained shear strength reported is the peak strength determined from the torque *vs*. strain plot (maximum value of torque recorded). In addition, the residual strength was determined from the same plot. After the peak strength the readings will decrease to a value that is more or less constant with continued rotation. This minimum value is a measure of the residual strength of the soil, that is, the strength of the soil after experiencing large strains.

For soft sediments, P -wave velocity was determined using a Digital Sound Velocimeter (DSV) of Dalhousie University/Bedford Institute of Oceanography (Mayer et al., 1987; Courtney and Mayer, 1993). For more consolidated material, measurements were made with the Hamilton Frame system on pieces of sample removed from the liner, usually along the axis of the core.

2.2. Post-cruise laboratory analyses

2.2.1. Grain-size analyses

As a first step, the sediment fraction (> 50 µ) was separated from the fraction (> 50 µ) by wet sieving. Subfractions (< 50 µ) were analyzed using a Sedigraph 5100D (Stein, 1985) using sodium hexametaphosphate for the dispersed medium. Subfractions (> 50 µ) were analyzed by means of a settling tube (Giró and Maldonado, 1987). These instruments measure the size distribution of particles dispersed in a liquid by assuming velocities of sinking particles in a viscose fluid using Stoke's law. The results of both measurements were integrated and the total distribution of size classes in the samples was calculated.

2.2.2. Calcium carbonate analyses

Calcium carbonate content in the samples was determined by the gasimetric method with a modified Bernard calcimeter, according to the method described by Vatan (1967). The bulk sample is pulverized to achieve total homogenization and is later attached with dilute HCl at atmospheric pressure. The weight percent of $CaCo_3$ in the sample is then calculated from the volume of CO_2 released.

3. Results

3.1. Multi-sensor core logger

3.1.1. GRAPE bulk density

Measured GRAPE density values of Leg 157 range between 1.25 and 2.0 g/cm^3, showing a large scatter. The downcore trend of average GRAPE density for the three holes is quite similar (Fig. 2). The values near the mudline vary between 1.27 g/cm^3 in site *950a* and 1.45 g/cc in sites *951a* and *952a* and increase continuously downcore to 1.75 - 1.80 g/cm^3 in the interval between 100 and 120 mbsf. Below this depth, the values show small variations. The downcore profile is centered around 1.75 g/cm^3 with some exceptions.

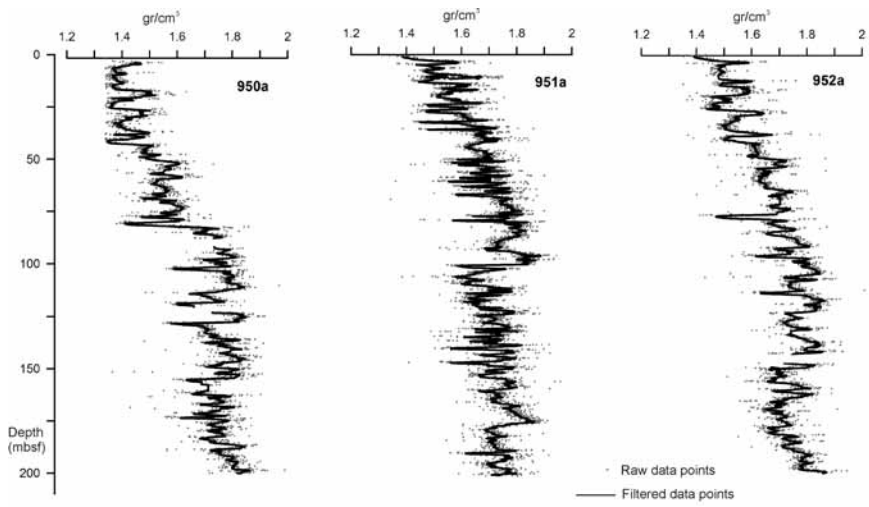

Fig. 2. GRAPE density profiles of the upper 200 mbsf of holes 950a, 951a and 952a.

A comparison among the p-wave velocity, magnetic susceptibility and density with regard to lithology (Fig. 3) shows that there is a sharp increase in density at the base of coarser-grained sediment layer (143 mbsf) that consist of volcanic or calcareous turbidite (1.8 to > 2.0 g/cm^3). The layer is interbedded between the lower density (avg. 1.65-1.70 g/cm^3), organic-rich turbidite layers. The major differences occur between 325-350 mbsf on site *950a* and 374-405 mbsf on site *952a*, where values between 1.8 and 2.0 g/cm^3 were recorded. These intervals correspond to more indurated sediments, either calcarenites, red clays or sandstones.

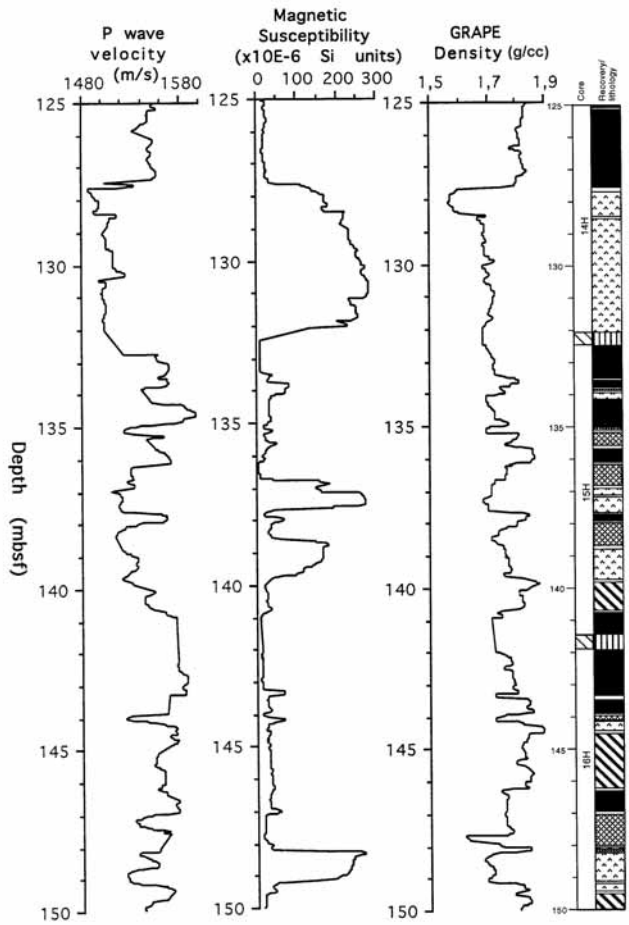

Fig. 3. Lithologic Log and MSCL record (P wave velocity, magnetic susceptibility, and GRAPE density) of a 25 m long section of hole 950a, from 125 to 150 mbsf.

3.1.2. Magnetic susceptibility

Magnetic susceptibility (MS) is a measure of the concentration of the magnetizable components within the sediment. Volume magnetic susceptibility (k) is a dimensionless ratio defined by the relation k=M/H, where M is a magnetization per unit volume induced by the applied magnetic field H (Collinson, 1983; Thompson and Oldfield, 1986). Magnetizable constituents of deep-sea sediments include ferromagnetic and paramagnetic minerals (compounds containing Fe^{2+}, Fe^{3+}, or Mn^{2+} ions, like clay minerals, particularly chlorite and smectite; ferromagnesian silicates like olivines, pyroxenes, biotite, and garnet); iron and manganese carbonates like siderite, ankerite, and rhodochrosite; and some iron sulphides like pyrite (Robinson, 1990; Sager and Hall, 1990). Therefore, downcore variations in the MS values of deep-sea sediments may reflect changes in lithology (proportion of biogenic -carbonate and silica to lithogenic -clay and labile minerals- components).

The susceptibility measurements of Leg 157 indicate that the recovered sediments are generally low in magnetic minerals and highly variable with depth, showing significant variations at a relatively fine scale probably related to changes in lithology. Susceptibility values at sites 950a to 952a show a back-ground level of about I to $20 \cdot 10^{-6}$ SI units, punctuated by high-amplitude spikes with values as great as 100 to $200 \cdot 10^{-6}$ SI units (Fig. 4). These peaks occur throughout the entire holes, but they are not uniformly distributed, nor can they be simply correlated between holes. The intervals of lower susceptibility coincide with the layers of thin (or absent gray) volcanic-rich turbidites and green (organic) or white (calcareous) turbidites and pelagite. The peaks of high magnetic susceptibility are correlated with gray, volcanic turbidites. Calcite and quartz are the dominant minerals in all sediments (ODP Leg 157 Shipboard Scientific Party, 1995), but differences in accessory mineral phases may account for the differences in magnetic susceptibility. Gray (volcanic) turbidites contain feldspar as an important component of the accessory phase, together with some clay minerals (illite, kaolinite, smectite, and some pyroxenes), contrasting with the other turbidites on which only illite, kaolinite, chlorite, or other clay minerals are present.

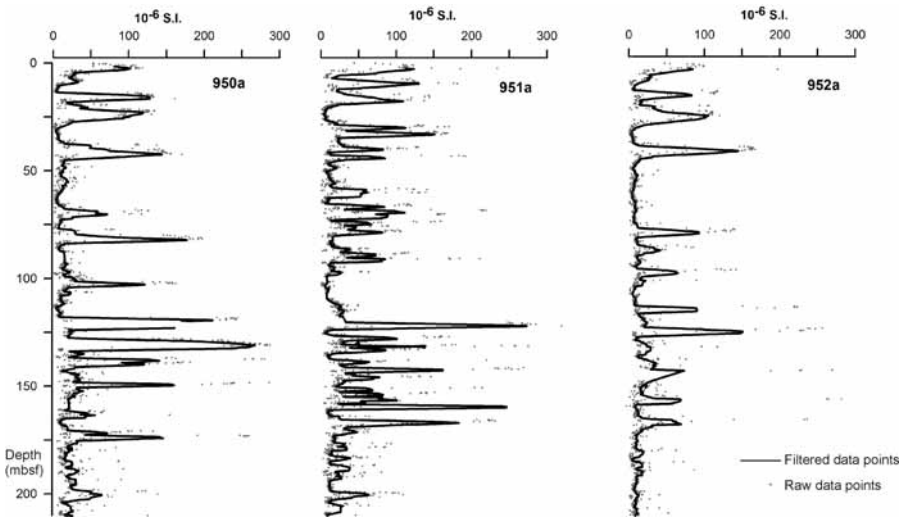

Fig. 4. Magnetic susceptibility profiles of the upper 200 mbsf os holes 5*950a*, 951a and 952a.

3.1.3. Acoustic velocity

An analysis of acoustic velocity is useful for geophysical modelling and interpretation, and may provide diagnostic information on the lithologic variations. Several studies have focussed on the relationship between acoustic velocity and porosity and lithology (Fulthorpe et al., 1989; Hamilton et al., 1982; Hamilton and Bachman, 1982; Mienert, 1984; Mienert et al., 1988; Nobes et al., 1986; Nobes et al., 1991), especially the dependence on clay and carbonate contents (Hamilton et al., 1982; Mienert, 1984; Nobes et al., 1991). Measured P -wave velocity values are anomalously low in cores and show a considerable scattering. Average acoustic velocities in holes *950a* to 952 are close to 1450-1475 m/s near the mudline and show a smooth downcore increase (1550 m/s) at 20 mbsf. Below this depth, there is an increase or decrease with a relatively homogeneous trend at about 1525 m/s (Fig. 5). In some cores, there are discontinuity measurements caused by core disturbance. Below 110 mbsf the average values of velocity are 1530 m/s and there is not a marked trend downcore. The most clear velocity discontinuities at the three holes can be correlated to thin pelagic intervals, where relative increases in velocity are recorded, as well as to the bases of some volcanic-rich turbidites intervals, where a relative decrease in velocity occurs.

3.2. Discrete measurements

The results of discrete physical properties measurement (bulk density, water content, and porosity) in the holes of the Madeira Abyssal Plain show in general a range of variability of index properties for normally consolidated, fine-grained deep-sea sediments. The downcore variation in the cores is indicative of gradual compaction of the sediment by increasing overburden, and shows information on compositional changes within the sediment. Furthermore, physical properties show a close relationship to the lithologic units in the different holes and also provide information for a further lithological differentiation within lithologic units (Shipboard Scientific Party, 1995).

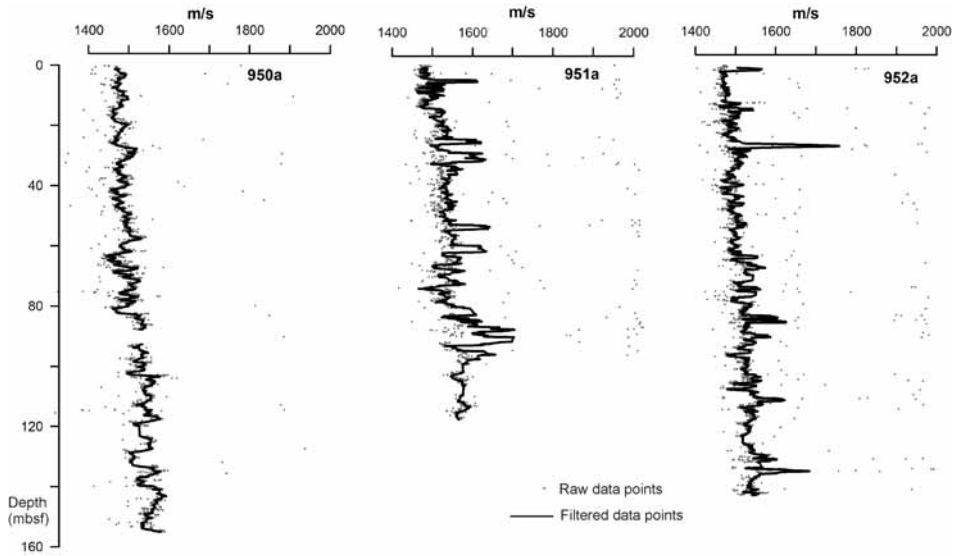

Fig. 5. P-wave velocity record of the sites *950a* (from 0 to 150 mbsf), 951a (from 0 to 120 mbsf) and 952a (from 0 to 140 mbsf).

3.2.1. Water content and porosity

Both water content and porosity decrease downcore. The rate of decrease is variable, probably related to major lithologic changes (Figs. 6, 7). The higher values of porosity (80%) occur at the surface and major decrease in water content and porosity occur below 100/120 mbsf. At this interval, porosity decreases by an average of 40%, from 80% at 0 mbsf to 35-60% at 100/ 120 mbsf. Water content decreases by a 20%, from 56% at 0 mbsf to 35% at 100/120 mbsf. Below this depth the rate decreases to about 200 mbsf. At this depth, porosity averages 52% and mean water content is 29%. In the upper

part, 100/120 mbsf, porosity and water content decrease by 20-40%. In the following 100 mbsf the average decreases to 4% for porosity and 6% for water content.

At three sites, variations in water content and porosity show a very similar but reversed pattern with wet-bulk density.

3.2.2. Bulk density

Between 0 and 200 mbsf the bulk density at holes *950a* to *952a* increases steadily downcore from a minimum value of about 1.45 g/cm^3 just beneath the sea floor to a maximum value of about 1.95 g/cm^3 (Fig. 8). Bulk density varies downcore the rate of change is within the top 100 mbsf it increases to about 1.80 g/cm^3 and then, it maintains a value between 110 and 200 mbsf. The highest bulk density (from 1.85 to 2.08 g/cm^3) corresponds to the relatively coarse-grained layers of volcaniclastic or calcareous turbidite intervals. The typical downcore profile of increasing bulk density (Fig. 8) and decreasing porosity and water content with depth (Fig. 6), suggests that the dominant process within the sediment in the upper 200 mbsf is the gravitational compaction from overburden pressure. The slower rate of decrease/increase in these index properties below 100/120 mbsf implies that sediments below that depth are almost completely consolidated.

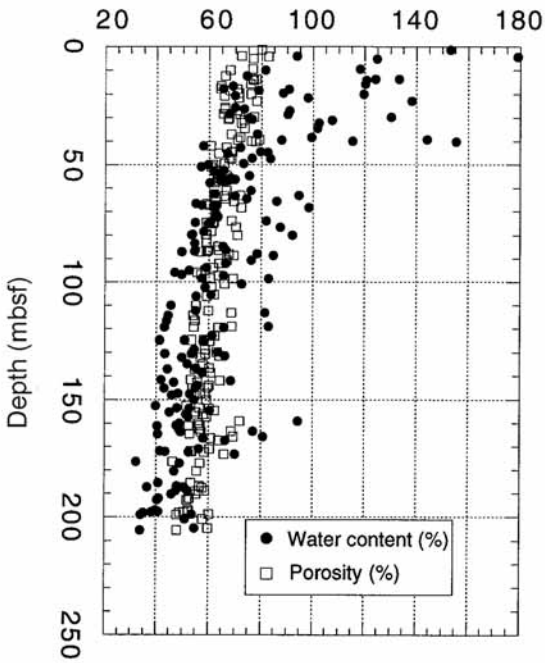

Fig. 6. Variation of water content and porosity *vs.* depth for all three holes *950a*, *951a*, and 952a.

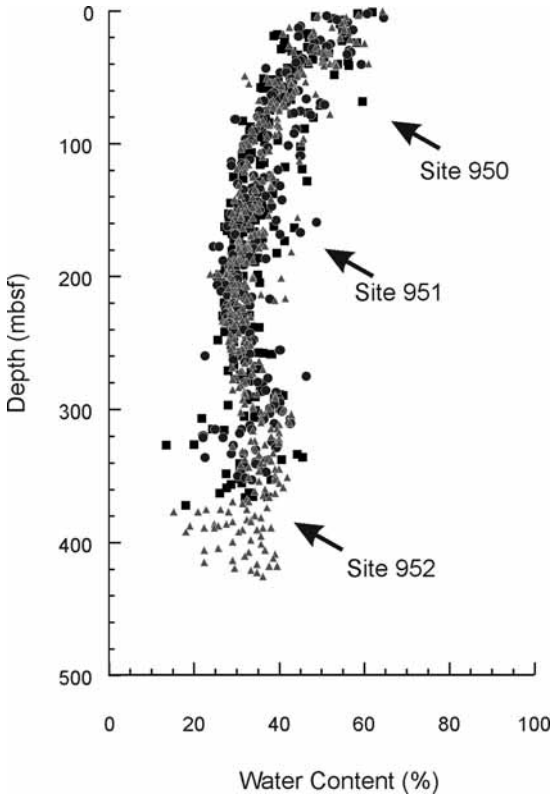

Fig. 7. Downcore variation of water content for sites *950a*, *951a*, and *952a*. Solid squares, solid circles and gray triangles represent samples from sites *950a*, *951a* and *952a*, respectively.

3.2.3. Grain density

Grain density depends on the minerals that form the sediment. It usually does not have a characteristic depth trend. The grain density profile shows, however, a marked trend downcore in holes 950a to 952a, which must be related to compositional changes in the sediment at a basin scale. Grain density profiles in holes *951a* and *952a* are quite similar, but they differ notably with respect to the profile measure for hole 950a, especially in the upper 220 mbsf (Fig. 9).

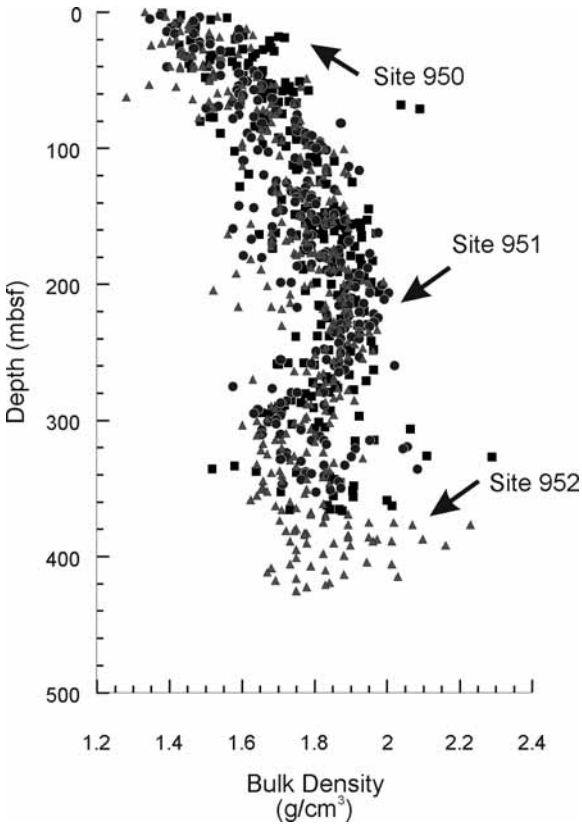

Fig. 8. Downcore variation of bulk density for sites *950a*, *951a* and *952a*. Solid squares, solid circles and gray triangles represent samples from sites *950a*, *951a* and *952a*, respectively.

In hole 950a grain density value decreases steadily down core from an average value of 2.86 g/cm^3 near the sea floor to an average value of 2.72 g/cm^3 at approximately 150 mbsf. The rate decreases below 100 mbsf, and below about 140 mbsf. Below 140 mbsf there is a sharp increase to an average value of 2.80 g/cm^3, decreasing to 2.77 g/cm^3 at 175 mbsf and then increasing again to 2.80 g/cm^3 at 200 mbsf. In holes 951a and 952a grain density values at the top are 2.68 g/cm^3 (average), and show a continuous increase to about 2.73 g/cm^3 at 100 mbsf. At this depth a relative discontinuity occurs together with a high scattering that continues down to 200 mbsf. The average grain density seems to decrease to 2.70 g/cm^3 at 125 mbsf, and then to increase again to 2.80 g/cm^3 at 200 mbsf. The larger values of grain density correspond to the silty and sandy intervals of turbidite beds.

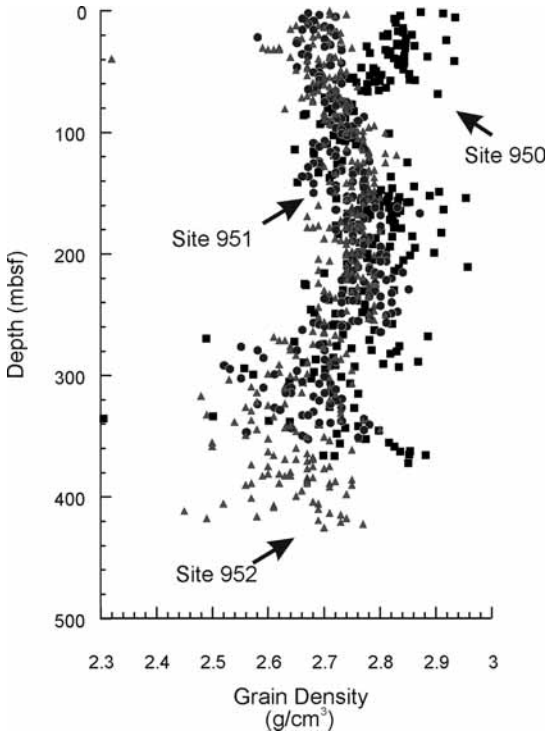

Fig. 9. Downcore variation of grain density for sites *950a*, *951a*, and *952a*. Solid squares, solid circles and gray triangles represent samples from sites, *950a*, *951a*, and *952a*, respectively.

3.3. Undrained shear strength

The measurements of laboratory vane shear strength were made at the interval between 85.7 m depth in hole 950a (Shipboard Scientific Party, 1995) and 167, 180 and 189 mbsf at holes 950a, 951a and 952a, respectively. Further downcore the hand-held penetrometer was used until the sediment strength exceeded its measuring limits (approximately 250 kPa). Both types of strength measurements were used simultaneously for 150 to 180 m in the holes (951a). A good correlation was observed between the data obtained by the two methods, although penetrometer readings tend to give higher values than those obtained with the laboratory vane shear and a large scatter of results.

Data obtained in the three holes show an expected trend of increasing strength downcore from near 0 kPa at the mudline to 200-230 kPa between 200-260 mbsf (Fig. 10). In some cases, strength variations seem to correspond to specific sediment types or lithologic changes within the turbidites. For instance, low strength values (50-100 kPa), e.g. below 200 mbsf in hole 950a, correspond to the weaker nannofossil-rich beds,

whereas in hole *952a* the deeper carbonate turbidites were strong or even stronger than the interbedded clay-rich turbidites, suggesting a change in the primary composition or perhaps the diagenetic history between the two holes.

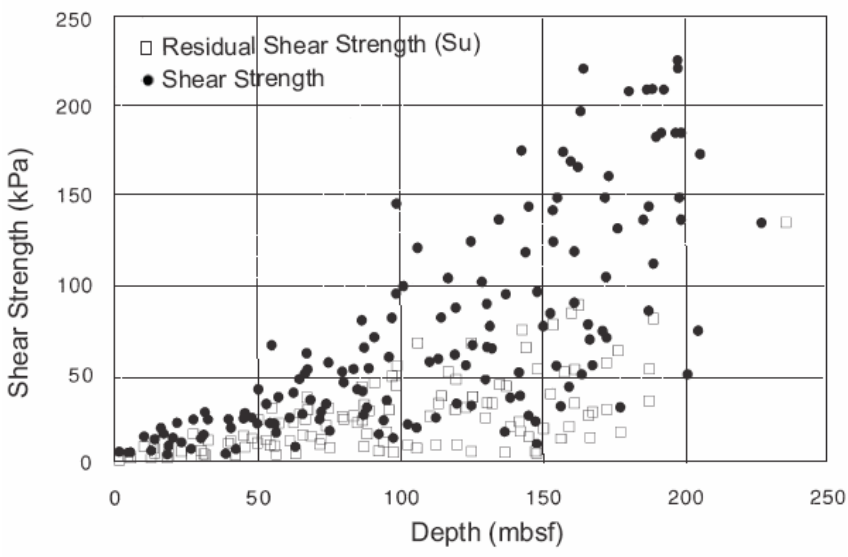

Fig. 10. Shear strength and residual strength *vs.* depth for holes *950a*, 951a, and 952a.

4. Post-cruise Laboratory Analyses

4.1. Grain-size distribution

Results of grain-size analysis show homogeneity of grain-size distributions among all three sites. Attending to the percentages of the three main size-fractions, most of the analyzed samples are classified as silty clays with only small amounts of sand (less than 17%). Mean silt content is about 23%, but it varies between 5 and 40%. Only three samples fall within the clayey silt range (silt content 53-64%), and one sample is sand (68%) with a small silty-clayey fraction. Figure 11 shows a triangular plot of these results, on which almost all samples fall just above the silt-clay axis. Mean grain sizes mainly vary between 8 and 9.6 phi although a small group of coarser samples from 4.5 to 7.2 phi is also identified (Fig. 12). The sandier samples are taken from near the base of some calcareous turbidite intervals, whereas those with higher silt content correspond to the lower section of organic or volcanic turbidites. The fine grain-size and low variability

observed for the samples is a reflection of the distal depositional environment where these turbidites accumulated.

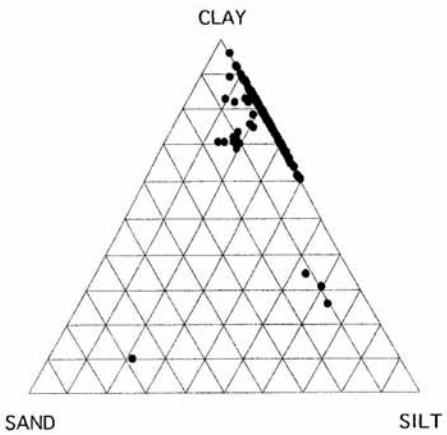

Fig. 11. Ternary diagram of sand, silt and clay percentages obtained from the analysed samples of all three holes *950a*, 951a, and 952a.

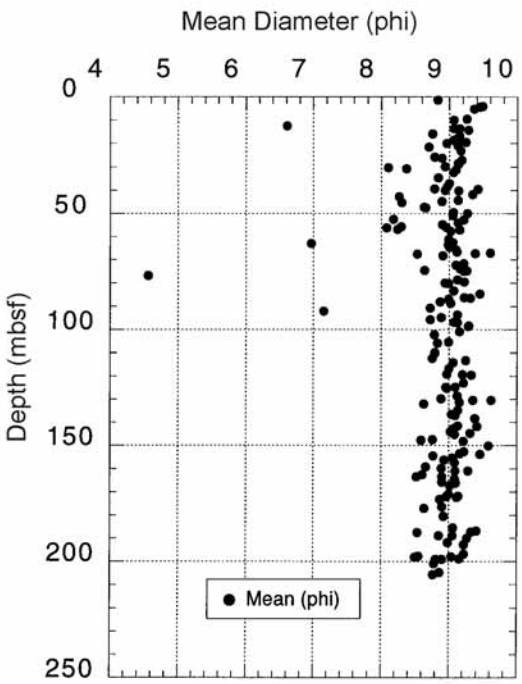

Fig. 12. Mean grain size diameter of samples *vs.* depth in holes *950a*, 951a, and 952a.

4.2. Carbonate content

Carbonate contents at the three sites range between 5% and 93%. Carbonate contents are greater than 40% in 85% of samples (Fig. 13) and a group of samples show especially high carbonate values (>75%) allowing the differentiation of certain sediment types based on this parameter. The higher carbonate contents correspond to the calcareous turbidites and to the nannofossil oozes that constitute some of the pelagic intervals. The reduced number of samples having the larger sand contents (generally less than 15%) are also characterized by higher carbonate contents (>80%) suggesting their initial attribution to basal foraminiferal sands of calcareous turbidite intervals based on GRAPE density data.

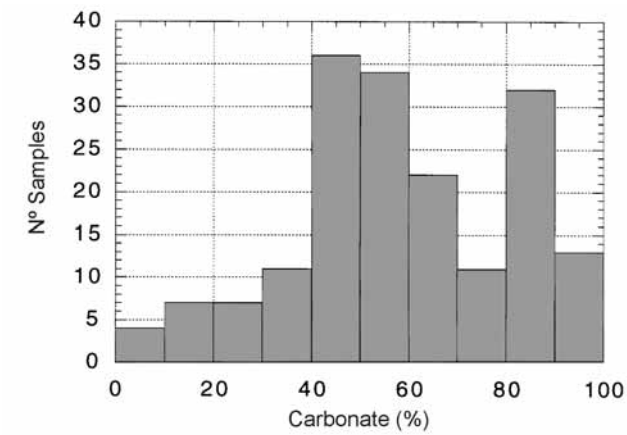

Fig. 13. Histogram representing the number of samples with carbonate contents for 10% intervals.

5. Discussion

5.1. Relationships among multi-sensor core logger

The turbidites that constitute the sedimentary record of Madeira Abyssal Plain, in spite of being quite easy to differentiate by visual observation due to differences in colour, they are very similar in respect to specific sedimentological aspects. They are all very fine grained and homogeneous, in contrast there are clear differences in other sedimentological or compositional aspects (i.e. carbonate content, mineralogy... etc).

These differences may be relevant to the physical identification of specific sediment types. The analysis of the high resolution MSCL data allows to identify relationships between these different physical properties and the corresponding sediment types.

In the present study, a marked correlation has been observed between some of the physical parameters measured with the MSCL sensors and the different lithologies recovered. In general, highs in magnetic susceptibility correspond to lows in GRAPE density and P-wave velocity. The core sections characterized by the highest magnetic susceptibility values always correspond to volcanic turbidite layers, whereas organic-rich turbidites show the lowest magnetic susceptibility and highs in density and velocity (Fig. 3). The larger peaks in GRAPE density always correspond to the coarser (silty) bases of some of the volcanic and organic-rich turbidite intervals. Calcareous- and intermediate turbidite-type intervals have values of physical properties typically within the range between the organic and volcanic intervals.

5.2. Index property-sediment relationships

Index properties are volumetric parameters calculated from the wet and dry weights and volumes of the samples. But the relationships between some of the index properties are also controlled by lithology, especially the grain density which is the only parameter that depends mostly on the mineralogy of the samples. Grain size laboratory analysis have shown that, despite the variability suggested by the differences visually observed among the turbidite types, almost all sediment types recovered are of similar size-range, with the exception of the bases of some thick turbidite intervals which contain large proportions of silt- or sand-size particles. Because of this low variability of sediment grain sizes, it is suggested that the major contribution to the variability observed on the physical properties would be controlled by either chemical/mineralogical variations or to processes related to the consolidation of the sediment by overburden.

5.3. P-wave velocity

Plots of velocity *vs.* porosity are particularly useful for distinguishing the state of consolidation of sediment *vs.* the extent of diagenesis. The compressional wave velocity behaviour of high porosity, unconsolidated sedimentary deposits is primarily controlled by properties of the pore fluid (Wood, 1941). In general, increasing consolidation in soft sediments tends to increase velocity through a decrease in porosity, which leads to increasing grain contact, whereas cementation produces a velocity increase through

increased rigidity of the sediment with little or no reduction in porosity (Willye et al., 1956; Dadey and Klaus, 1992). On a plot of velocity *vs.* porosity measurements of sediments from Leg 157 (Fig. 14) we observed a general trend to increase velocity as porosity decreases. Higher porosity samples (porosity between 65-82%) show velocities between 1510 and 1460 cm/sec, respectively. P-wave velocity increases at a higher rate for samples with porosities lower than 60%. A corresponding increase in P-wave velocity is observed for sediments with higher bulk densities (Fig. 15). In this case, a linear correspondence and a relatively good correlation exist for all two measurements. These observations suggest that, in the upper 200 mbsf of the holes, depth (i.e., increased consolidation) is a significant factor affecting the physical properties of the sediment, especially the velocity.

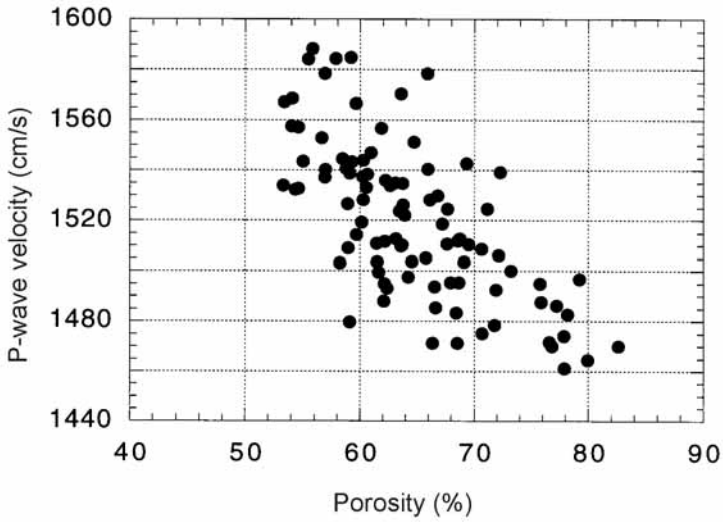

Fig. 14. Comparison of porosity *vs.* P-wave velocity for all samples.

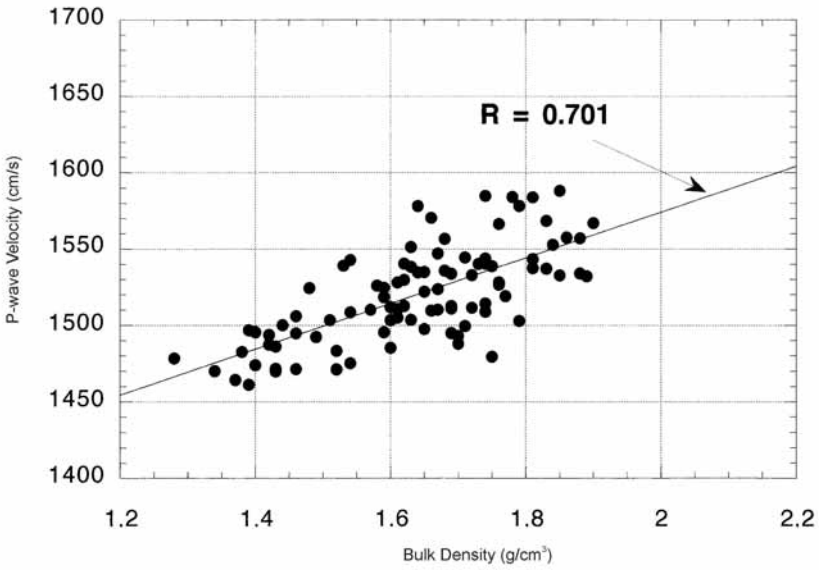

Fig. 15. Bulk density *vs.* P-wave velocity for all samples.

5.4. Bulk density

A plot of bulk density *vs.* porosity (Fig.16) for three holes shows that most samples follow a linear trend in which the higher porosities correspond to low bulk density samples. The linear regression through the sediments gives an equivalent grain density of 2.791 g/cm3, which is a little higher than the grain density of the more common constituents of sediments, like quartz (2.64 g/cm3) and calcite (2.71 g/cm3). The regression confirms that onboard measurements are somewhat imprecise. The linear trend shows lower porosities than those expected for bulk density. This lack of correspondence may be partially due to the relative uncertainties on calculating the volume of the high water content samples.

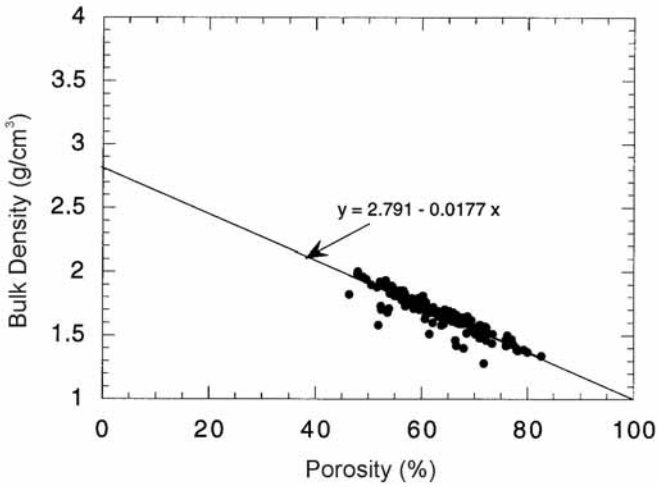

Fig. 16. Porosity *vs.* bulk density for all samples.

5.5. Carbonate content

Carbonate content is a parameter that normally has a major influence over the physical properties of the sediment. Silica and clay minerals in general have higher porosities than calcareous sediments, so increases in carbonate contend tend to be correlated with decreases in porosity (Nobes et al., 1991). Similar relationships are observed between bulk density and carbonate content (Hamilton et al., 1982). This relationship is not clear for the sediments recovered during Leg 157. A plot of carbonate content *vs.* porosity for all analyzed samples (Fig. 17) shows a scatter, where the higher porosities correspond to samples with intermediate values of carbonate. The only identifiable difference is that low carbonate samples are more dispersed, whereas intermediate- and carbonate-rich samples plot more clustered around certain values of porosity. The effect of porosity decrease by compaction with increasing depth of overburden is superimposed, and almost completely overwhelms, the effect probably caused by the carbonate content on the sediment. A plot of carbonate *vs.* grain density (Fig. 18) confirms that both parameters are independent of each other, as samples of varying carbonate content fall aligned along a horizontal line corresponding to a grain density of 2.79 g/cm^3. Grain density values are more scattered for the samples low in carbonate. This is a partially due to the fact that clay minerals have highly variable grain

densities, although the more common forms (illite, kaolinite and montmorillonite) have average grain densities of 2.6 to 2.7 g/cm^3. (Johnson and Olhoeft, 1984).

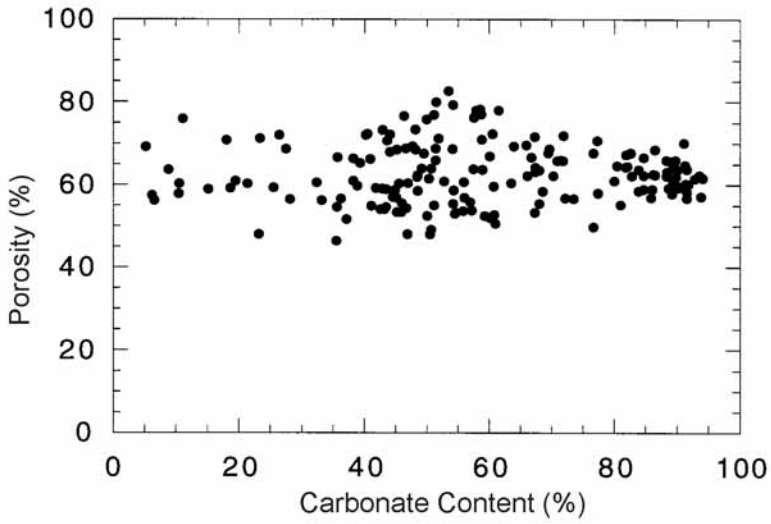

Fig. 17. Carbonate content *vs.* porosity for all samples.

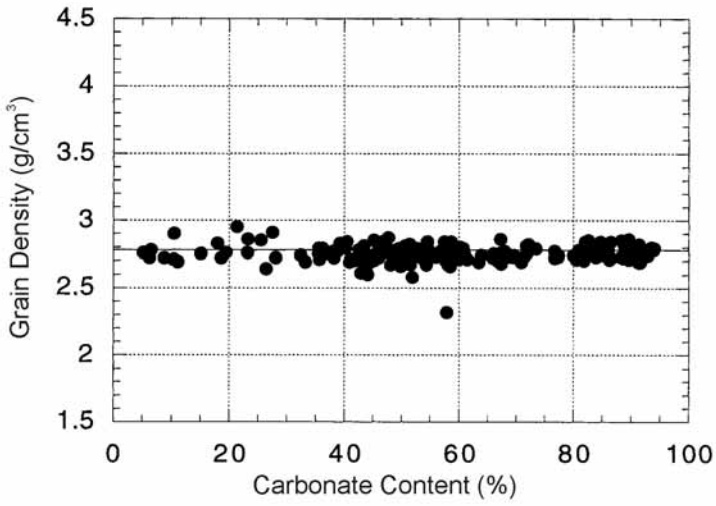

Fig. 18. Carbonate content *vs.* grain density for all samples.

5.6. Shear strength

Progressive consolidation due to overburden results in an expulsion of interstitial water and an increase of friction between particles on the sediment. The reduction of porosity and water content by progressive consolidation is the major factor controlling the increase in shear strength with depth (Schmincke et al., 1995). A plot of shear strength *vs.* water content for samples from all holes (Fig. 19) shows the higher strength values for samples having water content around 40% and a sharp decrease in strength as water content increases to 60%. Shear strength variations are smaller for samples with water contents between 70 and 150%. Part of these variations could be related to changes in cohesive forces developed in the clayey-rich sediments due to variations in the clay mineralogy, for instance. But it has to be noted that the laboratory vane shear apparatus was designed for use with clayey sediments with shear strengths less than 100 kPa, and some of the turbidite sediments recovered on Leg 157 have shear strength values exceeding that value. The scatter of strength data for values over 100 kPa is illustrated on Fig. 20, where shear strength is plotted against residual strength for each measurement. With the exception of a group of samples, a good correlation and continuity in data are observed between the two measurements for values up to 80 kPa, but above this value data points are scattered and the correlation in not so well defined. The control of the sediment strength by the consolidation of the sediments can also be deduced by the relationship between shear strength and P-wave velocity, a parameter that is commonly related to consolidation or diagenesis of the sediment (Dadey and Klays, 1992). Figure 21 represents the strength and corresponding value of P-wave velocity for each sample. A non-linear but progressive increase in P-w velocity is observed for increasing strength values, although some scattering exists, especially for strength values above 80 kPa.

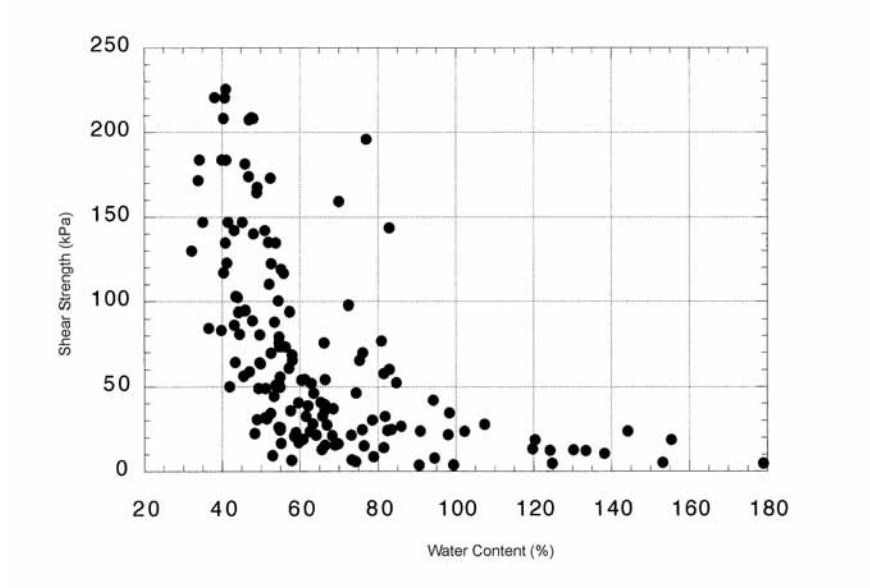

Fig. 19. Water content *vs.* shear strength for all samples.

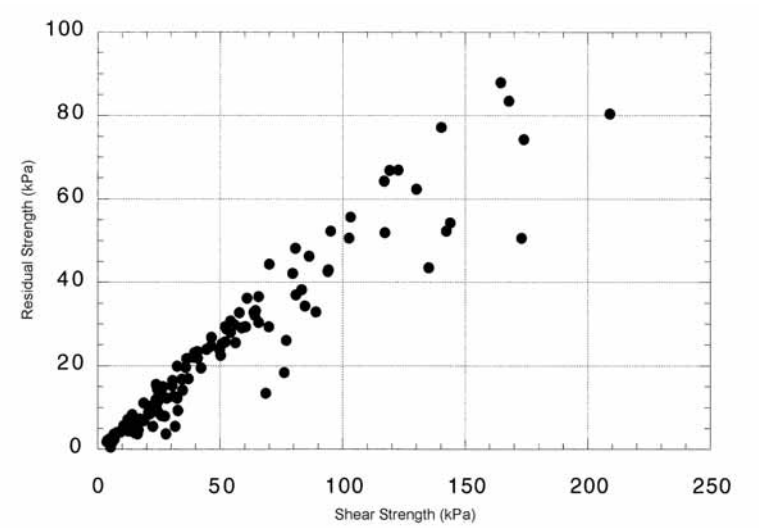

Fig. 20. Shear strength compared to residual strength for all samples.

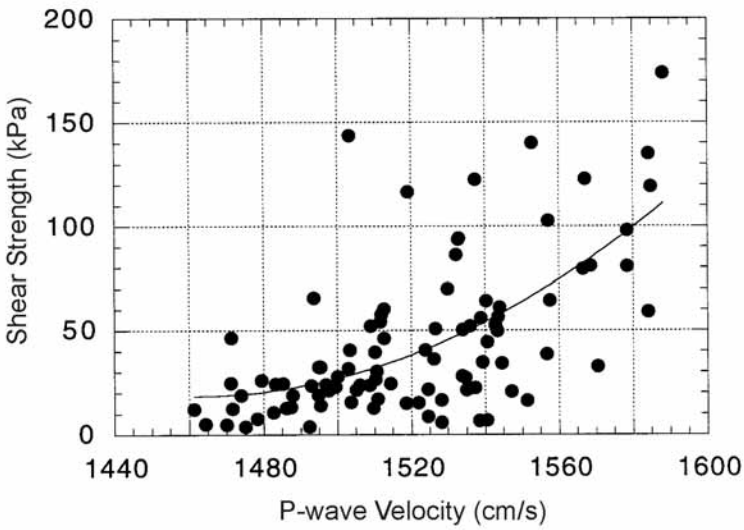

Fig. 21. P-Wave velocity *vs.* shear strength for all samples.

6. Conclusions

1. The physical properties of the upper 200 m of the sedimentary infill of Madeira Abyssal Plain are controlled by the degree of compaction, rather than by changes in lithology.

2. High-amplitude peaks of magnetic susceptibility clearly differentiate between the highly magnetizable, volcanic-rich turbidites and the low magnetic organic and calcareous turbidites. Differences in magnetic susceptibility appear to be related to changes in the mineralogical assemblage of the accessory phases.

3. GRAPE density and P-wave velocity appear mostly related to consolidation effects, but at a detailed scale shows variations related to the presence of thin, coarser-grained (silty) bases of some calcareous or organic-rich turbidite intervals.

4. Variations in grain density do not have a defined downcore trend, but they are mostly related to changes in composition (especially silica and carbonate) and primary bulk mineralogy. Grain densities are relatively higher in the volcanic turbidite intervals.

5. Index properties variations are mostly related to the decrease in porosity and increase in bulk density of the sediment due to compaction by overburden. Nevertheless, changes in the rate of downcore increase/decrease of given index properties, or sharp breaks in the downcore trends may be related to compositional changes (carbonate and silica content).

6. Carbonate content does not correlate with changes in porosity and grain density, and does not show any particular effect on the variation of physical properties of the sediments.

ACKNOWLEDGMENTS

This work was founded by the European Commission ANAXIMANDER project (EVK3-2001-00123), and by the “Ministerio de Ciencia y Tecnología” MARCONI (REN2000-0336-C03) project and MARSIBAL (REN2001-3868-C03) project. The support of these people and institutions is gratefully acknowledged. David Casas thanks the Generalitat de Catalunya for the PhD grant (1999FI 00002CSIC PG).

References

Baraza, J. and ODP Leg 157 Shipboard Scientific Party. 1996. Physical properties of sediments from Madeira Abyssal Plain: results from ODP Leg 157. Geogaceta 20 (2): 146-148.

Collison, D.W. 1983. Methods in Rock Magnetism and Paleomagnetism: Techniques and Instrumentation. London: Chapman and Hall.

Courtney, R.C. and L.A. Mayer. 1993. Calculating acoustic parameter by a filter correlation method. J. Acoust. Soc. Am. 93: 1145-1154.

Dadey, K. A. and A. Klays. 1992. Physical properties of volcaniclastic sediments in the Izu-Bonin area. In Taylor, B., Fujioka, K., et al., Proc. ODP, Sci. Res., 126: College Station, TX (Ocean Drilling Program): 543-550.

Fulthorpe, C.S., Schlanger, S.O. and R.D. Jarrard. 1989. In situ acoustic properties of pelagic carbonate sediments on the Ontong Java Plateau. J. Geophys. Res. 94: 4024-4032.

Giró, S. and A. Maldonado. 1987. Análisis granulométrico por métodos automáticos. Tubo de sedimentación y Sedigraph. Acta Geol. Hispánica 20 (1): 95-102.

Hamilton, E.L. 1970. Sound velocity and related properties of marine sediments. J. Geophys. Res. 75: 4423-4446.
Hamilton, E.L. and R.T. Bachman. 1982. Sound velocity and related properties of marine sediments. J. Acoust. Soc. Am. 72: 1891-1904.

Hamilton, E.L., Backman, R.T., Berger, WH., Johnson, T.C. and L.A. Mayer. 1982. Acoustic and related properties of calcareous deep-sea sediments. J. Sediment. Petrol. 52: 733-753.

Johnson, G.R. and G.R. Olhoeft. 1984. Density of rocks and minerals. In: Carmichael, R.S. (Ed.), CRC Handbook of Physical Properties of Rocks (Vol. 3): Boca Raton, FL (CRC Press, Ins.): 1-38.

Kim, D. C., Sung, J. Y., Park, S. C., Lee, G. H., Choi, J. H., Kim, G. Y., Seo, Y. K. and J. C. Kim. 2001. Physical and acoustic properties of shelf sediments, the South Sea of Korea. Mar. Geol. 179: 39-50.

Mayer, L.A., Courtney, R.C. and K. Moran. 1987. Ultrasonic measurements of marine sediment properties. Proc. Oceans´87: 1-139.

Mienert, J. 1984. The importance of carbonate content in the acoustic stratigraphy of Panama Basin. Mar. Geol. 54: 237-247.

Mienert, J., Curry, W.B. and M. Sarnthein. 1988. Sonostratigraphic records from equatorial Atlantic deep-sea carbonates: paleoceanographic and climatic conditions. Mar. Geol. 83: 9-20.

Nobes, D.C., Villinger, H., Davis, E.E. and L.K. Law. 1986. Estimation of marine sediments bulk physical properties at depth from seafloor geophysical measurements. J. Geophys. Res. 91: 14033-14043.

Nobes, D.C., Mienert, J. and G.J. Dirksen. 1991. Lithologic control of physical-property interrelations. In: Ciesielski, P.F., Kristoffersen, Y., et al., Proc. ODP, Int. Repts., 114: College Stations, TX (Ocean Drilling Program): 657-669.

Nobes, D.C., Langseth, M.G., Kuramoto, S., Holler, P. and N. Hirata. 1992. Comparison and correlation of physical-property results from Japan Sea Basin and Rise sites, legs 127 and 128. In: Tamaki, K., Suyehiro, K., Allan, J., McWilliams, M., et al., Proc. ODP, Int. Repts., 127/128, Pt. 2: College Station, TX (Ocean Drilling Program): 1275-1296.

ODP Leg 157 Shipboard Scientific Party. 1995. Gran Canaria Volcanic Apron and Madeira Abyssal Plain Drilled. EOS, Transactions, Am. Geophys. Union 76, 40.

Orsi, T.H., and D.A. Dun. 1991. Correlations between sound velocity and related properties of glacio-marine sediments: Barents Sea. Geo-Mar Lett. 11: 79-83.

Pisciotto, K., Tamaki, K., et al., 1990. Proc. ODP, Int. Repts. 127: College Station, TX (Ocean Drilling Program).
Robinson, S.G. 1990. Application for whole-core magnetic susceptibility measurements of deep-sea sediments: Leg 115 results. In: Duncan, R.A., Backman, J., Peterson, L.C., et al., Proc. ODP, Int. Repts., 115: College Station, TX (Ocean Drilling Program): 737-771.

Shipboard Scientific Party. 1995. Site *950a*. In: Scmincke, H.U., Weaver, P.P.E., Firth J.V., et al., Proc. ODP, Int. Repts., 157: College Station, TX (Ocean Drilling Program): 51-105.

Sager, W.W. and S. Hall. 1990. Magnetic properties of black mud turbidites from ODP Leg 116, distal Bengal Fan, Indian Ocean. In: Cochran, J.R., D.A.V et al., Proc. ODP, Int. Repts., 116: College Station, TX (Ocean Drilling Program): 317-336.

Scmincke, H.U. Ewaver, P.P.E., Firth, J.V. et al. 1995. Proc. ODP, Int. Repts., 116: College Station TX (Ocean Drilling Program).

Stein, R. 1985. Rapid grain size analyses of clay and silt fraction by Sedigraph 5000D: comparison with Coulter Counter and Atterberg methods. J. Sediment. Petrol. 55: 590-615.

Thompson, R. and F. Oldfield. 1986. Environmental Magnetism. London: Allen and Unwin.

Vatan, A. 1967. Manuel de Sédimentologie. Paris: Technip.

Weber, M., Niessen, F., Kuhn, G. and M. Wiedicke. 1997. Calibration and application of marine sedimentary physical properties using a multi-sensor core logger. Marine Geology 136: 151-172.

Willye, M.R.J., Gregory, A.R. and L.W. Gardner. 1956. Elastic wave velocities in heterogeneous and porous media. Geophysics 21: 41-70.

Wood, A.B. 1941. A Textbook of Sound. London: G.L. Bell.

CAPÍTULO 5

Physical properties and their relationship to sedimentary processes and texture in sediments from mud volcanoes in the Anaximander Mountains (Eastern Mediterranean). D. Casas, G. Ercilla, V. Lykousis. *Scientia Marina*. Enviado 2005. Aceptado 2006.

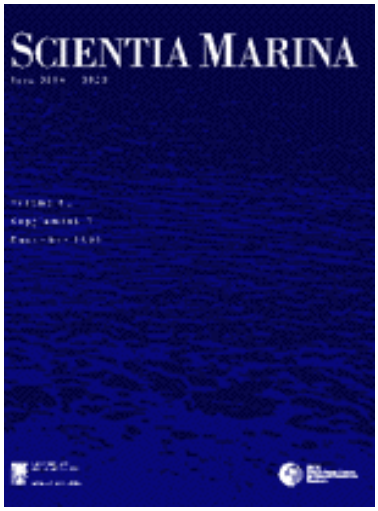

CAPÍTULO 5: PHYSICAL PROPERTIES AND THEIR RELATIONSHIP TO SEDIMENTARY PROCESSES AND TEXTURE IN SEDIMENTS FROM MUD VOLCANOES IN THE ANAXIMANDER MOUNTAINS (EASTERN MEDITERRANEAN)

PHYSICAL PROPERTIES AND THEIR RELATIONSHIP TO SEDIMENTARY PROCESSES AND TEXTURE IN SEDIMENTS FROM MUD VOLCANOES IN THE ANAXIMANDER MOUNTAINS (EASTERN MEDITERRANEAN).

David Casas[1], Gemma Ercilla[1], Vasilis Lykousis[2], Chryssanthi Ioakim[3], Constantine Perissoratis[3]

[1]Institut de Ciències del Mar-CSIC. Passeig Marítim de la Barceloneta. 37-49. Barcelona. Spain.
[2] National Centre for Marine Research- NCMR. Ag. Kosmas, Elliniko, 16604 Athens. Greece.
[3] Institute of Geology & Mineral Exploration.70 Messoghion St. Athens 11527, Greece.

Abstract

This research focuses on the mud volcanoes Amsterdam, Kazan and Kula located in the Anaximander Mountains (SW Turkey continental margin), which are characterized by the presence of sediments containing gas and gas hydrate. These mud volcanoes were sampled by recovering four gravity cores. For sediment located right on top (crater or active part of the summit) of the mud volcanoes, the physical properties are controlled by lithology and mud volcanic processes rather than degree of compaction. This could suggest the possibility of current mud volcanic activity. By contrast, the sediment located in the external flank of Kula mud volcano displays physical properties mostly related to consolidation effects and to the type of sediment at a detailed scale, as occurs typically in deep-sea fine grained sediments. This suggests a restricted influence of mud volcanic processes.

Keywords: Anaximander, Mud volcano, physical properties, sediment texture, index property, gas.

1. Introduction

This research project focuses on the mud volcanoes Amsterdam, Kazan and Kula (Fig.1), which are located in the Anaximander Mountains (SW Turkey continental margin) and are characterized by the presence of gas and gas hydrates (Woodside *et al .,* 1998; Lykousis *et al* .,. 2003; Lykousis *et al* .,. 2004; Werne *et al* ., 2004). The term mud volcanism refers to an array of sedimentary processes that result in the extrusion of argillaceous material, and occur both on land and on the seafloor (Milkov, 2000). The presence of mud volcanoes is associated with the presence of high seafloor methane fluxes as well as with the accompanying cold vents, seeps (Charlou *et al.,* 2003), carbonate crusts (Aloisi *et al .,* 2002) and gas hydrates under certain conditions. Therefore, they play an important role in scientific issues such as sediment stability, climate and environmental studies, and the interplay between microbial life and fluid seepage (Olu *et al .,* 2004).

Physical properties of marine sediments are important variables for an understanding of geological events in marine environments and play an important role in determining the nature of fluid and gas migration, which in turn affects the nature of microbial communities and gas hydrate formation. Several studies have been conducted to examine the relationship between physical and textural parameters of marine sediments (Orsi and Dunn, 1991; Weber *et al.*, 1997; Kim *et al.*, 2001; Casas *et al.*, 2004). Sediment physical properties depend to a large extent on lithology, grain size and the proportion of different components of the sediment (e.g. clay, quartz, biogenic carbonate and silica) (Hamilton *et al.*, 1982; Nobes *et al.*, 1991). The wet-bulk density, for example, is related to porosity and grain density, and is partially controlled by grain size (Johnson and Olhoeft, 1984). The acoustic velocity is controlled by porosity and carbonate and clay contents (Hamilton *et al.*, 1982; Mienert, 1984; Nobes *et al.*, 1986). Physical properties are also influenced by diagenetic effects, especially by the decrease in porosity with increasing compaction, but also by cementation and carbonate dissolution (Nobes *et al* ., 1992).

This research project addresses detail analysis and relationships of physical properties and sedimentological characteristics of the sediments containing gas hydrate recovered on mud volcanoes from the Anaximander Mountains (Fig.1). In particular, the aim of this work is to define the type of sediments associated with mud volcanoes, to establish the processes which formed them, and to determine the effects of sedimentological changes on the physical properties of these sediments.

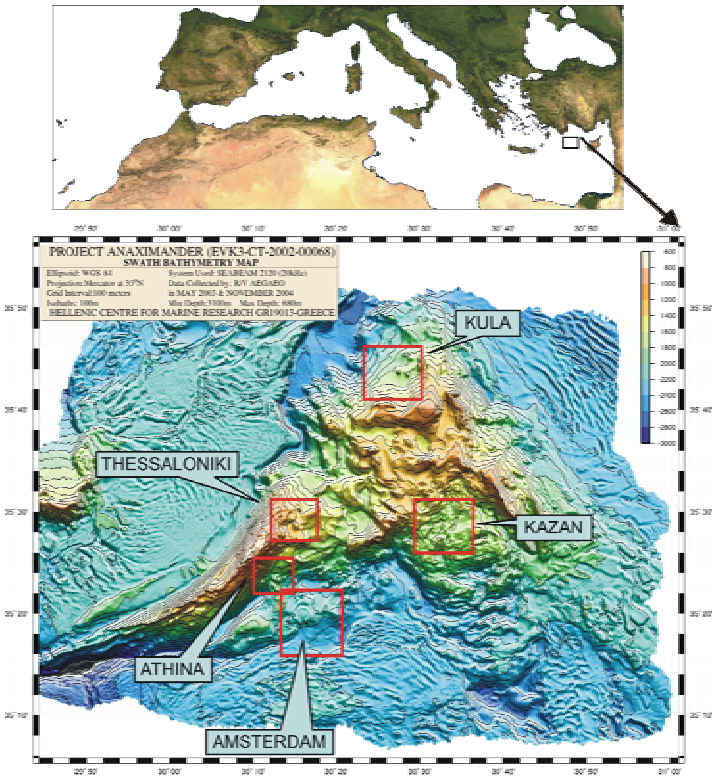

Fig. 1. Map showing the location of the Anaximander Mts.

2. Geological Setting

The Anaximander Mountains are located in one of the most rapidly subsiding sections of the Mediterranean (Fleming, 1972), where interaction between the Anatolian and African Plates takes place. These mountains are currently undergoing a neotectonic deformation phase characterized by strike slip faulting with subsidiary normal faulting and some minor thrusts within a zone of accommodation between the above-mentioned plates (McClusky *et al .,* 2002; Zitter *et al .,* 2003; Ten Veen at el., 2004). At least seven mud volcanoes (such as Amsterdam, Kula and Kazan) have been observed in the area, and more than 25 dome-like mud volcanoes have been identified (Woodside *et al*., 1997, 1998; Lykousis *et al* ., 2004*)*. The three mud volcanoes under study (Fig. 2) appear respectively as elliptical (about 100 m high and 3 km width), hemispherical (about 80 m high and 1 km width) and irregular (about 50 m high and 800 m width) reliefs (Zitter *et al* ., 2005). Their origin is associated with the structural situation characterized by a compression zone that favours the expulsion of overpressured fluids at the surface. There

are several acoustic evidences in the area that suggest the presence of gas in the sediments, such as acoustic turbidity, acoustic wipe-outs and pockmarks. Likewise, sediment containing interstitial free gas, gas hydrate, and carbonate crusts have been recovered on these volcanoes (Woodside *et al* ., 1988; Lykousis *et al* ., 2003).

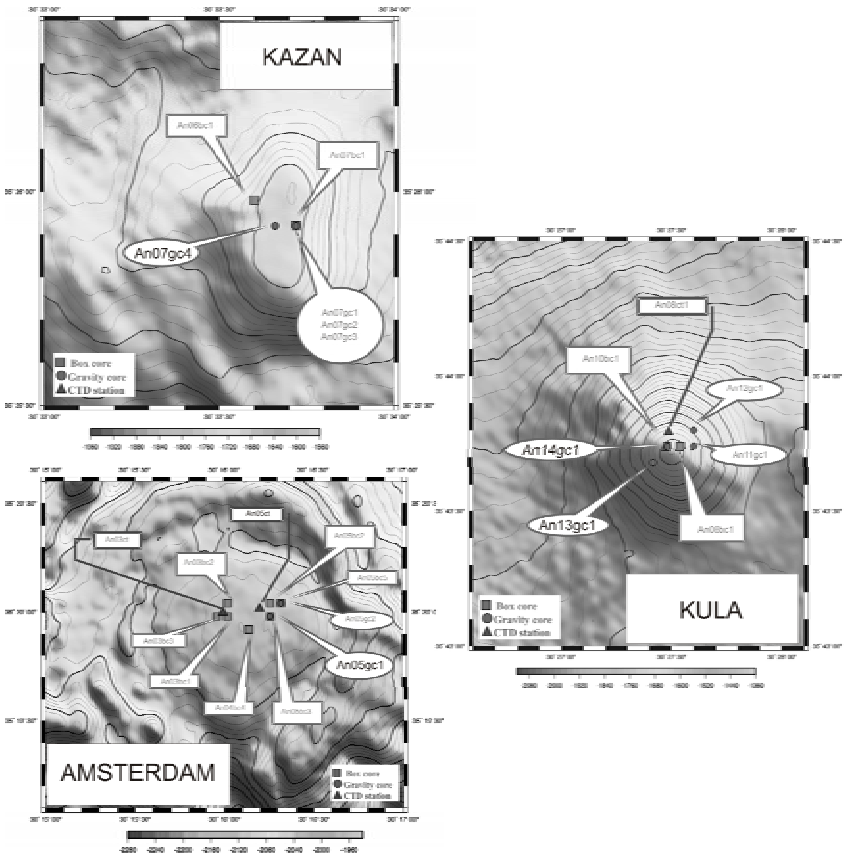

Fig. 2. - Amsterdam, Kula and Kazan mud volcanoes, showing the location of all cores recovered from each volcano. The location of the four cores under study has been highlighted.

3. Methodology

The present study was carried out on four gravity cores (An05GC1, An07GC4, An14GC1 and An13GC1, Table 1) recovered on the Amsterdam, Kazan and Kula mud volcanoes (Fig. 2) during the first cruise of the European project Anaximander, onboard the R/V *Aegaeo* of the Hellenic Centre for Marine Research. The laboratory methodology comprised measurements made in order to determine the textural and compositional

characteristics and the physical and index properties of the types of sediments. Textural and compositional analysis and index property measurements were made on discrete samples, whereas the physical properties comprise continuous measurements.

The textural analysis gives information about the grain-size of sediments which is of great interest for determining the mechanism of transport and deposition. Textural analysis on selected samples was conducted by hand sieving for the > 2000 μ fraction, settling tube (Giró and Maldonado, 1987) for the 2000 to 50 μ fraction, and Sedigraph 5100D (Stein, 1985) for the < 50 μ fraction.

Continuous, non-destructive high-resolution measurements of whole-round core sections were obtained with the Multi-Sensor Core Logger (MSCL). The measured parameters include wet-bulk density (by Gamma Ray Attenuation, GRAPE), magnetic susceptibility (MS) and P-wave velocity (Weber, 1997). The typical sampling rate was about one measurement every 1 cm.

Compositional analysis is important in order to determine the nature and origin of sediments. This analysis comprised the determination of the sand fraction composition and calcium carbonate content. The composition of the sand fraction was determined by visual identification and by counting 350 grains per sample with the use of a binocular microscope. Calcium carbonate content in the samples was determined by the gasimetric method with a modified Bernard calcimeter, according to the method described by Vatan (1967).

Discrete measurements of physical properties include the index properties water content, grain density, porosity and undrained shear strength. The index properties were determined by gravimetric techniques using the salt-corrected weights and volumes as outlined by Hamilton (1970), assuming an interstitial pore-water salinity of 35‰. Soft sediments were sampled and placed in precalibrated aluminium beakers. Mean sample weights were determined using an electronic balance. Sample volumes were determined using a helium-displacement AccuPyc 1330 Pycnometer. The samples were oven-dried for 24 h at about 105ºC, and the dry weight and volume were again measured. Porosity was calculated combining the index properties of discrete samples (grain density) and Gamma-ray density (MSCL). Porosity (Φ) and density (ρ_b) are related by the following equation using grain density (ρ_g), which was on average 2.7 g/cm^3, and pore-water density (ρ_w), which was assumed to be 1.025 g/cm^3

$$\Phi = (\rho_g - \rho_b)/(\rho_g - \rho_b)$$

The undrained shear strength (S_u) of soft cohesive sediments was measured with a Wyckeham-Farrance motorized vane shear device.

Core	Core length	Depth	φ	λ	Mud Volcano
An05gc1	131 cm	2030 m	35° 20' 002	30° 16' 263	Amsterdam
An07gc4	148 cm	1700 m	35° 25' 908	30° 33' 689	Kazan
An13gc1	81 cm	1636 m	35° 43' 701	30° 27' 400	Kula
An14gc1	85.5 cm	1636 m	35° 43' 716	30° 27' 502	Kula

Table 1. Location, depth of analysed cores and their location on mud volcanoes.

4. Results

4.1. Sedimentology

The four cores studied (Figs. 3, 4, 5, 6.) are located in different sedimentary environments. Cores An05GC1, An07GC4 and An14GC1 are sited inside the crater of the Amsterdam, and in the active summit of Kazan and Kula mud volcanoes respectively. Core An13GC1 is sited at the outflowing masses that form the external flank of the Kula volcano. Table 1 presents the details of the core locations. The stratigraphy of cores An05GC1, An07GC4 and An14GC1 comprises mud breccias (Figs. 3, 4, 6.) characterized by a muddy, matrix-supported and very poorly sorted sediment with angular to subangular clasts of mudstone of different compositions and grain sizes (0.5 to 2.5 cm). General porous gas-release structures are the predominant sedimentary structure. This is because disseminated gas hydrate was recovered in this type of sediment, but it dissociated during the sampling operation or minutes later onboard, when its stable P-T conditions changed (Kvenvolden, 1993; Pellenbarg and Max, 2000). Shells of bivalves (*Lucinoma kazani*) were observed in the top of core An05GC1. This mollusc is typically associated with cold seep venting in the eastern Mediterranean (Salas and Woodside, 2002) and described in other mud volcanoes in the area as "Athina" m.v. (Lykousis *et al* ., 2006).

By contrast, core An013GC1 (Fig. 5.) is defined by mud breccia which toward the top changes to hemipelagic mud (50 cm thick); the contact between the two types of sediment is sharp and the top of the mud breccia (firsts 12 cm) is oxidized. Within the hemipelagic sediments, an organic-rich (black) bed between 15 to 33 cmbsf (centimetres below sea floor) is identified as the early Holocene sapropel S1 (Rijk *et al* ., 1999).

The results of the grain-size analysis on the muddy matrix of the mud breccia and hemipelagic mud show low variability of grain-size distributions among cores. According to the percentages of the three main size-fractions, most of the analyzed samples are classified as silty clays (55-67% of clay) and clayey silts (46% silt), with only small amounts of sands (7%) and gravels (<10%). Mean grain sizes mainly vary between 5 and 8.7 phi.

The sand fraction of mud breccia is basically characterized by terrigenous components (Fig. 7A.). The average value of total terrigenous components ranges between 89 and 99%. They are essentially quartz, light minerals, rock fragments and a maximum of 7% oxidised pyrite (Fig. 7B). In core An05GC1 a greater relative weight of rock fragments can be observed, with a maximum of 32%. The sand fraction of hemipelagites shows the highest percentage of biogenic components, with values close to 100%. These components are basically planktonic foraminifera (Fig. 7C).

Calcium carbonate contents of mud breccias have average values of < 29%, showing small differences between the cores. In the hemipelagic muds the average carbonate value is 34%, with a maximum value of 49% (Fig. 8).

4.2. Physical properties

4.2.1. Bulk density

Measured density values range between 1.2 and 2.1 g/cm^3, but the values show a large scattering which may partially correspond to fine-scale lithologic variations. In spite of the variable profile marked by many spikes, the downcore trend of average density for cores An05GC1, An07GC4 and An14GC1 is quite similar. Therefore, density values vary between 1.46 g/cm^3 in An05GC1, 1.49 g/cm^3 in An07GC4 and An14GC1 near their tops, and 1.27 g/cm^3 in An05GC1, 1.45 g/cm^3 in An07GC4 and 1.48 g/cm^3 in An14GC1 near their bottoms (Figs. 3, 4, 6). Only the core An13GC1 showed a general trend to increase down core (Fig. 5). In this core, density value was 1.4 g/cm^3 near the top, increasing down core to 1.58 g/cm^3 from 75 and 80 cmbsf.

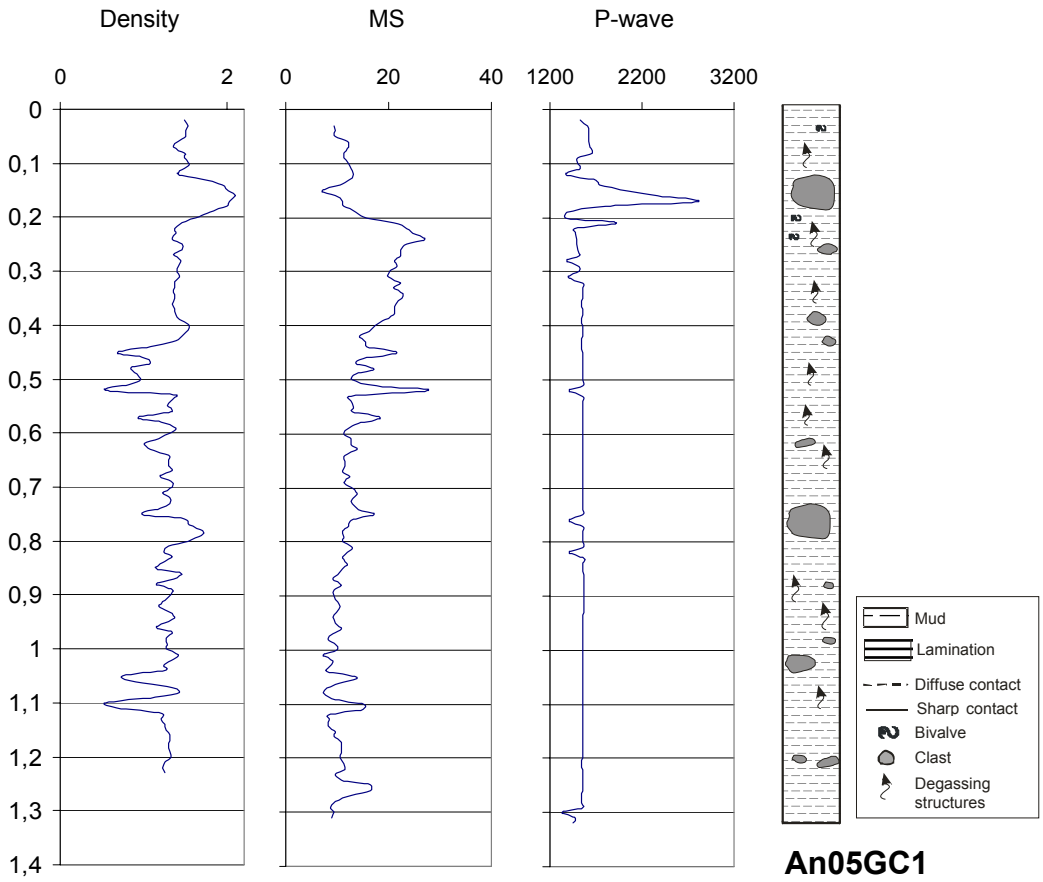

Fig. 3. - Core logs illustrating the vertical distribution of bulk density values (g/cm3), magnetic susceptibility (10-6 SI), P-wave velocity (m/s) and sediment for the core An05GC1. Vertical scale in meters.

The detailed study of the profiles illustrates the correspondence between density variations and sediment types. The above-mentioned general trend is locally interrupted with sharp increases, which usually correspond to the coarser-grained sediment or the presence of some large clast (rock fragments); these intervals show the greatest relative differences observed for each core and are where maximum values of density (1.93-2.1 g/cm3) were recorded. Some of these intervals are easily recognizable: e.g. the intervals 13-19 cm in An05GC1 (Fig. 3), 143-149 cm in An07GC4 (Fig. 4), 73-79 cm in An14GC1 (Fig. 6) and 62-64 cm in An13GC1 (Fig. 5).

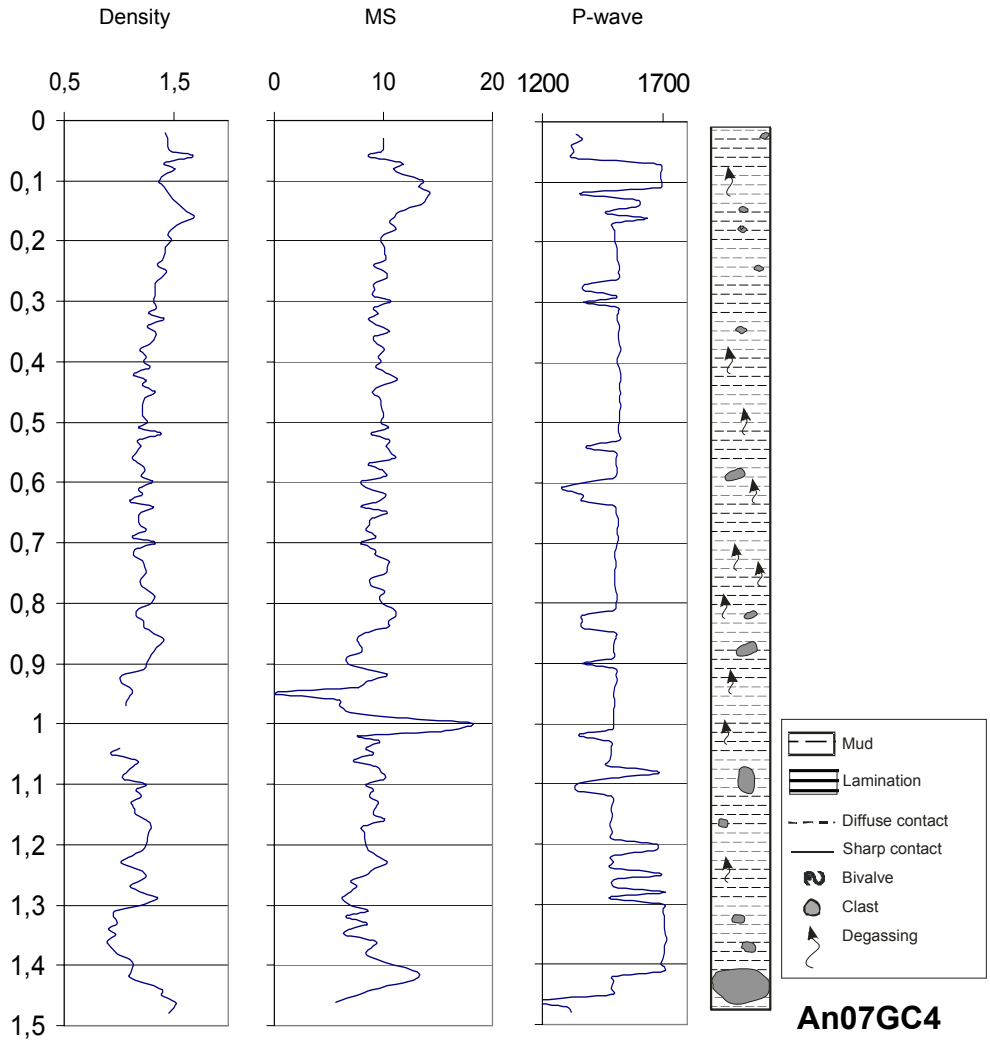

Fig. 4. - Core logs illustrating the vertical distribution of bulk density values (g/cm3), magnetic susceptibility (10-6 SI), P-wave velocity (m/s) and sediment for the core An07GC4. Vertical scale in meters.

4.2.2. Magnetic susceptibility

Magnetic susceptibility (MS) is a measure of the concentration of the magnetizable components within the sediment. Variations in the MS values of deep-sea sediments may reflect changes in lithology (the proportion of biogenic components-carbonate and silica-to lithogenic components-clay and labile minerals), which is essentially one of the bases for the lithological classification of deep-sea sediments (Robinson, 1990; Sager and Hall, 1990).

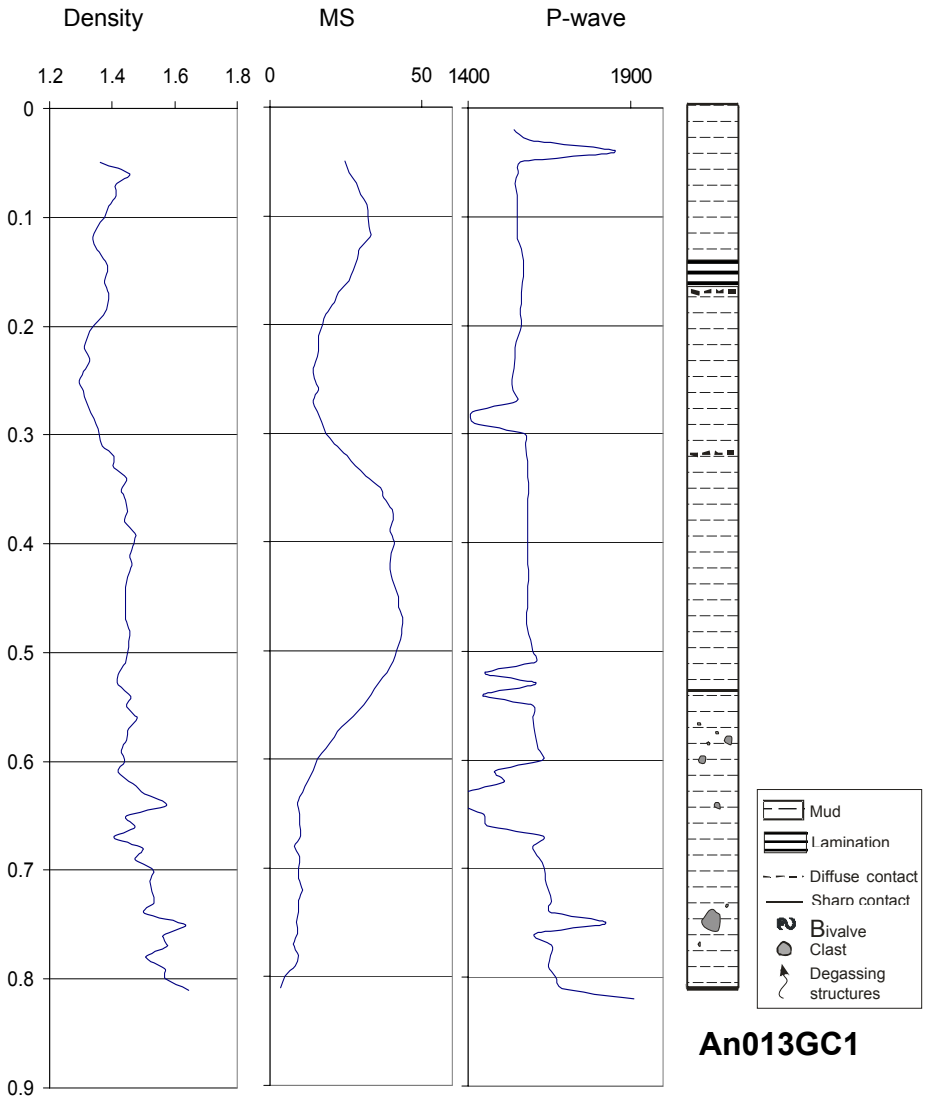

Fig. 5. - Core logs illustrating the vertical distribution of bulk density values (g/cm3), magnetic susceptibility (10-6 SI), P-wave velocity (m/s) and sediment for the core An13GC1. Vertical scale in meters.

MS measurements show average values of about $13 \cdot 10^{-6}$ SI units in An05GC1, $9 \cdot 10^{-6}$ SI units in An07GC4, $11 \cdot 10^{-6}$ SI units in An14GC1 and $24 \cdot 10^{-6}$ SI units in An13GC1. There are some differences regarding the general trend of the cores (Figs. 3, 4, 5, 6). Cores An05GC1, An07GC4 and An14GC1 have a comparable “behaviour” showing low variability with depth but the average trend is punctuated by spikes with values as great as $27 \cdot 10^{-6}$ SI units (52 cm in An05GC1), $18 \cdot 10^{-6}$ SI units (100 cm in An07GC4) and $22 \cdot 10^{-6}$ SI units (79 cm in An014GC1). The spikes observed in these cores

occur throughout the entire log, but they are not uniformly distributed. As occurs in the density log, all MS peaks seem to correlate with the presence of some rock fragments.

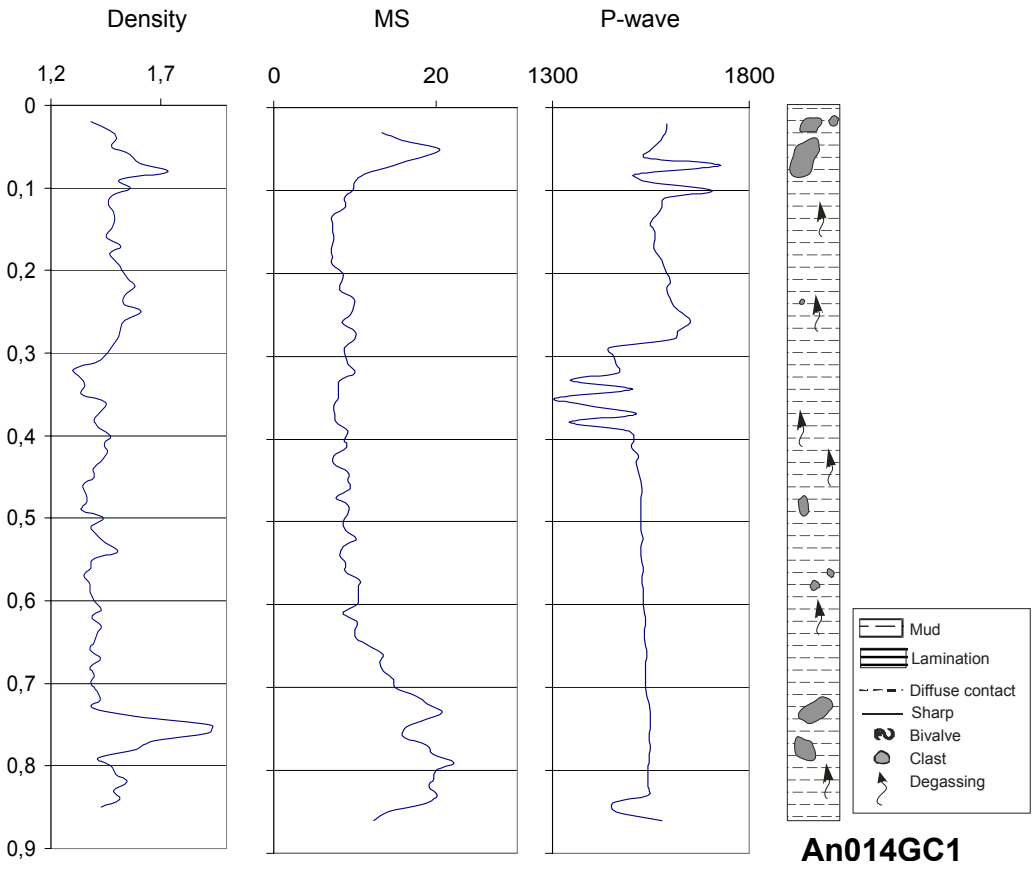

Fig. 6. - Core logs illustrating the vertical distribution of bulk density values (g/cm3), magnetic susceptibility (10-6 SI), P-wave velocity (m/s) and sediment for the core An14GC1. Vertical scale in meters.

By contrast, core An13GC1 shows a different trend. It displays a general decrease downcore from $24 \cdot 10^{-6}$ SI to $8 \cdot 10^{-6}$ SI. The detailed analysis of its vertical distribution allows three different intervals to be differentiated: i) 6 to 25 cmbsf, the MS values decrease downcore from 30 to 14 $\cdot 10^{-6}$ SI; ii) 25 to 50 cmbsf, the MS values increase downcore from 15 to 41 $\cdot 10^{-6}$ SI; and iii) 50 cm to bottom, the MS values decrease downcore from 40 to 3 $\cdot 10^{-6}$ SI units (Fig. 5). The described intervals seem to coincide with the stratigraphy of the core, reflecting the different types of sediment as hemipelagites *vs*. organic-rich hemipelagites *vs*. mud breccia.

4.2.3. Acoustic velocity

The analysis of the acoustic velocity is useful for geophysical modelling and interpretation, and it may provide diagnostic information about lithologic variations. Several studies have focused on the correlation of the acoustic velocity with porosity and lithology (Hamilton and Bachman, 1982; Nobes *et al* ., 1986; Mienert *et al* ., 1988; Fulthorpte *et al* ., 1989), especially the clay and carbonate content (Hamilton *et al* ., 1982; Mienert, 1984; Nobes *et al* ., 1991).

Measured P-wave velocity values are generally low. Average acoustic velocities on cores An05GC1, An07GC4, An13GC1 and An14GC1 are close to 1587 m/s, 1493 m/s, 1588 m/s and 1577 m/s respectively near the mudline (Figs. 3, 4, 5, 6). Only An13GC1 shows a smooth downcore increase with depth to values close to 1691 m/s at 80 cmbsf (Fig. 5). P-wave logs show a scattering probably caused by sediment disturbance or bad acoustic contact (for example, see the last 10 cm of core An07GC4, Fig. 4).

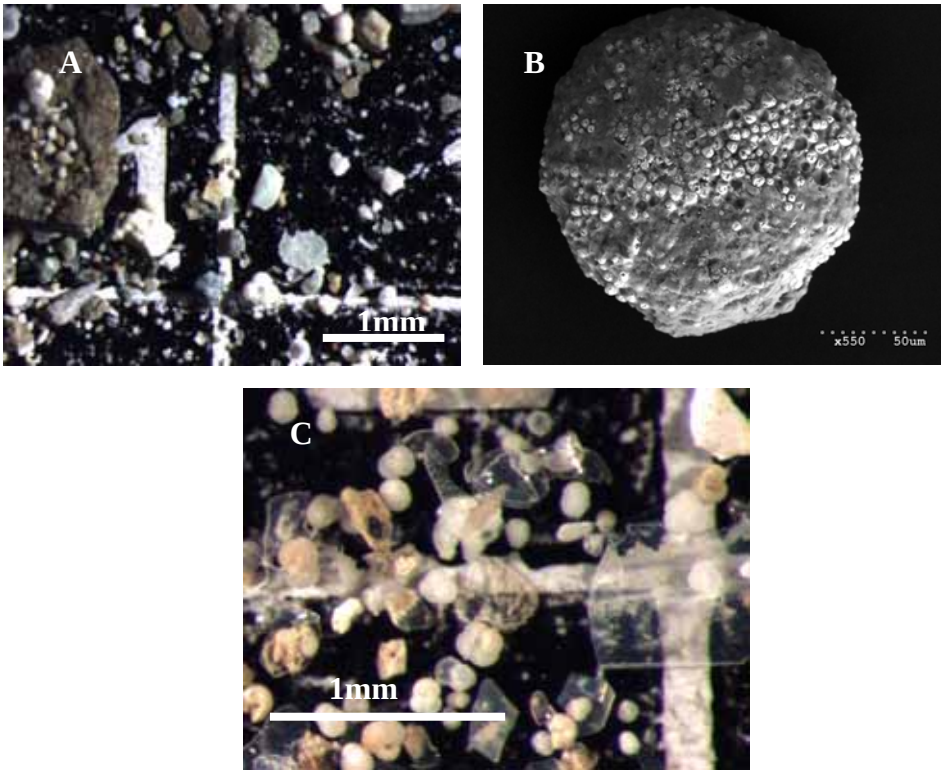

Fig. 7. - (A) Microscope picture of mud breccia showing the terrigenous components of sand fraction. (B) Electron microscope image showing the alterated crystals of pyrite found as component of mud breccia and (C) Microscope picture of hemipelagic sediment showing the biogenic components of sand fraction.

4.3. Discrete measurements

4.3.1. Water content

Water content (% dry weight) decreases downcore although the rate of decrease is variable (Fig. 9A). The higher values of water content (>50 %) correspond in general to the most surficial samples, but the general trend of water content distribution of cores An05GC1, An07GC4 and An14GC1 (where the trend to decrease downcore is very low or null) contrast with that of core An13GC1. The water content of the first group of cores decreases downward from 35-50% at the top to 21-35% at the bottom, while in core An13GC1 it decreases downward from 62% at the top to 41% at the bottom. These top-bottom differences may result from consolidation processes although their distribution may also indicate differences in texture and/or different sediment-forming processes (Lee and Baraza, 1999; Nelson *et al.*, 1999).

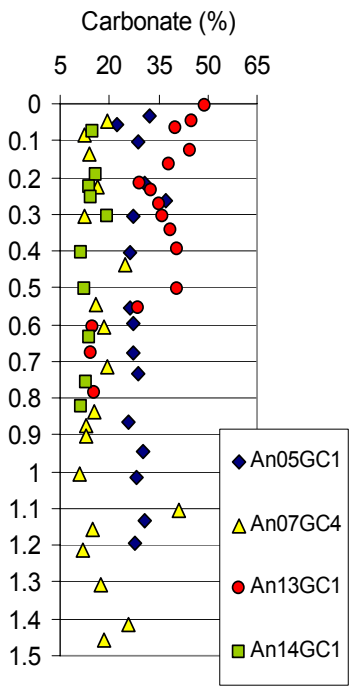

Fig. 8. - Downcore variation of carbonate content (%) for cores An05GC1, An07GC4, An13GC1 and An14GC1.

4.3.2. Grain density

Grain density depends on the minerals that form the sediment. It usually does not show a characteristic depth trend as water content and bulk density do. The grain density profile does not show marked trends downcore in the studied cores (Fig. 9B). In core An05GC1 the average grain density is 2.76 g/cm^3 but at 0.3 mbsf it increased sharply to 2.96 g/cm^3. In cores An07GC4 and An14GC1 the average grain density is 2.69 and 2.70 g/cm^3 respectively. The lowest grain density is recorded in core An13GC1, which shows an average value of 2.64 g/cm^3 and a minimum value of 2.56 g/cm^3 at 0.27 mbsf.

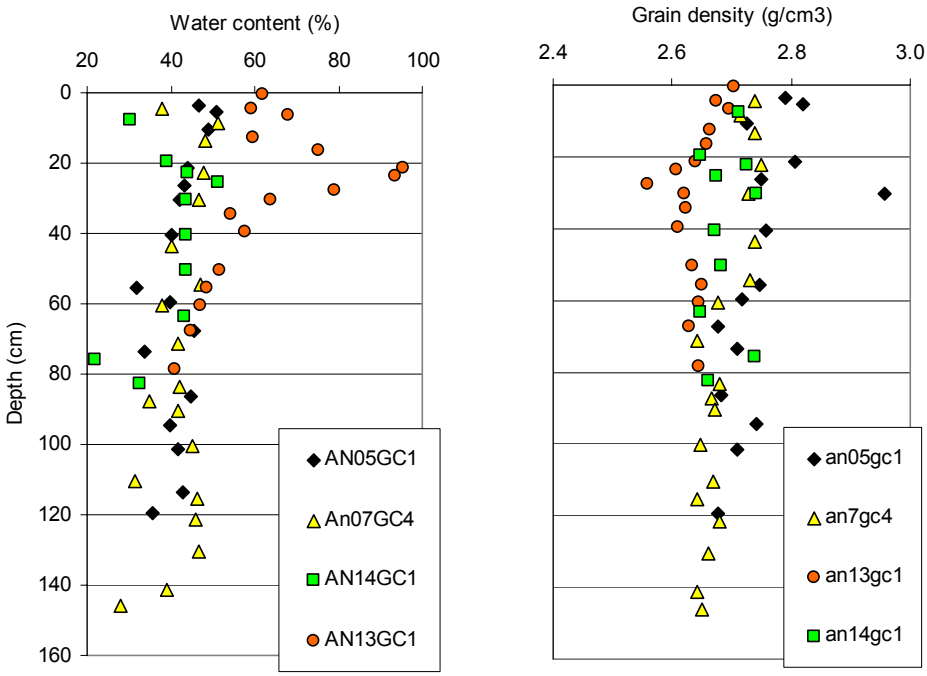

Fig. 9. - Downcore variation of (A) water content (%) and (B) grain density (g/cm3) for cores An05GC1, An07GC4, An13GC1 and An14GC1.

4.3.3. Porosity

The porosity profile does not show any trend in core An07GC4, whose average value was 85% (Fig. 10). The profiles in cores An05GC1 and An14GC1 increase downcore and their average values are 77 and 73% respectively. Only in core An13GC1 the porosity decreases downcore from 77% at the top to 66% at the bottom (Fig. 10). In this case an average value of 75% is calculated.

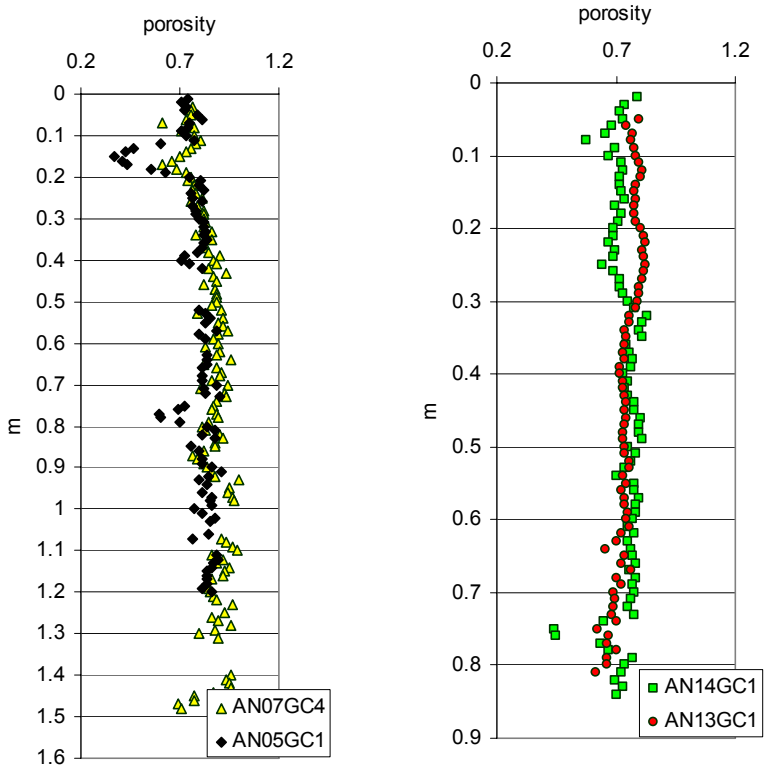

Fig. 10. - Core logs illustrating the vertical distribution of porosity (%).

4.3.4. Undrained shear strength

The data obtained show a general but very low trend of increasing average strength downcore (except in core An07GC4) from nearly 2 kPa at the top to 6 kPa at the bottom (Fig. 11). The highest shear strength is recorded in core An13GC1, which shows an average value of 7.7 kPa and a maximum value of 14 kPa at 0.6 mbsf.

In cores An05GC1, An07GC4 and An14GC1, with the same type of sediment along the core (mud breccia), the strength variations may be related to changes in the primary composition or to processes such as gas seepage which can break the internal structure of sediment. For core An13GC1, formed by mud breccia overlaid by hemipelagic sediments, strength variations seem to correspond to specific sediment types or lithologic/compositional changes in the same type of sediment. For instance, low relative strength values (6.4-6.7 kPa) correspond to the presence of the sapropel S1 between 15 to 33 cmbsf.

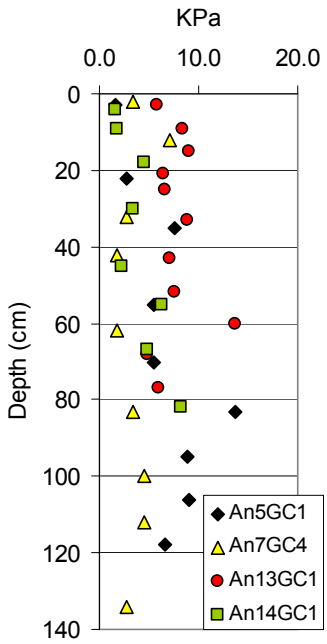

Fig. 11. - Downcore variation of shear strength (kPa) for cores An05GC1, An07GC4, An13GC1 and An14GC1.

5. Discussion

5.1. Sedimentology: geological significance

The geological interpretation of the sedimentology indicates that cores recovered on the crater of the Anaximander, Kula and Kazan mud volcanoes are formed by mud breccia on the surface, suggesting recent activity or at least that they are not in a dormancy period. Likewise, the mud breccia succession probably results from individual eruption events, due to the absence of phases of mud breccia oxidation and intercalations of hemipelagites. On the other hand, the sedimentology of core An13GC1, from the external flank of the Kula volcano, corresponds to an old extruded mudflow. After the deposition of the mud breccia this sediment was affected by an episode of oxidation due to its contact with the seawater, which was followed by a hemipelagic deposition. The 50 cm thick succession of hemipelagites suggests a prolonged period without mass flow deposition in the southwestern sector of the mud volcano flank.

Disseminated gas hydrate was recovered in the sediment cores, and this type of distribution implies low concentrations of gas hydrate, favouring its breakdown during the sampling and its disappearance in a short time when its stable P-T conditions change (Kvenvolden, 1993). The gas hydrate was observed in the mud breccia located in the active summits (or crater in the case of Amsterdam m.v.) of the mud volcanoes, but was absent from the mud breccia and hemipelagites located outside of the active areas of mud volcanoes (Lykousis *et al.*, 2003). These observations suggest three possible explanations for the presence and formation of the gas hydrate: a) its restricted location in the mud volcanoes, 2) the texture of the sediment, and 3) the mineralogy. Gas hydrate occurs at, or near the surface of mud breccia sediments in the summit (or crater); High gas fluxes through mud breccia due to the fluid dynamic processes (overpressured system) related to mud volcano formation and the presence of a relatively large volume of gas rising to the surface could favour the formation of gas hydrate (Casas *et al.*, 2003). The texture is similar for the matrix of the mud breccia and hemipelagites, so in this particular case a textural control of the conditions of formation of gas hydrate for the sediment hosting it is not justified. Finally, with respect to mineralogy, recent studies suggest a close relationship between the type of minerals and the presence of gas hydrate. The coincidence of areas with gas hydrate and areas with high percentages of smectite is a recent discovery (Collet and Wendlandt, 2000); the smectite may act as a catalyst in the formation of gas hydrate and may also alter its stability. The clay

mineralogy of the mud breccia from the Anaximander mud volcanoes is mostly characterized by the presence of smectite, with 89% in the Amsterdam and 85% in the Kazan mud volcanoes; illite and kailonite have been also identified, although in lower percentages (Zitter, 2004). High percentages of smectite in the muddy-matrix of mud breccia have been also observed in other mud volcanoes in the Mediterrean (Jurado-Rodríguez and Martínez-Ruiz, 1998; Zitter, 2004) and in other areas of the world, such as the Gulf of Cadiz (Martin, 2004) or Barbados (Lance *et al.*, 1998). Pyrite (Fig. 7) is a mineral that can be indicative of the presence of gas in one area, and it has been found in mud breccias of others mud volcanoes containing gas and gas hydrate (Martín, 2004). Its proposed genesis is related to the bacterial activity of the consortium of sulphide-reducing bacteria and archaeae, which oxidise the methane and reduce the sulphate, favouring carbonate precipitation and sulphurs (Michaelis *et al.*, 2002; Martín, 2004). Therefore, the presence of pyrite in mud breccia recovered on Anaximander, Kazan and Kula could also be related to the observed gas hydrate and carbonate crusts.

5.2. Physical properties

One of the greatest advantages of the MSCL is that it allows us to obtain a high-resolution, continuous record of the physical properties of the sediment. The data ensure that the physical signals of all sediment types are measured, which is especially relevant in the study of geological sections like the present studied cores, in which the variability of sediment types is very low. MSCL measurements performed in the lab do not represent the undisturbed physical state of the in situ environment of gas hydrate formation, but it can very useful to know the lithology and nature of the hosting sediment.

A low correlation was observed between some of the physical parameters measured with the MSCL sensors. In general, highs in density correspond to lows in magnetic susceptibility, but no statistical relationship confirmed this tendency. Only in core An13GC1 was a low positive correlation (R=0.47) between density and P-wave velocity observed. These observations suggest that depth (i.e. increased consolidation), which correlates with density (R=0.72), is a significant factor affecting the physical properties of the sediment, especially the velocity.

The relationship between physical properties and lithology has found correlations with density and MS. The maximums of density for cores An05GC1, An07GC4 and An14GC1 generally coincide with the presence of large clasts or clusters of them. But the variability of density in cores An07GC4 and An14GC1 seems to be controlled respectively by the variability of silt (R=0.69) and sand (R=0.47), and by the variability of gravel (R=0.78), silt (R=-0.75) and clay (R=-0.78).

The density for core An13GC1 also shows some relationships with sedimentological parameters such as sand-density (R=0.58), gravel-density (R=0.65) and clay-density (R=-0.73). These correlations are influenced by the percentage variations of sand, gravel and clay with the core-depth and the increase in density downcore (R=0.72) as an effect of consolidation (by overburden).

With respect to MS, an acceptable correlation was only found with clay (R=0.49) in core An07GC4, and with silt (R=-0.6) in core An14GC1. Thus, MS seems to be controlled by the fine fraction. The MS in core An13GC1 also correlates with carbonate (R=0.73), silt (R=0.43), gravel (R=-0.55) and sand (R=-0.58) content. These correlations also reflect the different types of sediment, with the highest MS values corresponding to the hemipelagic layers, and the lowest to the hemipelagic organic-rich sediment and mud breccia (Fig. 5). In this case, the silt probably plays an important role since it is the most independent of these variables and may thus be important for explaining the absolute magnetic susceptibility values for this core.

Plots of velocity *vs.* porosity are particularly useful for distinguishing the state of consolidation of sediment *vs.* the extent of diagenesis. In general, increasing consolidation in soft sediments tends to increase velocity through a decrease in porosity, whereas cementation produces an increase in velocity through increased rigidity of the sediment with little or no reduction in porosity (Dadey and Klaus, 1992). On a plot of velocity *vs.* porosity measurements of sediments from An014GC1 (Fig. 12A) and An013GC1 (Fig. 12B), we observed a general trend for velocity to increase as porosity decreases. A corresponding increase in P-wave velocity is only observed for sediments with higher bulk densities (R=0.47) in core An013GC1; in this case, a linear correspondence and a relatively good correlation exist for both measurements. These observations suggest that depth (i.e. increased consolidation) is a significant factor affecting the physical properties of the sediment, especially the velocity of core An013GC1.

5.3. Index properties

Index properties are all volumetric parameters calculated from the wet and dry weights and volumes of discrete samples. However, the relationships between some of the index properties are also controlled by lithology, especially the grain density which is the only parameter that depends mostly on the mineralogy of the samples. Grain size laboratory analysis showed that, despite the variability suggested by the differences observed visually between the types, almost all the sediment types recovered were of a similar size-range. Because of this low variability of sediment grain sizes, it is suggested that the greatest contribution to the variability observed in the physical properties would be made by either chemical/mineralogical variations or processes related to the consolidation of the sediment by overburden.

The average grain densities of the sediments described are 2.641 g/cm^3 for the hemipelagic sediment and 2.703 g/cm^3 for the matrix of mud breccia. These density values are close to the grain density of the most common constituents of the sediments, such as quartz (2.64 g/cm3), calcite (2.71 g/cm3) and clay minerals, which have highly variable grain densities, although the most common forms (smectite, kaolinite and montmorillonite) have average grain densities of 2.2 to 2.7 g/cm^3 (Johnson and Olhoeft, 1984).

There is a positive correlation between porosity and core-depth in cores An05GC1and An014GC1 (e.g. porosity increases with depth) and absence of correlation in core An07GC4, this can be explained by presence of porous gas-release structures resulting from depressurization following the collection of samples. This effect is less important in core An13GC1 since the coring site, which is located outside the crater of the mud volcano, has a different stratigraphy and lithology. In this case, the porosity and core-depth correlate negatively (R=-0.75).

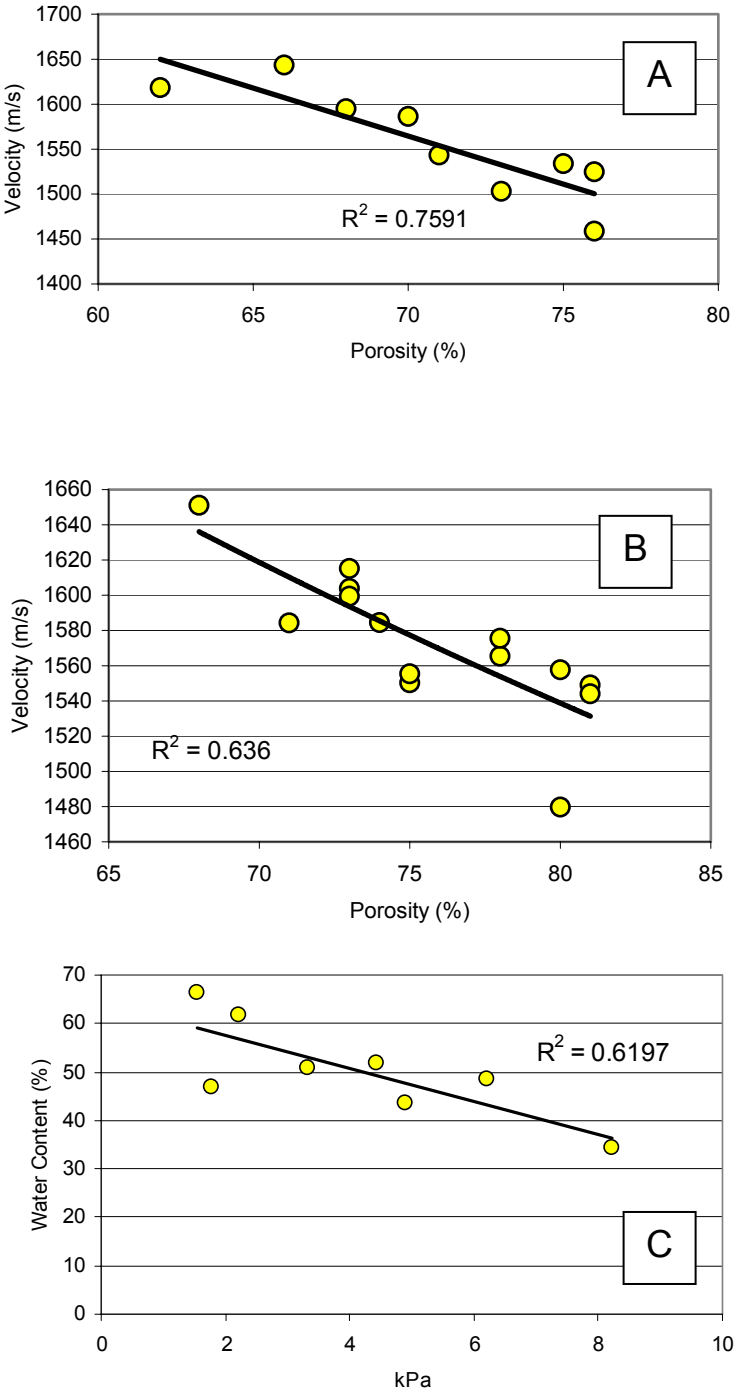

Fig. 12. - Graphic illustrating the relationship between porosity (%) and P-wave velocity (m/s) in core An014GC1 (A) and An013GC1 (B). And Diagram illustrating correlation between shear strength (kPa) vs. water content (%) for core An14gc1(C).

Carbonate content is a parameter that normally has a great influence on the physical properties of the sediment. Sediments with silica and clay minerals in general have higher porosities than calcareous, so increases in carbonate tend to correlate with decreases in porosity (Nobes *et al.*, 1991). Similar relationships are observed between bulk density and carbonate content (Hamilton *et al.*, 1982). This relationship is not clear for the sediments recovered in the Anaximander area. A plot of carbonate *vs.* porosity for all analyzed samples (Fig. 13) shows a cloud of points with no observable trends. A plot of carbonate *vs.* grain density (Fig. 13) confirms that the two parameters are independent of each other. Grain density values are clustered in different groups for the mud breccia samples with low carbonate content, and scattered for the hemipelagic samples with high carbonate content. This could due to the fact that the mud breccia is composed of a homogeneous group of minerals while the hemipelagic samples are composed of a greater variety of clay minerals and biogenic components.

Shear strength depends on the cohesion forces and on the friction between the coarser sediment particles. Progressive consolidation due to overburden results in the expulsion of interstitial water out of the sediment pores and the increase in the friction factor in the sediment strength. In general, in marine sediment shear strength values depend on water content. By contrast, in our results shear strength and water content show a very low correlation with depth and, as stated above, the physical properties were not especially controlled by the consolidation in cores An05GC1, An07GC4 and An14GC1. Shear strength and water content also fail to show any acceptable correlation (when all the samples measured are taken into account). Literature suggest that this could be related to changes in the cohesive forces developed in the clayey-rich sediments due to variations in the clay mineralogy (Schmincke *et al* ., 1995), but in our “gassy” cores an effect of presence of porous gas-release structures resulting from depressurization following the collection of samples is also possible. In one particular case (An14GC1) a negative correlation is described (Fig. 12C).The presence of gas hydrates in the mud breccia has to affect its shear strength, and it is expected this is greater than the measured values. Thus the depressurization may also be responsible for the relatively low strength values obtained.

Water content shows a low correlation with core-depth, but in all cases it shows a tendency to decrease downcore. The best result is found in core An13gc1 (R=-0.61), where we also find a “normal behaviour” of water content in comparison with the other variables, i.e. an increase in density (R=-0.82) and velocity (R=-0.56) is associated with a

decrease in water content and a decrease in porosity (R=0.80) and the mean grain size in phi units (R=0.67). For the rest of the cores, these relationships are not very clear or are achieved only partially.

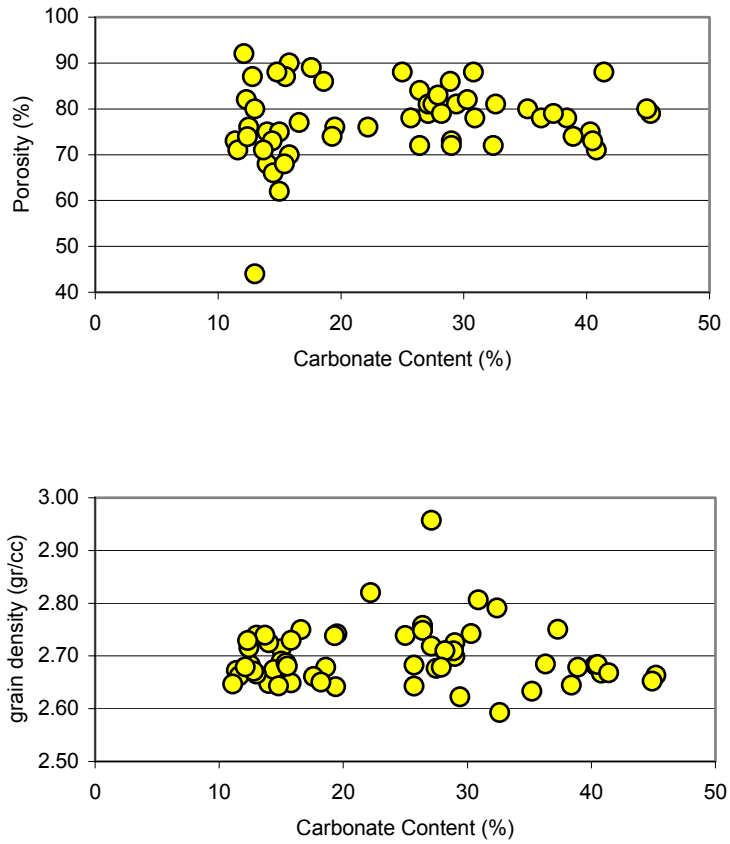

Fig. 13. - Graphic illustrating the relation between porosity (%) and carbonate content (%) and between grain density (g/cm3) and carbonate content (%) for all analysed samples.

6. Conclusions

1. Two different types of sediments have been defined, mud breccia and hemipelagic mud. Mud breccia is characterized by a high clay and silt content ranging between 67-56% and 19-30%, with a sand and gravel content of about 14%. Hemipelagic mud is characterized by a high clay and silt content and a sand content of only 3%. The stratigraphy of cores An05GC1, An07GC4 and An14GC1 comprises mud breccias, whereas the core An013GC1 is defined by mud breccias that toward the top changes to

hemipelagic mud (an organic-rich bed is identified within); the contact between the two types of sediment is sharp.

2. Some differences between cores were identified from the statistical correlation of the different parameters studied. For cores An05GC1, An07GC4 and An14GC1 the physical properties are mainly controlled by lithology. This is supported by the correlations found between density and sand or silt in core An07gc4 and between density and gravel or silt in core An14GC1. The MS of these cores seems to be controlled by the fine fraction. The physical properties of core An013GC1 are mostly related to consolidation (compactation by overburden), but at detail scale they show variations related to variations in the defined texture (hemipelagic mud *vs.* mud breccia). This is supported by the relationships found between density and core-depth (which is the most significant) and the correlation between density and P-wave or porosity and P-wave. The influence of variation in grain-size is observed due to the relationships between density and clay or gravel. In this case, the magnetic susceptibility seems to be controlled by the coarser fraction (gravel, silt and sand).

3. The statistical correlation indicates that carbonate content does not correlate with changes in porosity and grain density in the four cores. This may suggest that carbonate content does not show any evident effect on the physical properties of the sediments.
Water content shows a low correlation with core-depth, but in all cases it shows a tendency to decrease downcore. Only in core An13gc1 we find a “normal behaviour” of water content in comparison with the other variables, i.e. an increase in density and velocity is associated with a decrease in water content and a decrease in the porosity and mean grain size. The “normal behaviour” of this core is possible because it is from non active site, with fluids passing through it. For the rest of the cores, these relationships are achieved only partially.
Shear strength had mostly a low or null correlation with core-depth. A negative correlation was only observed between shear strength and water content in core An14Gc1. For the rest of the cores, the shear strength could reflect the effect of presence of porous gas-release structures resulting from depressurization after collection of samples containing gas hydrate.

4. The stratigraphy and the above-mentioned correlations suggest that for the sediment cores located in the active part of the mud volcanoes (An05GC1, An07GC4 and An14GC1), the physical properties are controlled by lithology and mud volcanic processes rather than by degree of compaction. This could suggest recent fluid circulation, and therefore the possibility of current mud volcanic activity in the studied volcanoes. By contrast, the core located in the inactive part of the Kula mud volcano (An13GC1) displayed physical properties mostly related to consolidation effects, (even though it is composed partially by mud breccias) and to the type of sediment at a detailed scale, as occurs typically in deep sea fine-grained sediments. This suggests a restricted influence of mud volcanic processes, i.e. fluid circulation out of the summit or crater of the mud volcanoes.

5. The Multi Sensor Core Logger measurements, do not represent the undisturbed or in-situ physical properties of sediment containing gas hydrates. Also it is difficult to establish the degree of disturbance after the gas hydrate dissociation. This is enough to justify the necessity of advanced tools to get pressurized sediment cores as APCA (Advanced Piston Core) which improve the recovery of sediment hosting free gas and gas hydrates (Amann *et al* ., 2000). In the studied cores, as it has noted, the release of gas has influenced the general structure of sediment, but it has not been distorted or destroyed. That's way the relationships showed are still convincing and describe, at least relatively, the behaviour in the different environments sampled. MSCL measurements are very useful to know the lithology and nature of the sediment hosting gas hydrates as well.

Acknowledgments

This work was founded by the European Commission ANAXIMANDER project (EVK3-2001-00123), and by the "Ministerio de Ciencia y Tecnología" MARCONI (REN2000-0336-C03) project and MARSIBAL (REN2001-3868-C03) project. The support of these people and institutions is gratefully acknowledged. David Casas thanks the Generalitat de Catalunya for the PhD grant (1999FI 00002CSIC PG).

References

Amann, H., J. Baraza, C. Marx, C. Perissoratis, J. Roberts, A. Skinner, P. Valdy and H. Zuidberg. - 2000. Hyace**,** An Autoclave Coring Equipment for Systematic offshore sampling, measurement and ground truthing. *Eurocean 2000* , 670-673.

Aloisi, G.I., I. Bouloubassi, K. Heijs, R.D. Pancost, J.S. Sinninghe and J.C. Gottschal. - 2002. Methane-consuming microorganisms and the formation of carbonate crusts at seeps. Earth and Plan. Sc. Lett., 203: 195 –203.

Casas, D., G. Ercilla and J. Baraza. - 2003. Acoustic evidences of gas in the continental slope sediments of Gulf of Cadiz (E Atlantic). Geo-Mar Lett., 23: 300-310.

Casas, D., H. Lee, G. Ercilla, R. Kayen, F. Estrada, B. Alonso, J. Baraza and F. Chiocci. - 2004. Physical and geotechnical properties and assessment of sediment stability on the continental slope and basin of the Bransfield Basin (Antarctica Peninsula). Marine Geores. and Geotech., 22 (4): 253-278.

Charlou, J.L., J.P. Donval, T. Zitter, N. Roy, P. Jean-Baptiste, J.P. Foucher, J. Woodside and the MEDINAUT Scientific Party. - 2003. Evidence of methane venting and geochemistry of brines on mud volcanoes of the eastern Mediterranean Sea. Deep-Sea Res., Part I, 50: 941-958.

Collet, T.S. and R.F. Wendlandt. - 2000. Formation evaluation of gas hydrate-bearing marine sediments on the Blake Ridge with downhole geochemical log measurements. Procc. ODP, Results, 164: 199-215.

Dadey, K.A. and A. Klays. - 1992. Physical properties of volcanoclastic sediments in the Izu-Bonin area. In: Taylor, B., Fujioka, K., et al ., Proc. ODP, Sci. Res., 126, pp. 543-550 College Station, TX (Ocean Drilling Program).

Fleming, N. - 1972. Eustatic and tectonic factors in the relative vertical displacement of the Aegean coast. In: Stanley, D. (ed.) The Mediterranean Sea, pp. 189-201. Dowden, Hutchinson & Ross,Stroudsberg.

Fulthorpe, C.S., S.O. Schlanger and R.D. Jarrard. - 1989. In situ acoustic properties of pelagic carbonate sediments on the Ontong Java Plateau. J. Geophys. Res., 94: 4024-4032.

Giró, S. and A. Maldonado. - 1987. Análisis granulométrico por métodos automáticos. Tubo de sedimentación y Sedigraph. Acta Geológica Hispánica, 20 (1): 95-102.

Hamilton, E.L. - 1970. Sound velocity and related properties of marine sediments. J. Geophys. Res., 75: 4423-4446.

Hamilton, E.L. and R.T. Bachman. - 1982. Sound velocity and related properties of marine sediments. J. Acoust. Soc. Am., 72: 1891-1904.

Hamilton, E.L., R.T. Backman, WH. Berger, T.C. Johnson and L.A. Mayer. - 1982. Acoustic and related properties of calcareous deep-sea sediments. J. Sediment. Petrol., 52: 733-753.

Johson, G.R. and G.R. Olhoeft. - 1984. Density of rocks and minerals. In: Carmichael, R.S. (ed.), CRC Handbook of Physical Properties of Rocks (Vol. 3): Boca Raton, FL (CRC Press, Ins.), 1-38.

Jurado-Rodríguez, M.J. and F. Martínez-Ruiz. - 1998. Some clues about the Napoli and Milano mud volcanoes from an integrated log-core approach. Proc. ODP, Sci. Res, 160: 607-623.

Kim, D. C., J. Y. Sung, S. C. Park, G. H. Lee, J. H. Choi, G. Y. Kim, Y. K. Seo and J. C. Kim. - 2001. Physical and acoustic properties of shelf sediments, the South Sea of Korea. Mar. Geol., 179: 39-50.

Kvenvolden, K.A. - 1993. Gas hydrates. Global perceptive and global change: Rev. Geophys., 31: 173-187.

Lance, S., P. Henry, X. Le Pichon, S. Lallement, H. Chamley, F. Rostek, J.C. Faugeres, E. Gonthier and K. Olu. - 1998. Submersible study of mud volcanoes seaward of the Barbados accretionary wedge: sedimentology, structure and rheology. Mar. Geol., 145: 255-292.

Lee, H. and J. Baraza. - 1999. Geotechnical characteristics and slope stability in the Gulf of Cadiz. Mar. Geol., 155: 173-190.

Lykousis, V., J. Woodside, G. de Lange, S. Alexandri, D. Sakellariou, P. Nomikou, Chr. Ioakim, A. Daehlman, D. Casas, G. Rousakis, D. Ballas, K. Kormas, S. Kioroglou and C. Perissoratis. - 2003. Mud volcanoes and related gas hydrates in Anaximander Mountains (Eastern Mediterranean). New discoveries from the 01/May03 cruise of R/V Aegaeo (Anaximander Project). Ocean Margin Research Conference (EC and UNESCO). Paris (France) 15-17 September.

Lykousis, V., S. Alexandri, J. Woodside, P. Nomikou, Chr. Ioakim, D. Sakellariou, G. de Lange, A. Daehlman, D. Casas, G. Rousakis, D. Ballas and C. Perissoratis. - 2004. New evidence of extensive active mud volcanism in the Anaximander Mountains (Eastern Mediterranean): The ATHINA mud volcano. Environ. Geol., 46(8). 1030-1037.

Lykousis, V., S. Alexandri, J. Woodside, G. de Lange, A. Daehlman, C. Perissoratis, Chr. Ioakim, D. Sakellariou, P. Nomikou, D. Casas, K. Kormas, G. Rousakis, D. Ballas and G. Ercilla. - 2006. Mud volcanoes and gas hydrates in Anaximander Mountains (Eastern Mediterranean): Marine and Petroleum Geology. Submitted.

Martín, C.- 2004. Caracterización mineralógica de estructuras ligadas a escapes de metano en el Golfo de Cádiz. Tesis de licenciatura. Universidad de Cádiz-Instituto Español de Oceanografía.

McClusky, S., S. Balassanian, A. Barka, C. Demir, S. Ergintav, I. Georgiev, O. Gurkan, M. Hamburger, K. Hurst, H. Kahle, K. Kastens, G. Kekelidze, R. King, V. Kotzev, O. Lenk, S. Mahmoud, A. Mishin, M. Nadariya, A. Ouzounis, D. Paradissis, Y. Peter, M. Prilepin, R. Reilinger, I. Sanli, H. Seeger, A. Tealeb, M.N. Toksoz and G. Veis. - 2002. GPS constraints on plate kinematics and dynamics in the eastern Mediterranean and Caucasus. J. Geophys. Res., 105:5695 –5719

Michaelis W., R. Seifert, K. Nauhaus, T. Treude, V. Thiel, M. Blumrnberg, K. Knittel, A. Gieseke, K. Peternecht, T. Pape, A. Boetius, R. Amann, BB. Jorgensen F. Widdel J. Peckmann, Pimenov NV and MB. Gulin. - 2002. Microbial reefs in the Black Sea fuelled by anaerobic oxidation of methane. Science, 297: 1013-5.

Mienert, J.- 1984. The importance of carbonate content in the acoustic stratigraphy of Panama Basin. Mar. Geol., 54: 237-247.

Mienert, J., W.B. Curry and M. Sarnthein. - 1988. Sonostratigraphic records from equatorial Atlantic deep-sea carbonates: paleoceanographic and climatic conditions. Mar. Geol., 83: 9-20.

Milkov, A.V.- 2000. Worldwide distribution of submarine mud volcanoes and associated gas hydrates. Mar. Geol., 167: 29-42.
Nelson, C.H., J. Baraza, A. Maldonado, J. Rodero, C. Escutia and J.H. Barber Jr. - 1999. Influence of the Atlantic inflow and Mediterranean outflow on late Quaternary sedimentary facies of the Gulf of Cadiz continental margin. Mar. Geol., 155: 99-129.

Nobes, D.C., H. Villinger, E.E. Davis and L.K. Law. - 1986. Estimation of marine sediments bulk physical properties at depth from seafloor geophysical measurements. J. Geophys. Res., 91: 14033-14043.

Nobes, D.C., J. Mienert and G.J. Dirksen. - 1991. Lithologic control of physical-property interrelations. In: Ciesielski, P.F., Kristoffersen, Y., et al ., Proc. ODP, Int. Repts., 114: College Stations, TX (Ocean Drilling Program), 657-669.

Nobes, D.C., M.G. Langseth, S. Kuramoto, P. Holler and N. Hirata. - 1992. Comparison and correlation of physical-property results from Japan Sea Basin and Rise Sites, legs 127 and 128. In: Tamaki, K., Suyehiro, K., Allan, J., McWilliams, M., et al ., Proc. ODP, Int. Repts., 127/128, Pt. 2: College Station, TX (Ocean Drilling Program), 1275-1296.

Olu-Le, R. K., M. Sibuet, Fiala-Medioni, A., S. Gofas, C. Salas, J.P. Foucher and J. Woodside. - 2004. Cold seep communities in the deep eastern Mediterranean Sea: composition and spatial distribution on mud volcanoes Deep-Sea Res. Part I: Oceanographic Research Papers. 51:12, 1915-1936.

Orsi, T.H. and D.A. Dun. - 1991. Correlations between sound velocity and related properties of glacio-marine sediments: Barents Sea. Geo-Mar Lett., 11: 79-83.

Pellenberg, R.E. and M.D. Max.- 2000. Introduction, Physical Properties, and Natural Occurrences of Hydrate. In: Max, D. (ed.) Natural Gas Hydrate: in Oceanic and Permagrost Environments. Kluwer Academic Publishers, Netherlands, 5: 1-8.

Rijk, S., A. Hayes and E.J. Rohling. - 1999. Eastern Mediterranean sapropel S1 interruption: an expression of the onset of climatic deterioration around 7 ka BP. Mar. Geol., 153: 337-343.

Robinson, S.G. - 1990. Application for whole-core magnetic susceptibility measurements of deep-sea sediments: Leg 115 results. In: Duncan, R.A., Backman, J., Peterson, L.C., et al ., Proc. ODP, Int. Repts., 115: College Station, TX (Ocean Drilling Program), 737-771.

Sager, W.W. and S.A. Hall. - 1990. Magnetic properties of black mud turbidites from ODP Leg 116, distal Bengal Fan, Indian Ocean. In: Cochran, J.R., D.A.V et al ., Proc. ODP, Int. Repts., 116: College Station, TX (Ocean Drilling Program), 317-336.

Salas C. and J.M. Woodside. - 2002. Lucinoma kazani n. sp.(Mollusca: Bivalvia): evidence of a living benthic community associated with a cold seep in Eastern Mediterranean Sea. Deep-Sea Res., 49: 991-1005.

Stein, R. - 1985. Rapid grain size analyses of clay and silt fraction by Sedigraph 5000D: comparison with Coulter Counter and Atterberg methods. J. Sediment. Petrol., 55: 590-615.

Ten Veen, J. H., J. Woodside, T. A.C. Zitter, J. Dumont, J. Mascle and A. Volkonskaia. - 2004. Neotectonic evolution of the Anaximander Mountains at the junction of the Hellenic and Cyprus arcs. Tectonophysics. 391: 1-4, 35-65.

Vatan, A. - 1967. Manuel de Sédimentologie. Technip.,Paris.

Weber, M., F. Niessen, G. Kuhn and M. Wiedicke. - 1997. Calibration and application of marine sedimentary physical properties using a multi-sensor core logger. Mar. Geol., 136: 151-172.

Werne J.P., R.R. Haese, T. Zitter, G. Aloisi, L. Bouloubassi, S. Heijs, A. Fiala-Medioni, R.D. Pancost, J.S.S. Damste, G. de Lange, L.J. Forney, J.C. Gottschal, J.P. Foucher, J. Mascle and J. Woodside. - 2004. Life at cold seeps: a synthesis of biogeochemical and ecological data from Kazan mud volcano, eastern Mediterranean Sea. Chem. Geol., 205 (3-4): 367-390.

Woodside, J.M., M.K. Ivanov and A.F. Limonov. - 1997. Neotectonics and fluid flow through the seafloor sediments in the Eastern Mediterranean and Black Seas. Part I: Eastern Mediterranean Sea. IOC technical series, 48:1-128.

Woodside, J.M., M.K. Ivanov, A.F. Limonov and Shipboard Scientists of the Anaxiprobre expeditions. - 1998. Shallow gas and gas hydrates in the Anaximander Mountains region, eastern Mediterranean Sea. In: Henriet, J.-P. & Mienert, J. (eds.) Gas Hydrates: Relevance to World Margin Stability and Climate Change. Geological Society, London, Special Publications, 137: 177-193.

Zitter, T. A., J.M. Woodside and J. Mascle. - 2003. The Anaximander Mountains: a clue to the tectonics of southwest Anatolia. Geol. J., 38: 375–394.

Zitter, T.A. - 2004. Clay mineral provenance in mud breccias of Eastern Mediterranean mud volcanoes. Free University of Amsterdam. Chapter 4. PhD Thesis. Free University of Amsterdam.

Zitter, T.A., C. Huguen and J.M. Woodside. - 2005. Geology of mud volcanoes in the Eastern Mediterranean from combined sidescan and submersible surveys. Deep Sea Research Part I. Oceanog. Res. Paper, 52 (3): 457-475.

CAPÍTULO 6

Physical and geotechnical properties and assessment of sediment stability on the continental slope and basin of the Bransfield Basin (Antarctica Peninsula). D. Casas, H. Lee, G. Ercilla, R. Kayen, F. Estrada, B. Alonso, J. Baraza, F. Chiocci. *Marine Georesources & Geotechnology*, *22(4): 253-278. 2004.*

H2 Version Number : 7.51c/W (Jan 11 2001)
File path : g:/Startpg/Journals/TaylorandFrancis/Umgt/22(4)/22(4)-44640/Umgt22(4)-44640.3d
Date and Time : 9/11/04 and 20:31

Marine Georesources and Geotechnology, 22: 1 26, 2004

ISSN: 1064-119X print/1521-0618 online
DOI: 10.1080/10641190490900853

Taylor & Francis
Taylor & Francis Group

Physical and Geotechnical Properties and Assessment of Sediment Stability on the Continental Slope and Basin of the Bransfield Basin (Antarctica Peninsula)

D. CASAS
G. ERCILLA
F. ESTRADA
B. ALONSO
J. BARAZA

Institut de Ciències del Mar. CMIMA
CSIC Barcelona, Spain

H. LEE
R. KAYEN

U.S. Geological Survey (USGS) Menlo Park
California, USA

F. CHIOCCI

University of Rome, Rome, Italy

Our investigation is centred on the continental slope of the Antarctic Peninsula and adjacent basin. Type of sediments, sedimentary stratigraphy, and physical and geotechnical characterization of the sediments have been integrated. Four different types of sediments have been defined: diamictons, silty and muddy turbidites, muddy, silty and muddy matrix embedded clast contourites. There is a close correspondence between the physical properties (density, magnetic susceptibility and p-wave velocity) and the texture and/or fabric as laminations and stratification. From a quantitative point of view, only a few statistical correlations between textural and physical properties have been found. Within the geotechnical properties, only water content is most influenced by texture. This slope, with a maximum gradient observed (20°), is stable, according to the stability under gravitational loading concepts, and the maximum stable slope that would range from 22° to 29°. Nevertheless, different

Received 2 April 2004; accepted 28 September 2004.
The research was supported by the "Ministerio de Ciencia y Tecnología" ANT97-0584 project and ANT1999-1462-E, by the MARSIBAL (REN2001-3868-C03) project and by the European Commission ANAXIMANDER project (EVK3-2001-00123). We are grateful for the cooperation of the members of Western Region Coastal and Marine Geology team of U.S Geological survey (USGS). We also thank Bradley A. Carkin and Benedicta Paracuellos for their help in geotechnical and sedimentological analyses, respectively. David Casas thanks the *Generalitat de Catalunya* for the Ph.D. grant (1999FI 00002CSIC PG).
Address correspondence to D.Casas, CSIC-Institut de Ciències del War, Passeig Marítim de la Barceloneta, 37-49, Barcelona 08003, Spain. E-mail: davidc@icm.csic.es

CAPÍTULO 6: PHYSICAL AND GEOTECHNICAL PROPERTIES AND ASSESSMENT OF SEDIMENT STABILITY ON THE CONTINENTAL SLOPE AND BASIN OF THE BRANSFIELD BASIN (ANTARCTIC PENINSULA)

PHYSICAL AND GEOTECHNICAL PROPERTIES AND ASSESSMENT OF SEDIMENT STABILITY ON THE CONTINENTAL SLOPE AND BASIN OF THE BRANSFIELD BASIN (ANTARCTIC PENINSULA)

D. Casas[1*], H. Lee[2], G. Ercilla[1], R. Kayen[2], F. Estrada[1], B. Alonso[1], J. Baraza[1], F. Chiocci[3]

[1] Institut de Ciències del Mar. CMIMA. CSIC. Passeig Marítim de la Barceloneta, 37-49. 08003 Barcelona. SPAIN.
[2] U.S. Geological Survey (USGS), Mail Stop 999, 345 Middlefield Road, Menlo Park, CA 94025. USA.
[3] University of Rome "La Sapienza" P.le Aldo moro 5, 00185, Rome. ITALY
*davidc@icm.csic.es

Abstract

Our investigation is centred on the continental slope of the Antarctic Peninsula and adjacent basin. Type of sediments, sedimentary stratigraphy, and physical and geotechnical characterisation of the sediments have been integrated.

Four different types of sediments have been defined: diamictons, silty and muddy turbidites, muddy, silty and muddy matrix embedded clast contourites.

There is a close correspondence between the physical properties (density, magnetic susceptibility and p-wave velocity) and the texture and/or fabric as laminations and stratification. From a quantitative point of view, only a few statistical correlations between textural and physical properties have been found. Within the geotechnical properties, only water content is most influenced by texture. This slope with a maximum gradient observed (20º) is stable, according to the stability under gravitational loading concepts, and the maximum stable slope that would range from 22 º to 29 º. Nevertheless, different instability features have been observed. Volcanic activity, bottom currents, glacial loading-unloading or earthquakes can be considered as potential mechanisms to induce instability in this area.

Keywords: Antarctica, Bransfield Basin, sedimentology, slope stability.

1. Introduction

Mass-physical and geotechnical studies are used by geologists in order to understand the sedimentary processes and controlling factors responsible of the nature and composition of marine sediments, and the causes of observed failures, in addition to evaluating the relative stability of specific undersea slopes. Little seems to be known about the geotechnical properties of glacial deposits occurring in marine environments and glaciomarine deposits (Anderson, 1999). The studies about sedimentation in glacial continental margins reveal significant variability in textural, mineralogical, and geochemical characteristics of the sediments (Anderson 1999). Likewise, these characteristics can change both, laterally along the margin, and vertically within the sediment column, suggesting that seafloor characteristics and dynamics can be also affected by physical and geotechnical properties.

Over the last 30 years data have been collected on the Bransfield Basin, located off the northern tip Antarctica, between the Antarctic Peninsula and the South Shetland Islands (Fig.1). These data have been mainly focused on tectonism, volcanism (Barker and Austin, 1994; Maldonado et al., 1994; Gràcia et al., 1996; Larter et al., 1997 among others), recent-most sedimentology and glacio-marine and marine processes (Yoon et al., 1997; Banfield and Anderson, 1995; Ercilla et al., 1998; Anderson, 1999), whereas geotechnical studies have received little attention (Holler, 1989). Recognizing the limitations in having four sediment cores recovering near-surface sediments in the present study, this paper correlates, discusses and contrasts the sedimentological, physical and geotechnical properties of the continental slope of the Antarctic Peninsula within the southwestern sector of the Bransfield Basin. Likewise, with the geotechnical results we have evaluated the relative stability of this section of the Bransfield Basin.

2. Geological Setting

The Bransfield Basin is a young and active rift basin, located off the northern tip Antarctica, between the Antarctic Peninsula and the South Shetland Islands (Fig.1). It can be divided into three sub-basins: eastern, central and western, separated by volcanic ridges (Jeffers and Anderson, 1990; Gràcia et al., 1996). The central Basin, which is the focus of the present paper, is an asymmetric ENE-WSW-trending basin 230 km long, 125 km wide and with a maximum depth of 1950 m. The sedimentary evolution of the

Antarctic Peninsula has been mainly controlled by successive advances and retreats of the ice sheet across the margin (Anderson et al., 1991; Canals et al., 2002). The active periods of sedimentation on the continental slope occurred during glacial periods and in the basin at the end of the glacial and interglacial periods (Jeffers and Anderson, 1990; Prieto et al., 1998; Prieto et al., 1999).

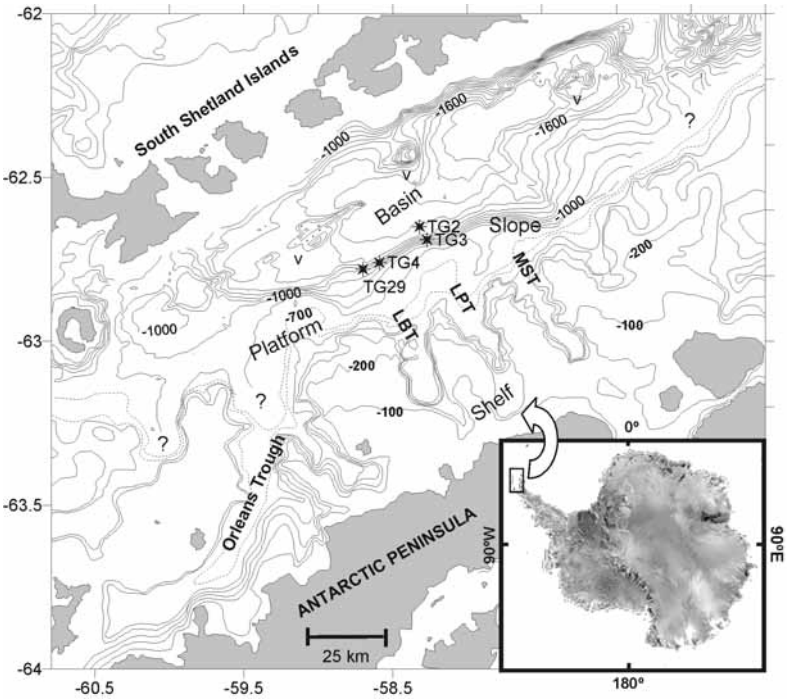

Fig.1. Map of location of the study area and bathymetry of Bransfield Basin. Black plots represent the position of sediment cores. Legend: LBT, Lanford Trough; LPT, Laclavere Troug; ST, Mott Snowfield Trough.

The area studied in the present paper comprises the southwestern sector of the Bransfield Basin, from offshore Laclavere to Lanford glacial troughs, and reaches from the continental slope down to the adjacent basin, at a water depth of 1575 m (Fig. 1). In this area, the detailed analysis of multibeam bathymetry indicates that the continental slope comprises two sub-provinces: platform and steep slope (terms based on Jeffers and Anderson, 1990). The platform, with lower gradients (0 to 8º), extends from 250 to 750 m water depth, and has a variable width (10-15 km). This sub-province is incised by the above mentioned glacial troughs (Fig. 1). The steep slope is defined by relatively higher gradients (Fig. 2), between 10 and 18º. It extends down to 1400 m water depth and is

relatively narrow (7 km wide). The steep slope passes downslope to the basin which has a smoother surface (Fig. 2), gradients between 0 a 4° and a maximum water depth of 1650 meters.

The most recent sediment of the studied area have been seismically analyzed by Ercilla et al (1998). These authors indicate that the platform area show a highly rough surface produced by the ice-sheet advanced during the last glaciation. Likewise, undisturbed stratified facies overlying the rough surface are identified on the most external areas. These deposits probably formed by particle vertical settling during the present-day interglacial period. Locally, these stratified deposits are incised by iceberg plough marks. The steep slope is characterized by mass-transport deposits, mostly comprising slumps. They appear as acoustically prolonged, transparent, chaotic or disrupted stratified deposits, which usually form mound-like reliefs.

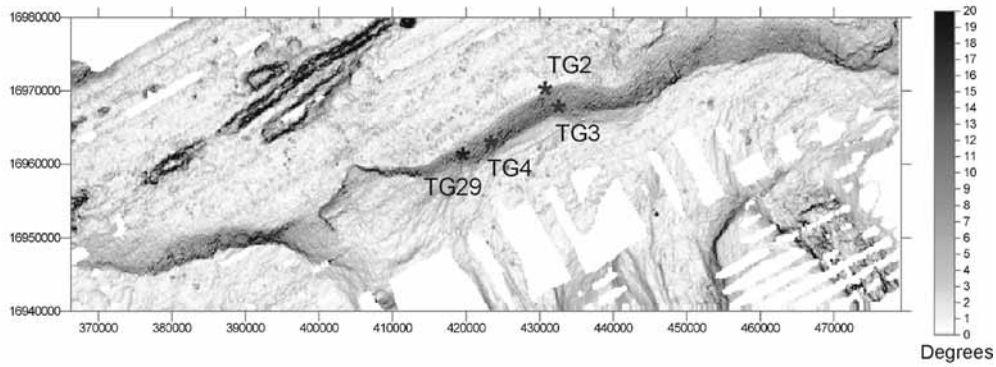

Fig. 2. Map of gradients (coordinates system in UTM) of the area of study, with the location of sediment cores.

3. Methodology

Multibeam bathymetry (Canals et al., 1994; Lawver et al., 1996), very high resolution seismic profiles obtained with the TOPAS (TOpographic PArametric Sonar) system and four gravity cores have been used in the present study. The cores are located on the continental slope and basin floor. The Table 1 shows the location, water depth, core length, physiographic province and slope gradient of the core sites.

The TOPAS records and cores were obtained onboard the R/V Hesperides, during the MAGIA cruise. The TOPAS system is a hull-mounted sea-bed and sub-bottom echosounder that operates using the non-linear acoustic properties of the water (Dybedal

and Boe, 1994). The penetration of the acoustic signal achieved with the TOPAS system varies between 30 and 200 milliseconds at full oceanic depths.

CORE	LATITUDE	LONGITUDE	WATER DEPTH (m)	CORE LENGTH (cm)	PROVINCE	GRADIENT
TG2	62.65S	58.32W	1575	148	Basin	3º
TG3	62.69S	58.27W	1200	84	Slope	14º
TG4	62.76S	58.59W	1200	230	Slope	15º
TG29	62.78S	58.70W	1200	120	Slope	10º

Table 1. Summary of sediment cores worked in this study.

The cores were capped, wrapped in cheesecloth, coated with parafin, and stored in a refrigerator at 4 ºC before consolidation and triaxial testing. The following sedimentological analyses have been carried out on the sediment samples: grain size, sand fraction composition, carbonate content, X-ray, and physical and geotechnical analysis.

Grain size analysis of selected sub-samples was conducted using a hand sieve and settling tube for the greater than 50 micron fraction and by the Sedigraph procedure (Micromeritics model 5100) for the smaller than 50 micron fraction. Composition of the sand fraction was determined with the aid of a binocular microscope. The carbonate content was obtained using a Bernard's calcimeter (Vatan, 1967). X-radiographs were made of the cores in order to recognise detailed sedimentary structure and disturbance features; so, that sections free of cracks or complex stratigraphy could be selected for advanced geotechnical testing.

Physical properties were obtained using a GEOTEK Multi Sensor Core Logger (MSCL) which measures P-wave velocity, bulk density (by Gamma Ray Attenuation) and magnetic susceptibility (MS) at 1 cm interval. MS is measured using a Bartington loop sensor and it is a measure of the concentration of the magnetizable components within the sediment. Therefore, downcore variations in the MS values of deep-sea sediments may reflect changes in lithology.

Water content in discrete samples was obtained measuring the sample wet weights using an electronic balance, drying the samples for 24 hr at about 105ºC, and measuring again their (dry) weights.

Consolidation characteristics were evaluated using an incremental consolidation test procedure conducted within a back-pressured, fixed ring GEOCOMP consolidometer.

The test results were used to obtain an estimate of the maximum past vertical stress that had been exerted on the sediment (Casagrande 1936). The shear strength was measured by a GEOCOMP triaxial testing device with monotonic axial loading under consolidated and undrained conditions.

4. Results

4.1. Near-surface seismic features of the core settings

The sediment cores are located in different depositional environments of the slope and basin offshore the Antarctic Peninsula. TG3, TG4 and TG29 locate on the steep slope, at 1200 m water depth, and TG-2 at the foot of the steep slope on the basin, at 1575 m water depth. The slope depositional environments sampled by TG3 and TG4 have been deduced from Ercilla et al (1998). This is because in our study, the seismic profiles display the absence of acoustic penetration, probably related to steeper gradients of the slope, that affect the acquisition and performance of the TOPAS system (Dybedal and Boe, 1994). Ercilla et al. (1998) studies indicate that the area is characterised by the predominance of sediment deposited from glacio-marine and mass-wasting processes (Fig. 3).

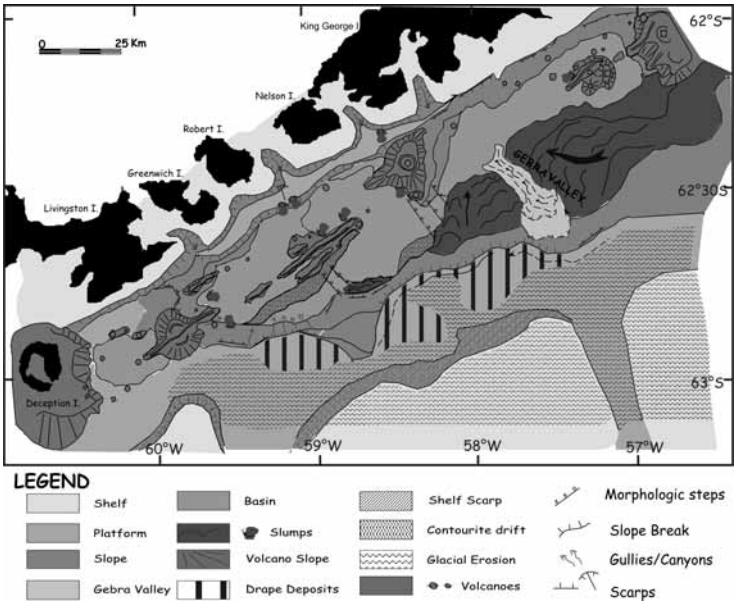

Fig. 3. Location of the surface geological features identified on the platform, slope and basin of the Central Bransfield Basin (after Ercilla et al. 1998).

The slope depositional environment of TG29 is also characterised by mass-movement features as mass-flow and/or slump deposits (Fig. 4). Among these features, TG29 was recovered from a lenticular body that seems to represent a rotational slump. This body is internally defined by deformed stratified reflections, partially back-rotated, that evolve downslope into chaotic facies. The stratified reflections abut against a concave-upward surface that represents the slide plane. These facies produce a wavy seafloor surface.

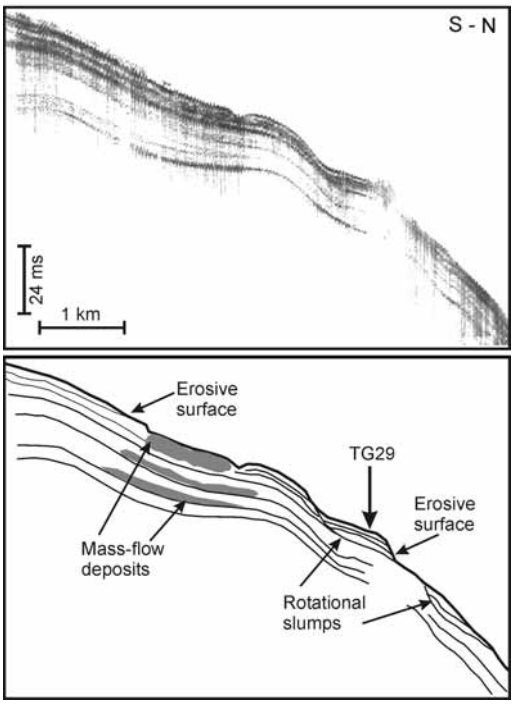

Fig. 4. Seismic profile and line-drawing illustrating the occurrence of mass-movement features. Those comprise Mass-flow, slumps and erosive surfaces on the seafloor.

The basin depositional environment of TG2 is characterised by the presence of contourite deposits (Fig. 5). These deposits form a depositional mound (24 ms thick and 1.5 km wide) associated with a moat (25 m deep and 1 km wide) located adjacent to the foot of the slope. Core TG2 is located on the moat (Fig. 5). The moat floor is mainly composed of irregular reflections of high and short lateral continuity and high acoustic amplitude.

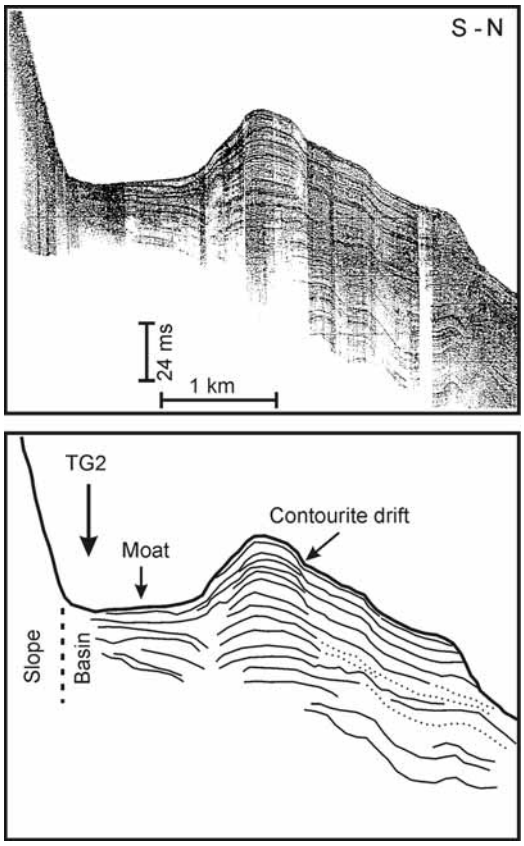

Fig. 5. Seismic profile and line-drawing illustrating the presence of contourite deposits. These deposits form a depositional mound associated with a moat located adjacent to the foot of slope.

4.2. Sediment types

4.2.1. Texture and composition

Different types of texture characterized the sediments of the four analyzed cores: muddy matrix-supported clasts, silts and muds. In spite of TG3, TG4 and TG29 being recovered on the steep slope, at the same water depth, they are texturally different. TG3 and TG-4 consist of matrix-supported and very poorly sorted (sorting 4 to 5 phi) sediment with clasts, that in TG3 appears interrupted by a 5 cm thick bed of poorly sorted (sorting 2 phi) silts (52 % silt and 42 % sand). The matrix is muddy consisting of 34 % silt, 28 % clay,

and 28 % sand. The clasts comprise heterometric (0.3 to 3 cm long) and sub-angular metamorphic rock fragments that appear embedded within the matrix. Based on charts for *a visu* estimating particle percentage (Swanson, 1981), their presence varies from common to abundant, ranging between 11 to 26 %.This sediment appears structureless, suggested by a chaotic distribution of the clasts within the matrix (Figs. 6 and 7). Core TG-29 consists of two major units: muddy matrix supported clasts and muds. The muddy matrix-supported clasts are similar to that of TG3 and TG4, but in this core the sediment appears poorly stratified. This stratification is suggested by both the presence of very thin beds of faint lamination where locally the clasts appear orientated (Fig. 8) and an upward fining grain size trend of the matrix. This type of sediment grades topward to muds that are interrupted by a centimetric bed of poorly sorted (sorting 2 phi) silts. These muds consist of 42 % silt, 33% clay and 24% sand with isolated lithic fragments (1.5 cm long), and are predominantly structured displaying planar-parallel and cross laminations. This configuration appears locally deformed by the presence of isolated clasts.

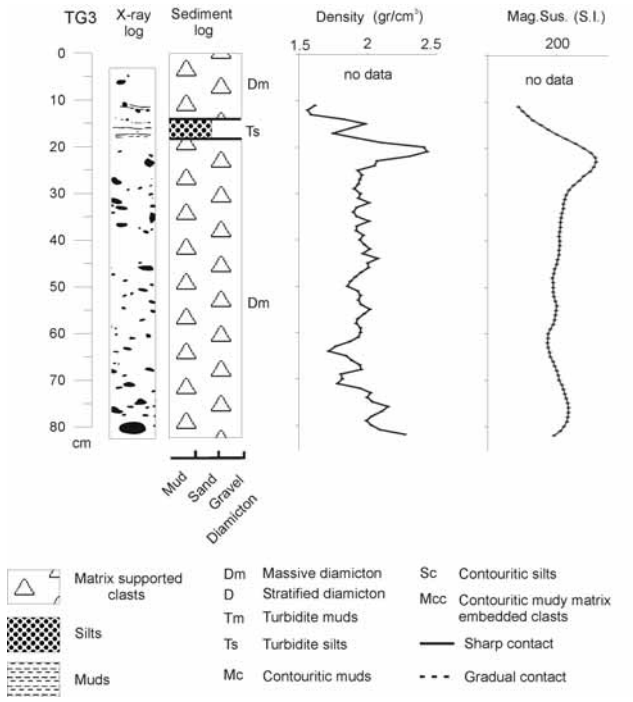

Fig. 6. X-ray log, sediment log, density and magnetic susceptibility for the slope core TG3.

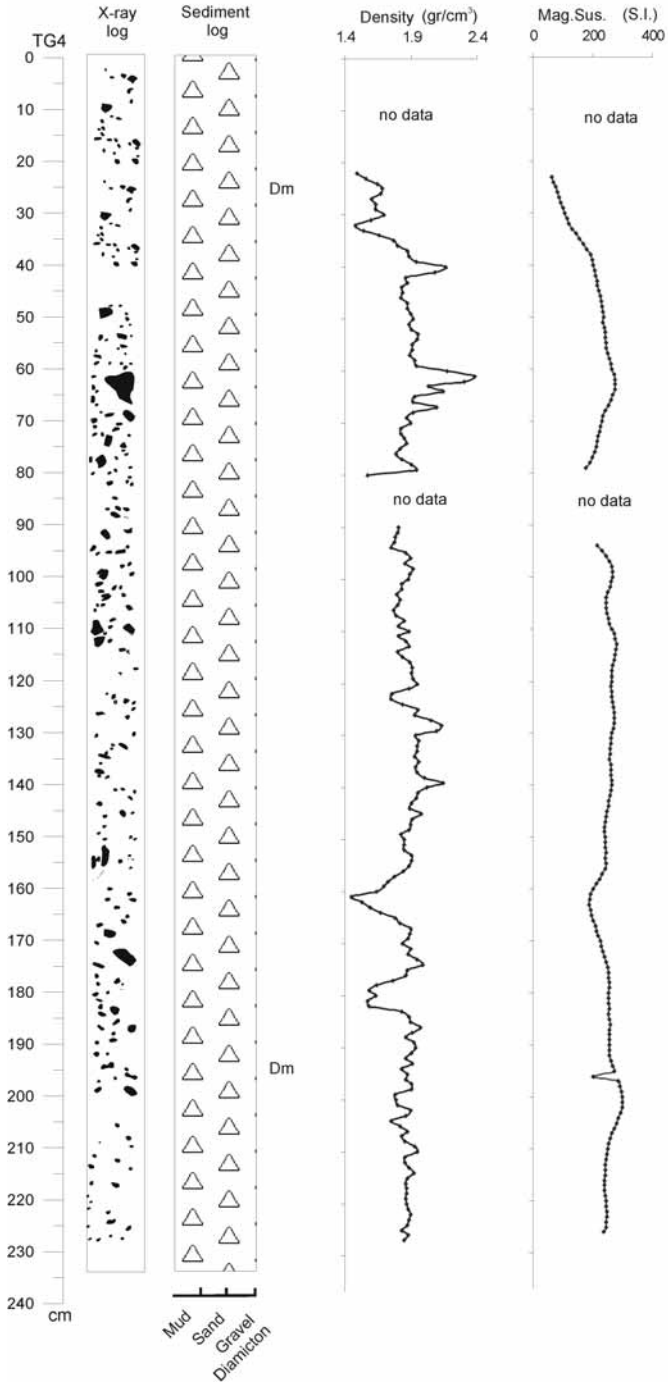

Fig. 7. X-ray log, sediment log, density and magnetic susceptibility for the slope core TG4. Legend in Fig. 6.

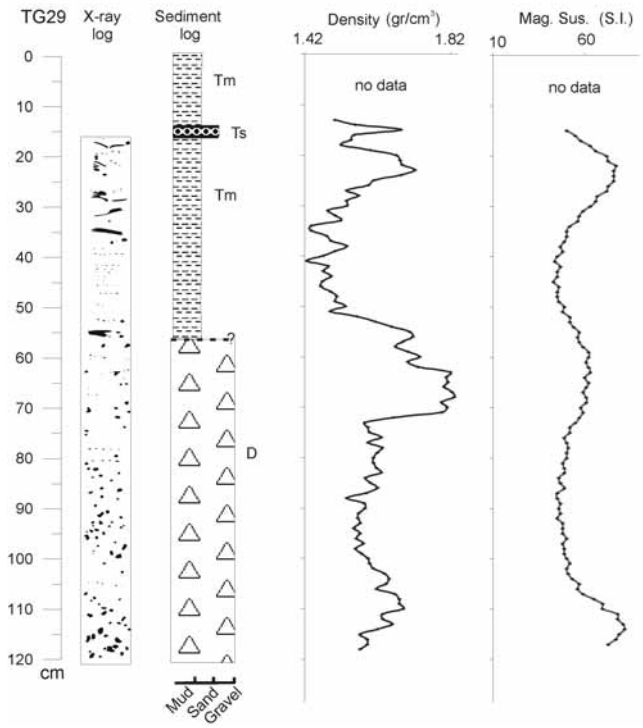

Fig. 8. X-ray log, sediment log, density and magnetic susceptibility for the slope core TG29. Legend in Fig. 6.

Basin core TG-2 consists of four distinct units: muds overlaid by a muddy matrix-supported clasts, sandy silts, and again muds. The muds consist of 51 % clay, 46 % silt and 7 % sand, with sorting of 2.4 phi. The X-ray images show that planar-parallel and cross laminations are typical of this sediment, and they often contain dispersed sub-angular clasts, which locally appear re-orientated according to the lamination. Likewise, some clasts deform the underlying layered sediments (Fig. 9). The sandy silts consist of 46% silt, 40% sand and 13% clay, and are poorly sorted (sorting 2.6 phi). The muddy matrix-supported clasts consist of less than 11 % sub-angular lithic fragments that are up to 2 cm long. The matrix contains 53 % clay, 46 % silt and 5 % sand. The X-ray radiographs show beds of oriented clasts. The silts consist of 40% sand, 46% silt and 13% clay, and are poor-sorted (sorting 2.6 phi). The X-ray images indicate a structureless muddy sediment (Fig. 9).

The sand fraction and calcium carbonate content show small variations among the cores and very small differences between each type of sediment. The sand fraction composition is mainly terrigenous (85 to 95 %). Their components are a mixture of light

minerals (quartz and feldspars) and plutonic and magmatic rocks. Calcium carbonate content is very low with an average of 3 %.

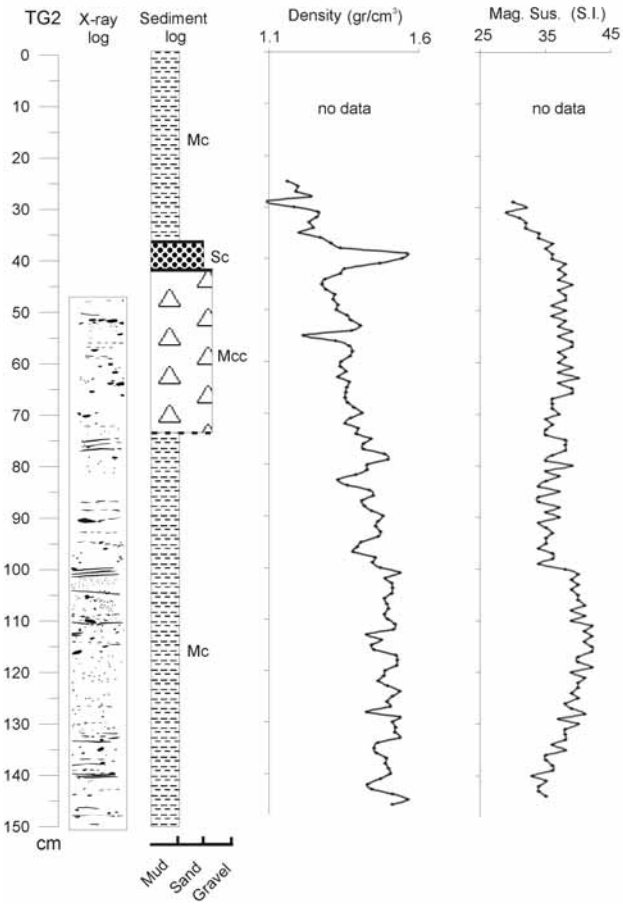

Fig. 9. X-ray log, sediment log, density and magnetic susceptibility for the basin core TG2. Legend in Fig. 6.

4.2.2. Sedimentary processes

The textural character and composition of these sediments have been compared with the previous sedimentological studies carried out in the Bransfield basin (Anderson, 1999; Anderson et al., 1991). Based on this comparison, all retrieved slope sediments are believed to result from glacio-marine and marine deposits. The muddy matrix supported clasts of TG-3, TG-4 and TG-29 would be diamicton sediments deposited by glacio-marine processes. These processes consist of debris release from the melting of floating ice shelves and/or icebergs, probably during the last glacial stage. The silts and muds are

believed to result from unchannelised turbidity currents flowing downslope. This interpretation is suggested by our seismic and sedimentological data. Seismic profiles suggest that these deposits occur in a depositional environment where mass gravity flows of variable slurries are dominant. The sedimentological evidences include identification of sharp boundaries, massive to parallel and cross-laminated structures, and sorting.

The retrieved basin sediments are believed to result from bottom currents. The depositional environment from which TG-2 was sampled indicates that bottom currents produced a zone of non-deposition or erosion (moat) against the slope, which is associated to a contouritic drift. Bottom currents influenced deposition of sediments probably derived from glacio-marine processes, as evidenced by the clasts embedded within the different textures, and/or marine instability processes derived from sliding upslope. Then, the sedimentary features displayed by these deposits are interpreted in terms of bottom current variations. The variety of their structures from massive to parallel and cross laminations, most probably represent variations in the intensity of bottom current flow, respectively from weak to stronger (Howe, 1995). Likewise, the presence of oriented clasts may indicate the action of strong bottom currents that re-oriented the deposited clasts (McCave and Tucholke, 1986; Faugères et al., 1993; Mariani et al., 1993).

4.3. Physical properties

The compressional-wave velocity (Vp) records are incomplete because of poor acoustic contact. Nevertheless, by selecting all valid values of Vp from all studied cores, we have obtained values ranging from 1500 to 1620 m/s. Records of density and magnetic susceptibility show different vertical distribution patterns, although slope cores TG3 and TG4 show similar trends. They have density values ranging from 1.5 to 2.4 g/cm^3, and susceptibility values from 100 to 300 SI (Figs. 6 and 7). The vertical distributions of both density and magnetic susceptibility does not display an overall trend but are marked by isolated maximums; maximum values are displayed by TG3 at 25 cm downcore and TG4 at 60 cm. Locally, TG3 shows a relative maximum (2 g/cm^3) near the top.

The slope core TG29 has bulk density values varying between 1.4 g/cm^3 to 1.8 g/cm^3, and magnetic susceptibility between 32 to 80 SI (Fig. 8). Although the vertical distributions of both measures show a great variability. It is possible to define levels of relative high and low values. Also, the depths at high and low values of density and

susceptibility are coincident for both logs. High values of density and magnetic susceptibility occur from 120 to 115 cm, 75 to 55 cm, and 25 to 20 cm below the sediment surface. A detailed analysis of the vertical distribution of these higher values in the two first levels shows a decrease upward.

The basin core TG2 has density values from 1.1 g/cm^3 to 1.6 g/cm^3 and magnetic susceptibility from 23 SI to 42SI (Fig. 9). The vertical pattern of both measures is different from those mentioned above, being characterised by a toothed shape produced by numerous changes of relatively minor order. Likewise, in TG2, the general trend is toward increasing values of bulk density with depth.

4.4. Geotechnical properties

4.4.1. Index properties: water content

The general trend of water content (% dry weight) within the slope cores (TG3, TG4 and TG29) contrasts with the basin core (TG2). The water content of the slope cores varies between 30 and 65 % at the bottom and increases upward to between 77 and 80 % at the top. In spite of the similarity of the distributions a detailed comparative analysis suggests the water content of TG3 and TG4 is as much as 30 % lower than that of TG29 (Fig. 10). Basin core TG2 has a higher water content relative to that of the slope cores. It has values of 120 % at the bottom increasing to values of 140 % at the top.

4.4.2. Consolidation properties

The results of consolidation tests (Fig. 11) were used to estimate the maximum past stress (σ'_{vm}) which is the greatest effective overburden stress to which the sediment has ever been exposed. Estimates of maximum past stress were obtained by the Casagrande (1936) construction on plots of void ratio *versus* log of the applied vertical effective stress (Fig. 11). The values of σ'_{vm} for TG2, TG4 and TG29 are similar, varying between 24 kPa and 28 kPa; these values contrast with that of TG3 (75 kPa, Table 2).

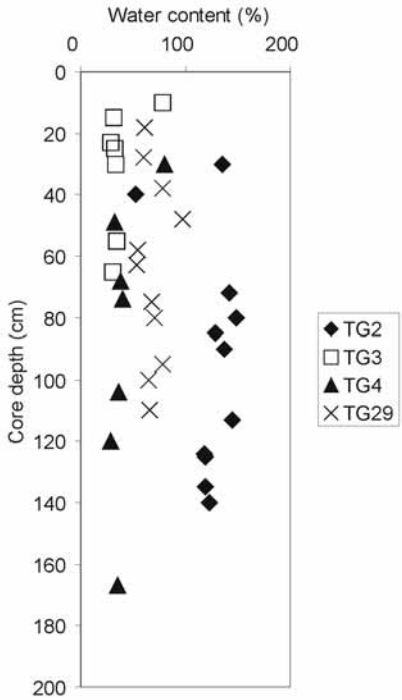

Fig. 10. Variation of water content *versus* depth for all four cores. Different symbols represent the different cores.

The overconsolidation ratio (OCR) is the ratio of the maximum past stress (σ'_{vm}) to the effective stress (σ'_v) at the time of sampling. Table 2 indicates that OCR varies between 3 and 5 for TG2, TG4 and TG29, and there is an increase to 15 for TG3. Values of OCR greater than 1 indicate overconsolidation conditions; for superficial sediment they can also suggest the loss of part of the sediment load that previously existed; and in surficial sediments, they can also indicate apparent overconsolidation. This apparent consolidation is considered to result from processes not related to normal mechanical compactation but to strong bonding of argillaceous and other particulate matter due to physico-geochemical processes, biogeochemical processes (Bryant and Bennett, 1988), electrostatic forces between particles (Wetzel, 1990) or secondary compression (Lee et al., 1981). To discriminate between the true and apparent overconsolidation, values of excess maximum past stress σ'_e ($\sigma'_e = \sigma'_{vm} - \sigma'_v$) are calculated (Lee and Edwards, 1986). Values of σ'_e are between 15 and 22 kPa for TG2, TG4 and TG29, contrasting with the value of 70 kPa for TG3. These values are typically associated with normally consolidated sediments, confirming then that the OCR values are reflecting an apparent

overconsolidation (Lee et al., 1981) except for core TG3 where a true overconsolidation is likely.

The compression index, C_c, which is the amount of compression (change in void ratio) that occurs during a tenfold increase in vertical effective stress (or one *log* cycle of change in pressure), is a measure of the compressibility of the sediment. Intermediate to high compressibility (C_c = 0.29 to 0.60) is present in TG3, TG4, TG29, and bottom parts of TG2; high compressibility (C_c = 0.98) is present in the upper part of TG2 (Table 3). That property is consistent with the tendency observed in the bulk density log, where bulk density increases with depth.

CORE	DEPTH (cm)	B. DENSITY (gr/cm^3)	MAX. P.STRESS σ'_{vm} (kPa)	V.EFF.ESTRESS σ'_v (kPa)	OCR	σ'_e
TG2	85	1.35	25.6	2.7	9.435	22.9
TG2	140	1.70	24.5	9.2	2.660	15.3
TG3	55	1.88	75.1	4.6	16.323	70.5
TG4	74	1.81	26.5	5.7	4.639	20.8
TG29	95	1.54	27.5	4.8	5.673	22.6

Table 2. Results of incremental consolidation tests.

The coefficient of consolidation, C_v, is a measure of the rate at which the sediment consolidates. Values of C_v are approximately one order of magnitude lower for TG3, TG4 and TG29 ($C_v = 10^{-4}$ cm^2/s) than for TG2 ($C_v = 10^{-3}$ cm^2/s) (Table 3). All these values are typical for mineral soils with a medium plasticity (25-5 plasticity index range) (Lambe and Whitman, 1969).

CORE	DEPTH (cm)	COEFFICIENT OF CONSOLIDATION (C_V) (cm^2/s)	COMPRESSION INDEX (C_C)
TG2	85	10^{-3}	0.98
TG2	140	10^{-3}	0.60
TG3	55	10^{-4}	0.35
TG4	74	10^{-4}	0.29
TG29	95	10^{-4}	0.63

Table 3. Values of Coefficient of consolidation and Compression index for the cores studied.

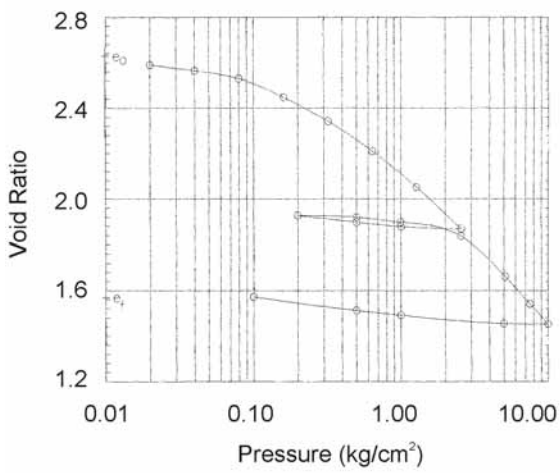

Fig. 11. Example of consolidation curve (void ratio *versus* log applied stress).

4.4.3. Shear strength properties

Consolidated, undrained triaxial tests were run to measure the strength of sediment under an axial load and to obtain the ratio of undrained shear strength (Su) to effective consolidation stress (σ'_c) for normal consolidation (Su/ σ'_c = S). The results of such tests are presented as a stress path (shear stress applied to the sample, q, *versus* mean effective confining stress, p', throughout the test). Stress paths provide information about the sediment behaviour during shear.

The shear strength of the sediment was determined using the normalised soil parameter (NSP) method (Ladd and Foott, 1974). Static undrained triaxial tests were conducted on samples consolidated to four times their estimated maximum past stress (σ'_{vm}) in order to determine the normalised shear strength (Su/ σ'_c = S) of normally consolidated sediment. The average values of this ratio, S, are 0.36 for TG2, 0.43 for TG3, 0.44 for TG4 and 0.48 for TG29. Fig. 12 represents the stress paths for one sample of the retrieved cores (TG4), consolidated to 150 kPa prior to shearing to compensate the effects of sediment disturbance during coring (Lee and Edwards, 1986). A contractive response during shear (stress path trending to the left) is observed for all sections of cores. This reflects a development of positive pore pressures during shear and results in the rapid collapse of the sediment fabric at further strain and a rapid drop of the shear resistance.

Calculations of estimated shear strength as a function of depth are based on Equation (1).

$$Su = \gamma' * z * S * (OCR)^m = \rho' * g * z * S * ((\sigma'_v + \sigma'_e)/ \sigma'_v)^m \quad (1)$$

where; γ' = sediment submerged unit weight (bulk density minus seawater density times gravity). ρ'= bulk density minus seawater density (bulk density values come from MSCL density values); g = gravity acceleration; z = subbottom depth; S= ratio of undrained shear strength (Su) to effective consolidation stress (σ'_c); σ'_v= vertical effective stress; σ'_e= excess maximum past stress and m= soil constant (Lee and Edwards, 1986). Average values of S and σ'_e for each core are used. With respect to m, previous research has shown that values of m = 0.8 are suitable (Lee and Edwards, 1986).

Bulk density values come from MSCL density values. Bulk density values obtained from gamma-ray attenuation provides the greatest amount of information about fine-scale sedimentology. In addition, bulk density of sediment is often typically a good proxy for engineering classification (Lee and Baraza, 1999; Lee et al., 1999). Thus, the gamma-ray density is the best quantitave approximation to the fine-scale sedimentology, and in consequence the density log has to be used in shear strength equation (1).

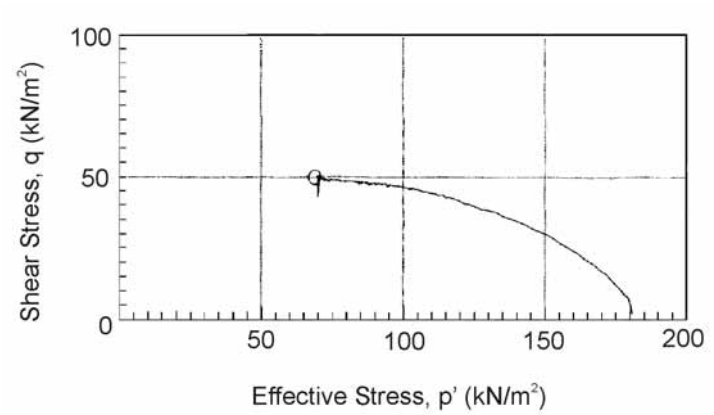

Fig. 12. Example of result of undrained triaxial test (stress paths). Sample showing contractive behaviour during shear.

Using equation (1) values of Su can be extrapolated down to 5 m subbottom depth. Fig. 13 shows how the estimated strength varies with depth below the seafloor for each core. The estimated Su values are less than 10 kPa on surficial sediment (for all cores), whereas at 5 m core depth Su ranges from 50 kPa for TG3, 25 kPa for TG4 and TG29 to less than 20 kPa for TG2.

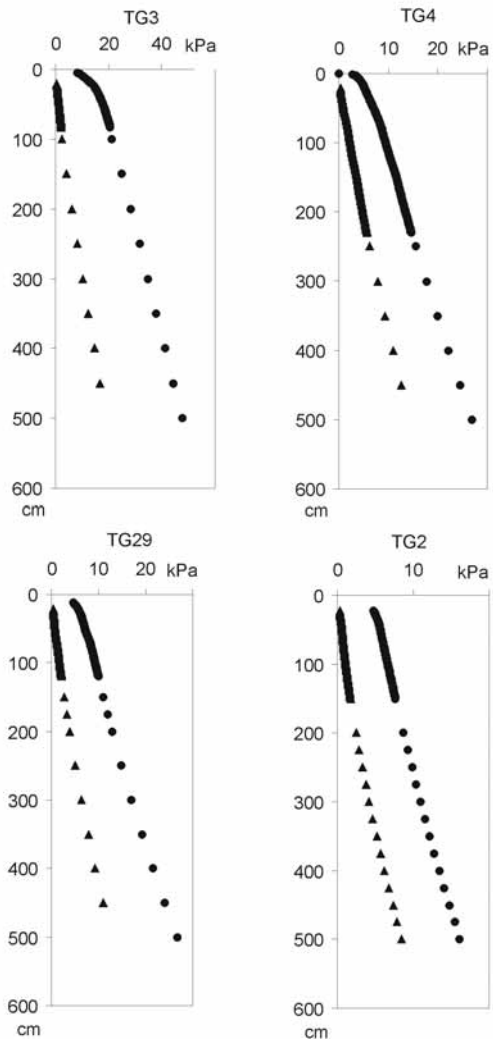

Fig. 13. Comparison of strength (dots) *versus* environmental stress (triangles). Both curves have been extrapolated down to 5 m subbottom depth. Discussion in the text.

5. Discussion

5.1. Effects of texture and stratigraphy in physical properties

The physical (P-wave velocity, density and magnetic susceptibility) behaviour of the Brandfield Basin sediments obtained from the MSCL reflects a close association between physical properties and texture and/or fabric as laminations and stratification (vertical size trending). These associations are expected because geometric configuration of particles, pore volume, matrix effects and grain-to-grain interactions determine the physical properties. We have expressed these associations qualitatively and some of them quantitatively based on statistical bi-variate relationships between P-wave velocity and density, and textural variables.

In spite of the incomplete information about compressional-wave velocity (Vp), all valid values of Vp have been selected from studied cores, obtaining a relationship (Fig. 14) between Vp and clay content of these sediment types. This relationship is numerically expressed in Equation (2) as

$$Vp = 1608 - 1.75 * (\%\ clay) \quad R = -0.64 \quad (2)$$

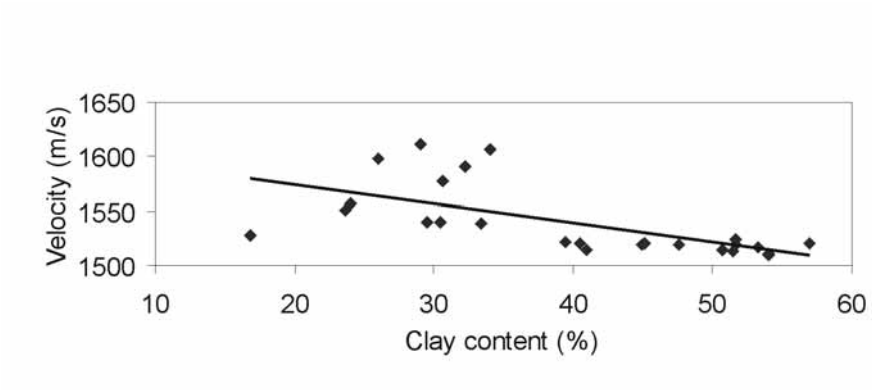

Fig. 14. Comparison of P-wave *versus* clay content for all samples studied.

This inverse correlation indicates that Vp decreases with increasing clay content. A similar relationship was observed by Hamilton (1970) and Kim et al. (2001). Generally, velocity decreases with increasing clay content for a matrix-supported sediment (Yin, 1993). Hamilton and Bachman (1982) also indicate that clay content in marine sediment affects velocity through its influence on porosity and bulk density.

Two main factors account for the observed variation in bulk density and magnetic susceptibility: texture and macrofabric. With respect to texture effect, in all cores the maximum values of bulk density and magnetic susceptibility coincide with the presence of large clasts or clusters of them within the muddy matrix of the diamicton and contourite sediments. Likewise, pronounced maximums are associated to centimetric interbedded beds of turbidite silts in slope cores TG3 and TG29, and contourite sandy silts in basin core TG2. The silt increases in about 20 % compared to the finer grained host sediment in TG-4 and TG29, and the sand increases in about 35 % compared to the above and below host sediment in TG-2.

From a quantitative point of view, a few statistical correlations between textural and physical properties have been found. Bulk density and texture are correlated statistically in TG29; the relationship between bulk density and % gravel (amount of clasts) is defined by a positive correlation index of 0.72. There also exists a very good inverse correlation between % clay with % sand (R= -9) in TG2 for all type of sediments. Both variables have a good correlation with bulk density, R= -0.78 (for % sand) and R= 0.78 (for % clay); i.e, bulk density decreases with % sand and increases with % clay. These correlations could explain the relatively minor changes recorded in the bulk density log and the toothed shape of vertical distribution.

The above mentioned statistical correlations only reflect general trends for some cores, and they cannot explain some particular cases, e.g. bulk density maximums associated with the presence of thin silt layers. This may imply that not enough “statistical entity” and/or a secondary data set is available to gain insight into variations in the physical properties. Those factors influencing physical properties can be among others such as; microfabric, mineralogy, chemical activity (authigenec mineralization), biological activity (bioturbation), or post physical/mechanical processes (e.g. bottom currents, ice gouging).

The effect of macrofabric on bulk density and magnetic susceptibility values are observed in slope core TG29 and basin core TG2 in two main features: textural trend and sedimentary structures. The upward decreasing trend observed in both properties in TG29 is correlated with the fining upward trend of the diamicton muddy matrix. The toothed appearance in the vertical distribution of both values in TG2 is coincident with the presence of planar-parallel and cross laminations in the contourite sediments. Likewise, in core TG2, the general trend of increasing values of bulk density with depth has a good correlation (R=0.86). No relationship exists between depth and texture, so this effect is probably due to consolidation and consequent porosity reduction (McGregor et al., 1979). Such a correlation is less evident in the other cores because they are mostly characterised by greater textural variability as well as anisotropic fabric.

5.2. Effects of texture and stratigraphy in geotechnical properties

Water content was found in this study to be mostly influenced by the texture of the sediment. Texture helps to explain the differences in this index property between the slope (TG3, 4 and 29) and basin (TG2) cores. The dominant basin sediments (contourite muds and muddy matrix supported clasts) display a higher content in clay (more than 50 %) and lower in sand (less than 7 %) with respect to predominant sediments (diamicton and turbidite muds) on the slope (less than 33 % silt and 28 % sand). Due to this high content in clay and low content in sand fractions the natural water content of the basin deposits is higher. Then, variations in water content between slope and basin cores seem to result mostly from porosity differences due to textural changes. It is widely known that the greater the content of clay-size material, the greater the water content (also void ratio and porosity). Similar changes in water content, resulting from grain size variation are found in silty and clayey sediments from the Bransfield Strait and Weddell Sea (Holler, 1989) where an increase in the coarse material produces a reduction in the natural water content. On the other hand, the generalized downcore decrease (from 77 and 80% to 30 and 65 %) in water content that display the cores, independently of their location, seem to be conditioned from reduction in porosity due to consolidation effects.

It has to be emphasized that this study found only very slight differences in measured consolidation and triaxial strength properties between the different types of sediment and their stratigraphy. Shear strength can be a useful criterion for distinguishing different types of diamicton, for example glacio-marine sediments versus logdment tills or deformation tills (Anderson, 1999), and therefore different mechanisms of transport. The

little differences observed in shear strength are consistent with the glacio-marine and marine origins without the effect of a lodgement (lodgement till). The similarity of the composition of the sand fraction, carbonate content, and tentatively of the mineralogical composition of the clay fraction, dominated by illite (Yoon et al., 1994) originating from Antarctic Peninsula can play a significant role as well.

Sediment erosion by removal of overburden by mass wasting, that is a sedimentary processes dominant on the steep slope (Ercilla et al., 1998), is the most probable cause of the overconsolidation obserserved in core TG3. To evaluate this mechanism for generating overconsolidation, we converted the measurements of excess maximum past stress into equivalent thickness of sediment (Edwards et al., 1987). For the calculation of excess sediment thickness, we assumed that the preloading sediment would be diamicton because it is the predominant sediment in the Bransfield Basin. Such a sediment has a submerged unit weight of about 7 kN/m^3 (0.7 g/cm^3). Dividing excess maximum past stresses by this value yields 9 m as the equivalent thickness of sediment that would have been needed to preload the overconsolidated sediment to the observed levels.

5.3. Slope stability analysis. Stability under gravitational loading conditions

The stability of a sedimentary deposit on a given slope depends on the shear strength of the sediment, how that strength varies with depth below the seafloor, and how that strength compares with the environmental stresses that are imposed on the sediment. A slope will become unstable whenever the average imposed shearing stress along the potential surface of sliding becomes equal to the average shearing resistance along this same surface (Scott and Zuckerman, 1970). In the absence of downslope forces other than gravity, the stability of a sedimentary body on a slope is inversely related to the thickness of a potentially unstable mass (z), the slope angle (α), and the unit weight of sediment (γ') (Hampton et al., 1978). The stability is directly proportional to the shear strength of the sediment at the depth, z.

Environmental stress for this area is calculated based on Equation (3) using the maximum measured slope in the area (20º):

$$Su = 0.5 * (\sin 2\alpha) * \sigma'_v \quad (3)$$

$$\text{Where} \quad \sigma'_v = \gamma' * z = \rho' * g * z$$

The calculated stress values for each core is shown in Fig. 13. These values vary between 0 kPa at the seafloor to less than 15 kPa at 5m down core for all cores. These values are always lower than shear strength values estimated using Equation (1) (compare curves in Fig. 13). Therefore, we can establish that this slope with a maximum gradient of 20 º is stable, according to the stability under gravitational loading concepts. It is possible to calculate the maximum stable slope by determining which angle causes the stress curve to cross the shear strength curve (Fig. 13). For the studied margin, the maximum stable slope would range from 27º for TG4, 29º for TG29, 25º for TG3 to 22º for TG2.

Our slope instability analysis suggests that the continental slope (subprovince slope) and basin are stable under gravitational loading concepts. Nevertheless, different instability features have been observed on seismic profiles or deduced by numerical models. Other high-resolution seismic and morphologic studies (Anderson et al., 1991; Ercilla et al., 1998) also indicate the presence of instability features along the slope and basin of the study area and surroundings.

We have no way of evaluating the triggering mechanism with existing data, but based on the geologic and oceanographic framework the following triggers are considered as potential mechanisms to induce instability: volcanic activity, glacial loading-unloading, bottom currents, earthquakes, and the presence of gas. Large volcanic seamount lineations characterise the central Bransfield Basin, and they show active mid-ocean ridge basalt volcanism interpreted as a result of incipient seafloor spreading (Gràcia et al., 1996). Volcanic emplacement may have caused earthquake shaking, triggering instability processes on the continental margin of the Bransfield Basin.

The effect of glacial loading-unloading could be, another mechanism to induce instability. Ice sheet loading on a continental shelf may induce far-field pore-pressure effects (Mulder and Moran,1995), and the isostatic rebound related to the retreat of glacial loading (Anderson, 1999) could produce a crustal uplift with a probable influence on the instability processes.

Bottom-current-related processes have played a role in the most recent sedimentary history of the basin, favouring the formation of contourite drifts and associated moats at the foot of the continental slope. Such processes were also described by Ercilla et al. (1998). The formation of a moat at the foot of a slope as a consequence of an erosive current could become a trigger to initiate instability processes on the adjacent slope.

A moderate level of intermediate-focus microseismicity, more or less stable with time has been defined in the Bransfield Basin and surrounding areas (Ibáñez et al., 1997). These authors considered the Bransfield Basin to be a zone with moderate seismic activity. Earthquake magnitudes varying between 4.8 and 6 (Richter magnitude) have been measured in the last 16 years. The lack of cyclic triaxial tests does not allow us to quantify the effect of earthquake loading on slope stability. Nevertheless, infrequent strong earthquakes with magnitudes greater than 6 can be tentatively considered as a major mechanism for instability features (Baraza et al., 1990). Likewise, the high activity of weaker earthquakes (Mb 2-4) registered in the area (Robertson et al., 2001) could be taking into account because they can reduce the sediment shear strength (Hampton et al., 1996).

Evidence of gas as acoustic blanking and pockmarks has been observed in the recent sediment deposited on the distal sectors of the Orleans and Gerlache Troughs (Ercilla, pers. com.). Nevertheless, the area of gassy sediment is well constrained and outside of the study area. According, this trigger is relatively insignificant.

6. Conclusions

The near-surface deposits from the SW Bransfield slope and basin consist of diamicton, turbidite and contourite sediments deposited respectively from glacio-marine, gravitative and bottom current processes. They are made of a variable mixture of muddy matrix-supported clasts, muds, silts, sandy silts and silty muds, with terrigenous components. The stratigraphy indicates that sedimentation and related processes on the continental slope display lateral variations in short distances.

The physical properties appear to be controlled by textural differences and stratigraphy (sedimentary structures, vertical grain size trending). Vp decreases with increasing clay content. Density and magnetic susceptibility values increase with the presence of gravel-size clasts or clusters of them. From a quantitative point of view, only a few statistical correlations between textural and physical properties have been found in some cores. They cannot explain some particular cases so this may imply that they have not enough “statistical entity” and/or a secondary data set (e.g., microfabric, mineralogy, chemical activity, biological activity, or post physical/mechanical processes) is necessary to gain insight into variations in the physical properties. Density and magnetic susceptibility also appear to be controlled by effects in two main macrofabric features:

textural trend (vertical trending of grain size) and sedimentary structures (parallel and cross laminations).

Within the geotechnical properties, only water content is most influenced by texture. The major presence of clays in basin deposits explains the water content of these sediments with respect to those of the slope. However, the generalized downncore decrease in water that is displayed in all cores, are conditioned by consolidation effects and not by texture or stratigraphy. Consolidation and shear strength properties are similar in all cores. Sediments in Branfield Basin are normally consolidated, except for slope core TG3, where lightly overconsolidation condition can be considered. This overconsolidation results from the occurrence of mass wasting processes, a dominant process on the Bransfield slope. The loss of about 9 m of sediment overburden is suggested as the most probably cause.

According to the stability under gravitational loading concepts we can establish that the present slope with a maximum gradient of 20º is stable and the maximum slope stable would range from 22º to 29º. This data is important because it could explain why this slope, as others in high latitudes (i.e. continental slope off Palmer Archipelago, Estrada et al., 2000) are very sharp, with high gradient slope even when they have a sedimentary control. Nevertheless, different instability features have been seismically observed or deducted from the consolidation tests. To explain their presence we have to resort to external triggering since all sediments studied are stable by themselves. Based on the geological and oceanographic frameworks, volcanic activity, bottom currents, tidal waves, glacial loading-unloading or earthquakes can be considered as potential mechanisms to induce instability in this area.

Acknowledgements

The research was supported by the “Ministerio de Ciencia y Tecnología” ANT97-0584 project and ANT1999-1462-E, by the MARSIBAL (REN2001-3868-C03) project and by the European Commission ANAXIMANDER project (EVK3-2001-00123). We are grateful for the cooperation of the members of Western Region Coastal and Marine Geology team of U.S Geological survey (USGS). We thank Bradley A. Carkin and Benedicta Paracuellos for their help in geotechnical and sedimentological analyses respectively. David Casas thanks the *Generalitat de Catalunya* for the PhD grant (1999FI 00002CSIC PG).

References

Anderson, J.B. 1999. Antarctic marine geology. Cambridge: Cambridge University Press.

Anderson, J.B., Barket, L.R. and Thomas, M.A. 1991. Seismic and sedimentological record of glacial events on the Antarctic Peninsula shelf. In: Thomson, M.R.A., Crame, J.A. Thomson, J.W. (Eds.) Evolution of Antarctica. Cambridge: Cambridge University Press, pp. 687-691.

Banfield, L. and Anderson, J.B. 1995. Seismic facies investigation of the Late Quaternary glacial history of Bransfield Basin, Antarctica. In: Cooper, A.K., Barker, P.F., Brancolini, G. (Eds.), Geology and Seismic Stratigraphy of the Antarctic Margin. Am. Geophys. Union, Antarct. Res. Ser. (68): 123-140.

Baraza, J., Lee, H. J., Kayen, R.E. and Hampton, M.A. 1990. Geotechnical characteristics and slope stability on the Ebro margin, western Mediterranean. Mar. Geol. (95): 379-393.

Barker, D.H.N. and Austin, J.A. 1994. Crustal diapirism in Bransfield Strait, West Antarctica. Evidence for distributed extension in marginal basin formation. Geology (22): 657-660.

Bryant, W.R. and R. H. Bennett. 1988. Origin, physical, and mineralogical nature of red clays: the Pacific Ocean basin as a model. Geo-Mar. Lett. (8): 189-249.

Canals, M., Acosta, J., Baraza, J., Bart, P., Calafat, A.M., Casamor, J.L., De Batist, M., Ercilla, G., Farran, M., Francés, G., Gràcia, E., Ramos-Gerrero, E., Sanz, J.L., Sorbías J.L. and Tassone, A. 1994. La Cuenca Central de Bransfield (NW de la Península Antártica): primeros resultados de la campaña GEBRA-93. Geogaceta (16): 132-135.

Canals, M., Casamor, J.L., Urgeles, R., Calafat, A.M., Domack, E.W., Baraza, J., Farran, M., De Batist, M. 2002. Seafloor evidence of a subglacial sedimentary system off the northern Antarctic Peninsula. Geology 30(7): 603-607.

Casagrande, A. 1936. The determination of the pre-consolidation load and its practical significance. Proceddings 1st International Conference Soil Mechanics and Foundation Engineering. pp. 60-64.

Dybedal, J. and Boe, R. 1994. Ultra high resolution subbottom profiling for detection of thin layers and objects. Oceans'94. Osates, Brest, France.

Edwards, B. D., Lee, H. J., Karl, H. A., Reimnitz, E. and Timothy, L. A. 1987. Geology and Physical Properties of Ross Sea, Antarctica, Continental Shelf Sediment. In: Cooper, A. K., Davey, F. J. (Eds.), The Antarctic Continental Margin: Geology and Geophysics of the Western Ross Sea. CPCEMR Earth Science Series, Circum-Pacific Council for Energy and Mineral Resources. Houston, Texas, 5B.

Ercilla, G., Baraza, J., Alonso, B. and Canals, M. 1998. Recent geological processes in the Central Bransfield Basin (Western Antarctic Peninsula). In: Stoker, M. S., Evans, D., Cramps, A. (Eds.), Geological Processes on Continental Margins: Sedimentation, Mass-Wasting and Stability. Geol. Soc., Spec. Publ., London,129, pp. 205-216.

Estrada, F., Canals, M., Ercilla, G. and Alonso, B. 2000. Análisis morfosedimentario detallado del Margen Pacífico septentrional de la Península Antártica. Geotemas 1(4): 135-138.

Faugères, J.C., Mézerais, M.L. and Stow, D. A.V. 1993. Contourite drift types and their distribution in the North and South Atlantic Ocean basins. Sed. Geol. (82): 189-203.

Gràcia, E., Canals, M., Farran, M., Prieto M.J. and Sorribas, J. GEBRA team, 1996. Morphostructure and evolution of the Central and Eastern Bransfield Basins (NW Antarctic Peninsula). Mar. Geophys. Res. (18): 429-448.

Hamilton, E. L. 1970. Sound velocity and related properties of marine sediments, North Pacific. J. Geophys. Res. (75): 4423-4446.

Hamilton, E.L. and Bachman, R.T. 1982. Sound velocity related properties of marine sediments. J. Acoust. Soc. Am. (72): 1891-1904.

Hampton, M.A., Bouma, A.M., Carlsn, P.R., Molnia, B.F. and Clukey, E.C. 1978. Quantitative study of slope instability in the Gulf of Alaska. 10th Proc. Annu. Offshore Technol. Conf. Houston, pp. 2307-2318.

Hampton, A.M., Lee, H. and Locat, J. 1996. Submarine landslides. Reviews of geophysics 34 (1), 33-59.

Holler, P. 1989. Mass-physical properties of sediment from Bransfield Strait and North Weddell Sea. Mar. Geotech. (8): 1-18.

Howe, J. A. 1995. Sedimentary processes and variations in slope-current activity during the glacial-interglacial episode on the Hebrides slope, northern Rockfall Trough, North Atlantic Ocean. Sed. Geol. (96): 201-230.

Ibáñez, J.M., Morales, J., Alguacil, G., Almendros, J., Ortiz, R., Pezzo, E., Posadas, A. and Luzón, F. 1997. Regional seismic activity around Livingston and Deception islands from 1992 to 1996: shallow and intermediate-depth earthquakes. Bol.R.Soc.Hist. Nat. (Sec. Geol.). 93, 1-4.

Jeffers, J.D. and Anderson, J.B. 1990. Sequence stratigraphy of the Bransfied Basin, Antarctica. Implications for the tectonic history and hydrocarbon potential. In: John, B. St. (Ed.) Antarctica as a Exploration Frontier: Hydrocarbon Potential Geology and Hazards. AAPG Stud. Geol. (31): 13-30.

Kim, D. C., Sung, J. Y., Park, S. C., Lee, G. H., Choi, J. H., Kim, G. Y., Seo, Y. K. and Kim. J. C. 2001. Physical and acoustic properties of shelf sediments, the South Sea of Korea. Mar. Geol. (179): 39-50.

Ladd, C.C. and Foott, R. 1974. New design procedure for stability of soft clays. J. Geotech. Eng. Div. 100 (GT7), 763-786.

Lambe, T.W. and Whitman R.V. 1969. Soil Mechanics. New York: Wiley.

Larter, R.D., Rebesco, M., Vanneste, L.E., Gambôa, A.P. and Barker, P.F. 1997. Cenozoic tectonic, sedimentary and glacial history of the continental shelf west of Graham land, Antarctic Peninsula. Geology and seismic stratigraphy of the antarctic margin, part2. Antarc. R. Ser. 71, pp. 1-27.

Lawer, L. A., Sloan, B. J., Barker, D. H. N., Ghidella, M., Herzen, R. P. V., Keller, R. A., Klinkhammer, G. P. and Chin, C. S. 1996. Distributed, active extension in Bransfiels Basin, Antarctic Peninsula: Evidence from Multibeam. GSA Today 6 (11): 1-7.

Lee, H.J., Edwards, B.D. and Field, M.E. 1981. Geotechnical analysis of submarine slumps, Eureka, California. 13 th Proc. Annu. Offshore Technol. Conf. Houston, Usa, pp. 53-59.

Lee, H.J. and Edwards, B.D. 1986. Regional method to assess offshore slope stability. J. Geotech. Eng. (112): 489-509.

Lee, H., Locat, J., Dartnell, P., Israel, K. and Wong, F. 1999. Regional variability of slope stability: application to the Eel margin, California. Mar. Geol. (154): 305-321.

Lee, H. and Baraza, J. 1999. Geotechnical characteristics and slope stability in the Gulf of Cadiz. Mar. Geol. *(155): 173-190.*

Maldonado, A., Later, R.D. and Aldana, F. 1994. Forearc tectonic evolution of the South Shetland Margin, Antarctic Peninsula. Tectonics 13 (6): 1345-1370.

Mariani, M., Argnani, A., Roveri, M. and Trincardi, F. 1993. Sediment drifts and erosional surfaces in the central Mediterranean: Seismic evidence of bottom-current activity. Sed. Geol. (82): 207-220.

McCave, N. and Tucholke, B.E. 1986. Deep current-controlled sedimentation in the western North Atlantic. The Geology of North America. The Western North Atlantic Region. Geol. Soc. Am. Vol. M.

McGregor, B. A., Bennett, R.H. and Lambert, D.N. 1979. Bottom processes, morphology, and geotechnical properties of the continental slope. South of Baltimore Canyon. App. Ocean Res. (1): 177-187.

Mulder, T. and Moran, K. 1995. Relationship among submarine instabilities, sea level variations, and the presence of an ice sheet on the continental shelf: An example from the Verrill Canyon Area, Scotian Shelf. Paleoceanography (10): 137-154.

Prieto, M.J., Canals., Ercilla, G., M. and Batist, M. 1998. Structure and geodynamic evolution of the Central Bransfield Basin (NW Antarctica) from seismic reflection data. Mar. Geol. (149): 17-38.

Prieto, M.J., Ercilla, G., Canals., M. and Batist, M. 1999. Seismic stratigraphy of the Central Bransfield Basin (NW Antarctic Peninsula): interpretation of deposits and sedimentary processes in a glacio-marine environment. Mar. Geol. (157): 47-68.

Robertson, S.D., Wiens, D.A., Dorman, L.M. and Vera, E. 2001. Seismicity and tectonics of the South Shetland Islands region from a combined land-sea seismograph deployment. Eos. Trans. AGU, 82 (47), Fall Meet. Suppl., Abstract S12B-0596.

Scott, R.F. and Zuckerman, K.A. 1970 Study of slope instability in the ocean floor. Calif. Inst. Technol., Soil Mech. Lab. Rep. CR-70007, 61p.

Swanson, R. G. 1981. Sample Examination Manual. Methods in Exploration Series. AAPG.

Vatan, A. 1967. Manuel de Sédimentologie. Paris: Technip.

Wetzel, A. 1990 Interrelationships between porosity and other geotechnical properties of slowly deposited, fine-grained marine surface sediments. Mar. Geol. (92): 105-113.

Yin, H. 1993. Acoustic velocity and attenuation of rocks: isotropy, intrinsic anisotropy, stress-induced anisotropy. Ph.D. thesis. Stanford Univ. USA.

Yoon, H.I., Han, M.W., Park, B.K., Oh, J. and Chang, S. 1994. Depositional environment of near-surface sediments, King George Basin, Bransfield Strait, Antarctica. Geo-Mar. Lett (14):1-9

Yoon, H.I., Han, M.W., Park, B.K., Oh, J. and Chang, S. 1997. Glaciomarine sedimentation and palaeo-glacial setting of Maxwell Bay and its tributary embayment, Marian Cove, South Shetland Islands, West Antarctica. Mar. Geol. (140): 265-282.

CAPÍTULO 7

DISCUSIÓN Y CONCLUSIONES

CAPÍTULO 7: DISCUSION Y CONCLUSIONES

DISCUSION Y CONCLUSIONES

En cada uno de los trabajos presentados se ha incidido especialmente en una característica concreta del estudio de las inestabilidades submarinas. Para obtener una imagen completa de este fenómeno las diferentes técnicas utilizadas deben poderse integrar (Fig. 1). Este paso no es trivial ya que a las marcadas diferencias entre las técnicas (escala, resolución o densidad de los datos) hay que añadir, con frecuencia, la poca disponibilidad de todo el abanico de datos necesarios por su coste económico o por falta de desarrollo técnico y científico.

Dos grandes grupos de técnicas se han utilizado en los diferentes trabajos presentados, el registro sísmico y las técnicas analíticas de laboratorio (análisis sedimentológico y geotécnico). El análisis sísmico nos ofrece la posibilidad de observar indirectamente el marco tecto-sedimentario donde los deslizamientos se producen así como definir el plano de deslizamiento, estructura interna, escala, geometría o la distancia que ha recorrido el sedimento deslizado. El análisis sedimentológico y geotécnico, por su parte, nos ofrece datos directos sobre el sedimento y las propiedades índice, resistencia y consolidación.

Los modelos sísmicos y geotécnicos, a menudo, son insuficientes por si solos para explicar en detalle la variabilidad de movimientos de masa y ambientes deposicionales en donde ocurren. Este hecho sugiere que cada evento descrito debería ser estudiado individualmente para conocer en detalle la dinámica del deslizamiento y su impacto sobre la estabilidad del talud. La necesidad del conocimiento exhaustivo de las condiciones tanto generales del área a estudiar como particulares de cada evento descrito es especialmente importante en sedimentos con hidratos de gas, ya que en este caso se nos presenta un problema doble, el de describir como afecta la presencia de hidratos de gas (o su descomposición) en las propiedades mecánicas del sedimento y en la de encontrar un método eficaz para estudiar el proceso. Durante la extracción de sedimentos con hidratos de gas, éstos se descomponen, proceso que aporta agua dulce al sedimento. La incorporación de agua a la matriz del sedimento sumado a la desaparición de un elemento sólido en ella evidentemente cambia las propiedades mecánicas y geotécnicas en general, por lo que es difícil caracterizar el comportamiento de dicho sedimento en estadios anteriores a un posible deslizamiento, ya que en la práctica es imposible obtener muestras intactas que se puedan analizar desde un punto geotécnico. En este caso concreto sólo es concebible la obtención de información fiable

pre-rotura, mediante técnicas de medición de propiedades in-situ, y los datos obtenidos sobre muestras en donde los hidratos ya se han descompuesto sólo aportan datos parciales sobre las características y posible comportamiento de esos sedimentos durante el estadio de post-rotura.

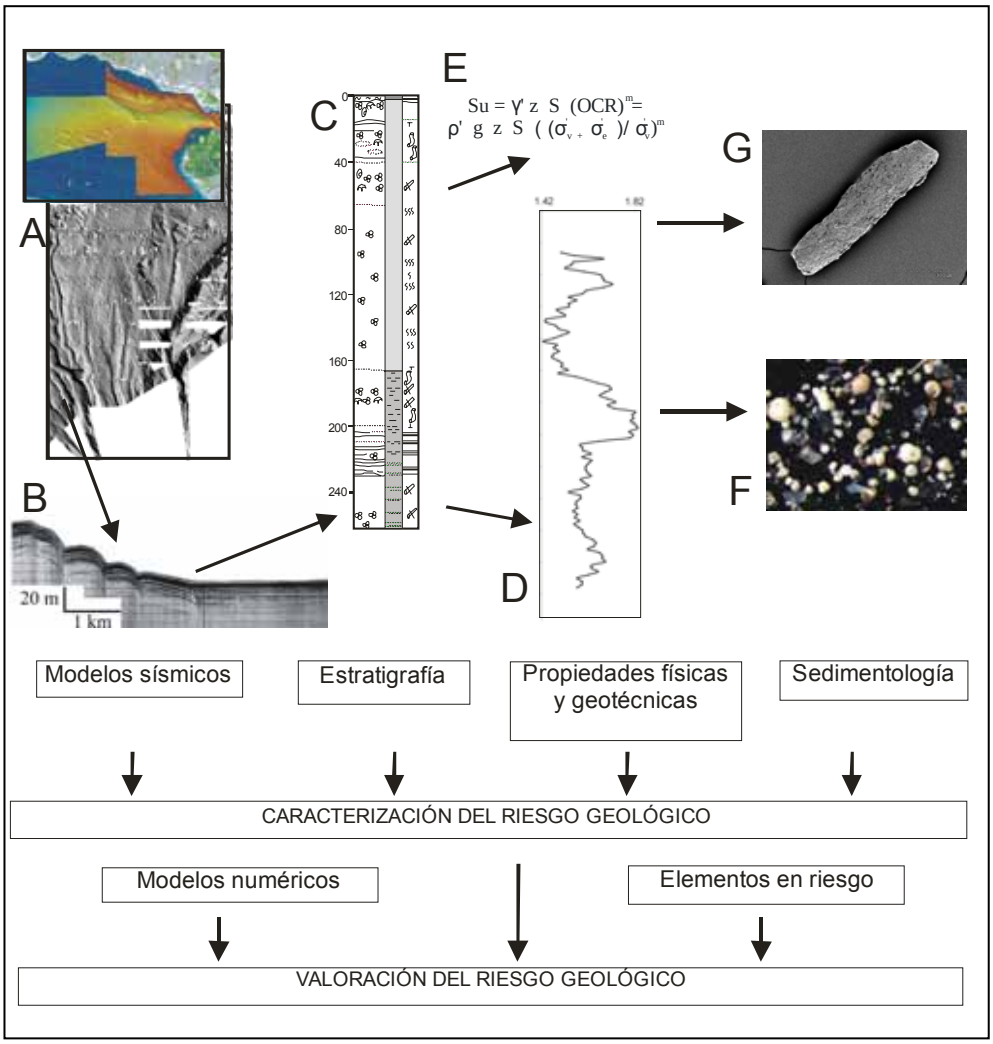

Fig. 1. La estrategia de estudio para abordar el estudio de las inestabilidades submarinas, implica una aproximación multidisciplinar (facies acústicas, morfología, sedimentología, propiedades físicas y geotécnicas…) y multiescala: kilométrica (multihaz y perfiles sísmicos, A y B respectivamente) métrica (testigos de sedimento, C; propiedades físicas, D) decimétrica (propiedades geotécnicas, E) milimétrica (características texturales, F) y micrométrica (características composicionales, G).

1. Caracterización del Margen Continental y Registro Histórico de las Inestabilidades Observables en un Talud Continental

El estudio de la distribución de procesos de inestabilidad sedimentaria en un área determinada, y las características de un talud continental que pueden favorecer su ocurrencia es esencial en el conocimiento de este tipo de procesos y de las variables que determinan su comportamiento. En este sentido el estudio regional de la distribución, tamaño y morfología de las inestabilidades submarinas se ha realizado en el capítulo 2.

Los movimientos de masa (37% de la superficie) son un importante proceso que controla la estructura y evolución sedimentaria del talud continental del Ebro durante el Cuaternario. Y tienen una distribución, tamaño y morfología muy variable. Los tres sectores diferenciados en el talud continental del Ebro (norte, centro y sur) se caracterizan por el relativo decrecimiento de la anchura y aumento del gradiente de norte a sur. Los sectores norte y central están básicamente afectados por cañones erosivos con cárcavas en los cursos superiores y deslizamientos masivos y caóticos en los cursos inferiores. El sector sur y la parte meridional de la parte central están básicamente afectados por deslizamientos de gran escala, Columbretes y Torreblanca (> 10 km de longitud), y depósitos de colada de derrubios, BIG'95 (Canals et al., 2000; Willmott et al., 2001; Urgeles et al., 2003). Los tres sectores además presentan deslizamientos de pequeña escala (> 4 km de longitud).

Las inestabilidades submarinas presentes en el área comprenden superficies erosivas asociadas a valles submarinos, cárcavas, deslizamientos en los cañones submarinos, deslizamientos de pequeña y gran escala, cicatrices de deslizamientos y coladas de derrubios en el talud "abierto". Los deslizamientos de pequeña y gran escala no actúan como agentes importantes de transporte hacia las zonas profundas del margen continental ya que aunque estos procesos modifican la estructura interna de los paquetes de sedimento movilizados éstos mantienen su coherencia. Son los cañones submarinos los principales agentes de transporte de sedimento aguas abajo.

La presencia y distribución de elementos críticos que pueden afectar a la estabilidad del talud, como sedimentos cargados con gas libre o hidratos de gas, es otro punto importante a integrar en el estudio regional y esto se ha abordado en el capítulo 3.

El área con sedimentos cargados de gas libre en el Golfo de Cádiz se ha identificado en forma de "blanket" que aparece como turbulencia acústica en los registros sísmicos y se da por absorción de la energía acústica. El área con gas libre está afectada por procesos de inestabilidad sedimentaria, en forma de deslizamientos, aunque éstos se

dan aguas abajo al oeste de la zona de turbidez acústica. Localmente, en las partes proximales de los deslizamientos, aparecen limitados basalmente por una zona contenedora de gas con reflexiones claras en forma de “bright spots”.

Los “pockmarks” aparecen en una área de 30 km de largo por 2 a 7 km de ancho en la zona centro-este del talud continental superior, entre los 300 y 400 m de profundidad, desde la zona cargada con gas libre y con diapiros. Los pockmarks presentan una gran variedad de tamaños y formas, con diámetros de entre 125 y 850 m y profundidades de entre 1 y 19 m. Los pockmarks presentes son tanto modernos como antiguos aunque ambos tienen una forma similar. Asociados a los pockmarks hay perturbaciones acústicas verticales que aparecen como difracciones de alta amplitud, y que pueden representar columnas de gas expulsado. Diferentes características acústicas (“wipe-outs” o perturbaciones columnares transparentes) indican la presencia de gas en el sedimento en las áreas con presencia de “pockmarks”. Plumas acústicamente reflectivas se han observado en la columna de agua, inmediatamente encima de los pockmarks, sugiriendo emanaciones de gas desde el sedimento superficial en la actualidad.

Junto a las evidencias ya mencionadas de la presencia de gas en el Golfo de Cádiz, existe una nueva característica, en forma de anomalía acústica, que puede constituir la prueba de la presencia de hidratos de gas en el área. Ésta anomalía, de la que se presentan varios ejemplos, sería comparable a los BSR (reflector simulador de fondo). Una reflexión fuerte, de alta amplitud y discontinua de unos 3 km de largo aparece en el talud superior central en la misma área en la que se desarrollan los “pockmarks”. Otro ejemplo de esta anomalía acústica se localiza en el talud superior, a lo largo de una cresta diapírica. Todas estas anomalías acústicas tipo BSR, que aparecen intermitentemente en algunas áreas del talud superior, se dan en condiciones de presión y temperatura deducidas que no corresponden a las condiciones de estabilidad de los hidratos de gas. En este sentido se sugiere que la intrusión de los edificios volcánicos/ diapíricos puede inducir localmente una presión anómalamente alta en las áreas inmediatamente colindantes, afectando el campo de estabilidad de los hidratos de gas y permitiendo su formación.

La presencia de gas e hidratos de gas también se ha confirmado en las montañas submarinas Anaximander (capítulo 5). La distribución de sedimentos cargados de gas en el área, parece estar condicionada por los procesos asociados a los volcanes de fango presentes. Se ha detectado la presencia de hidratos de gas en los cráteres de los

volcanes Kula, Kazan y Ámsterdam, aunque la extensión de la distribución de los hidratos de gas fuera de los edificios volcánicos parece estar limitada al talud sur del volcán Ámsterdam que es el más activo del área en términos del volumen de flujos de fango extruidos (Lykousis et al., 2005).

1.1. Valoración de los parámetros geológicos de un margen

La complejidad en los estilos de rotura y en la evolución de las inestabilidades sedimentarias, así como en la identificación de los mecanismos detonantes necesitan el análisis conjunto de todos aquellos parámetros geológicos que caracterizan a la zona de estudio en cuestión. En este sentido, los estudios arriba mencionados establecen que la caracterización geológica del margen continental ofrece información sobre aquellos factores críticos que pueden afectar a la estabilidad del talud continental (fondo y subfondo marino), tales como parámetros fisiográficos (pendientes, anchuras), localización y profundidad de sistemas deposicionales, morfología y configuración interna de las inestabilidades sedimentarias, facies litológicas y acústicas de las inestabilidades y del sedimento circundante, edad y génesis de los elementos morfo-sedimentarios y morfo-estructurales, dinámica de fluidos, elementos tectónicos, etc. Es decir, comprenden todos aquellos factores críticos a tener en cuenta en un análisis detallado del terreno y de la estratigrafía del subfondo marino.

Por otro lado, el estudio regional de la distribución, tamaño y morfología de las inestabilidades submarinas es importante para valorar su efecto en los sistemas sedimentarios de los taludes y su papel como mecanismo para modelar los márgenes continentales (Fig. 2). Además, ofrecen criterios para entender la dirección de transporte, que es generalmente talud abajo. Cuando se cuantifica el número de deslizamientos submarinos en función de la profundidad, se observa que éstos son más abundantes en el talud continental (Pratson y Laine, 1989; Booth et al., 1993). Asimismo su estudio regional permite establecer a grandes rasgos dos zonas principales en el talud continental: una zona depletiva y de evacuación y una zona acumulativa. La zona depletiva está caracterizada por el adelgazamiento del material deslizado y presencia de estructuras de tensión y la formación de superficies erosivas tales como cañones, cárcavas y cicatrices. Es decir, son zonas donde predominan lo procesos gravitativos erosivos. La zona acumulativa se caracteriza por la presencia de pliegues, estructuras de compresión y cuerpos deposicionales tales como debritas, turbiditas, diques

sedimentarios asociados a canales, es decir cuerpos sedimentarios formados por procesos gravitativos deposicionales los cuales contribuyen a la agradación/progradación del margen.

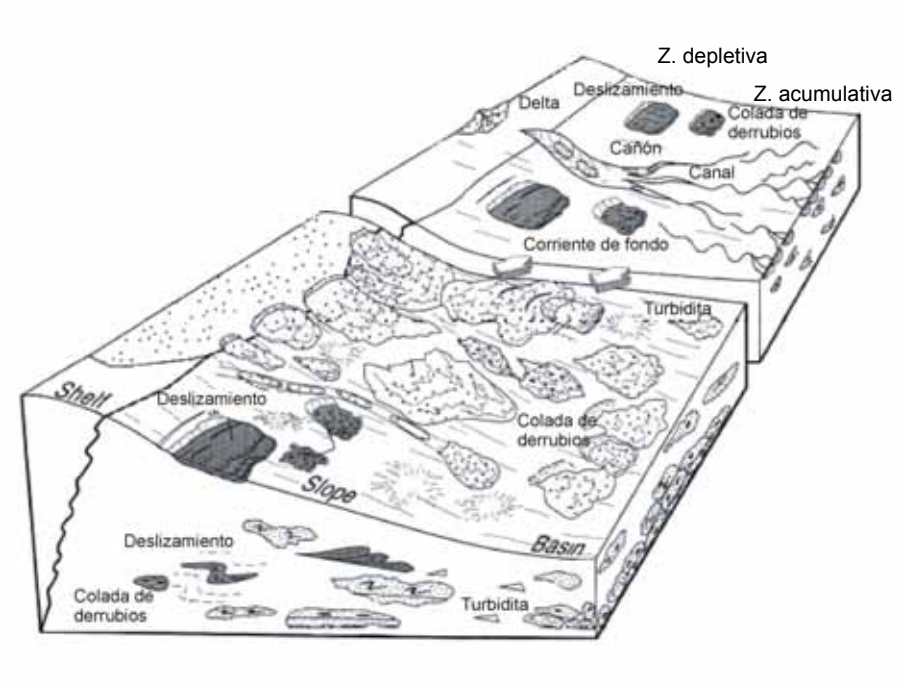

Fig. 2. Bloque diagrama representando la gran variedad de procesos de inestabilidad sedimentaria presentes en los taludes continentales y su distribución.

2. Definición de las Facies Sedimentarias, Geometría, Dinámica de Rotura y Evolución de los Deslizamientos Submarinos Observados

La variabilidad y distribución de los cuerpos de pequeña escala descritos en el margen continental del Ebro, han permitido efectuar una aproximación a su evolución. En este sentido son dos los factores que parecen controlar dicha evolución (asumiendo la presencia del mismo tipo de sedimento), el espesor del sedimento involucrado y la frecuencia de rotura.

De entre todos los cuerpos deslizados descritos en los trabajos presentados, los deslizamientos de Columbretes y Torreblanca, en el talud continental del Ebro son los depósitos individuales que mejor permiten caracterizar su geometría, sus facies y deducir

su dinámica de rotura. Columbretes es un deslizamiento enraizado en el talud superior a una profundidad de 170 m y que termina cerca del pie de talud aproximadamente a una profundidad de 1100 m. La cicatriz se extiende desde los 170 a 454 m de profundidad y se caracteriza por una superficie de pendiente alta (> 4º) que trunca los depósitos progradantes del borde de plataforma. El cuerpo deslizado, de 20 km de ancho se extiende unos 10 km aguas abajo y tiene un espesor medio de 150 ms (unos 113 m); y un volumen de unos 23 km^3. De hecho, el espesor del cuerpo principal varía aguas abajo (desde 150 a 80 ms). Sísmicamente, el cuerpo de Columbretes se puede diferenciar como un depósito caótico claramente diferenciado de las áreas bien estratificadas.

El deslizamiento Torreblanca ha sido identificado en la parte más meridional del sector central y se extiende hacia el pie de talud (al menos hasta los 1350 m de profundidad). La parte más proximal, cerca del Cañón de Torreblanca está a 360 m de profundidad, donde la pendiente aumenta de manera abrupta de 15 a 29 %. Este cambio marca la cicatriz que tiene aproximadamente una extensión vertical de unos 300 m. Entre la cicatriz y el cuerpo principal, situado a 655 m de profundidad, hay un pequeño valle en forma de V, que corresponde a una estructura tensional característica de la cabecera de muchos deslizamientos submarinos. El cuerpo principal del deslizamiento Torreblanca se define sísmicamente por reflectores estratificados discontinuos afectados por facies hiperbólicas caóticas. El cuerpo tiene una longitud de hasta 40 km y presenta una sección de forma lenticular. El deslizamiento posee una superficie rugosa y un espesor de unos 300 ms que afecta a un complejo canal-dique. El plano de deslizamiento se localiza entre 90 y 260 m por debajo de la superficie del deslizamiento. El plano es bastante continuo, concordante con la estratificación regional.

Aunque sólo se dispone de un perfil sísmico que atraviesa el deslizamiento de Torreblanca, se pueden deducir algunos aspectos sobre el mecanismo de rotura y su evolución, ya que presenta una morfología, geometría y estructura interna bien desarrollada constituida por diversas unidades litológicas que están incididas oblicuamente por un complejo canal-dique. Cuatro estadios forman el modelo propuesto por Baraza 1989 para la génesis y desarrollo de este deslizamiento, en esta Tesis estos estadios se definen como: metaestable, rotura, deslizamiento y parada (Fig. 3). En el momento inicial, un equilibrio metaestable caracteriza el talud y en esta situación los planos de estratificación pueden actuar como niveles de debilidad; esto queda sugerido por el hecho que el plano de deslizamiento parece estar formado por un nivel subparalelo a la estratificación. Los paquetes de sedimento estratificados se depositaron durante

estadios de bajo nivel del mar con una alta tasa de sedimentación, lo que implicaría que el sedimento está subconsolidado y por tanto tendríamos niveles débiles proclives a la inestabilidad (Hampton et al., 1996; Larberg y Vorren, 2000; Canals et al., 2004). El estadio de rotura se iniciaría cuando el equilibrio metaestable se rompe. Esto ocurriría cuando las fuerzas movilizadoras superan la resistencia del sedimento.

El estadio de rotura se inicia con un desplazamiento a lo largo del plano de rotura. Este desplazamiento consistiría en un movimiento rotacional y un desplazamiento horizontal a lo largo del plano de rotura. En este estadio, se genera la cicatriz principal así como la depresión tensional que resulta de la separación de ambas caras del plano de deslizamiento. En un estadio de madurez, el deslizamiento progresa siguiendo este régimen tensional. El deslizamiento rotacional a lo largo del plano de rotura es más aparente en la cicatriz principal, así como el desplazamiento traslacional del cuerpo principal lo es a lo largo del plano de rotura. Este régimen distensivo sería el responsable de la formación de estructuras tensionales, como son las fallas normales o antitéticas en la parte proximal del cuerpo deslizado. Simultáneamente, el deslizamiento progresa aguas abajo y el volumen y área que involucra aumenta.

El estadio de parada se inicia cuando las fuerzas conductoras que actúan decrecen como resultado de los menores gradientes del talud en las partes más profundas de éste. Este efecto se suma al incremento de las fuerzas de resistencia por fricción en el plano de deslizamiento lo que reduce progresivamente la velocidad del cuerpo movilizado produciendo estructuras compresivas. El estadio final se produce cuando las fuerzas de fricción superan las fuerzas conductoras en la parte superior del área deslizada. Como consecuencia de este balance se produce un régimen compresivo en la parte final del deslizamiento, lo que implica el desarrollo de pequeños pliegues de arrastre y la parada definitiva del cuerpo deslizado.

Las diferencias de comportamiento durante los estadios de rotura y post-rotura de los movimientos de masa observados en sedimentos aparentemente equivalentes, así como la detección de las variables que controlarían una posible reactivación es un aspecto poco conocido y no suficientemente caracterizado. Los dos movimientos de mayor tamaño descritos, Columbretes y Torreblanca, están en una posición, en el talud, equivalente pero presentan unas características sísmicas y morfológicas bien diferenciadas. La estructura interna del deslizamiento de Torreblanca al presentar una entidad geométrica definida, indica que el sedimento está sólo ligeramente alterado, y que el transporte pendiente abajo sólo produjo “rumpling” y “folding". En el caso del

deslizamiento de Columbretes se produce una fragmentación progresiva durante el movimiento pendiente abajo. La falta de estratificación observable indica que durante el desplazamiento, el bloque deslizado de Columbretes sufrió una intensa distorsión y mezcla. Además el hecho de que la profundidad a la que se localiza el plano de deslizamiento sea variable (está a menos profundidad en el sector noreste) y que afecte a diferentes niveles estratigráficos sugiere que este deslizamiento no está arraigado en un sólo paquete de sedimento. Los datos disponibles hasta el momento no sugieren una respuesta satisfactoria a las diferencias de comportamiento durante los estadios de post-rotura en sedimentos *a priori* equivalentes.

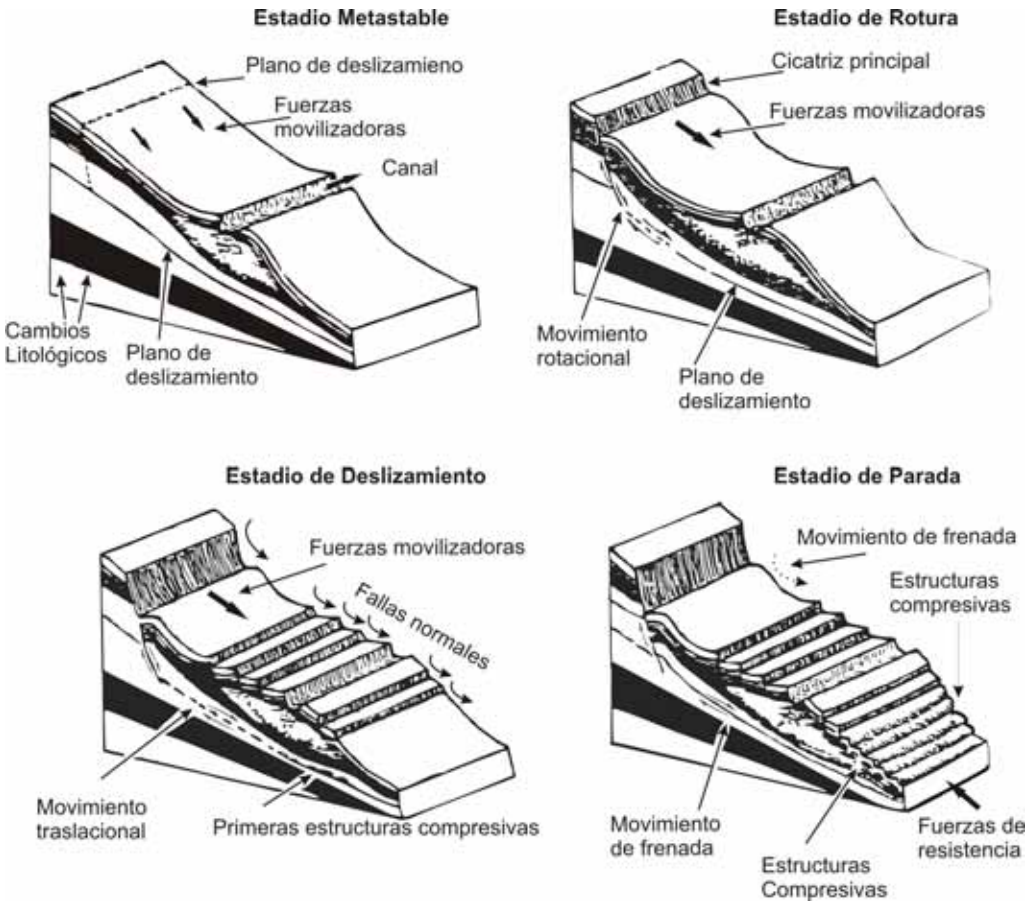

Fig. 3. Bloques diagrama mostrando los cuatro estadios propuestos, metaestable, rotura, deslizamiento y parada, en la evolución del deslizamiento de Torreblanca. Modificado de Baraza, 1989.

2.1. Comparación entre los modelos sísmicos y geotécnicos

Los estudios llevados a cabo en el talud continental del Ebro y talud continental de la Península Antártica y la Cuenca de Bransfield ponen de manifiesto diferencias de comportamiento reflejados en los datos sísmicos y geotécnicos. Una vía para explicar las diferencias sería la integración de los modelos geotécnicos y sísmicos. Esto se puede llevar a cabo en el talud del Ebro dada la disponibilidad de un modelo geotécnico de la misma área realizado por Baraza et al. (1990). Dicho modelo se basa en el análisis de testigos de sedimento (< 3 m de longitud) en los sectores central y sur del talud continental del Ebro (Fig. 1 del capítulo 2) y define dos áreas diferenciadas en función de sus propiedades geotécnicas: el talud continental superior (< 500 m de profundidad) e inferior (>500 m de profundidad). En líneas generales, el talud superior es más estable bajo condiciones estáticas no drenadas y el talud continental inferior es más estable bajo condiciones con drenaje o de largo período, aunque el máximo gradiente observado en el área de estudio (talud superior e inferior) sería estable bajo condiciones de carga estática (gravitacional).

Este modelo geotécnico puede explicar sólo en cierta medida la distribución y características de los movimientos de masa observados en el talud continental del Ebro. Es una buena aproximación para empezar a entender qué propiedades físicas y geotécnicas generales tienen los sedimentos del área y cual es su comportamiento más probable. De hecho, la zonación geotécnica propuesta podría explicar porqué la mayoría de depósitos de flujos de derrubios están concentrados en el talud inferior, ya que es donde el sedimento presenta una mayor plasticidad (respecto al talud superior). Igualmente, la zonación geotécnica propuesta puede ayudar a entender porqué los movimientos de gran escala presentan sus cicatrices en el talud superior; esto sería por la mayor susceptibilidad de los sedimentos situados entre 200 y 700 m ante una carga sísmica.

Aún y así el modelo es ciertamente insuficiente para explicar con satisfacción la variabilidad de contextos, tipos, escalas y geometrías de las inestabilidades descritas en los perfiles sísmicos. El análisis de los perfiles de sísmica del talud continental sugiere una diversidad de ambientes deposicionales (talud superior e inferior, sectores norte, central y sur, cañones e intercañón) mucho mayor que la reflejada por el modelo geotécnico (talud superior e inferior). Este hecho sugiere que la distribución y variabilidad de los movimientos de masa y su detonante más probable se debe estudiar

individualmente desde el punto de vista geotécnico para de esta forma conocer las condiciones locales de estabilidad y rotura del sedimento. Este sería un buen principio para saber las causas de que una región se mantenga intacta mientras que la región vecina se rompe y desliza y porqué lo hace en la forma en la que lo hace.

Nuevos datos obtenidos en el flujo de derrubios llamado BIG'95 en el talud continental del Ebro (Willmott et al., 2001) presentan diferencias en las propiedades físicas, en concreto en el contenido en agua, respecto a los valores obtenidos para el modelo geotécnico. El contenido en agua medido en los testigos distribuidos a lo largo de BIG'95 presenta un reducción general del 43% respecto el valor medio obtenido por el modelo geotécnico (Baraza, 1989) en las áreas colindantes. Por tanto, si las propiedades índice del sedimento están condicionadas por el contenido en agua en la zonación propuesta por Baraza (1989), el comportamiento de esta parte del talud podría ser significantemente diferente, reforzando así la idea de la necesidad de un estudio individualizado de los diferentes ambientes observados.

3. Estudio de las Propiedades Físicas, Mecánicas y Elásticas del Sedimento

Las propiedades físicas (densidad, velocidad de ondas P y susceptibilidad magnética) de sedimentos marinos son variables importantes para entender tanto los ambientes marinos como los eventos geológicos que se dan en ellos. Diferentes estudios se han centrado en las relaciones existentes entre las propiedades físicas y parámetros texturales de los sedimentos marinos, ya que estas dependen en gran medida de la litología, el tamaño de grano y la composición de los sedimentos. La densidad total, por ejemplo está relacionada con la porosidad, la densidad de grano y está parcialmente controlada por el tamaño de grano. La velocidad de ondas P está controlada por la porosidad, el contenido en carbonato y minerales de las arcillas. Las propiedades físicas también pueden estar fuertemente influenciadas por procesos diagenéticos, como el decrecimiento de la porosidad por compactación, por cementación o por la disolución de carbonato (Fig. 4). El conocimiento de las propiedades físicas es básico en el estudio de la estabilidad sedimentaria ya que proporciona información básica sobre el sedimento e intervienen en el cálculo de las propiedades geotécnicas, esenciales en la estimación de la estabilidad de una zona en concreto. El estudio de las propiedades físicas se ha realizado de forma extensa en los capítulos 4, 5 y 6 de la presente memoria.

Los sedimentos recuperados en la Llanura Abisal de Madeira (mayoritariamente turbiditas carbonatadas, orgánicas y volcánicas) son sedimentológicamente parecidos pero muy variables en lo que a su contenido en carbonato se refiere y presentan unas propiedades físicas e índice características, controladas básicamente por el grado de compactación más que por cambios litológicos. La distribución textural y la baja variabilidad en los sedimentos analizados reflejan la típica deposición en ambientes marinos distales, donde predomina la acumulación de turbiditas.

Los registros de susceptibilidad magnética presentan picos de alta amplitud que diferencian claramente los minerales altamente magnetizables de las turbiditas volcánicas, de las turbiditas orgánicas y carbonatadas con una baja susceptibilidad magnética. Las diferencias observadas en la susceptibilidad magnética están pues relacionadas con cambios mineralógicos. Los registros de densidad total y velocidad de ondas P están relacionados básicamente por el efecto de consolidación que se da en la columna sedimentaria, aunque en detalle presentan variaciones que se pueden relacionar con la presencia de intervalos limosos o algunas de las turbiditas orgánicas o carbonatadas.

Las variaciones en la densidad de grano no presentan ninguna tendencia definida en la vertical, aunque si están relacionadas con los cambios composicionales del sedimento, especialmente entre sílice y carbonato, presentando valores relativamente más altos en los intervalos turbidíticos volcánicos. Las propiedades índice están básicamente relacionadas con el decrecimiento de la porosidad e incremento de la densidad debido a la compactación por presión litostática. Localmente algunas tendencias, o la presencia de picos abruptos pueden estar relacionados con cambios composicionales, y pueden marcar especialmente las diferencias entre sedimentos ricos en sílice y en carbonato. El contenido en carbonato no se correlaciona con cambios en la porosidad ni con la densidad de grano, por lo que parece no tener un particular efecto sobre las variaciones en las propiedades físicas de estos sedimentos.

De la consolidación progresiva del sedimento resulta la expulsión del agua intersticial y un aumento de la fricción y por tanto de la resistencia del sedimento. La reducción de la porosidad y del contenido en agua es el primer factor de control en el incremento de la resistencia en profundidad. La comparación entre el contenido en agua y la resistencia del sedimento pone de manifiesto la correlación entre valores altos de resistencia con contenidos en agua medios de 40% y un decrecimiento abrupto de la resistencia para valores de contenido en agua del 60%. Las variaciones en la resistencia

son menores para contenidos en agua entre 70 y 150%. Parte de las variaciones observadas se podrían relacionar con la presencia de fuerzas cohesivas desarrolladas en sedimentos ricos en arcillas. El control de la resistencia del sedimento por la consolidación también se puede deducir por la relación entre la resistencia y la velocidad de ondas P, un parámetro relacionado con la consolidación y/o diagénesis del sedimento. Un incremento progresivo pero no lineal de la velocidad de ondas P se relaciona con un incremento en los valores de resistencia.

Dos tipos de sedimento básicos se han definido en los volcanes de fango localizados en las montañas de Anaximander, brechas fangosas, producto de la actividad volcánica (coladas de fango) y fangos hemipelágicos. La estratigrafía de los testigos que muestrean los ambientes internos de los cráteres de los volcanes Ámsterdam, Kula y Kazan (An05GC1, An07GC4, An14GC1) se caracteriza por el apilamiento vertical de brechas de fango, mientras que el testigo An013GC1 localizado en el flanco externo del volcán Kula presenta brechas fangosas que hacia el techo pasan a fangos hemipelágicos.

Las propiedades físicas de los sedimentos del interior de los cráteres están básicamente controladas por la litología; ésto queda reflejado por algunas correlaciones entre la densidad y diferentes variables texturales (arena, limo o grava). La susceptibilidad magnética en estos sedimentos está controlada por la fracción más fina. Contrariamente, el testigo en el flanco externo de Kula está básicamente controlado por el efecto de la consolidación (compactación) de la columna sedimentaria en profundidad, aunque a escala de detalle refleja las variaciones texturales o composicionales (hemipelágico *versus* brechas fangosas). La susceptibilidad magnética parece estar controlada en este caso, por la fracción grosera.

El contenido en carbonato parece no tener una influencia significativa en las propiedades físicas de estos sedimentos. El contenido en agua no presenta tendencias claras en los testigos excepto para el situado en el flanco exterior de Kula, donde se da un incremento de contenido en agua asociado a un decrecimiento de la densidad y porosidad. La resistencia a la cizalla no presenta ninguna tendencia general clara en la vertical, en general parece estar controlada por el efecto de la disturbación resultante de la despresurización que se da durante la recuperación de los testigos por escape de gas o disociación y escape de hidratos de gas.

La estratigrafía y las relaciones comentadas anteriormente en los testigos situados en el interior de los tres volcanes de fango indican que las propiedades físicas

están controladas por la litología y procesos volcánicos más que por el grado de compactación. Esto sugiere la existencia reciente (actual) de circulación de fluidos y por tanto de actividad volcánica reciente. En contraste el testigo situado en el flanco exterior de Kula presenta unas propiedades físicas controladas por la compactación y a menor escala por el tipo de sedimento, como ocurre normalmente en sedimentos finos y profundos. Esto sugiere una influencia restringida de los procesos volcánicos fuera del edificio.

Las propiedades físicas de los sedimentos analizados en el talud continental de la Península Antártica y zona profunda de la Cuenca de Bransfield, están controladas por las diferencias texturales descritas y por la estratigrafía (estructuras sedimentarias, tendencias verticales en la distribución del tamaño de grano). La velocidad de ondas P decrece con el incremento del contenido en arcilla, y los valores de densidad y susceptibilidad magnética aumentan con la presencia de clastos de tamaño grava o grupos de clastos. Las correlaciones entre éstas variables no pueden explicar totalmente el comportamiento de las propiedades físicas por no tener suficiente entidad estadística y que por tanto sería necesario tener en cuenta otro grupo de variables (por ejemplo la microfábrica, mineralogía, actividad química, actividad biológica o procesos físicos/mecánicos). La densidad y la susceptibilidad magnética también parecen estar controladas por el efecto de dos características principales de la macrofábrica: la tendencia vertical de los cambios texturales y estructuras sedimentarias como las laminaciones paralelas y cruzadas.

Respecto a las propiedades geotécnicas, sólo el contenido en agua está influenciado por la textura. El mayor contenido de arcillas en los depósitos de la cuenca explicaría el mayor contenido en agua de estos respecto a los del talud continental, aunque la disminución generalizada del contenido en agua de techo a base en todos los testigos estaría condicionada por la consolidación del sedimento y no por cambios en la estratigrafía o texturales. La consolidación y resistencia del sedimento son similares en todos los testigos. Los sedimentos en el margen de la Península Antártica están normalmente consolidados, excepto para el testigo de talud TG3, en el que una ligera sobreconsolidación puede ser considerado. Esta sobreconsolidación en los sedimentos superficiales sería el resultado de la pérdida de carga sedimentaria producto de las inestabilidades submarinas que son un proceso dominante en el talud estudiado. Se ha calculado que la pérdida de unos 9 m de sedimento es la causa más probable sugerida para la sobreconsolidación observada.

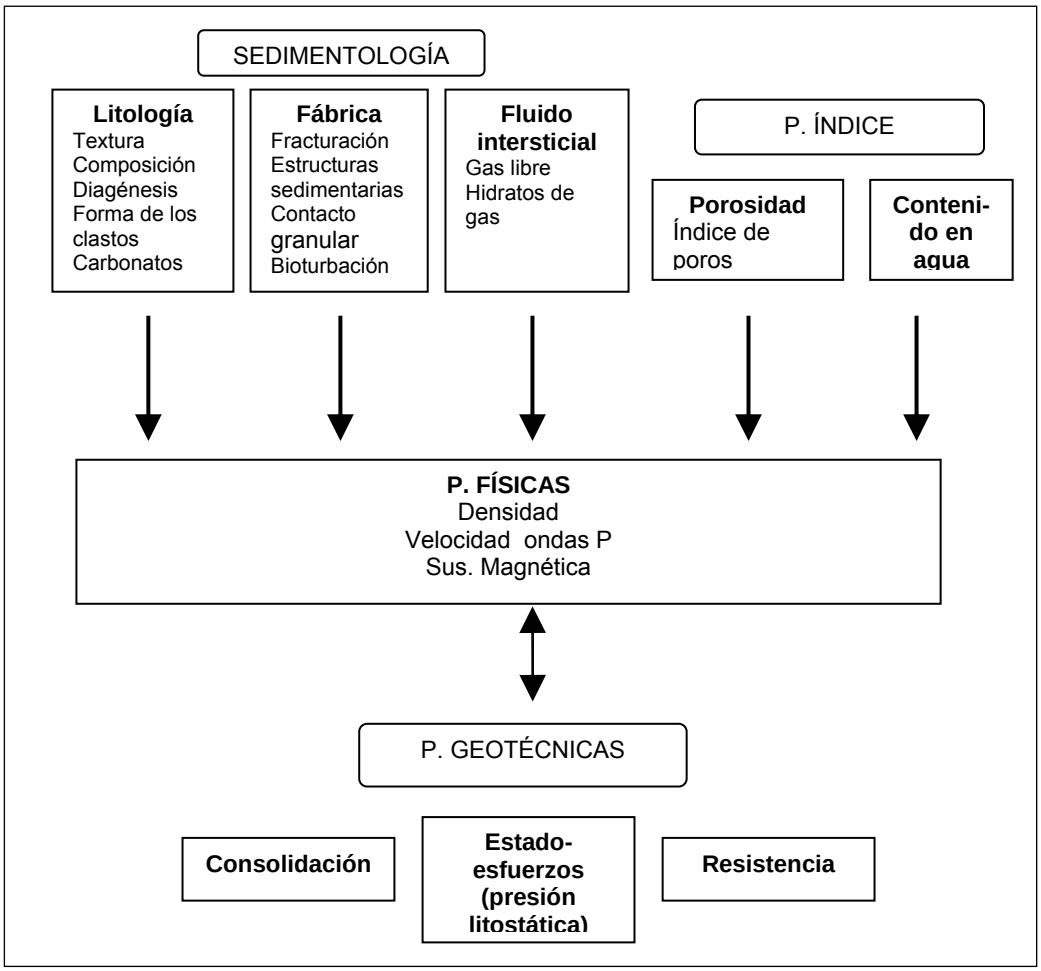

Fig. 4. Esquema que ilustra la compleja interdependencia multi-variable de las propiedades físicas de un sedimento marino. Ponderar la influencia de cada variable sedimentológica e índice es un ejercicio muy complejo ya que éstas están, a su vez, íntimamente interrelacionadas.

3.1. Relaciones entre las propiedades físicas y las sedimentológicas. El problema inverso

Las propiedades físicas obtenidas en continuo y a alta resolución se han mostrado una herramienta muy valiosa y útil en el estudio de los sedimentos marinos. Nos permite estudiar en detalle la estratigrafía, las tendencias verticales en los sedimentos, su correlación lateral y afinar las características de los sedimentos descritos. También se ha demostrado su gran utilidad cuando se integran en los cálculos de estabilidad.

Una de las ambiciones en el conocimiento de las propiedades físicas es la

predicción del sedimento a partir del registro de sus propiedades físicas. El problema para este ejercicio es que en la práctica, las propiedades físicas dependen de muchas variables que a su vez se interrelacionan de forma compleja (Fig. 4). Estamos pues delante de un problema multi-variable, matemáticamente complejo y que no tiene una solución única. Aunque sea parcialmente, si que es posible observar qué variables, al menos para unos testigos en concreto, tienen un mayor peso o son críticas en la definición de sus propiedades físicas. Esto se puede observar en los capítulos 4, 5 y 6 donde se han descrito diferentes relaciones estadísticamente aceptables entre las propiedades físicas y las variables sedimentológicas. Estas relaciones no son constantes, y dependen en gran medida de las características de cada tipo de sedimento (ambiente geológico), pero si que hay ciertos patrones en el comportamiento de los registros de densidad, susceptibilidad magnética y velocidad de ondas P que se cumplen coincidiendo con el "estilo" de la sedimentación. Esto se puede observar en las características generales de los registros que son relativamente parecidos en los testigos recuperados en el talud de la Península Antártica y en los volcanes de fango de Anaximander. En ambos casos el "estilo" de los registros del diamicton (de procedencia glacio-marina) y de la brecha fangosa (de procedencia volcánica) es parecida y contrasta con el de los sedimentos recuperados de la base del talud o cuenca, es decir con sedimentos estrictamente marinos (p.e. turbiditas). A pesar de que evidentemente el diamicton y la brecha fangosa tienen una génesis totalmente diferente, y que la composición no es en absoluto comparable, si tienen en común el ser sedimentos matriz soportados que contienen clastos de diversos tamaños y formas. Parece pues que la fábrica de un sedimento tiene una importancia clave en sus propiedades físicas relativas mientras que la composición mineralógica tendrá un efecto más relevante en el valor absoluto de estas propiedades.

En los testigos TG2 (Bransfield), an13GC1 (Anaximander) y los sondeos 950, 951 y 952 (Llanura Abisal de Madeira) donde dominan los procesos marinos, las propiedades físicas están básicamente controladas por la consolidación (compactación de la columna sedimentaria) presentando variaciones de orden menor que corresponden a grandes rasgos a cambios litológicos o variaciones internas del sedimento. Contrariamente, en los testigos con sedimentos depositados por procesos glacio-marinos (TG3, TG4, TG29 en Bransfield) y volcánicos (an05GC1, an14GC1 y an07GC4 en Anaximander) las propiedades físicas parecen estar controladas por las características del sedimento y el efecto de la compactación, si se observa, es muy secundario.

4. Determinación de las Fuerzas y Procesos Mecánicos que Pueden Controlar la Detonación de Deslizamientos y su Evolución

Las fuerzas y procesos que pueden originar los deslizamientos observados en las diferentes áreas estudiadas (capítulos 2, 3 y 6) dependen tanto del marco regional como de factores locales, involucrando procesos característicos de ambientes sedimentarios particulares. Entre los **factores de predisposición** detectados en las áreas de estudio se pueden citar la actividad sísmica, la presencia de hidratos de gas, la actividad volcánica, la erosión o las altas tasas de sedimentación. Entre los mecanismos o **factores detonantes** deducidos se pueden citar la carga litostática (subconsolidación), los terremotos y la incidencia de tormentas y olas internas o corrientes de marea sobre el sedimento durante los estadios de bajo nivel del mar, la actividad volcánica, corrientes de fondo, carga-descarga glacial o la presencia de sedimentos cargados con gas libre. Entre los **factores revelantes** observados se pueden citar la evidencia de inestabilidades previas, la presencia de pockmarks o de estructuras diapíricas (Tabla 1).

El desarrollo de las inestabilidades en el talud continental del Ebro ha sido favorecido por la tectónica local y las altas tasas de sedimentación en el talud superior, que corresponden a depósitos deltaicos regresivos. Bajo estas condiciones, los posibles mecanismos detonantes son la carga litostática, los terremotos y la incidencia de tormentas y olas internas sobre el sedimento durante los estadios de bajo nivel del mar. La distribución espacial, la variabilidad, los tipos de movimientos en masa y la evolución post-deslizamiento están influenciados por factores independientes. Estos factores incluyen un aporte desigual de sedimento, la frecuencia de rotura la potencia del sedimento involucrado, el gradiente del talud y la proximidad a los epicentros de terremotos. Las pendientes relativamente altas presentes en el talud continental del Ebro, y la rápida deposición directamente sobre el talud superior durante los periodos de bajo nivel del mar son los principales factores responsables del estado de subconsolidación del sedimento y la consecuente disminución de la resistencia del sedimento. Bajo estas condiciones es probable que la carga sedimentaria fuese suficiente para generar los deslizamientos. Aunque este mecanismo fue seguramente favorecido por la acción cíclica de tormentas y ondas internas durante los estadios de bajo nivel del mar. Las coladas de derrubios depositadas en el talud continental inferior serían resultado de la evolución de deslizamientos. La carga sísmica se puede considerar como el mecanismo responsable de generar los deslizamientos de gran escala Torreblanca y Columbretes, probablemente también favorecido por otros factores secundarios inestabilizadores.

En el talud continental del Golfo de Cádiz, se ha observado una zona afectada por procesos de inestabilidad sedimentaria, en forma de deslizamientos, en el área con gas libre al oeste de la zona en la que se ha registrado turbidez acústica. Localmente, en las partes proximales de los deslizamientos, aparecen limitados basalmente por una zona de gas con reflexiones claras en forma de “bright spots”. La presencia de pockmarks y diapiros son factores revelantes específicos de esta área y la presencia de hidratos de gas es un factor de predisposición, aunque la poca extensión geográfica en hidratos, asociados básicamente a la presencia de edificios diapíricos hace pensar que la disociación de estos hidratos no es un factor detonante relevante. Por el contrario se puede correlacionar la presencia de deslizamientos a la presencia de sedimentos cargados de gas libre, por lo que se podría considerar este factor como un elemento crítico en la estabilidad sedimentaria de la zona.

En el área de las montañas de Anaximander y según los pocos datos disponibles, como pasa en el Golfo de Cádiz la distribución de hidratos de gas en el sedimento parece ser limitada, aunque en este caso al interior de los volcanes de fango y al flanco sur del talud del volcán Ámsterdam. Esto hace pensar que aunque su presencia se puede considerar un factor de predisposición, su disociación tampoco sería un factor detonante relevante.

	Ebro	**Cádiz**	**Anaximander**	**Bransfield**
Factores predisposición	• Tectónica • Tasa sedimentación • Pendientes del talud	• Sedimentos cargados de gas libre e hidratos de gas	• Sedimentos cargados de gas libre e hidratos de gas	• Zona de actividad sísmica
Factores detonantes	• Carga litostática • Terremotos • Oleaje de tormenta • Ondas internas	• Sedimentos cargados de gas libre • Formación de diapiros		• Actividad volcánica • Terremotos
Factores revelantes	• Inestabilidades previas	• Pockmarks • Diapiros	• Inestabilidades previas	• Inestabilidades previas

Tabla 1. Factores de control más relevantes de las inestabilidades sedimentarias descritas en las diferentes áreas de estudio.

En el talud de la Península Antártica, al contrario que en el margen continental del Ebro, la carga litostática (subconsolidación) no es un factor detonante, debido a las características del sedimento presente en el talud. Según los resultados de los análisis geotécnicos realizados, la pendiente máxima medida en el área de estudio (20º) sería estable según los conceptos de estabilidad bajo carga estática (litostática), y según estos preceptos se puede establecer que el ángulo máximo estable variaría entre 22º y 29º. Este dato, además podría explicar porqué los taludes en altas latitudes, construidos con sedimentos glaciomarinos, son muy abruptos a pesar de tener un control estrictamente sedimentario. Las inestabilidades observadas o deducidas en la zona, no se podrían explicar por las características del sedimento ya que estos son estables por si mismos, por tanto se debe recurrir a factores detonantes externos al sedimento. Basándonos en el marco oceanográfico y geológico, la actividad volcánica, corrientes de fondo, corrientes de marea, carga-descarga glacial o terremotos pueden ser considerados como potenciales mecanismos inducidores de inestabilidades en el área.

5. Consideraciones Finales y Perspectivas de Futuro

Esta Tesis Doctoral contribuye al conocimiento de las inestabilidades submarinas, que por su singularidad y significado tienen un alto interés científico. Pero de los trabajos presentados afloran aspectos poco resueltos y derivan nuevas preguntas…

La concepción dinámica de las inestabilidades submarinas, que implica diferentes estadios (pre-rotura, rotura, post-rotura y reactivación) con diferentes leyes y parámetros de control, genera inevitablemente nuevas incógnitas. Se ha observado (capítulo 2) que existen diferencias significativas en el comportamiento post-rotura incluso en sedimentos equivalentes. ¿Cómo predecir este comportamiento?, ¿qué factores son determinantes en la posible evolución de un deslizamiento a una colada de derrubios y/o a una corriente de turbidez?. Esto último es relevante, no sólo desde un punto de vista científico, también lo es para la evaluación del riesgo y vulnerabilidad al que pueden estar sometidos diferentes infraestructuras, ya que las corrientes de turbidez, como ya se ha apuntado, pueden presentar distancias de transporte muy importantes y por tanto afectar a estructuras muy alejadas de las áreas en las que se generan.

Gran parte de los trabajos publicados sobre inestabilidades submarinas, se centran en movimientos de masa localizados en márgenes divergentes y pasivos. Es en estos márgenes donde se han descrito algunos de los ejemplos más espectaculares. Es evidente que en otros marcos geológicos, márgenes convergentes e insulares (por ejemplo volcánicos) los procesos de inestabilidad sedimentaria son importantes. ¿Hay diferencias respecto a las inestabilidades entre estos contextos geológicos?, ¿los movimientos de masa son más frecuentes pero de menor magnitud en márgenes activos tectónicamente?.

En el capítulo 3, se estudia el papel del gas libre e hidratos de gas en el sedimento, como un factor crítico en la estabilidad de un talud continental. El objetivo de este artículo es el estudio de dicho elemento en si mismo, y se ha visto como la presencia de gas se puede relacionar con inestabilidades sedimentarias, con la formación de “pockmarks” o con la formación de plumas de gas en la columna de agua. Parece que la expulsión de gas del sedimento puede obedecer a diversos mecanismos que provocan diferentes efectos, que no siempre son la detonación de inestabilidades. Aunque la idea de que es un factor de predisposición es rotunda, ¿bajo que condiciones es un factor detonante?, ¿depende sólo de la concentración y de la presión intersticial que es capaz de generar?, ¿de la velocidad de expulsión?, ¿qué otros factores son importantes?.

Se han discutido en los capítulos 4, 5 y 6 las relaciones existentes entre las propiedades físicas y otras variables sedimentológicas de los sedimentos estudiados. Es evidente que por ejemplo, la precipitación de carbonatos y minerales de neoformación, con los cambios en la fábrica del sedimento que esto conlleva, debe tener un efecto importante sobre el comportamiento mecánico de los sedimentos, y por tanto sobre sus propiedades físicas. ¿En que grado la diagénesis afecta a las propiedades físicas?. ¿Cómo ponderar este efecto?.

El avance en el estudio de las inestabilidades submarinas no sólo requiere aproximaciones conceptuales adecuadas o la integración de diferentes disciplinas, sino también de la mejora tecnológica para la recuperación de datos representativos y de calidad (propiedades físicas in situ), y de la implementación de técnicas digitales que proporcionen una visión integral y detallada del problema a estudiar. El análisis morfológico 3D mediante herramientas digitales de representación y procesado de datos geofísicos (por ejemplo Kingdom Suite), permiten una mejora en el conocimiento de los procesos erosionales y deposicionales asociados a los cañones submarinos (Bertoni y Cartwright, 2005) o en el estudio de los movimientos de masa, y por tanto el análisis detallado de la estructura interna de las masas deslizadas. Otra herramienta que se ha mostrado muy eficaz, tanto en la ordenación del territorio como en la predicción de riesgos geológicos, pero que hasta el momento se ha aplicado básicamente en sistemas terrestres (Carrara et al., 1991; Jibson et al., 1998), son los sistemas de información geográfica (SIG). Dichos sistemas tienen un gran potencial en sistemas marinos (Lee et al., 1999; Lee, 2000; León, 2005) cuando se adaptan a las características específicas que diferencian estos ambientes de los terrestres ya que permite combinar de forma flexible la gran cantidad y diversidad de información que se requiere para el estudio de los riesgos geológicos asociados a un área concreta. Esto podría sentar las bases metodológicas que proporcionen una aproximación objetiva al riesgo geológico en el medio marino, la identificación de áreas potencialmente expuestas a fenómenos destructivos (como por ejemplo los maremotos), el cálculo de la probabilidad de su ocurrencia y por tanto para la determinación de las posibles medidas de mitigación que se pueden adoptar, si son necesarias.

Bibliografía

Baraza, J., 1989. Procesos de Edificación y Características Geotécnicas del Talud del Ebro. Tesis Doctoral. Universitat Politècnica de Catalunya.

Baraza, J., Lee, J., Kayen, R., Hampton, M.A., 1990. Geotechnical characteristics and slope stability on the Ebro margin, Western Mediterranean. En C.H. Nelson, A. Maldonado (Eds.), The Ebro margin. Marine Geology, 95: 379-393.

Bertoni, C., Cartwright, J., 2005. 3D seismic analysis of slope-confined canyons from the Plio-Pleistocene of the Ebro Continental Margin (Western Mediterranean). Basin Research, 17: 43-62.

Booth, J.S., O'Leary, D. W., Popenoe, P., Danforth, W.W., 1993. US Atlantic continental slope landslides: their distribution, general attributes and implications. Submarine landslides: selected studies in the US exclusive economic zone. W.C. Schwab. US Geological Survey Bulletin, 2002: 14-22.

Canals, M., Casamor, J. L., Urgeles, R., Lastras, G., Calafat, A. M., Masson, D. G., Berne, S., Alonso, B., 2000. The Ebro continental margin, western Mediterranean Sea: interplay between canyon-channel system and mass wasting processes. GCSSEPM Foundation 20th Annual Research Conference Deep-water Reservoirs of the World, Houston, Texas, pp. 152–174.

Canals, M., Lastras, G., Urgeles, R., Casamor, J.L., Mienert, J., Cattaneo, A., De Batist, M., Haflidason, H., Imbo, Y., Laberg, J.S., Locat, J., Long, D., Longva, O., Masson, D.G., Sultan, N., Trincardi, F., Bryn, P., 2004. Slope failure dynamics and impacts from seafloor and shallow sub-seafloor geophysical data: case studies from the COSTA Project. Marine Geology, 213: 9– 72.

Carrara, A., Cardinali, M., Detti, R., Guzzetti, F., Pasqui, V., Reichenbach, P., 1991. GIS Techniques and statistical models in evaluating landslide hazard. Earth Surface Processes and Landforms, 16: 427-445.

Hampton, A.M., Lee, H., Locat, J., 1996. Submarine landslides. Reviews of Geophysics, 34 (1): 33-59.

Jibson, R.W., Harp, L.H., Michael, J.A., 1998. A method for producing digital probabilistic seismis landslides hazard maps: an example from the Los Angeles, California Area. USGS Open-File Report, 98-113.

Larberg, J.S., Vorren, T.O., 2000. The Traenadjupet Slide, offshore Norway - morphology, evacuation and triggering mechanisms. Marine Geology, 171: 95-114.

Lee, H., Locat, J., Dartnell, P., Kenneth, I., Wong, F., 1999. Regional variability of slope stability: application to the Eel margin, California. Marine Geology, 154: 305-321.

Lee, H., 2000. A GIS-based regional analysis of the potential for shallow-seated submarine slope failure. Proc. 8 International Symposium on Landslides. June. Cardiff, Wales.

León, R., 2005. Modelo S.I.G. del campo de estabilidad de los hidratos de gas: aplicación a las estructuras geológicas ligadas a las emisiones submarinas de fluidos hidrocarburos en el Golfo de Cádiz. Tesis Doctoral. Universidad Complutense de Madrid.

Lykousis, V., Alexandri, S., Woodside, J., de Lange, G., Daehlman, A., Perissoratis, C., Ioakim, Chr., Sakellariou, D., Nomikou, P., Casas, D., Kormas, K., Rousakis, G., Ballas, D., 2005. Mud volcanoes and gas hydrates in Anaximander Mountains (Eastern Mediterranean). Journal of Geological Society of London. En revisión.

Pratson, L. F., Laine, E. P., 1989. The relative importance of gravity-induced versus current-controlled sedimentation during the Quaternary along the mideast US outer continental margin revealed by 3.5 kHz echo character. Marine Geology, 89: 87-126.

Urgeles, R., Lastras, G., Canals, M., Willmott, V., Moreno, A., Casas, D., Baraza, J., Berne, S., 2003. The BIG'95 debris flow and adjacent unfailed sediments in the NW Mediterranean Sea: geotechnical sedimentological properties, and dating. En J. Locat, J. Mienert (Eds.), Submarine Mass Movements and Their Consequences. Advances in Natural and Technological Hazards Research, 19: 479-487. Netherlands, Kluwer Academic Publishers.

Willmott, V., Canals, M., Lastras, G., Casas, D., 2001. Caracterización sedimentológica de un debris flow reciente en el margen continental del Ebro. Geotemas, 3(2): 117-120.

✐ Recent mass-movement processes on the Ebro continental slope (NW Mediterranean). D. Casas, G. Ercilla, J. Baraza, B. Alonso, A. Maldonado. *Marine and Petroleum Geology*, 20: 445-457. 2003.

✐ Acoustic evidences of gas in the continental slope sediments of the Gulf of Cadiz (E Atlantic). D. Casas, G. Ercilla, J. Baraza. *Geo-Marine Letters*, 23: 300-310. 2003.

✐ Physical properties and their relationship to texture and consolidation effects in Pliocene-Quaternary sediments from Madeira Abyssal Plain. D. Casas, G. Ercilla, J. Baraza, B. Coakley. *Marine Georesources & Geotechnology*, enviado. 2005.

✐ Physical properties and their relationship to sedimentary processes and texture in sediments from mud volcanoes in the Anaximander Mountains (Eastern Mediterranean). D. Casas, G. Ercilla, V. Lykousis. *Scientia Marina,* enviado. 2005.

✐ Physical and geotechnical properties and assessment of sediment stability on the continental slope and basin of the Bransfield Basin (Antarctica Peninsula). D. Casas, H. Lee, G. Ercilla, R. Kayen, F. Estrada, B. Alonso, J. Baraza, F. Chiocci. *Marine Georesources & Geotechnology*, 22(4): 253-278. 2004.

David Casas Layola

Tesis Doctoral

2005

Universitat de Barcelona

Institut de Ciències del Mar. CSIC